# EVALUATION OF RESERVOIR QUALITY OF THE DERDERE FORMATION WITHIN THE SEQUENCE STRATIGRAPHIC FRAMEWORK IN DIYARBAKIR REGION, SE TURKEY

A THESIS SUBMITTED TO
THE GRADUATE SCHOOL OF NATURAL AND APPLIED SCIENCES
OF
MIDDLE EAST TECHNICAL UNIVERSITY

BY

SUZAN MÜGE YETİM

IN PARTIAL FULFILLMENT OF THE REQUIREMENTS
FOR
THE DEGREE OF DOCTOR OF PHILOSOPHY
IN
GEOLOGICAL ENGINEERING

FEBRUARY 2021

Approval of the thesis:

**EVALUATION OF RESERVOIR QUALITY OF THE DERDERE FORMATION WITHIN THE SEQUENCE STRATIGRAPHIC FRAMEWORK IN DIYARBAKIR REGION, SE TURKEY**

submitted by **SUZAN MÜGE YETİM** in partial fulfillment of the requirements for the degree of **Doctor of Philosophy** i**n Geological Engineering, Middle East Technical University** by,

Prof. Dr. Halil Kalıpçılar
Dean, Graduate School of **Natural and Applied Sciences** _____

Prof. Dr. Erdin Bozkurt
Head of the Department, **Geological Engineering** _____

Prof. Dr. Demir Altıner
Supervisor, **Geological Engineering, METU** _____

**Examining Committee Members:**

Prof. Dr. Bora Rojay
Geological Eng, METU _____

Prof. Dr. Demir Altıner
Geological Eng, METU _____

Prof. Dr. Turhan Ayyıldız
Geological Engineering, Ankara University _____

Assoc. Prof. Dr. Kaan Sayit
Geological Eng., METU _____

Assoc. Prof. Dr. Ayşe Atakul Özdemir
Geophysical Eng., Van Yüzüncüyıl University _____

Date: 04.02.2021

**I hereby declare that all information in this document has been obtained and presented in accordance with academic rules and ethical conduct. I also declare that, as required by these rules and conduct, I have fully cited and referenced all material and results that are not original to this work.**

Name, Last name : Suzan Müge, Yetim

Signature :

# ABSTRACT

## EVALUATION OF RESERVOIR QUALITY OF THE DERDERE FORMATION WITHIN THE SEQUENCE STRATIGRAPHIC FRAMEWORK IN DIYARBAKIR REGION, SE TURKEY

Yetim, Suzan Müge
Doctor of Philosophy, Geological Engineering
Supervisor : Prof. Dr. Demir Altıner

February 2021, 248 pages

An integrated sequence stratigraphic study based on well samples and well log data reveals the signals of eustatic sea level change during the Cenomanian-Turonian time interval in Diyarbakır, southeastern Turkey. The depositional model of the Derdere Formation based on detailed microfacies analysis is proposed as the carbonate ramp model consisting of inner ramp (tidal flat, lagoon and shoal), proximal middle ramp, distal middle ramp and outer ramp depositional settings.

In the direction of east to west seven wells are selected in order to correlate with the depositional sequences defined in the outcrops of the Derik section. Third-order depositional sequences typical of Cretaceous greenhouse carbonate systems are defined in the wells based on lithofacies, paleontological data and INPEFA log data. Highstand systems tracks contain a greater abundance of grain-dominated shoal lithofacies with various benthic foraminifers while transgressive systems tracks are represented by pelagic facies with high amount of mud dominated

lithofacies containing calcisphaerulids and planktonic foraminifers. The deposition of the Derdere Formation is considered to be diachronic since the oldest levels of the formation are still Cenomanian age in the Diyarbakır Region different from the field section measured in Derik, Mardin Region; hence the number of sequences defined in well sections is nine during Cenomanian-Turonian time interval.

Carbon isotope studies are conducted to detect C-T boundary and OAE-2 with biostratigraphy, microfacies and INPEFA logs. Oxygen isotope studies are considered as a secondary tool to define sequences and major stratigraphic surfaces and should be used together with other primary tools including microfacies change, INPEFA logs and biostratigraphy. During the early Cenomanian time interval carbonate content increases with the decreasing rate of relative sea level and causes negative $\delta^{18}O$ values at the bottom of the Derdere succession. There are some negative shifts on the oxygen isotope curves in Turonian time interval which is explained by the meteoric diagenesis.

A model for highstand deposition on the Derdere ramp platform and diaganetic mechanisms generated during sea level fluctuations is proposed. At the time of the deposition of highstand systems tract, facies deposited on the inner ramp depositional setting were subaerially exposed and meteoric water infiltration caused dissolution and dolomitization type diagenetic mechanisms. Cloudy core-clear rimmed dolomite, which is associated with highstand systems tracts and meteoric diagenesis, enhances reservoir quality of the formation whereas dolomitization observed in the transgressive systems tract does not have any constructive effect on the reservoir quality of the Derdere Formation.

Keywords: SE Turkey, Derdere Formation, Sequence Stratigraphy, Reservoir Quality, Eustatic Sea Level Change, 3rd Order Sequences

# ÖZ

## DİYARBAKIR BÖLGESİ'NDE SEKANS STRATİGRAFİ ÇERÇEVESİ İÇERİSİNDE DERDERE FORMASYONU'NUN REZERVUAR ÖZELLİKLERİNİN DEĞERLENDİRİLMESİ

Yetim, Suzan Müge
Doktora, Jeoloji Mühendisliği
Tez Yöneticisi: Prof. Dr. Demir Altıner

Şubat 2021, 248 sayfa

Güneydoğu Anadolu Bölgesi Diyarbakır'da kuyu örnekleri ve kuyu loglarına dayalı yürütülen sekans stratigrafi çalışmaları Senomaniyen-Turoniyen zaman aralığında östatik deniz seviyesi değişimlerini ortaya koymaktadır. Detaylı mikrofasiyes çalışmaları ile Derdere Formasyonu için ortaya koyulmuş olan çökel model karbonat yokuş modeli olup, iç şelf (gelgit düzlüğü, lagün ve sığlık kısımları), yakınsak orta şelf, ıraksak orta şelf ve dış şelf olarak ayrılmıştır.

Diyarbakır Bölgesi'nde doğu-batı doğrultusunda yedi adet kuyu Derik mostrasında tanımlanan çökel sekans paketleri ile korele edilmek üzere seçilmiştir. Kratese dönemi karbonat sisteminin tipik 3. dereceden çökel sekans paketleri bu öncelikli kuyuda litostratigrafi, paleontoloji ve kuyu log verilerine dayalı olarak tanımlanmıştır. Sekansların sığlaşan sistem paketleri çeşitli bentik foraminiferlerden oluşan fazla miktarda tane dokulu sığ fasiyeslerinden oluşurken, derinleşen sistem paketleri kalsisferli ve planktonik foraminiferli çamur dokulu pelajik litofasiyesleri ile temsil edilmektedir. Diyarbakır Bölgesi'ndeki kuyularda tanımlanmış olan kuyularda Derdere Formayonu en yaşlı seviyelerinin hala Senomaniyen yaşlı ve Mardin Bölgesi Derik kesitinden farklı olması sebebiyle,

Derdere Formasyonu çökelimi diyakronik olarak değerlendirilmiş olup, Senomaniyen-Turoniyen zaman aralığında tanımlanmış olan sekans paketlerinin sayısı kuyularda dokuz olarak tanımlanmıştır.

Karbon izotop çalışmaları Senomaniyen-Turoniyen sınırını koymak ve Denizel Anoksik Olay-2' nin sınırlarını belirlemek amacıyla biyostratigrafi, mikrofasiyesler ve INPEFA logları ile birlikte değerlendirilmiştir. Oksijen izotop çalışmaları sekansların ve ana sekans yüzeylerinin belirlenmesinde ikinci dereceden bir yöntem olarak değerlendirilmiş olup, mikrofasiyes değişimleri, INPEFA logları ve biyostratigrafi ile birlikte değerlendirilmesi gerektiği sonucuna varılmıştır. Erken Senomaniyen zaman diliminde, azalan deniz seviyesi ile karbonat miktarında artış olması sebebiyle, Derdere Formasyonu tabanında negatif $\delta^{18}O$ değerleri kaydedilmiştir. Turoniyen döneminde oksijen izotop eğrisi üzerinde görülen negatif sapmalar meteoric diyajenez ile açıklanmıştır.

Derdere yokuş tipi karbonat platformu sığlaşan çökelleri ve deniz seviyesi değişimleri esnasında oluşan diyajenetik mekanizmalar için bir model ortaya koyulmuştur. Sığlaşan sistem paketlerinin çökelimi esnasında, iç şelf çökel ortamında bulunan fasiyeslerin yüzeylendiği ve meterorik su girişinin çözünme ve dolomitizasyon gibi diyajenetik işlergelerin gözlenmesine sebep olmuştur. Sığlaşan sistem paketleri ve meteoric diyajenez ile ilişkili olarak oluşmuş olan bulutlu merkezli-temiz kenarlı dolomitlerin rezervuar gelişimine olumlu etkiler yaparken, derinleşen sistem paketleri içinde oluşmuş olan dolomitlerin rezeruar gelişimine herhangi bir olumlu etkisinin olmadığı gözlenmiştir.

Anahtar Kelimeler: Güneydoğu Anadolu Bölgesi, Derdere Formasyonu, Sekans Stratigrafisi, Rezervuar Kalitesi, Östatik Deniz Seviyesi Değişimleri, 3. Dereceden Sekanslar

To my beloved family...

## ACKNOWLEDGMENTS

I would like to thank, Prof. Dr. Demir Altıner for his continues support during my Phd study and research, thoughtful guidance, motivation, enthusiasm, and broad knowledge of general geology, biostratigraphy, sedimentology and sequence stratigraphy. My gratitude is also due to my committee members, Prof Dr. Bora Rojay, Prof. Dr. Turhan Ayyıldız, Assoc. Prof. Kaan Sayıt, and Assoc. Prof. Ayşe Özdemir. I would like to express my appreciation to Prof. Dr. Sevinç Altiner for her recommendations.

This study is also one of the research and development projects of Turkish Petroleum Coorporation. Hence I would like to offer my special thanks to Turkish Petroleum Corporation for providing well data, for making my laboratory work possible and for financial support to have light microscope based cathodoluminescence and to conduct isotope studies. Another special thanks to my manager in Turkish Petroleum Coorporation, Macide Zeynep Yücel, my colleagues in Sedimentology and Reservoir Geology Department of Turkish Petroleum and Recep Özkan and Mehtap Pınar from Stratigraphy Department for their support and knowledge about biostratigraphy.

I am also grateful to all my friends for their friendship and endless encouragements.

Lastly, I would like to thank my family for their love, guidance, patience and support they provided during difficult times and offer special thanks to my husband and my mother for their continuous support and motivation throughout my study.

## TABLE OF CONTENTS

## LIST OF TABLES

### TABLES

## LIST OF FIGURES

**FIGURE**S

## LIST OF ABBREVIATIONS

### ABBREVIATIONS

Integrated Prediction Error Filter Analyses (INPEFA)

Field-emission scanning electron microscopy (FE-SEM)

Cathodoluminescence (CL)

Energy dispersive system (EDS)

Gamma ray (GR) and Gamma ray total (GRTO)

Gamma ray potassium-thorium (GRKT)

Sonic (DT)

Resistivity (LLD, LLS, MSFL)

Density (RHOB, NPHI)

Photoelectric (PE)

Spectral Gamma-ray (SGR)

Potassium (K)

Uranium (U)

Thorium (Th)

Cenomanian-Turonian (C-T)

Oceanic Anoxic Events (OAEs)

Highstand systems tract (HST)

Transgressive systems tract (TST)

Maximum flooding surface (MFS)

Sequence boundary (SB)

# LIST OF SYMBOLS

## SYMBOLS

### General Lithology


SANDSTONE


SILTSTONE


MUDSTONE


SHALE


MARL


SILTY MARL


DOLOMITIC MARL


LIMESTONE


DOLOMITIC LIMESTONE


DOLOMITE

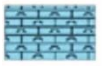
BIOCLASTIC LIMESTONE


CLAYEY LIMESTONE


CONGLOMERATE


NODULAR LIMESTONE


MELANGE

## Fossils and Microfacies Symbols

# CHAPTER 1

# INTRODUCTION

## 1.1 PURPOSE AND SCOPE

A sequence stratigraphic study based on core and cutting samples, and well log data documents the effects of the Cenomanian-Turonian sea level change on the lithofacies of the Derdere Formation deposited in the Diyarbakır Region, southeastern Turkey. In the study of Özkan and Altiner (2019), a field section, measured in the Mardin Group carbonates including Areban, Sabunsuyu and Derdere Formations, a sequence stratigraphic study has been carried out in the Derik Area, Mardin and the sequences are defined as the records of the global sea level changes. This study is intended to correlate the sequences defined in these outcrop sections with well data from Diyarbakır Region in this study and to evaluate the reservoir quality of the Derdere Formation within the sequence stratigraphy frame. Seven wells, penetrated totally or partially into the Derdere Formation, are selected from the foreland area of the Diyarbakır Region. Among these seven wells (from west to east K-11, K-8, K-3, K-2, K-4, K-9, K-7 wells), the K-11 well is selected as the pilot well in order to develop the sequence stratigraphic framework based on the numerous cores taken from the Derdere Formation. Deepening and shoaling (transgressive and regressive) third-order depositional sequences interpreted based on microfacies and well log data are defined in this pilot well. As a general speaking, facies defined in highstand systems tracts are more tend to be grain-dominated shoal and peritidal type environments in inner ramp settings while facies defined in transgressive systems tracts are more tend to be pelagic with high amount of mud dominated lithofacies and calcisphaerulid and planktonic foraminifers type primary constituents. Sequence boundaries are not simple to define in the well studies different from the field studies since hematitic crust at the top of the sequence, iron oxide rich limestone surface or irregular

erosional surface as a result of subaerial exposure surface can easily be observed at field sections. Sequence boundaries are discriminated with the drastic changes in microfacies and located at the top of highstand systems tracts. Where sea level is high in order to define third-order of sequences relative shoaling and deepening trends of facies are considered. Third-order sequences defined in the K-11 Well are correlated with the sequences of other wells interpreted from the turning points of Integrated Prediction Error Filter Analyses (INPEFA), which is considered as a sensitive instrument to sea level changes. These sequences and sequence stratigraphic surfaces are tested whether they correspond to the depths of change in lithofacies which have an influence on INPEFA log.

The main purpose of the study is to reveal the varieties and similarities in terms of microfacies, number of sequences, types of sequence boundaries and the reasons behind these on the depositional trends of Derdere Formation using well data in the Diyarbakır Region by the application of sedimentology and sequence stratigraphy principles. For this purpose, Derdere Formation is aimed to be studied at seven selected wells regarding sea level changes, sequence divisions and testing whether sequence correlation can be applicable on the wells by the consideration of variations on lateral and vertical microfacies changes and biostratigraphy. Biostratigraphy and observations on the change of microfacies, which can be detected both laterally and vertically and stacking patterns whether they are progradational, retrogradational or aggradational, are used for sequence stratigraphic interpretations. The main reason behind the differences of deposition of platform carbonates is whether, non-deposition or erosion, will be revealed.

In addition to depositional differences, determination of syn-depositional and post-depositional diagenetic mechanisms (cementation, dolomitization, dissolution, fracturing, recrystallization, replacement etc.) and relative timing of these mechanisms (earliest to latest) provides data for the reservoir quality determination and the relationship with the sequences and sequence boundaries within the seqeuence stratigraphic framework. With the help of lithological, sedimentological,

petrographical, biostratigraphical and well log data study will be completed at three phases:

- Comparison of depositional and diagenetic trends of the Derdere Formation in the wells of the Diyarbakır Regions,
- Correlation of sequences defined in the wells of the Diyarbakır Region with sequences defined in the section measured at the Derik Section, Mardin and
- Sequence stratigraphic correlation with other carbonate platforms worldwide during the Early-Late Cretaceous time.

## 1.2 GEOLOGIC SETTING AND DATA DISTRIBUTION

### 1.2.1 Geologic Setting of the Study Area

The study area is located in the foreland area of Diyarbakır which is the XI. Petroleum District of Southeastern Turkey (**Figure 1**). Seven wells are selected by the consideration of three parameters, which are entire penetration to Mardin Group Carbonates, being located in the foreland area (being away from the thrust fault zone on the north) and the presence of cores taken from the Derdere Formation which is the main focus of this study (**Figure 2**). Mardin Group Carbonates which are defined in Southeast Anatolian Region become focus point of most of the studies conducted on petroleum exploration due to the existence of facies showing both source and reservoir rock properties and providing opportunity of production. Adiyaman and Diyarbakir Regions are considered as the part of foreland area at the southern side of Late Miocene and Late Cretaceous thrust fault zone (Perinçek, 1980; Fontaine et. al., 1989; Demirel ve Güneri, 2000; Aydemir, 2011) and can be taken into account as promising regions in terms of petroleum exploration (Demirel ve Güneri, 2000).

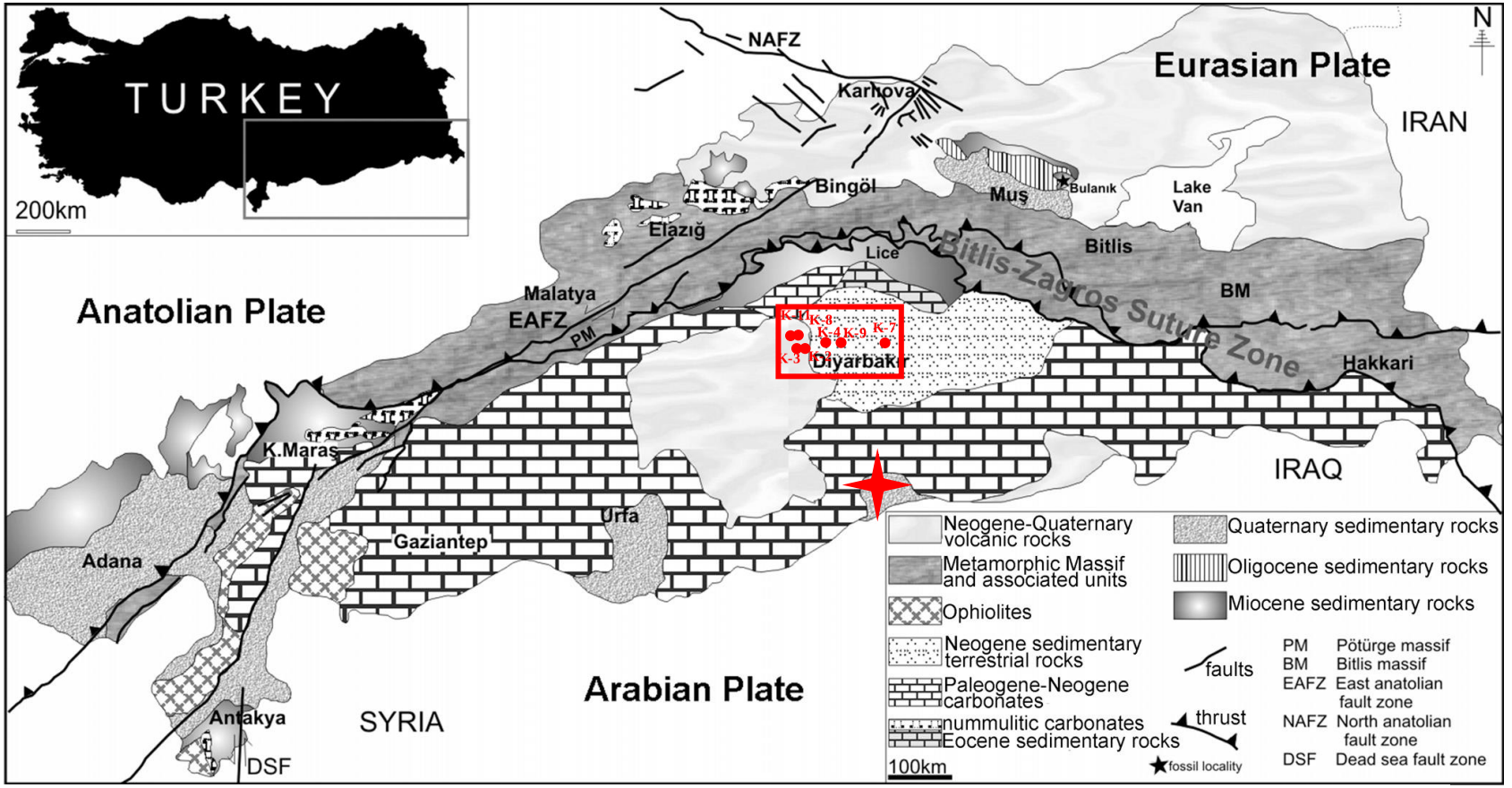


**Figure 1.** Geological map of Southeast Turkey (Aydemir, 2011). Study area is shown with red rectangular around Diyarbakır Region and well locations are plotted on the map. Location of fieldwork completed around Derik, Mardin area is shown with red star (modified after Şenel, 2002 and Hüsing et. al.,2009).

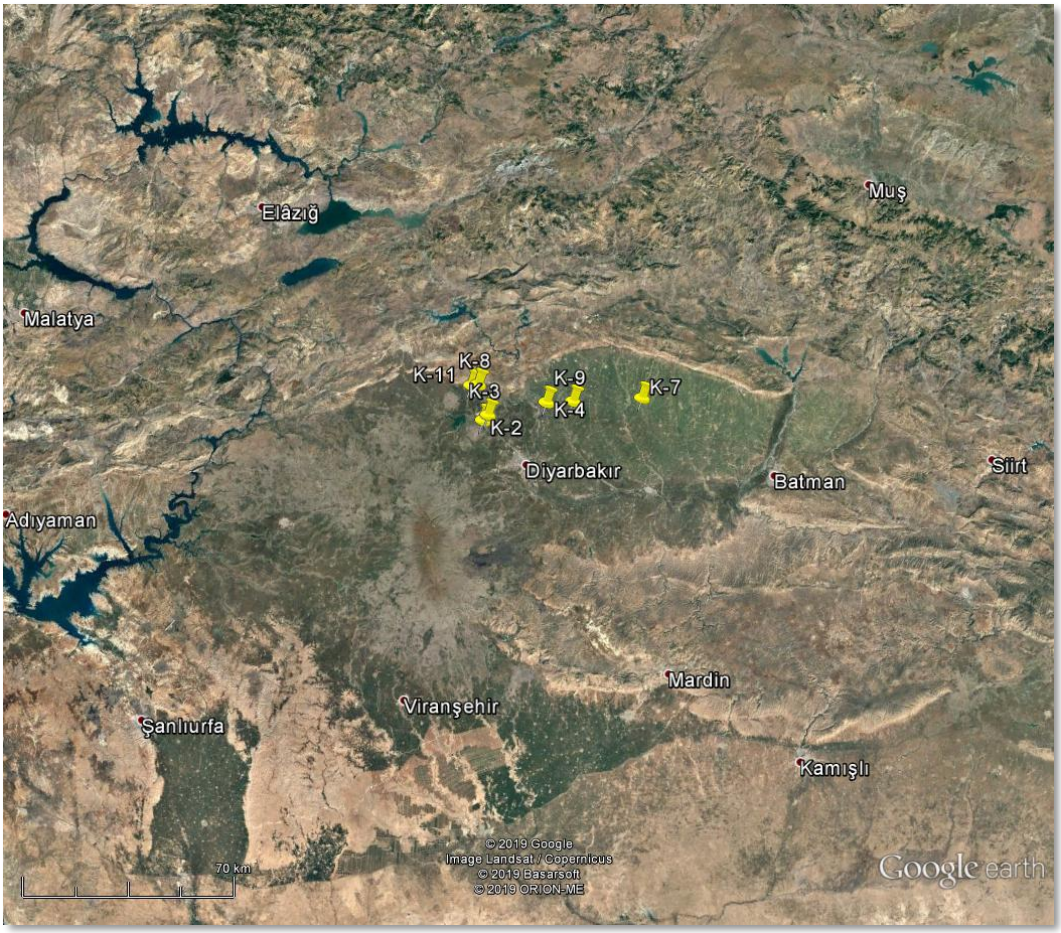


**Figure 2.** Locations of the studied wells from west to east K-11, K-8, K-2, K-3, K-9, K-4 and K-7 are plotted on Google Earth image.

The main concept behind doing this research is the sequence stratigraphic study based on a fieldwork at which succession of Mardin Group Carbonates are measured in Derik, Mardin Region by Özkan and Altıner in 2014. As a result of this fieldwork, sequences which can be correlated with global cycle chart of Haq, 2014 are defined and this study is published in 2019 by Özkan and Altıner. From west to east seven wells are picked up in order to test whether they can be correlated with the section measured in the field. Westernmost well is K-11 well and easternmost well is K-7 and the distance between these wells are approximately 100 kilometers **(Figure 1** and **Figure 2)**.

### 1.2.2 Data Distribution

This study mainly focuses on well data including core and cutting samples. K-11 well is chosen as the pilot well in order to reveal the depositional model and sequence stratigraphic framework of the Derdere Formation (**Figure 2**). The reason of selecting this well as a pilot well is the presence of five cores and the high resolution sampling from the Derdere Formation which is the main focus of this study **(Table 1)**. Cutting samples with 2 meters resolution are studied where core samples are absent. Other than cores of the K-11 well, two cores of the K-8 well are also studied by high resolution sampling. The rest of the K-8 well and other wells are studied from the cutting samples.

Lithological and petrographical analyses are conducted on these core and cutting samples (**Table 2-4**). Core samples provide approximately 5 centimeters resolution in order to observe the lithologic heterogeneity in the Derdere Formation. This high resolution sampling provides an opportunity to define fourth- to fifth- order parasequences; however, cutting samples do not have that much of high resolution sampling, mainly third-order sequences are differentiated by taking into consideration of sequences' thicknesses. Where data resolution is not available for the sequence discrimination in the shoaling and deepening successions, well log data is used which is going to be explained in the following chapters.

K-11 pilot well drilled in 2011, which is located at northwest of the Diyarbakir Region and in the XI. Petroleum District. The well was completed in the Derdere Formation at 1798 m with the discovery of oil with the five cores (**Table 1**).

K-8 well drilled in 2011, which is located at north of the Diyarbakir Region and in the XI. Petroleum District. The well was completed in the Derdere Formation at 1872 m with oil discovery with two cores taken from the Derdere Formation (**Table 1**).

For the other wells, K-2, K-3, K-4, K-7 and K-9 wells only cutting samples are available to study. Total thickness of the Derdere Formation varies from west to east. The total thickness of the Derdere Formation is 152 m in K-11 well (without

whole penetration), 166 m in K-8 well (without whole penetration), 167 m in K-3 well (with whole penetration), 166 m in K-2 well (with whole penetration), 160 m in K-4 well (with whole penetration), 186 m in K-9 well (with whole penetration)and 156 m in K-7 well (with whole penetration).

All cutting samples, core samples and thin sections are prepared in the Research and Develeopment Center of Turkish Petroleum Corporation (R&D Center of TPAO), Ankara. All of the well samples are used by the permission obtained from TPAO.

**Table 1.** Wells with the cores in the study area

| Name of the well | Number of the core | Depth Interval (m) | Recovery (%) | Formation |
|---|---|---|---|---|
| **K-11** | 1 | 1649-1658.5 | 100 | Derdere |
| **K-11** | 2 | 1694-1702.4 | 95 | Derdere |
| **K-11** | 3 | 1719-1727 | 96 | Derdere |
| **K-11** | 4 | 1763-1773.3 | 100 | Derdere |
| **K-11** | 5 | 1773-1782.2 | 100 | Derdere |
| **K-8** | 1 | 1712-1717.5 | 82 | Derdere |
| **K-8** | 2 | 1822-1827.5 | 28 | Derdere |
| **K-9** | 1 | 2430-2436 | 70 | Derdere |

**Table 2.** Thin section sample depths' of cores and cuttings of K-8 well

| | K-8 WELL | | | | |
|---|---|---|---|---|---|
| | Core Samples | | Cutting Samples | | |
| | Core#1 | Core#2 | | | |
| Sample Depths (m) | 1712.05 | 1822.04 | 1672 | 1770 | 1824 |
| | 1712.17 | 1822.17 | 1678 | 1772 | 1826 |
| | 1712.28 | 1822.45 | 1690 | 1774 | 1828 |
| | 1712.32 | 1822.56 | 1718 | 1776 | 1830 |
| | 1712.44 | 1822.78 | 1720 | 1778 | 1832 |
| | 1712.56 | 1822.95 | 1724 | 1780 | 1834 |
| | 1712.85 | 1823.03 | 1726 | 1782 | 1836 |
| | 1713.12 | 1823.52 | 1730 | 1784 | 1838 |
| | 1713.34 | | 1732 | 1786 | 1840 |
| | 1713.59 | | 1734 | 1788 | 1842 |
| | 1713.7 | | 1736 | 1790 | 1844 |
| | 1713.79 | | 1738 | 1792 | 1846 |
| | 1713.88 | | 1740 | 1794 | 1848 |
| | 1714.19 | | 1742 | 1796 | 1850 |
| | 1714.2 | | 1744 | 1798 | 1852 |
| | 1714.4 | | 1746 | 1800 | 1854 |
| | 1714.53 | | 1748 | 1802 | 1856 |
| | 1714.78 | | 1750 | 1804 | 1858 |
| | 1714.9 | | 1752 | 1806 | 1860 |
| | 1715.31 | | 1754 | 1808 | 1862 |
| | 1715.55 | | 1756 | 1810 | 1864 |
| | 1715.72 | | 1758 | 1812 | 1866 |
| | 1715.97 | | 1760 | 1814 | 1868 |
| | 1716.11 | | 1762 | 1816 | 1870 |
| | 1716.3 | | 1764 | 1818 | 1872 |
| | 1716.4 | | 1766 | 1820 | |
| | 1716.49 | | 1768 | 1822 | |

**Table 3.** Thin section sample depths' of cores and cuttings of K-11 well

| | K-11 WELL | | | | | | | | | | | |
|---|---|---|---|---|---|---|---|---|---|---|---|---|
| | Core Samples | | | | | | | | | | Cutting Samples | |
| | Core#1 | | Core#2 | | Core#3 | | Core#4 | | Core#5 | | | |
| Sample Depths (m) | 1649.07 | 1654.15 | 1694.02 | 1699.21 | 1719.06 | 1726.73 | 1764.03 | 1770.50 | 1773.25 | 1781.11 | 1604 | 1754 |
| | 1649.21 | 1654.20 | 1694.16 | 1699.32 | 1719.91 | 1726.75 | 1764.16 | 1770.69 | 1773.35 | 1781.28 | 1608 | 1756 |
| | 1649.35 | 1654.38 | 1694.24 | 1699.6 | 1720.21 | | 1764.37 | 1770.80 | 1773.65 | 1781.47 | 1616 | 1758 |
| | 1649.43 | 1654.40 | 1694.46 | 1699.64 | 1720.27 | | 1764.42 | 1771.01 | 1773.80 | 1781.52 | 1620 | 1760 |
| | 1649.50 | 1654.66 | 1694.55 | 1699.73 | 1720.50 | | 1764.54 | 1771.30 | 1774.10 | 1781.69 | 1628 | 1762 |
| | 1649.62 | 1654.71 | 1694.68 | 1699.77 | 1720.60 | | 1764.67 | 1771.40 | 1774.18 | 1781.92 | 1634 | 1764 |
| | 1649.76 | 1654.86 | 1694.72 | 1699.96 | 1720.64 | | 1764.84 | 1771.56 | 1774.46 | 1782.11 | 1638 | 1774 |
| | 1649.83 | 1654.91 | 1694.82 | 1700.03 | 1720.81 | | 1764.89 | 1771.65 | 1774.77 | | 1642 | 1776 |
| | 1650.01 | 1655.05 | 1694.87 | 1700.14 | 1720.89 | | 1765.08 | 1771.76 | 1775.01 | | 1646 | 1778 |
| | 1650.11 | 1655.09 | 1695.03 | 1700.28 | 1721.05 | | 1765.16 | 1771.85 | 1775.28 | | 1648 | 1784 |
| | 1650.23 | 1655.21 | 1695.09 | 1700.39 | 1721.16 | | 1765.40 | 1772.07 | 1775.49 | | 1674 | 1786 |
| | 1650.43 | 1655.25 | 1695.18 | 1700.48 | 1721.78 | | 1765.53 | 1772.17 | 1775.79 | | 1680 | 1788 |
| | 1650.48 | 1655.40 | 1695.22 | 1700.56 | 1721.84 | | 1765.78 | 1772.30 | 1775.89 | | 1682 | 1790 |
| | 1650.57 | 1655.60 | 1695.33 | 1700.61 | 1722.01 | | 1765.84 | 1772.36 | 1776.12 | | 1684 | 1792 |
| | 1650.69 | 1655.65 | 1695.4 | 1700.82 | 1722.09 | | 1766.00 | 1772.67 | 1776.30 | | 1686 | 1794 |
| | 1650.79 | 1656.05 | 1695.79 | 1701.03 | 1722.16 | | 1766.28 | 1772.78 | 1776.64 | | 1690 | 1796 |
| | 1650.85 | 1656.20 | 1695.86 | 1701.19 | 1722.21 | | 1766.53 | 1772.91 | 1776.70 | | 1692 | 1798 |
| | 1651.00 | 1656.30 | 1696.05 | 1701.24 | 1722.37 | | 1766.67 | 1773.15 | 1776.86 | | 1694 | |
| | 1651.07 | 1656.45 | 1696.1 | 1701.37 | 1722.45 | | 1766.79 | | 1777.00 | | 1696 | |
| | 1651.18 | 1656.60 | 1696.24 | 1701.53 | 1722.72 | | 1766.89 | | 1777.25 | | 1698 | |
| | 1651.25 | 1656.82 | 1696.29 | 1701.77 | 1722.82 | | 1766.97 | | 1777.31 | | 1704 | |
| | 1651.40 | 1657.00 | 1696.53 | 1701.82 | 1722.89 | | 1767.39 | | 1777.54 | | 1706 | |
| | 1651.50 | 1657.04 | 1696.64 | 1701.97 | 1722.96 | | 1767.43 | | 1777.77 | | 1708 | |
| | 1651.53 | 1657.22 | 1696.75 | 1702.04 | 1723.05 | | 1767.61 | | 1777.97 | | 1710 | |
| | 1651.62 | 1657.30 | 1696.80 | 1702.21 | 1723.17 | | 1767.78 | | 1778.04 | | 1712 | |
| | 1651.75 | 1657.50 | 1696.95 | 1702.27 | 1723.47 | | 1767.92 | | 1778.34 | | 1714 | |
| | 1651.82 | 1657.60 | 1697.01 | 1702.55 | 1724.01 | | 1768.13 | | 1778.45 | | 1716 | |
| | 1651.92 | 1657.75 | 1697.2 | | 1724.16 | | 1768.33 | | 1778.59 | | 1718 | |
| | 1652.07 | 1657.93 | 1697.42 | | 1724.40 | | 1768.47 | | 1778.76 | | 1728 | |
| | 1652.21 | 1658.10 | 1697.5 | | 1724.60 | | 1768.61 | | 1778.92 | | 1730 | |
| | 1652.27 | 1658.24 | 1697.64 | | 1724.81 | | 1768.74 | | 1778.96 | | 1732 | |
| | 1652.50 | 1658.44 | 1697.97 | | 1724.90 | | 1768.80 | | 1779.18 | | 1734 | |
| | 1652.55 | 1658.50 | 1698.06 | | 1725.05 | | 1769.03 | | 1779.41 | | 1736 | |
| | 1652.70 | | 1698.17 | | 1725.20 | | 1769.16 | | 1779.53 | | 1738 | |
| | 1652.75 | | 1698.33 | | 1725.25 | | 1769.35 | | 1779.74 | | 1740 | |
| | 1652.89 | | 1698.4 | | 1725.35 | | 1769.52 | | 1779.80 | | 1742 | |
| | 1652.96 | | 1698.55 | | 1725.49 | | 1769.66 | | 1780.01 | | 1744 | |
| | 1653.10 | | 1698.6 | | 1726.48 | | 1769.77 | | 1780.34 | | 1746 | |
| | 1653.33 | | 1698.79 | | 1726.99 | | 1769.95 | | 1780.53 | | 1748 | |
| | 1653.50 | | 1698.99 | | 1726.85 | | 1770.16 | | 1780.79 | | 1750 | |
| | 1653.55 | | 1699.13 | | 1726.58 | | 1770.29 | | 1780.93 | | 1752 | |

**Table 4.** Thin section sample depths' of cuttings of K-3, K-2, K-4, K-9 and K-7 wells

| | WELLS | | | | | | | | | | | | |
|---|---|---|---|---|---|---|---|---|---|---|---|---|---|
| | K-3 | | K-2 | | | K-4 | K-9 | | | K-7 | | | |
| | Cutting Samples | | | | | | | | | | | | |
| Sample Depths (m) | 2234 | 2380 | 2270 | 2420 | 2612 | 2448 | 2400 | 2528 | 2658 | 2776 | 2856 | 2922 | 3008 |
| | 2266 | 2382 | 2278 | 2424 | 2616 | 2458 | 2404 | 2532 | 2662 | 2780 | 2858 | 2924 | 3010 |
| | 2278 | 2384 | 2282 | 2428 | 2620 | 2464 | 2408 | 2536 | | 2782 | 2860 | 2926 | 3014 |
| | 2292 | 2386 | 2284 | 2432 | 2624 | 2498 | 2412 | 2540 | | 2786 | 2862 | 2928 | 3018 |
| | 2312 | 2388 | 2298 | 2436 | 2628 | 2530 | 2416 | 2544 | | 2792 | 2864 | 2930 | 3022 |
| | 2314 | 2390 | 2304 | 2440 | 2632 | 2536 | 2420 | 2548 | | 2794 | 2866 | 2932 | 3026 |
| | 2316 | 2392 | 2308 | 2448 | 2636 | 2546 | 2424 | 2552 | | 2796 | 2868 | 2934 | 3034 |
| | 2320 | 2394 | 2316 | 2452 | 2640 | 2550 | 2428 | 2556 | | 2798 | 2870 | 2936 | 3042 |
| | 2322 | 2396 | 2320 | 2460 | 2644 | 2554 | 2432 | 2560 | | 2800 | 2872 | 2938 | 3050 |
| | 2326 | 2398 | 2324 | 2468 | 2648 | 2562 | 2434 | 2564 | | 2802 | 2874 | 2940 | 3058 |
| | 2328 | 2400 | 2328 | 2472 | 2652 | 2566 | 2438 | 2568 | | 2804 | 2876 | 2942 | 3062 |
| | 2330 | 2402 | 2332 | 2484 | 2664 | 2572 | 2440 | 2572 | | 2806 | 2878 | 2944 | 3070 |
| | 2332 | 2404 | 2336 | 2488 | | 2576 | 2444 | 2576 | | 2808 | 2880 | 2946 | 3078 |
| | 2336 | 2406 | 2340 | 2496 | | 2594 | 2448 | 2580 | | 2810 | 2882 | 2948 | 3082 |
| | 2338 | 2408 | 2344 | 2500 | | 2598 | 2452 | 2584 | | 2812 | 2884 | 2950 | 3094 |
| | 2340 | 2410 | 2348 | 2504 | | 2604 | 2456 | 2588 | | 2814 | 2886 | 2952 | 3122 |
| | 2342 | 2412 | 2352 | 2508 | | 2610 | 2460 | 2592 | | 2816 | 2888 | 2954 | 3142 |
| | 2344 | 2414 | 2356 | 2512 | | 2648 | 2464 | 2596 | | 2818 | 2890 | 2956 | 3154 |
| | 2346 | 2414 | 2360 | 2516 | | 2664 | 2468 | 2600 | | 2820 | 2892 | 2958 | 3158 |
| | 2348 | 2416 | 2364 | 2520 | | 2666 | 2472 | 2602 | | 2822 | 2896 | 2960 | 3162 |
| | 2350 | 2418 | 2368 | 2520 | | 2668 | 2476 | 2606 | | 2824 | 2898 | 2962 | 3166 |
| | 2352 | 2420 | 2372 | 2524 | | 2670 | 2480 | 2610 | | 2826 | 2900 | 2964 | 3172 |
| | 2356 | 2422 | 2376 | 2528 | | 2720 | 2484 | 2614 | | 2828 | 2902 | 2966 | 3178 |
| | 2360 | 2424 | 2380 | 2532 | | 2722 | 2488 | 2618 | | 2830 | 2904 | 2968 | 3210 |
| | 2362 | 2426 | 2384 | 2536 | | 2728 | 2492 | 2622 | | 2832 | 2906 | 2970 | 3338 |
| | 2364 | 2428 | 2388 | 2544 | | 2740 | 2496 | 2626 | | 2834 | 2908 | 2872 | |
| | 2366 | 2430 | 2392 | 2556 | | 2774 | 2500 | 2630 | | 2838 | 2910 | 2974 | |
| | 2368 | 2432 | 2396 | 2564 | | | 2504 | 2634 | | 2840 | 2912 | 2976 | |
| | 2370 | 2434 | 2400 | 2580 | | | 2508 | 2638 | | 2844 | 2914 | 2980 | |
| | 2372 | 2436 | 2404 | 2584 | | | 2512 | 2642 | | 2846 | 2916 | 2982 | |
| | 2374 | 2438 | 2408 | 2588 | | | 2516 | 2646 | | 2848 | 2916 | 2984 | |
| | 2376 | 2440 | 2412 | 2598 | | | 2520 | 2650 | | 2852 | 2918 | 2986 | |
| | 2378 | | 2416 | 2608 | | | 2524 | 2654 | | 2854 | 2920 | 3000 | |

## 1.3 METHODS OF STUDY

### 1.3.1 Petrographic Methods

In this study, methods mainly depend on microscopical studies including transmitted light microscopy, reflected light microscopy, field-emission scanning electron microscopy (FE-SEM), X-ray mapping and light microscopy based-cathodoluminescence (CL).

Light microscopy can be used to delineate the majority of lithological, textural, and faunal assemblage variations. For the microfacies description and biostratigraphic studies light microscopy based studies are conducted. Other methods mentioned are used to reveal diagenetic mechanisms and diagenetic environment of the Derdere Formation in different wells of Diyarbakır. Field-emission scanning electron microscopy is used to observe small components including calcisphaerulids which are commonly observed in some levels of the Derdere Formation and X-ray mapping technique is to observe 2D compositional map of the sample. Light microscopy based-cathodoluminescence method is crucial to reveal cement stratigraphy of the samples.

Understanding and interpreting the evolution of the carbonate platform and the depositional environment of the Derdere Formation is one of the main purposes of this study. In order to reveal the depositional model, detailed microfacies analysis is conducted by examining the allochems, macro- and microfossil associations of the samples according to Dunham classification (**Figure 3**). Carbonate rock classification is based on the comparison charts for visual estimation percentage composition defined by Terry and Chilingar (1955) (**Figure 4**). By this semi-quantitative method and Dunham classification facies analyses are completed.

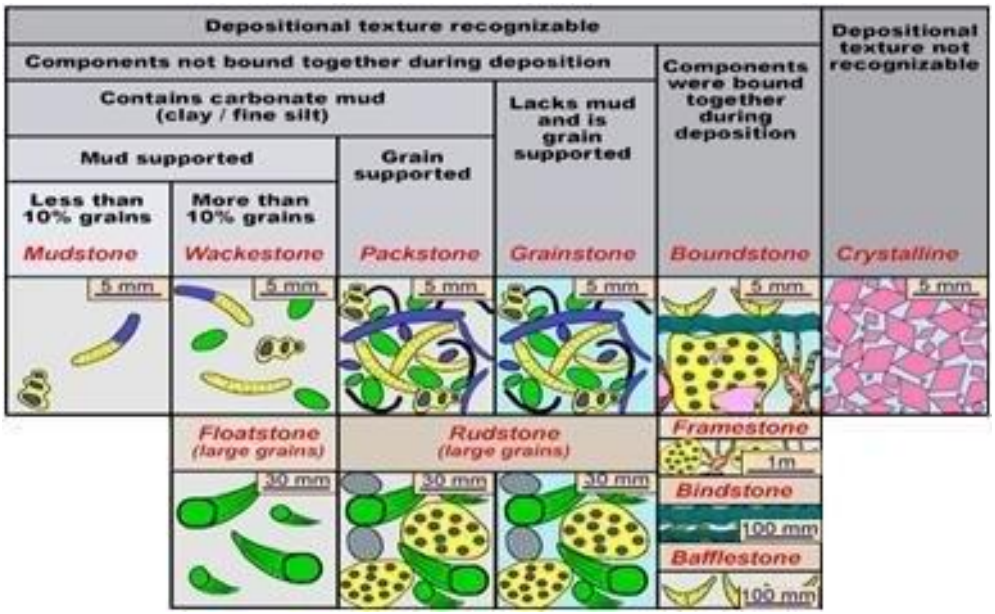


**Figure 3.** Dunham's carbonate rock texture classification (1962) with modifications by Embry and Klovan (1971)

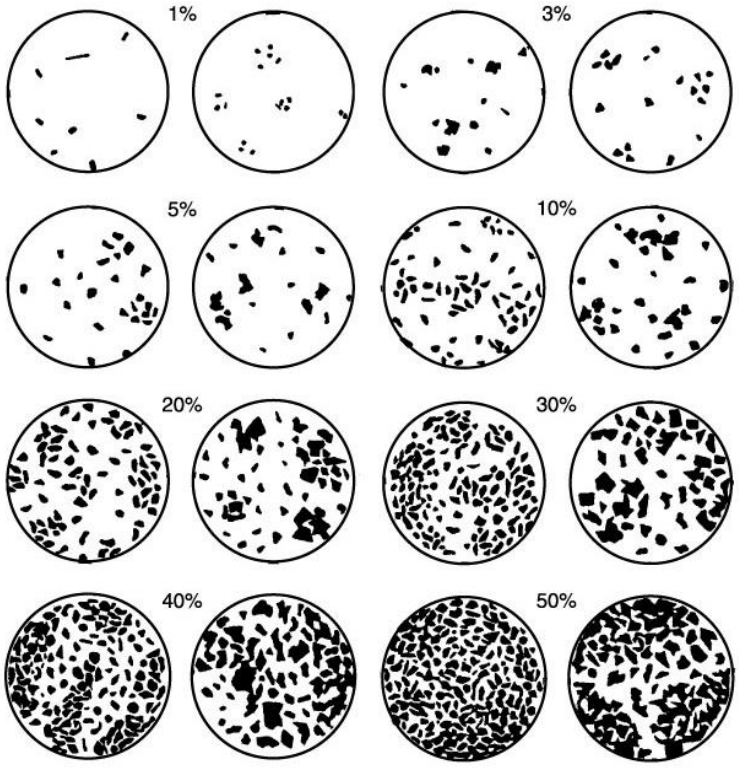


**Figure 4.** Comparison chart for visual percentage estimation (after Terry and Chilingar, 1955)

For the X-ray mapping technique, the principle behind the characteristics of X-rays for individual elements is used by energy dispersive system (EDS) detectors. In order to have 2D compositional map of the polished sample surface, distinct colors are assigned for the particular elements and by gathering these element maps together, mineral maps showing mineral composition can be achieved (Tovey and Krinsley, 1991; Ergene, 2014). Since the resolution of the element maps does not allow us to have multi-layer imaging for the mineral compositions, only element maps are used to make an observation for composition. The main point of using X-ray mapping technique for the Derdere Formation which is completely made up of carbonate minerals is to observe whether there are any authigenic quartz minerals due to possible dissolution of radiolaria in the Derdere.

CL for carbonate minerals is applied to make fabrics visible that are not visible by light microscopy for instance; recrystallization or dolomitization can cause disappearing of the skeletal and nonskeletal fragments and by the application of light microscopy based cathodulimine sence, these components may be visible if they are not intensely altered. CL is used to infer cement sequences with the interpretation of equally luminescing zones, which are diagenetically coeval and so have a conclusion about cement stratigraphy which means that relative timing of different cements according to different trace element content (Machel, 1985). The most common trace elements that affect the intensity of luminescence in carbonate minerals are manganese (Mn) and iron (Fe). According to the enhancing and inhibiting properties of luminescence, trace elements are named as activators or quenchers, respectively. In terms of this definition, Mn is an activator and Fe is a quencher. Existence of Mn and absence of Fe causes more energetic luminescence (bright orange color), absence of both causes darker color and existence of both causes dull (middle-colored) color (Machel, 1985; Ergene, 2014). It means that, if there is more than one luminescence of carbonate minerals including two of bright orange color, dark color and dull orange color on the same sample, there is more than one stage of cementation, dolomitization due to different trace element compositions (**Figure 5-8**).

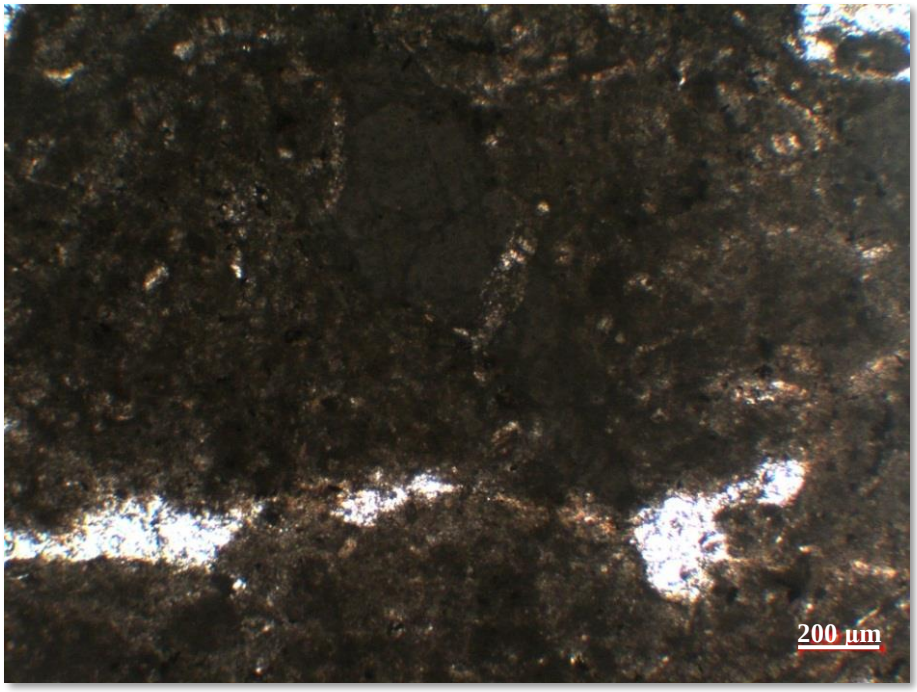


**Figure 5.** Plane polarized light microscopy photomicrograph of peloidal facies and fracture of K-2 well

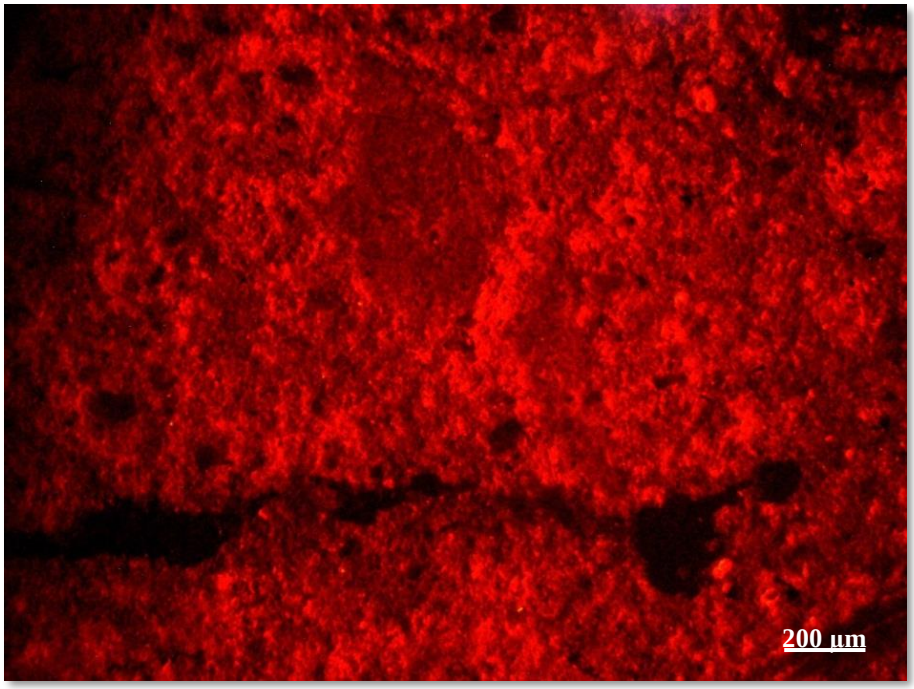


**Figure 6.** Light microscope based cathoduluminescence photomicrograph of peloidal facies and fracture of K-2 well

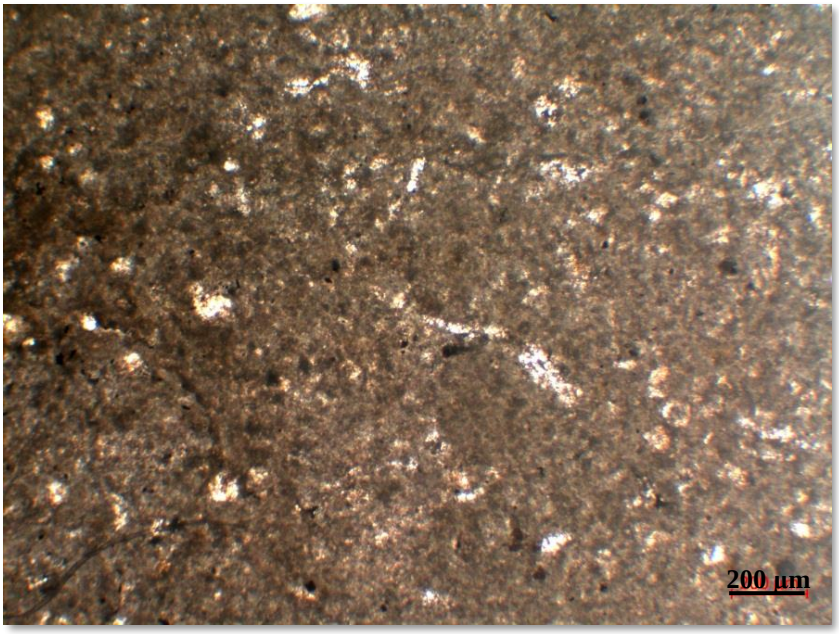


**Figure 7.** Plane polarized light microscopy photomicrograph of calcisphaerulid-bearing wackestone facies and microfractures and micro pores of K-2 well

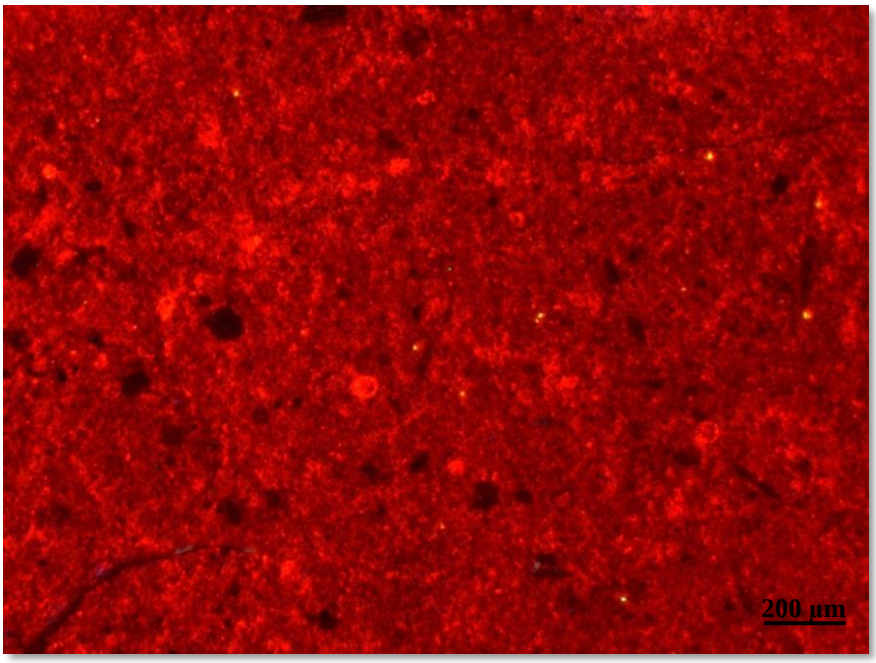


**Figure 8.** Light microscope based cathodoluminescence photomicrograph of calcisphaerulid-bearing wackestone facies and microfractures and micro pores of K-2 well

Light microscopy studies are also used for biostratigraphic analyses in order to detect the Cenomanian-Turonian Boundary Event. Benthic and planktonic foraminifer biostratigraphy studies are conducted on the same thin sections used for detailed microfacies descriptions.

All petrographical methods including reflected light, transmitted light microscopes, light microscope based cathodoluminescence and scanning electron microscope are completed in R&D Center of TPAO.

### 1.3.2 Principle Core Plug Analyses (Porosity and Permeability Measurements)

Since one of the main purposes of the study is to have a conclusion about reservoir parameters (basically porosity and permeability) and reservoir quality of Mardin Group Formations in terms of petroleum exploration, the reasons of porosity loss and gain are revealed. Where core samples are available and core plugs are taken, porosity and permeability measurements are completed by using helium method.

Porosity is calculated quantitatively by using core plug analysis and can be estimated by using petrographical methods qualitatively. Depositional (primary) and diagenetic (secondary) mechanisms which affect the porosity evolution are studied using petrographical methods including light microscopy, scanning electron microscopy, EDS and X-ray mapping and light microscopy based cathodoluminescence. Light microscopy studies and porosity measurements show that depositional environments and depositional features have a significant impact on reservoir development. On the other hand, it can be obviously interpreted that dolomitization is one of the most effective mechanisms on porosity gain and loss among secondary processes (Amthor and Friedman, 1991) due to volume change during dolomitization (Weyl, 1960; Morrow, 1990; Lucia and Major, 1994). Hence, dolomite rock textures should be examined in terms of crystal size distribution and crystal boundary shape which have a direct relationship with burial history and thermal maturation of rock (Amthor and Friedman, 1991).

Porosity and permeability of the cores of the K-11, K-8 and K-9 wells are measured by applying principle core plug analyses. These analyses are conducted on 63 samples of the five cores of K-11 well, 9 samples of the two cores of K-8 well and 8 samples of the core of K-9 well and reservoir parameters are quantitatively obtained.

Porosity and grain density are calculated using Helium Porosimeter and Boyle's Law method. As a result of these measurements grain volume of core plugs are obtained and pore volume, porosity and grain density data are calculated.

Permeability measurements are completed by passing dry air from the core plugs which are inside the Hassler type triaxial cell under the 250 psig overburden pressure and calculated by using Darcy Law. Hence, in laboratory conditions, principle reservoir parameters including porosity, permeability and grain densities are calculated on core plugs and these values are used to make interpretation about the effects of depositional environments and diagenesis and sequence stratigraphy at the end.

All of the porosity and permeability measurements are conducted in Research and Development Center of Turkish Petroleum Corporation.

### 1.3.3 Well Logs

Studying with cutting samples is not as easy as studying with core samples since resolution of cutting samples is 2 meters and it is hard to decide what is in situ and what is caving in 2 meters interval. Well logs are useful tool to study with cutting samples for the detection of lithology which is supposed to be in situ.

In this study, well logs are drawn using CycloLog software where LAS or ASCII data is available for the selected seven wells. CycloLog software is used for well log interpretation; it provides log based well correlations and helpful tool to visualize logs, making cross-plots, classifying colors according to changing lithology and facies.

For wells gamma ray (GR), sonic (DT), resistivity (LLD, LLS, MSFL), density (RHOB, NPHI), Photoelectric (PE) log data are used where they are available and well log data is obtained from Turkish Petroleum Company Exploration Department. Well log data obtained from the Exploration Department of Turkish Petroleum Company is in the format of ASCII and LAS and they are drawn using CycloLog software which is commonly used in the oil and gas industry by providing well log correlation and interpration.

Well logs are useful tools to make interpretation about lithology, sedimentology and reservoir properties of facies and formations while studying with cuttings and core samples. The most important point of studying with well logs is the combining of logs rather than using only one type of log in order to decide lithology, porosity or fluid type (whether there is oil, water or gas).

GR log is the measurement of the radioactivity of the rock, which is the directly proportional to the amount of the radioactive elements, potassium (K), uranium (U), and Thorium (Th) (Serra, 1983). Due to existence of K and Th in aluminosilicates (Ehrenberg and Savana, 2001), GR log tool can be considered as a direct function of the clay mineral content, grain size and depositional environment. Decrease in depositional energy can be resulted in increase in clay content which can be detected on GR log tool which provides link between GR log measurements and depositional environement (Emery and Myers, 1996). In the study of Ehrenberg and Svana (2001) spectral GR profiles are used to make interpretation of stratigraphic surfaces on carbonate platform. GR peaks show that K and Th are correlated and they a directly indicate siliciclastic (aluminosilicate) content, whereas U is uncorrelated with K, Th, and all other chemical components measured. Where the U becomes enriched, lithology of the interval can be interpreted as shale or argillaceous carbonate layers rather than carbonate-dominated layers. U is thus associated with aluminosilicate minerals and is not particularly concentrated in dolomite (Ehrenberg and Svånå, 2001). In this study mainly two types of GR logs are used which are gamma ray total (GRTO) and gamma ray potassium-thorium (GRKT). GRTO measures the amount of all

radioactive elements including K, T and U, while GRKT only measures the amount of K and T and it is free from the amount U. In order to observe the effect of radioactive elements on lithology directly, GRKT log can be preferred where it is available due to the fact that the amount of U can be affected by organic matter.

#### 1.3.3.1 Integrated Prediction Error Filter Analyses (INPEFA)

INPEFA log of gamma ray data is used to document facies association (Soua, 2012) and reveal trends and other patterns that are not generally apparent from the original log data and leads directly to a method for the objective subdivision of geological successions by the identification of key surfaces, somewhat analogous to the 'sequence' analysis of seismic profiles (Nio et. al., 2005). Also, study of Soleimani et. al. (2013) makes approach to sea level fluctuations using INPEFA logs. INPEFA logs are also generated by using CycloLog software.

In this study, INPEFA logs based on gamma ray logs are used to observe deepening and shoaling trends with the same working principle of gamma ray log. Since in the gamma ray log increasing values correspond to deepening (increasing rate of relative sea level) with the increase in clay and organic matter content, and shoaling (decreasing rate of relative sea level) with the increasing rate of carbonates, on the INPEFA log curve going through right shows deepening and vice versa (**Figure 9**). As mentioned above, turning points become more obvious on INPEFA logs (**Figure 9**) which make interpretation of relative sea level changes more clear and correlation with microfacies change easier. Scale of INPEFA logs and working interval is also important in order to observe turning points. In the wells optimum scale (1/500) and working intervals (mostly restricted interval of the Derdere Formation) are picked up (**Figure 10**). In terms of sequence stratigraphic framework according to deepening and shoaling upward sequences, transgressive systems tracts, highstand systems tracts and major key surfaces including sequence boundaries and maximum flooding surfaces are able to be defined. INPEFA log curves also provide correlation of two or more studied sections.

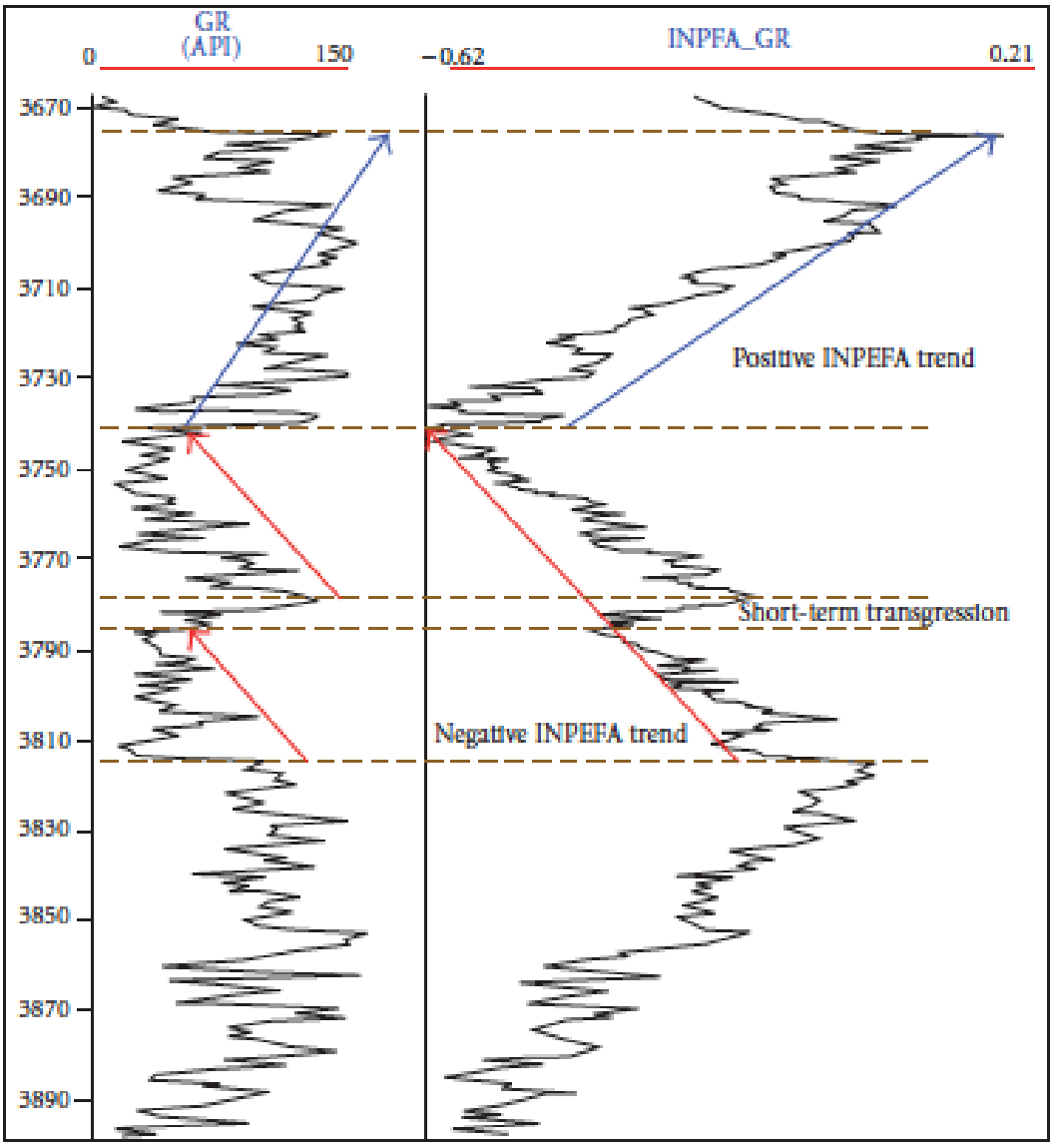


**Figure 9.** Presentation and correlation of the integrated predictive error filter (INPEFA) short-term curve (Nio et al. 2005; Soua, 2012) showing working principle depend on GR-log. Red arrows show negative INPEFA trend (decreasing upward values of GR and INPEFA-GR shoaling) while blue arrow shows positive INPEFA trend (increasing upward values of GR and INPEFA-GR and deepening). Trends are more visible on INPEFA-GR log compared to GR log.

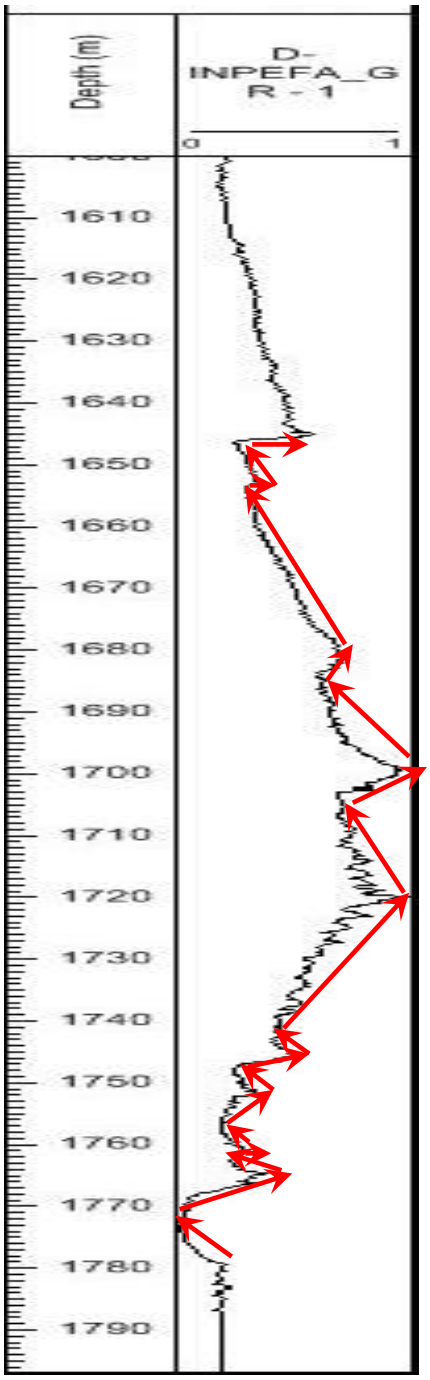


**Figure 10.** INPEFA log curves of K-11 pilot well on which going through lowest "zero" value shows shoaling trend and going through highest "one" value shows deepening trend. Red arrows show negative INPEFA trend which is shoaling and positive INPEFA trend which is deepening.

### 1.3.4 Stable Isotope Studies

Stable isotope studies are conducted for two wells including K-11 and K-2 wells. Totally 102 cutting and core samples are selected from these two wells in order to test whether they can be correlated with the sea level changes and sequences. 64 core and cutting samples of K-11 well and 38 cutting samples of K-2 well are studied isotopically. Stable isotope studies are conducted in the stable isotope laboratory of Rosenstiel School Department of Marine Geosciences in University of Miami by Peter K. Swart. Cutting and core samples of K-11 and K-2 wells were also analysed using a Kiel III device attached to a Finnigan Delta plus. Data produced by this device was corrected for isobaric interferences using the procedures defined by in the study of Craig (1957) modified for a triple collector mass spectrometer. Data used in this study is relative to Vienna Pee Dee Belemnite (V-PDB) using the conventional notation. Average standard deviation based on replicate analyses of internal standards is less than 0.1‰ (Swart et. al., 2009).

**Table 5.** Sample depths of stable isotope studies conducted on K-11 and K-2 wells

| Well Name | Depth | Well Name | Depth |
|---|---|---|---|
| K-11 | 1642 | K-2 | 2316 |
| K-11 | 1644 | K-2 | 2320 |
| K-11 | 1646 (a) | K-2 | 2324 |
| K-11 | 1646 (b) | K-2 | 2328 |
| K-11 | 1648 | K-2 | 2332 |
| K-11 | 1649,12 | K-2 | 2336 |
| K-11 | 1650,9 | K-2 | 2340 |
| K-11 | 1653,1 | K-2 | 2344 |
| K-11 | 1655,1 | K-2 | 2348 |
| K-11 | 1657,1 | K-2 | 2352 |
| K-11 | 1658,5 | K-2 | 2356 |
| K-11 | 1660 | K-2 | 2360 |
| K-11 | 1664 | K-2 | 2364 |
| K-11 | 1668 | K-2 | 2368 |
| K-11 | 1672 | K-2 | 2372 |
| K-11 | 1676 | K-2 | 2376 |
| K-11 | 1680 | K-2 | 2380 |
| K-11 | 1684 | K-2 | 2384 |
| K-11 | 1688 | K-2 | 2388 |
| K-11 | 1692 | K-2 | 2396 |

**Table 5** (continued). Sample depths of stable isotope studies conducted on K-11 and K-2 wells

| Well Name | Depth | Well Name | Depth |
|---|---|---|---|
| K-11 | 1694,02 | K-2 | 2400 |
| K-11 | 1695,79 | K-2 | 2404 |
| K-11 | 1696 | K-2 | 2408 |
| K-11 | 1696,75 | K-2 | 2412 |
| K-11 | 1698,4 | K-2 | 2416 |
| K-11 | 1700,56 | K-2 | 2420 |
| K-11 | 1702,55 | K-2 | 2424 |
| K-11 | 1704 | K-2 | 2428 |
| K-11 | 1708 | K-2 | 2436 |
| K-11 | 1712 | K-2 | 2440 |
| K-11 | 1716 | K-2 | 2444 |
| K-11 | 1719,06 | K-2 | 2448 |
| K-11 | 1721,05 | K-2 | 2452 |
| K-11 | 1723,05 | K-2 | 2456 |
| K-11 | 1725,25 | K-2 | 2460 |
| K-11 | 1726,85 | K-2 | 2464 |
| K-11 | 1728 | K-2 | 2468 |
| K-11 | 1730 | K-2 | 2472 |
| K-11 | 1730 | | |
| K-11 | 1734 | | |
| K-11 | 1738 | | |
| K-11 | 1742 | | |
| K-11 | 1746 | | |
| K-11 | 1750 | | |
| K-11 | 1754 | | |
| K-11 | 1758 | | |
| K-11 | 1762 | | |
| K-11 | 1764,16 | | |
| K-11 | 1766 | | |
| K-11 | 1768,13 | | |
| K-11 | 1770,16 | | |
| K-11 | 1772,07 | | |
| K-11 | 1774 | | |
| K-11 | 1774,1 | | |
| K-11 | 1776,12 | | |
| K-11 | 1778 | | |
| K-11 | 1778,04 | | |
| K-11 | 1780,01 | | |
| K-11 | 1782,11 | | |
| K-11 | 1784 | | |
| K-11 | 1788 | | |
| K-11 | 1792 | | |
| K-11 | 1796 | | |

## 1.4 PREVIOUS WORKS

Derdere Formation has been the subject of numerous studies since it is one of the most important lithostratigraphic units in Souteastern Anatolia due to its source and reservoir rock properties in terms of petroleum exploration perspective. There are several outcrops of the Derdere Formation and petroleum wells drilled through the Derdere Formation are abundant in different parts of the southeastern part of Turkey. These outcrop and well studies provide pronounced data for the Derdere Formation, hence literature is rich in academic papers and non-academic reports regarding the lithostratigraphy, sedimentology, reservoir quality, geochemistry and tectonic setting of the Derdere Formation (Sungurlu, 1974; Perinçek, 1980; Keskin and Can, 1986; Altıner, 1989; Yılmaz, 1993; Cater and Gillcrist, 1994; Yılmaz and Duran, 1997; Demirel and Güneri, 2000; Robertson et al., 2016; Özkan and Altıner, 2019). On the other hand, studies related with the sequence stratigraphy of Mardin Group Carbonates and eustatic control on the deposition of Mardin Group Carbonates are limited (Tardu, 1991; Cater and Gillcrist, 1994; Mülayim, 2013; Mülayim et al., 2016; Mülayim et. al. 2019; Özkan and Altıner, 2019; Mülayim, 2020). In the previous studies the age of the Derdere Formation is defined as Cenomanian to Turonian; however in the study of Özkan and Altiner (2019), the age of Derdere Formation is reported as Albian-Cenomanian-Turonian from Derik section, Mardin. During the deposition of the Sabunsuyu Formation (early Albian-Aptian) neritic depositional environmental conditions are dominant while during the deposition of the Derdere Formation (late Albian-early Turonian) both neritic and pelagic environmental conditions are observed due to the increasing rates of relative sea level. Since similar depositional environments of the Derdere Formation and Sabunsuyu Formation will cause some problems to differentiate them lithologically, the deposition of the Derdere Formation varies from neritic to pelagic environmental conditions while the Sabunsuyu Formation is considered to be deposited in more neritic environment in the study of Özkan and Altiner (2019).

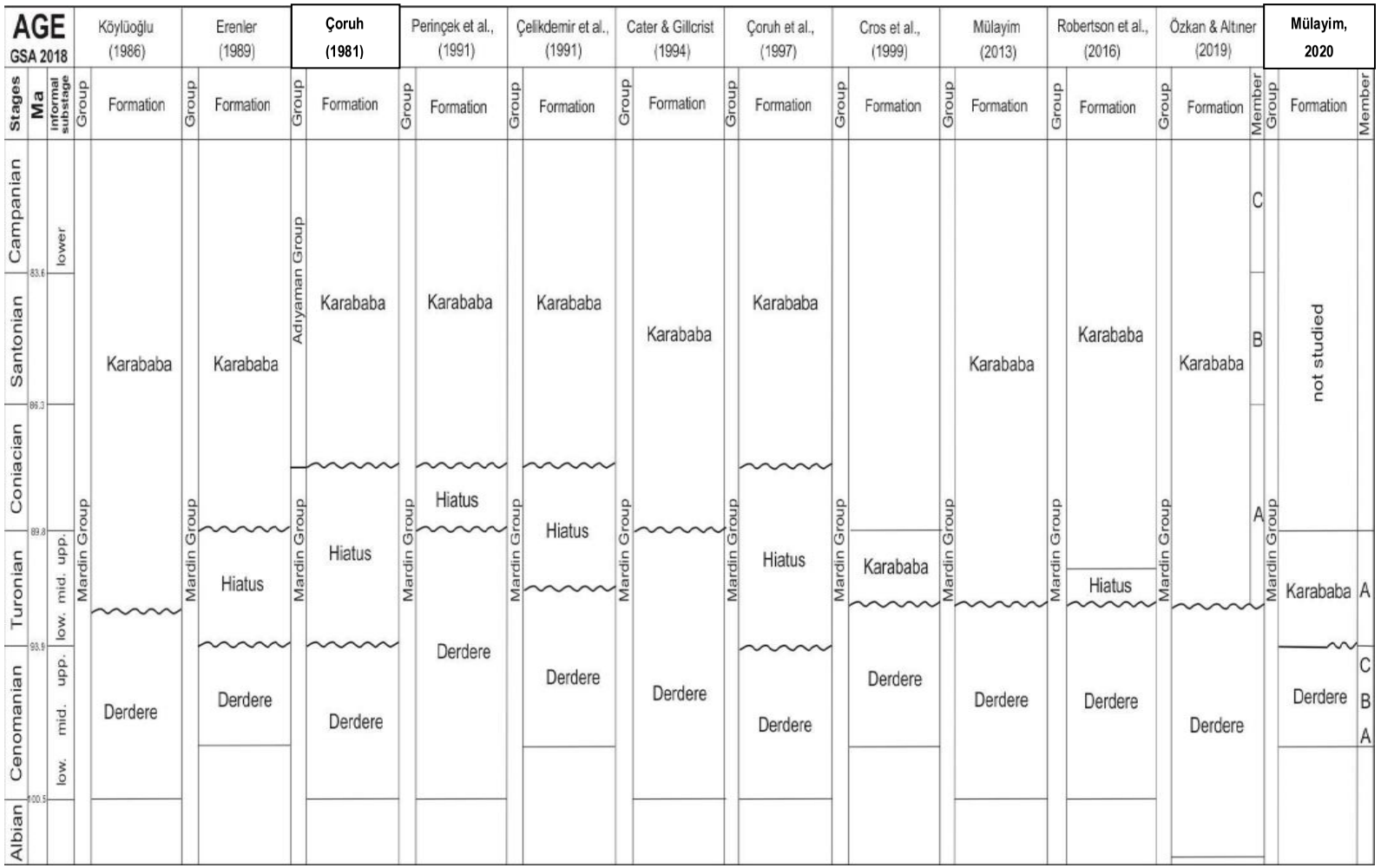


**Figure 11.** Age correlation chart of Albian to Campanian formations from previous studies (modified after Mülayim, (2020))

At the end of 1960s, one of the most known petroleum companies Exxon Production and Research Company introduced Sequence Stratigraphy concept while working on seismic sections as an alternative to lithostratigraphy (Posamentier and Wiemer, 1993) and then applications of sequence stratigraphy become widespread all over the world (Posamentier et. al., 1992; Posamentier and Weimer, 1993; Williams et. al., 1998). In sequence stratigraphic framework, shallow marine successions are commonly organized as upward-coarsening (upward-shoaling) units. Genetic stratigraphic sequences are bounded by periods of widespread basin margin flooding and record a significant episode of basin filling according to the definition of Galloway (1989). Within the sequence, parasequences may be bounded either above or below by sequence boundaries. The marine flooding is the surface between younger and older strata, which is associated with increase in water depth and it has also correlative surface in the coastal plain/shelf (Emery and Myers, 1996). In the study of Catuneanu (2002) sequence stratigraphic models based on a curve of base-level fluctuations affecting the accommodation space at the shoreline are stated. The balance between sedimentation rate and base-level fluctuations causes the transgressive and regressive shifts of the shoreline and timing of the formation of systems tracts and sequence stratigraphic surfaces (Catuneanu, 2002). The model created for the Derdere Formation depends on the principle of this sequence stratigraphy model of Catuneanu (2002).

In the previous studies, deposition of the Mardin Group Carbonates is evaluated regarding sequence stratigraphy principles (Tardu, 1991; Mülayim, 2013; Mülayim et. al., 2016). In the study of Mülayim et. al. (2016; Mülayim, 2020), facies descriptions, environmental analyses and definitions of sequence boundaries and systems tracts are completed for the productive levels of the Mardin Group Carbonates, which are oriented to Karababa and Derdere formations in Çemberlitaş Production Area. The conclusive points of their study is (1) depositional environments of the Derdere Formation and the Karababa Formation which are defined as lagoonal to shelf and deep to shallow marine intrashelf basin, respectively and (2) two third order sequence boundaries which correspond to late

Turonian and early Campanian in age and (3) transgressive and highstand systems tracts (Mulayim et. al., 2016). They concluded that the differences are mainly caused by the local variations in relative sea level and local tectonic events that have a pronounced influence on deposition. In the study of Mülayim et. al. (2020), three depositional sequences are defined in the interval of Cenomanian to Turonian including both Derdere and Karababa formations in the Sabunsuyu section and they are compared with the global chart of Haq (2014) and other carbonate platforms from Jordan, northern Sinai and Gulf of Suez. It is also stated that the deposition of Derdere and Karababa formations is under the control of global sea level change (Mülayim et. al., 2020; Mülayim, 2020).

There are numerous sequence stratigraphic studies in the world regarding the same time interval of the deposition of Derdere Formation (Albian-Cenomanian-Turonian). In the study of van Buchem et. al. (1996), a high resolution sequence stratigraphic study is conducted for Cenomanian to Turonian deposits of the Adam Foothills of Northern Oman. Similarly sequence stratigraphy studies of the Sarvak Formation, Iran located at the eastern side of the Arabian plate and by the side of Neo-Tethys ocean margin are presented in the study of Razin et. al. (2010).

Sequence stratigraphic model suggested for Oman (van Buchem et. al., 1996) and the model of Sarvak Formation (Razin et. al., 2010) have lots of similaries. The main difference is the significant siliciclastic influx in the Oman sequence during the third order transgression which is related with being close to the exposed Arabian Shield in Saudi Arabia (Razin et. al., 2010). Oman sequence also differs from the succession of the Derdere Formation in the aspect of siliciclastic influx.

In west-central Jordan the upper Albian to Turonian platform deposits are studied and stated in the paper of Schulze et. al. (2005). They state that during Cenomanian times, rudist-bearing packstones are deposited in the higher energy shallow subtidal zone and fossiliferous wackestones and packstones are typical of an open shallow subtidal environment. During Turonian time, oolithic or bioclastic grainstones and packstones and dolomitic wackestones with dolomitic wackestones in peritidal environments are observed in high energy environments. Although there are some

similarities between the depositional features and sequences of the Derdere Formation and the sequences defined in Jordan, such as, the grainstone/packstone facies described in the high energy environments of the Turonian time, facies deposited during the Cenomanian time are deeper compared to facies deposited in Cenomanian of Jordan.

Study of Wilmsen (2003) reveals the sequence stratigraphic systems tracts of northern Germany including transgressive systems tracts, maximum flooding events, highstand systems tracts. Maximum flooding events are described as blooms of specialist taxa adapted to maximum flooding conditions (low-energy and oligotrophy with low amount of food). Hence, microfacies including calcareous nonnoplankton, planktonic foraminifera and radiolaria can be considered to be indicating the maximum flooding zone. There are carbonate aggregates identified in some samples which are thought to be rich in coccolithoproids and coccoliths. Highstand bioevents are observed where shell concentrations are increasing in relatively coarse grained limestone with decreasing accommodation space. Therefore, microfacies where large shell fragments are observed between the pelagic microfacies can be interpreted as the deposits of highstand systems tracts. On the other hand, calcisphaerulid rich microfacies, where the accommodation space is largely increasing, can be considered as a kind of transgressive systems tract deposits.

Global cycle chart and 3$^{rd}$ order events recorded on the eustatic sea level curve of Haq (2014) is depend mainly on globally provided sequence stratigraphic data (Sarg, 1988; VanWagoner et al., 1988; Handford and Loucks, 1993) and oxygen isotope data where it is available. Oxygen isotope data of carbonates are not reliable for quantitative amplitude measuremets of the sea level changes; however they are considered as helpful to make an approach to qualitative relative magnitude and the timing of sea level fall corresponds to sequence boundaries. Additionaly, lithological and paleontological data are used to make interpretations of system tracks, depositional surfaces and sequence boundaries in outcrop sections (Haq, 2014). Long term and short term sea-level curves of Haq (2014) is correlated

with INPEFA logs of the studied wells and sequence boundaries defined in the Haq (2014) correspond to the sequence boundaries defined in C-T interval of the Derdere Formation.

## 1.5 REGIONAL GEOLOGIC SETTING

Turkey is composed of several continental fragments (**Figure 12**) and they have become single landmass during late Tertiary (Okay, 2008; Moix et. al., 2008). Although these small continental fragments are known, the exact boundaries between these fragments are disputatious. The boundary between Anatolide-Tauride Platform and the Arabian Plate is an ophiolitic imbricate zone which characterizes the suture zone formed due to the collision of the Anatolide-Tauride Platform and Arabian Plate (Şengör and Yılmaz, 1981; Yılmaz, 1993). Oceans, whose remainings are dispersed throughout the Anatolia as ophiolites and accretionary prisms, separate the continental fragments named as terranes (Okay, 2008).

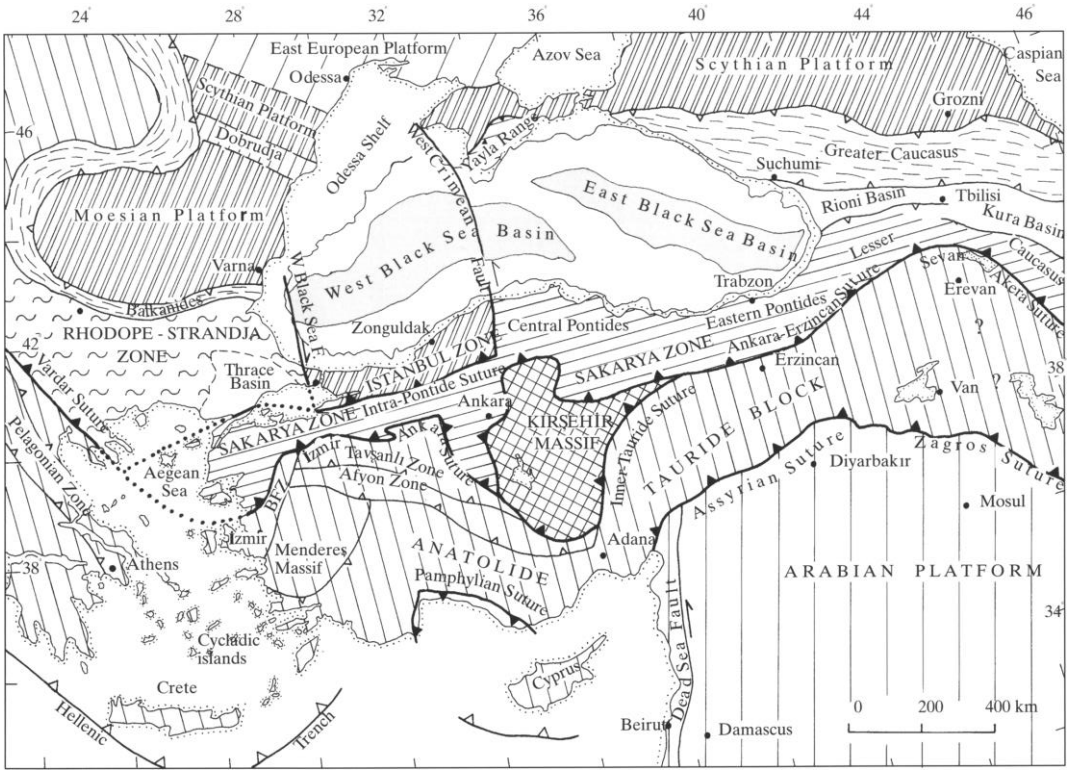


**Figure 12.** Tectonic map showing the major sutures and continental blocks. Sutures are shown by heavy lines with the polarity of former subduction zones indicated by filled triangles. Heavy lines with open triangles represent active subduction zones. The Late Cretaceous oceanic crust in the Black Sea is shown by grey tones. Small open triangles indicate the vergence of the major fold and thrust belts. BFZ denotes the Bornova Flysch Zone (Okay and Tüysüz (1999))

Southeast Turkey, which is the northernmost extension of the Arabian Platform, is separated from Anatolia by Taurus Mountain Range, which is the extension of Zagros Mountains (**Figure 13**) (Okay, 2008). Anatolides-Taurides shows similar stratigrapy with Southeast Anatolia regarding clastic-carbonate dominated Paleozoic and carbonate dominated Mesozoic succession and in Oligo-Miocene, final amalgamation of terranes is observed in Anatolia (Okay, 2008).

Zagros Mountains, which are formed as a result of the collision of Arabian and Eurasia, and part of Himalayan orogeny system, are the one of the largest mountain zone (Mouthereau et. al., 2012). The geodynamic evolution around the Zagros Region during the Mesosoic time is mainly explained by the subduction of the Neo-Tethys Ocean (Mouthereau et. al., 2012). A foreland basin that is formed

parallel to the mountain zone is located at the southern part of the Taurus-Zagros orogeny belt (Rigo de Righi and Cortesini, 1964). Anatolian and Arabian plates are separated by the southern branch of the Neo-Tethys ocean during the Early Cretaceous time (Şengör and Yılmaz, 1981; Fontaine et. al., 1989; Okay, 2008) (**Figure 13**) and the stratigraphy of the foreland basin is shaped under the influence of the closure of the Southern Branch of Neo-Tethys ocean and the collision of the Arabian Plate with Taurus Mountains (Mouthereau et. al., 2012; Robertson et. al., 2016).

During the Cretaceous time (Aptian-Campanian) a large carbonate platform was formed and on this platform which constitutes the northern edge of Arabian Plate, Mardin Group Carbonates (Areban Formation, Sabunsuyu Formation, Derdere Formation, Karababa Formation) are deposited (Sungurlu, 1974; Perincek, 1979; Cater and Gillcrist, 1994; Okay, 2008). Foreland basins are considered as where sediments are deposited, are hosts for evidences of local and regional geological events (Martin, 2001; Robertson et. al., 2016) and prospect areas for petroleum exploration (Bordenave and Hegre, 2010; Mouthereau et. al., 2012). Studied wells are situated in this foreland area in order to observe the complete succession of the Derdere Formation instead of seeing the Derdere Formation as segmented by thrust faults.

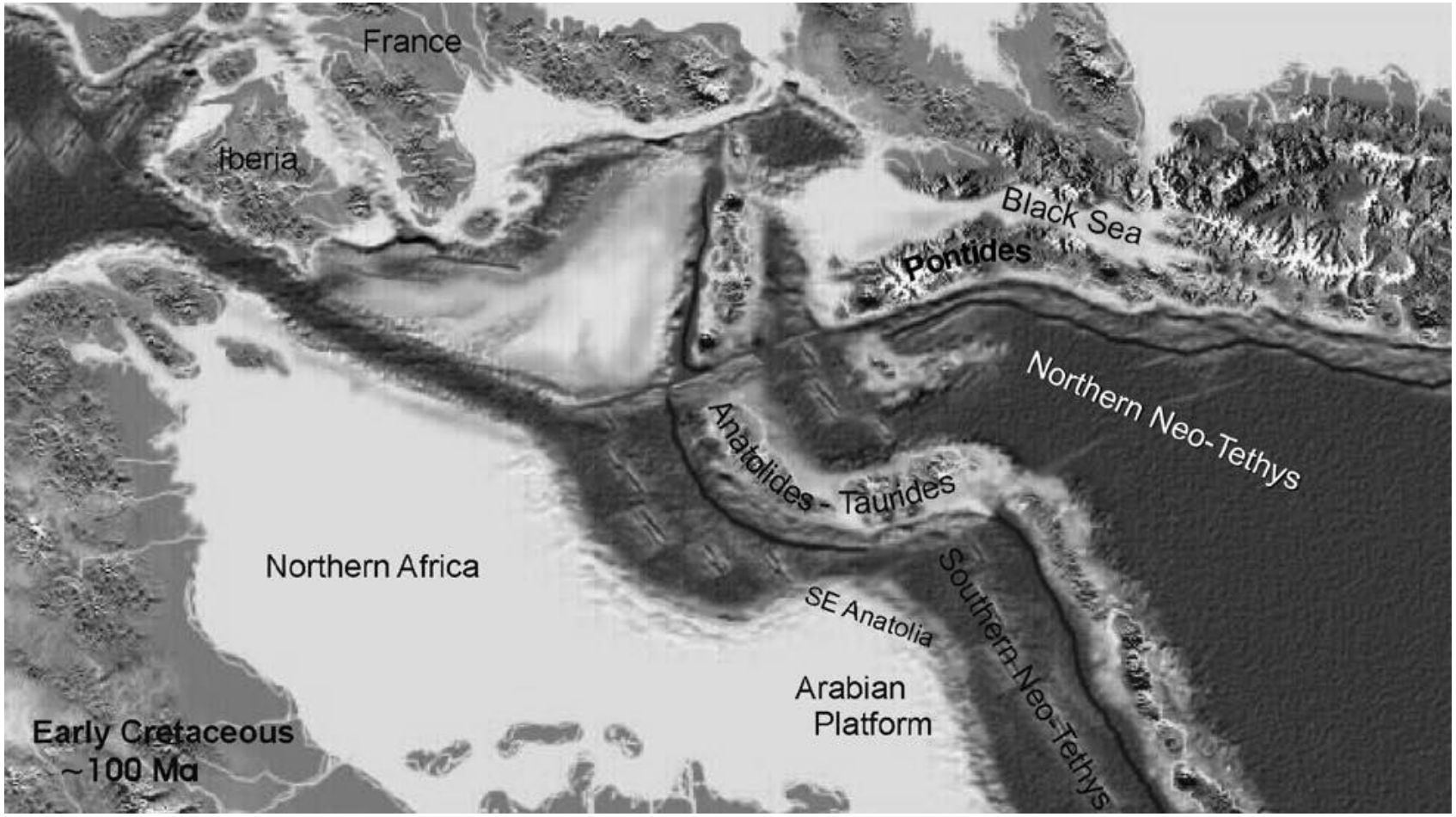


**Figure 13.** Mediterranean paleogeography during the Early Cretaceous (110 Ma) Modified after http://jan.ucc.nau.edu/~rcb7/globaltext.html. Note the absence of Anatolia as a single landmass (Okay, 2008)

There are three major structural units in southeast Turkey; east-west trending tectonic zones in the region from south to north of the Arabian Platform, one is the zone of imbrication, which is a transition between the Arabian Platform and the others are lower and upper nappes (Rigo de Righi and Cortesini, 1964; Ketin, 1966; Yilmaz, 1993). These major structural units are separated from one another by major thrusts (**Figure 14**).

There is thick sedimentary succession deposited from the early Cambrian to middle Miocene and ophiolite nappes which were trusted during the Late Cretaceous on the Arabian Platform. Mainly four units are idenitified on Arabian Platform which are from bottom to top, the lower autochthonous succession, the lower allochthonous units, the upper autochthonous succession and the upper allochtonous units (Yılmaz, 1990; 1993) (**Figure 15**).

The lower autochthonous succession is composed of siliciclastic rocks including sandstone and shale, marl, siltstone and carbonate rocks including dolomite and limestone from Precambrian to upper Cretaceous time interval and it overlies Precambrian Basement rocks (**Figure 15**).

The lower allochthonous zone is composed of a series of stacked thrust nappes which are, from top to bottom the ophiolite nappe (Yılmaz, 1993), the Kocali Complex (Rigo de Righi and Cortesini, 1964) and the Karadut Complex (Sungurlu, 1974; Perincek, 1979). The Karadut Complex is derived from the erosion of ophiolite nappes and is mostly formed by clasts of igneous rocks. The lower part of the Karadut Complex, is the time equivalent of the Mardin Group, composed of hemipelagic limestone and calcareous turbidite deposits and laid down on the outer shelf and the continental slope (Şengör and Yılmaz, 1981; Fourcade et al., 1991; Tuncer, 2013). The Kocali Complex, which consists of sheared serpentinite, chert, shale and interlayered basaltic lavas which are originated from the Tethyan ocean floor (Şengör and Yılmaz, 1981), overlies the Karadut Complex with a thrust fault contact (Sungurlu, 1974).

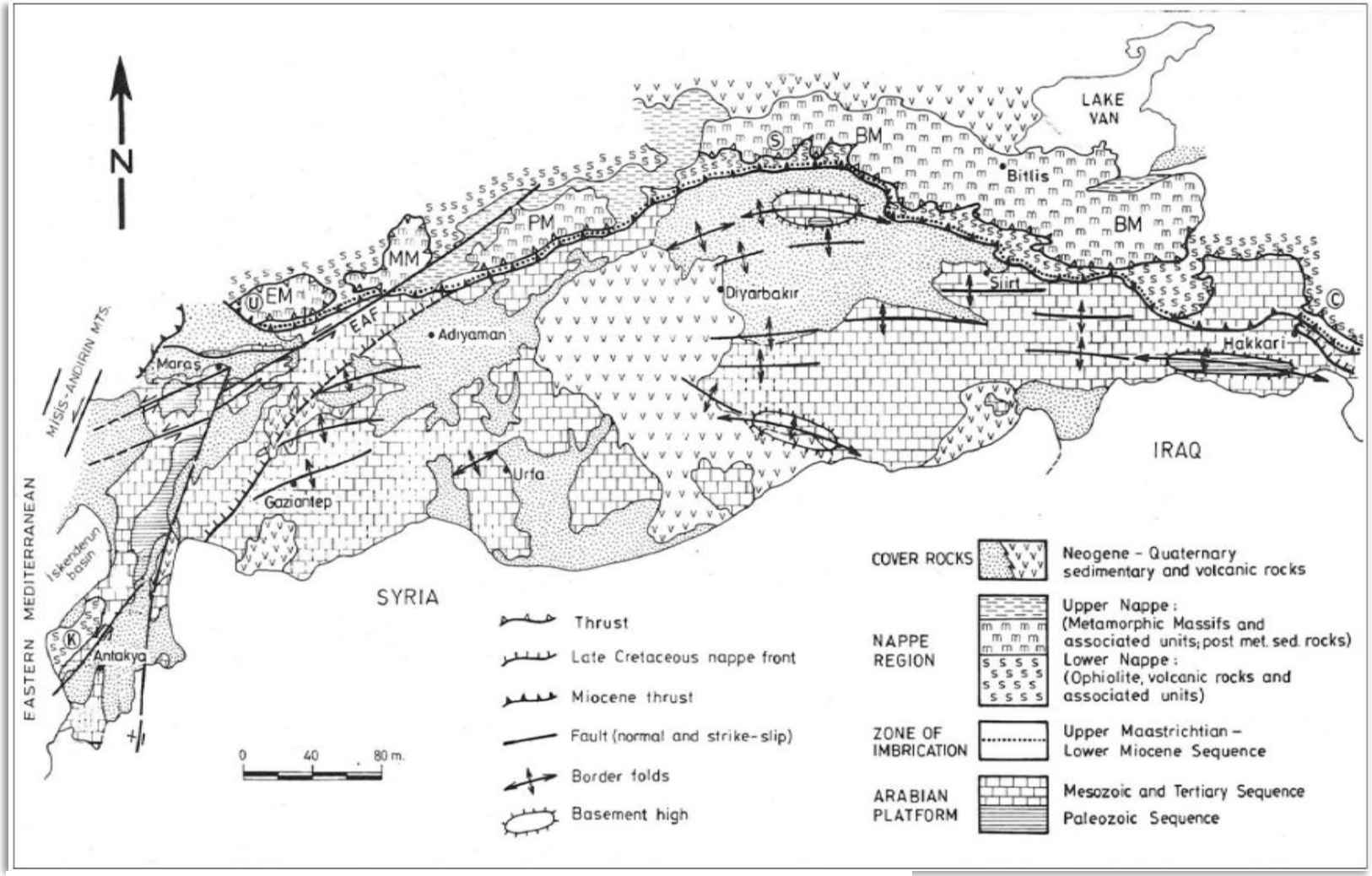


**Figure 14.** Geological map of Southeast Anatolia (Yılmaz, 1993)

In the upper autochthonous succession, during the Maastrichtian, marine carbonates were deposited without any interruption in the succession in the southern areas. The Terbüzek Formation, composed of basal sandstone and conglomerate, rests on the nappe units in the northern areas. The Besni Formation consisting of conformable thin, reefal limestone units conformably overlies the Terbüzek Formation and underlies the Germav Formation composed of thick shale-siltstone units deposited during the Late Maastrichtian to Paleocene time (Tuncer, 2013) (**Figure 15**).

The upper allochthonous units include the rock packages of the second nappe emplacement in the region during the Early Miocene time. There are two nappe zones including the lower nappe and the upper nappe corresponding to the Yüksekova Nappe and the Bitlis-Pötürge Massifs, respectively (Yalçın 1976; Yılmaz 1993; Okay, 2008).

As a result of this deformation, the present mountain ranges were formed and defined as the Zone of Imbrication and Nappe Zone are formed (Tuncer, 2013) (**Figure 15**). The Zone of Imbrication is an east-west trending zone and between the Arabian plate at the south and the nappe zone at the north (Yılmaz et. al., 1987; Yılmaz, 1990: Tuncer, 2013).

In the study of Yılmaz (1993), it is stated that the carbonate platform of Southeast Anatolian Orogenic Belt experienced rifting, normal faulting and volcanism during the Triassic period which corresponds to the early stages of continental breakup. The development of the carbonate platform, continental slope and abyssal plain occurred during the Jurassic and Early Cretaceous (**Figure 16**).

The estimated time of the movement of ophiolitic nappe towards the continental margin is Turonian to Santonian. Continental shelf extended to a continental slope and abyssal plain. On the abyssal plain foredeep and forebulge basins formed on the edge of the Arabian plate in front of the nappe. As a consequence of the subsidence of the foredeep basin, eroded material from the carbonate bank, slope and outer-shelf region were transported and deposited into the foredeep. The shelf area deepened northwards towards the southern branch of Neo-Tethys Ocean (Perinçek and Özkaya, 1981; Şengör and Yılmaz, 1981).

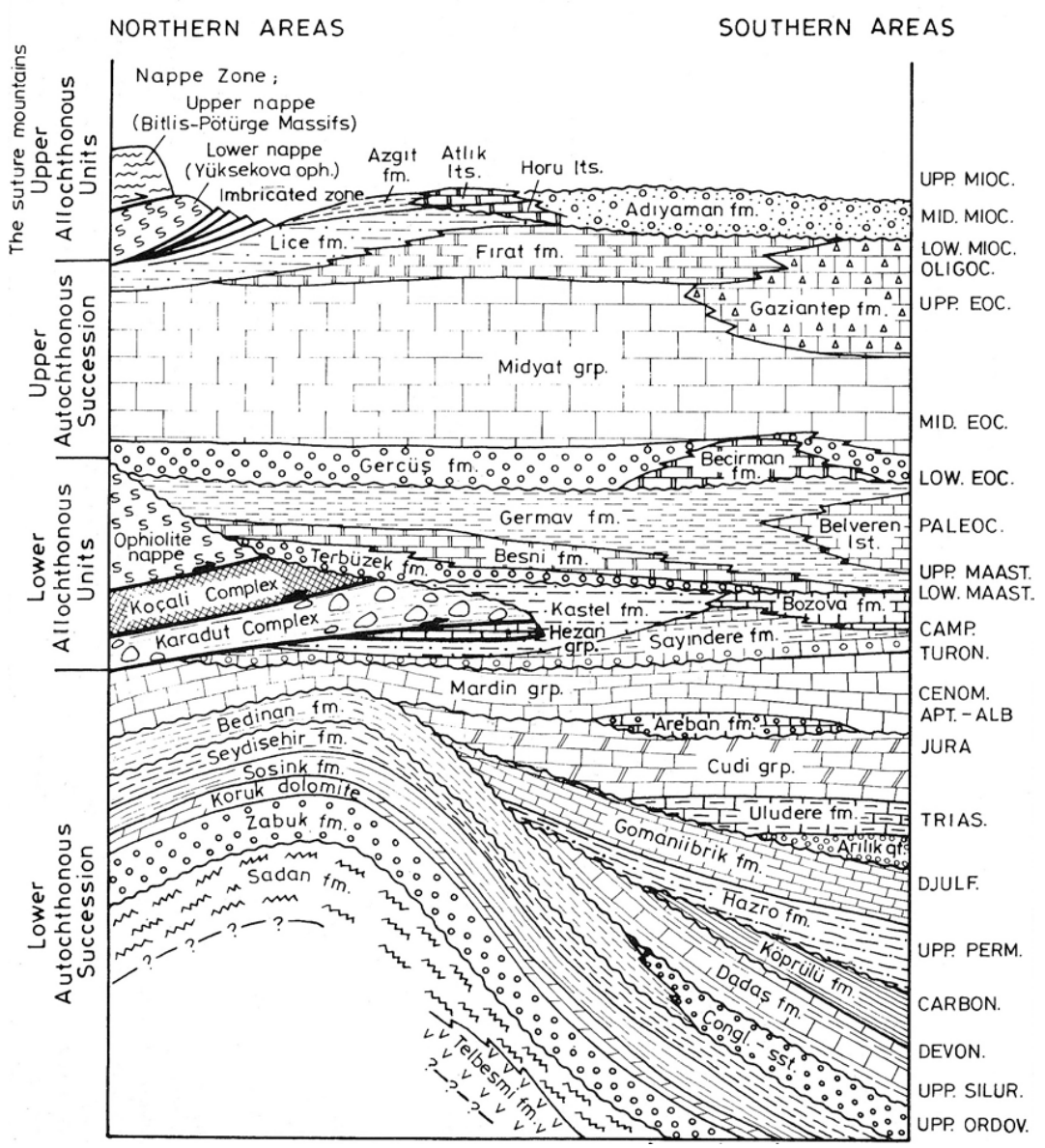


**Figure 15.** Stratigraphic section of the Arabian platform in southeast Anatolia (Yalçın 1976; Yılmaz 1993; Okay, 2008)

On the forebulge part, a regional unconformity formed due to the uplift and erosion. Due to emplacement of thrusted nappe pile on the uplifted and eroded edge of the platform, the margin was lowered beneath the sea level and a deep basin formed during the Campanian time. The thick nappe pile became a structural high and blocks derived from this high were deposited in the basin in front of the nappes as a debris flow (Righi and Cortesini, 1964) (**Figure 16**). These rock fragments derived from the nappes were deposited during the Late Maastrichtian to

Early Eocene and the red beds, which are believed to be the indicator of the regression. This has resulted in the formation of a sharp unconformable contact at the northern part of the basin and local sedimentary gaps in some parts of the basin (Righi and Cortesini, 1964).

The development of the foreland area where the wells are chosen for this study is far away from the orogenic belt where epirogenic movements are effective (Righi and Cortesini, 1964). The foreland area evolved into the folded belt nearby the orogenic zone towards the north. The main structural features observed are large east to west trending elongate anticlines (Şengör and Yılmaz, 1981). East-west trending studied wells are approximately 200km away from the northern suture zone. The distance between easternmost and westernmost wells is approximately 100km in the study area.

The late Mesozoic and the late Tertiary tectonism are the most significant time intervals of the formation of the most of the structures in the Southeatern Turkey (Righi and Cortesini, 1964). During Late Miocene and Pliocene uplift and compressional orogeny caused to the regression of the sea and shaped the present structural framework of the Southeastern Turkey (Temple and Perry, 1962).

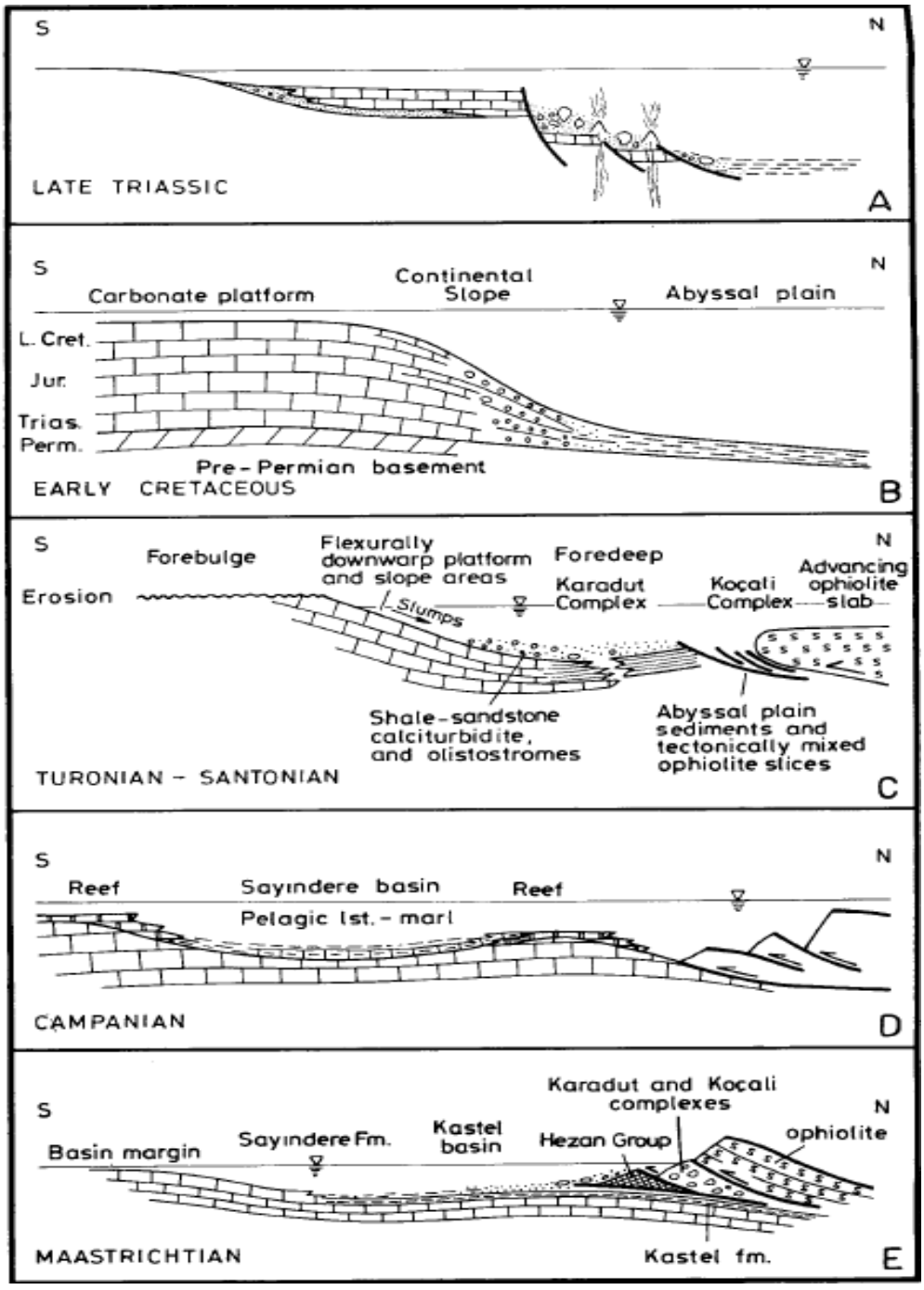


**Figure 16.** Plate-tectonic models for the Mesozoic evolution of southeast Anatolia (Yilmaz, 1993; Tuncer, 2013).

# CHAPTER 2

# STRATIGRAPHY

Southeastern Turkey has two major sedimentary cycles in the Paleozoic. The first sedimentary cyle is from Cambrian to Devonian age and the second is from Carboniferous to Permian. These cycles were deposited during the regional transgressions onto the Arabian platform (Temple and Perry, 1962). The outcrops of Cambro-Ordovician sediments are observed at around southwest of Mardin close to the Syrian Border. In the Paloezoic section, Silurian, Devonian and Lower Carboniferous sediments are absent in some parts of the basin due to later periods of uplift and erosion (Temple and Perry, 1962). Southeastern Turkey has also two main cycles during the Mesozoic time and there is a regional unconformity at the base of Cretaceous (Righi and Cortesini, 1964). The first cyle is composed of shallow marine to tidal flat carbonates which were deposited in the Triassic and Jurassic while the second cycle includes the Mardin Group Carbonates (Aptian-Santonian) and the formations of Campanian to Maastrichtian age. At the time of deposition of Mardin Group Carbonates including Aptian, Cenomanian and Turonian time intervals, shallow shelf conditions were dominant and neritic carbonate deposition throughout the basin is observed (Temple and Perry, 1962).

## 2.1 LITHOSTRATIGRAPHY

At the base of the stratigraphic column there are Precambrian and Lower Paleozoic shallow-marine sedimentary rocks in the Adiyaman Region and this succession was deformed during Late Paleozoic orogenesis (Demirel and Güneri, 2000). The main difference between the Adiyaman Region and nearby Diyarbakir and Gaziantep Regions is non-deposition at the end of the Ordovician and the beginning of the Aptian when the Adiyaman Region was emergent (Rigo de Righi and Cortesini, 1964; Sungurlu, 1974; Demirel and Guneri, 2000). Paleozoic-Lower Mesozoic

basement is unconformably underlying Aptian-Campanian Mardin Group Carbonates, which is deposited on the southern passive margin of the Neo-Tethys. During Cretaceous time, tectonic events, which are related by plate tectonics at northern part of Southeast Anatolia, caused lateral variations on the facies deposited on Arabian Continental Crust (Koyluoglu, 1986).

Mardin Group deposition starts with thin siliciclastic succession filling topographic lows and unconformably overlies Paleozoic rocks. Subdivisions of Mardin Group Formations depending on biostratigraphical studies were described in the studies of Cordey (1971), Perincek (1979), Celikdemir et. al. (1991), and Koyluoglu (1986). In Southeast Anatolia, 3 Aptian formations, which are the Areban Formation, the Latdagi Formation and the Sabunsuyu Formation, are detected (Koyluoglu, 1986). After Barremian non-deposition detected in the study of Farinacci and Koyluoglu (1982) in the Southeast Anatolian Region, deposition of the Mardin Group Carbonates started with transgression (**Figure 17** and **Figure 18**). Areban Formation is known as the base of the group and due to transgressive deposition of the formation, the Areban Formation becomes younger from west to east (time-transgressive) (Koyluoglu, 1986). At the southern part of Amanos, age of the formation is Barremian, while at Ceylanpinari Region it is Aptian to Albian and Lower Cenomanian at Hakkari Region. Latdagi Formation is only detected at around Hakkari Region and characteristic benthic fossil groups defined in the formation are more or less the same of the fossil groups detected in Sabunsuyu and Derdere formations (Koyluoglu, 1986).

During the Albian time, depositional environments of the formations and facies defined in the formations are similar to Aptian time.

After the Aptian transgression, until the late Cenomanian time, shallow marine conditions are dominant in Southeast Anatolia. Then platform submerged and the relative sea level started to rise and the planktonic foraminifers spread out to the platform (Koyluoglu, 1986).

During the Campanian time South Anatolia experiences regional marine transgression and rapidly subsiding foredeep Kastel Basin is developed at the

southern part of Campanian to Early Maastrichtian thrust belt (Ala and Moss, 1979; Sungurlu, 1974; Yilmaz, 1993). As a consequence of this rapid regional marine transgression, marl and shale is deposited over the Maastrichtian neritic limestone and marly limestone in the eastern and southern parts of the basin with the increasing accommodation space.

At the northern passive margin of the Arabian Plate, Southeastern Anatolia become intrashelf basin during the Aptian-Lower Maastrichtian time (Horstink, 1971) and reefoidal buildups and shelfal limestones are covered by shale and marls. During the Late Maastrichtian to the Late Eocene, restricted shallow marine environmental conditions are dominant.

In Southeastern Turkey, marl and shale deposition is continuous without any sedimentary gap at the at the K/T boundary during Tertiary time. One of the main sources of the Paleocene deposition is ophiolitic areas bounding the northern part of the basin (Temple and Perry, 1962). Due to regression started in Early Eocene time, local reefoidal carbonates alternates and/or covered with red beds (Righi and Cortesini, 1964) and due to regional transgression during Middle Eocene time which pursues regression, shallow marine carbonates are deposited throughout the whole basin all over Southeastern Turkey (Righi and Cortesini, 1964). The Oligocene evaporates and chalky marls cover the Eocene limestones and underlain Lower Miocene deposits which is the time of shallow marine transgression (Temple and Perry, 1962; Righi and Cortesini, 1964).

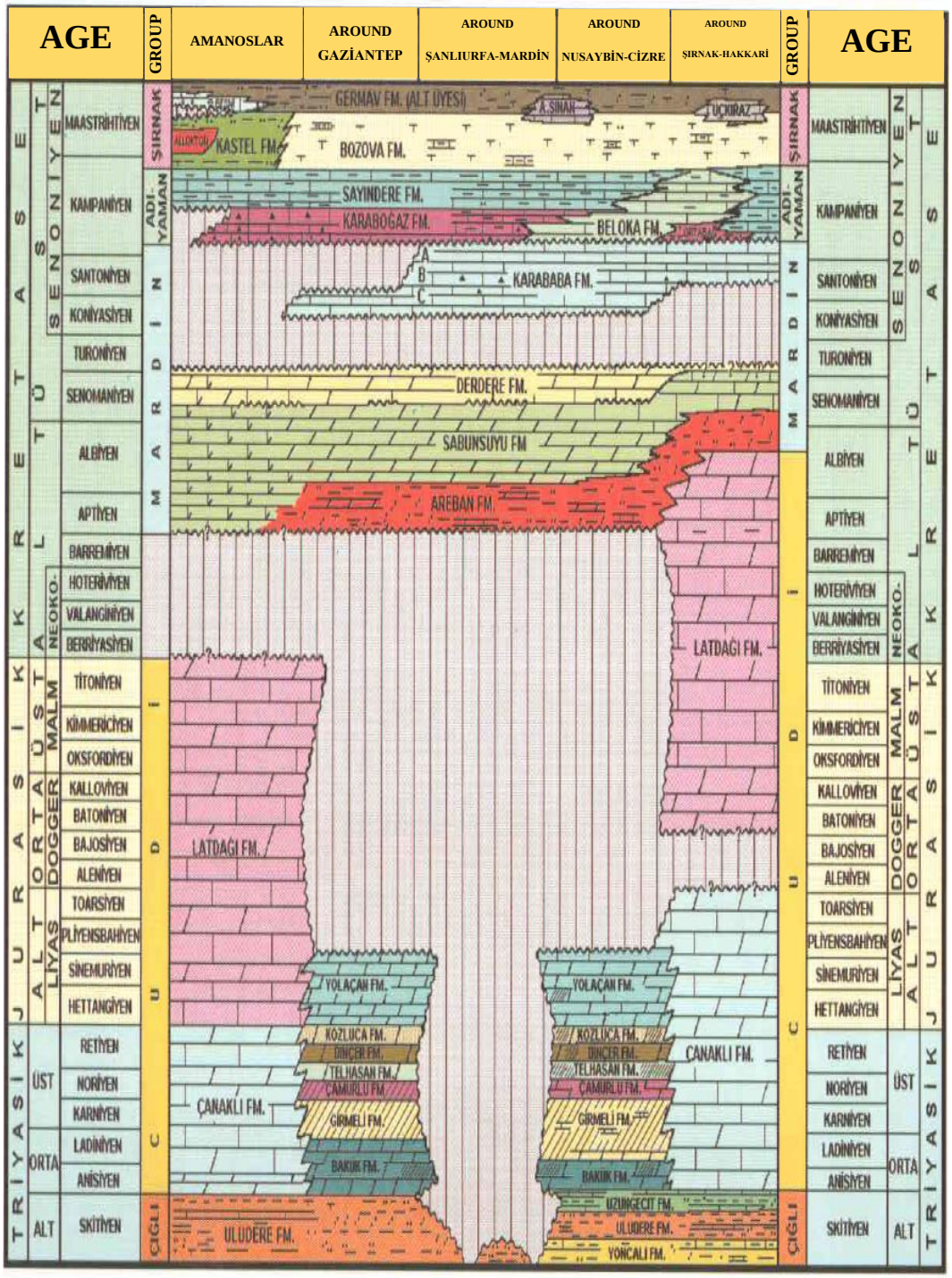


**Figure 17.** Stratigraphy and correlation of Mesosoic aged autochthonous units at the southern part of Southeastern Turkey (modified after Yılmaz and Duran, 1997)

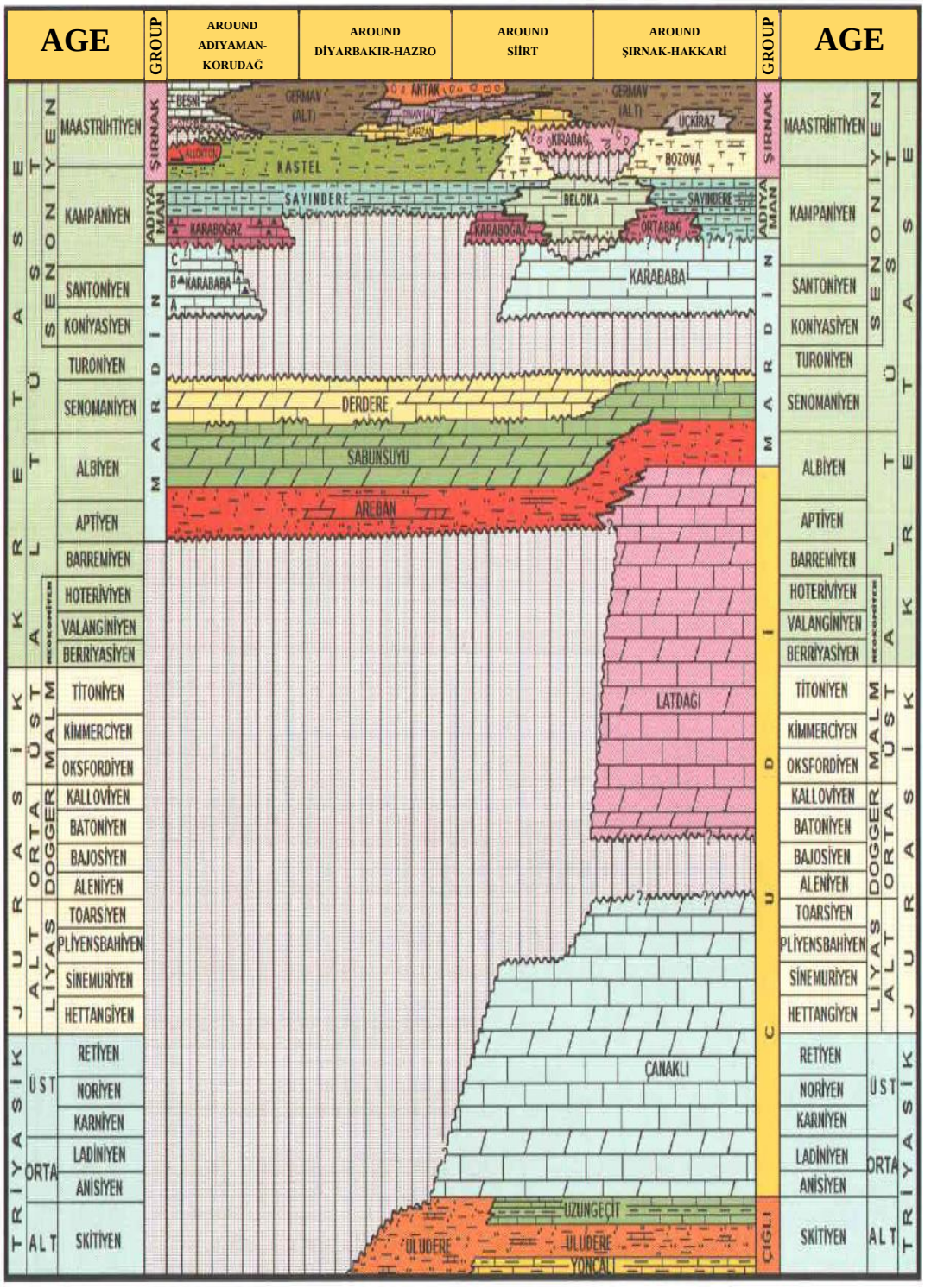


**Figure 18.** Stratigraphy and correlation of Mesosoic aged autochthonous units at the northern part of Southeastern Turkey (modified after Yılmaz and Duran, 1997)

### 2.1.1 Stratigraphy of the Mardin Group in Southeastern Turkey

Mardin Group name is firstly used by Tuna (1973) and Sungurlu (1973) for the Aptian-Turonian carbonates (**Figure 19**). According to these authors, from bottom to top, the Mardin Group is composed of Areban Formation, Sabunsuyu Formation, Derdere Formation and Karababa Formation. At the northern passive margin of the Arabian Plate, the depositional environment of the Mardin Group is defined as shelf and intrashelf basins (Horstink, 1971; Celikdemir et al., 1991; Demirel and Güneri, 2000).

The Mardin Group with these formations rests unconformably on either Precambrian or Paleozoic to Lower Mesozoic rocks in southeast Anatolia (Çelikdemir and Dülger, 1990; Yılmaz and Duran, 1997).

Mardin Group Carbonates are mainly composed of limestone, calcareous dolomite, dolomitic limestone and dolomite in the Southeast Anatolian Region (**Figure 19**).

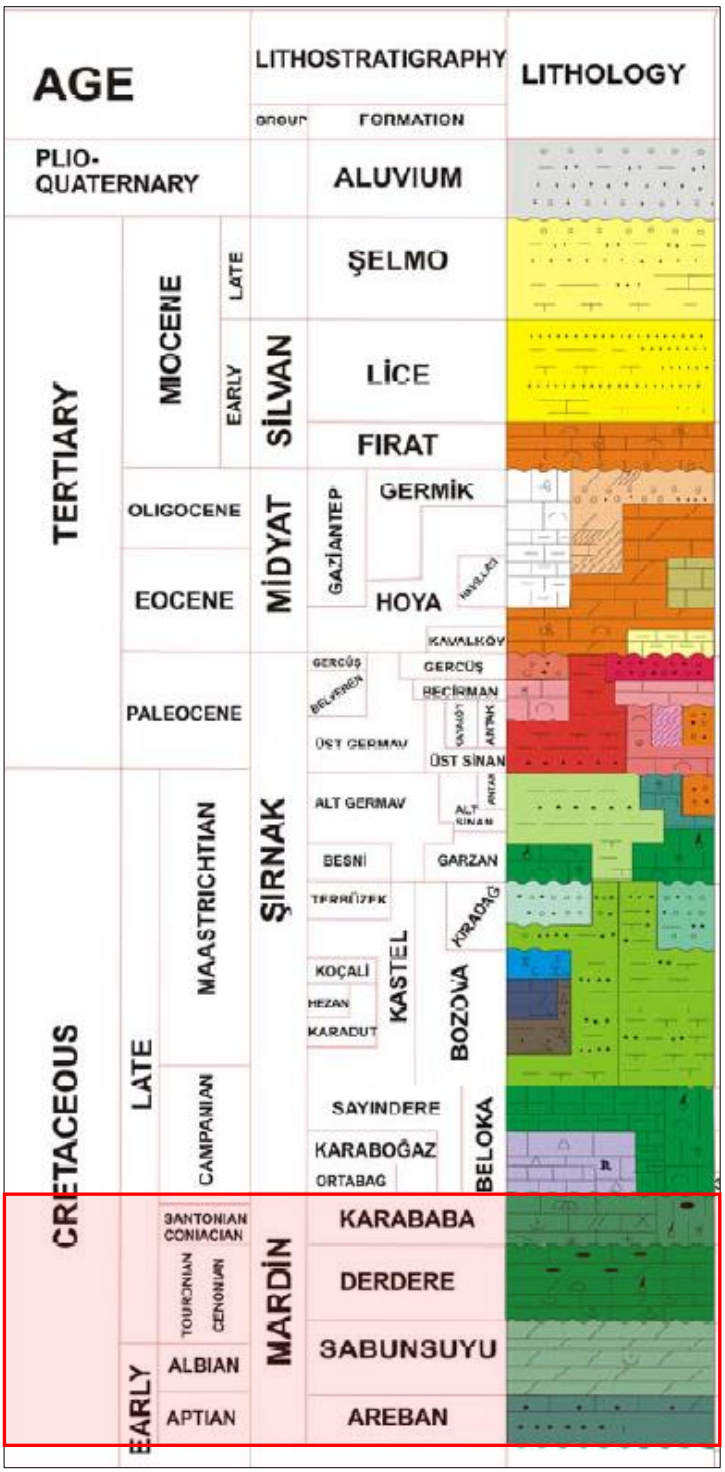


**Figure 19.** Generalized stratigraphic columnar section of autochthonous lithostratigraphic units of Southeast Anatolian Region (Güven et.al., 1991) Red triangle shows the stratigraphic position of Mardin Group Carbonates.

Mardin Group Carbonates are penetrated in most of the wells drilled in Southeastern Turkey and the thickness of Mardin Group is variable. The thickest carbonate succession is around 700 meters in the wells drilled at the east of Gaziantep. At the northern trend of Adıyaman, Diyarbakır and Batman, the thickness of the Mardin Group is 150-450 meters, at the southern trend of these, the thickness becomes 400-700 meters, at the eastern part of Şırnak and Cizre, thickness of the succession decreases to 100-200 meters (Çelikdemir and Dülger, 1990; Araç and Yılmaz, 1991; Duran et. al., 1996, Yılmaz and Duran, 1997).The Mardin Group has a contact with the Sayındere Formation at the southwestern part of Dicle District of Diyarbakır and at the core of Dicle High, northern slope of Cudi Mountain of Şırnak, western part of Hizil Stream, southwest and southeast of Beytüşşebap District (Yılmaz and Duran, 1997). Sayındere Formation is deposited in deep marine environmental conditions and overlain by the Karaboğaz Formation (Perinçek et. al., 1991). Regional marine transgression has a significant impact on the depositional trends of Southeastern of Turkey during Campanian time interval. The Karaboğaz Formation which is mainly composed of organic rich pelagic carbonates with the contributions of phosphate and glauconite nodules is the representative of anoxic deep marine environmental conditions similar to the Sayındere Formation (Demirel and Güneri, 2000).

#### 2.1.1.1 Areban Formation

Bedinan Formation is covered by transgressive siliciclastic sediments of the Areban Formation at its neostratotype. It is conformable and transitional with the Sabunsuyu Formation at the top at the neostratotype. The Areban Formation is also conformable and transitional with the Sabunsuyu Formation at the top and unconformable with the Paleozoic aged older units and the Cudi Formation at the other parts of the basin (Yılmaz and Duran, 1997).

The age of the Areban Formation is defined as Aptian-Albian (Sinanoglu and Erkmen, 1980; Erenler, 1989) and the depositional environment is determined as shoreline to shallow marine (Yılmaz and Duran, 1997).

The Areban Formation has different lithologies at different parts of the basin. Areban Formation is mainly composed of limestones, dolomites, interbedded shales, and sandstones and deposited in a restricted lagoonal to tidal-flat setting. Generally, in the Southeastern Turkey, brownish colored, rigid, medium to thick bedded, cross-laminated sandstone with carbonate cement and iron content and yellow, brown colored, compact, rigid, thin bedded limestone without any fossil content and rarely with sand contribution (Perinçek, 1980; Yılmaz and Duran, 1997). At around Derik area in Mardin, there are red-colored, medium grained conglomerates at the base of the formation, and continues with light yellow and bordo colored sandstone with conglomerates. The upper parts of the sequence are composed of thick bedded, yellow colored, very rigid dolomites and dolomitic limestones (Yılmaz and Duran, 1997).

#### 2.1.1.2 Sabunsuyu Formation

Unit is firstly defined by Wilson and Krummenacher (1959) in the measured section of the Sabunsuyu Stream at the western side of Kilis which includes whole Mardin Group with the name of "Sabun Suyu formation". In the study of Sungurlu (1973) the "Sabunsuyu formation" is defined in the Sabunsuyu Valley as it is used as today.

The Lower and the upper contacts of the Sabunsuyu Formation are conformable with the Areban Formation and the Derdere Formation, respectively. In the Korudağ area which is close to the Derdere Village in the Çüngüş District of Diyarbakır, it is unconformable with the Dadaş Formation at the lower contact and conformable with the Derdere Formation at the upper contact (Tuna, 1973; Pasin et. al., 1982).

The age of the Sabunsuyu Formation is determined as Albian-Cenomanian in the study of Erenler (1989) and the depositional environment is defined as restricted, semi-restricted shallow carbonate platform in the study of Perincek et. al. (1991). Sabunsuyu Formation consists of tidal-flat to subtidal carbonates.

The Sabunsuyu Formation is mainly composed of dolomite, dolomitic limestone and limestone lithologies (Tuna, 1973; Sungurlu, 1974; Perinçek, 1979; Aksu, 1980; Yılmaz, 1982; Pasin et. al., 1982; Güven et. al., 1988; Yılmaz and Duran, 1997).

The Sabunsuyu Formation is penetrated in most of the wells drilled in Souteastern Turkey and its thickness is variable from 40 m to 410 m (Çelikdemir and Dülger, 1990; Duran et. al., 1996; Yılmaz and Duran, 1997). In Diyarbakır, the thickness of the formation becomes 200-300 m.

#### 2.1.1.3 Derdere Formation

Unit is firstly named and described by Handfield et. al., (1959) in the section measured at the outcrop of the Korudag anticline of the Derdere village in the Çüngüş District of Diyarbakır as the "Derdere formation".

Upper contact of the Derdere Formation is sharp and unconformable with the Karababa Formation according to studies of Handfield et. al. (1959) and Bryant (1960). The lower contact of the formation is conformable with the Sabunsuyu Formation (Kellogg, 1960; 1961). At around the Derik District of the Mardin, the lower contact of the Derdere Formation is unconformable with the Sabunsuyu Formation in the previous studies (Aksu, 1980; Pasin et. al., 1982; Yılmaz and Duran, 1997); however it is stated in the study of Özkan and Altiner (2019) that, the contact between Derdere and Sabunsuyu formations is conformable. In the Sabunsuyu valley, the Karababa Mountain, surroundings of the Korudag-Çermik-Çüngüş of Diyarbakır, northern side of the Cudi Mountain in Şırnak and western part of Beytüşşebap District, upper contact of the Derdere Formation is with Sayındere Formation. At the southern flank of the Hazro anticline of Diyarbakır and the Mazıdağı District of Mardin, Karababa Formation and Derdere Formation are transitional and have conformable contact (Aksu, 1980; Yılmaz, 1982; Yılmaz and Duran, 1997).

In the previous studies, the age of the formation is defined as Cenomanian by Köylüoğlu (1981), and Erenler (1989) and depositional environment of Derdere is restricted to semi-restricted shallow marine (Perincek et. al., 1991); however the age of Derdere Formation is updated as late Albian to early Turonian and the depositional environment ranges from outer ramp to peritidal in the study of Özkan and Altiner (2019).

The Derdere Formation is composed of grayish beige, beige, gray, blackish gray, yellowish gray, white, dirty white, cream, earth-brown colored, rigid-very rigid, compact, brittle, thinly fractured, thin-medium-thick-very thick bedded, fossiliferous, clayey, sandy limestone and dolomitic limestone with mollusk fragments, partly porous, hydrocarbon smell, stylolites and chert nodules. It also consists of beige, grayish beige, gray, earth-brown, white, brown colored, rigid-very rigid, compact, medium-thick-very thick bedded, fine to coarse crystalline, sugary texture, fractured, partly porous dolomite with hydrocarbon smell and chert nodules (Perincek, 1979; 1980; 1989; 1990; Aksu, 1980; Yilmaz, 1982; Pasin et. al., 1982; Güven et. al., 1988; Yılmaz and Duran, 1997).

In the İnişdere section of the Besni District, the thickness of the formation is 118-152 m (Saltık and Saka, 1971a; Perinçek, 1980; Pasin et. al., 1982; Yılmaz and Duran, 1997). At the surroundings of Karababa Mountain of the Adıyaman, it is measured as 138-150 m (Saltık and Saka, 1971b; Pasin et. al., 1982; Güven et. al., 1988). In the Çermik-Çüngüş of Diyarbakır, the thickness of the formation is 15-40 m (Perinçek, 1979), in the Korudag close to the Derdere Village of Çüngüş District it is 104 m (Sungurlu, 1974). In the area of Hazro High, the thickness of formation is 12-68 m (Yılmaz, 1982; Pasin et. al., 1982). At around Mardin, the average thickness of the formation is 150 m (Güven et. al., 1988) and in the Derik District of Mardin it becomes 182-186 m (Aksu, 1980; Pasin et. al., 1982; Yılmaz and Duran, 1997). The thickness of the formation is measured as 314 m in the study conducted by Özkan and Altıner (2019) in the Derik District of Mardin. The Derdere Formation is penetrated in most of the drilling wells in Southeastern Turkey. The thickness of the formation changes from 50 m to 250 m (Çelikdemir

and Dülger, 1990; Yılmaz and Duran, 1997). On the Adıyaman-Diyarbakır line, the range of the thickness of the formation is from 100 to 150 m although the maximum thickness is 200-275 m towards Gaziantep. At the central part of the Southeastern Turkey, formation thickness is variable from 100 to 200 m.

#### 2.1.1.4 Karababa Formation

Karababa Formation is the youngest formation of the Mardin Group Carbonates and it has three members, named as A Member, B Member and C Member. The "Karababa limestone formation" is firstly used by Stager (1955). Karababa Formation is firstly named and defined as the "Karababa limestone" by Gossage (1956).

The Karababa Formation is unconformable with the Derdere Formation at the lower contact and unconformable with the Karaboğaz Formation at the upper contact (Tuna, 1973; Aksu, 1980; Pasin et. al., 1982; Güven et. al., 1988; Yılmaz and Duran, 1997).

The age of the formation is defined as late Coniacian to early Campanian (Erenler, 1989; Çoruh, 1981) and the depositional environment is determined as semi-restricted to restricted shelf lagoon and shallow marine (Şengündüz and Aras, 1986; Çelikdemir and Dülger, 1990; Araç and Yılmaz, 1991; Yılmaz and Duran, 1997). In the study of Özkan and Altıner (2019), the age of the Karababa Formation starts from late Turonian different from the previous studies.

The A Member of Karababa Formation is composed of brown beige, brown, dark gray, blackish gray colored, clayey, compact, thinly fractured limestone with marl transition, silt size echinoid, mollusk fragments, planktonic foraminifers, organic matter, phosphate and glauconite. The B Member consists of nodular, lenticular and banded cherts and it is gray, brownish gray, dark beige, brown colored, compact, thinly fractures, partly siliceous, fine-medium-thick and irregular bedded, rigid and brecciated-like limestone with macro and micro fossil content, chert globules. The C Member is beige, light cream, light gray, earth-brown, dirty white, white colored,

compact, rigid, medium-thick-very thick bedded, thinly fractured micritic limestones with fracture and dissolution and intraparticle porosity, sand size quartz, skeletal fragments including rudist, gastropod, echinoid, coral and partly with chert globules (Yılmaz, 1982; Yılmaz and Duran, 1997).

### 2.1.2 Stratigraphy of the Derdere Formation in the studied wells

The Derdere Formation is the main focus of this study among the Mardin Group Carbonates and it was studied in the seven wells. A complete succession of the Derdere Formation is studied in the five of the seven wells (K-3, K-2, K-4, K-9 and K-7); the two wells have partial penetration into the Derdere Formation (K-11 and K-8).

The formation conformably overlies the Sabunsuyu Formation and is unconformably overlain by the Sayındere Formation in Diyarbakır Region. From west to east, the thickness of the Derdere Formation is 152 m, 166 m, 167 m, 166 m, 160 m, 186 m, 156 m in the studied wells of K-11, K-8, K-3, K-2, K-4, K-9, K-7 wells, respectively with the alternations of limestone, dolomite, dolomitic limestone and calcareous dolomite.

Shallow-marine conditions were dominant during the deposition of Mardin Group Formations, particularly during the deposition of Sabunsuyu and Derdere Formations, and similar microfacies are observed both in Derdere and Sabunsuyu which make differentiation of the formations challenging without drawing biostratigraphical framework. The sequence stratigraphic study based on biostratigraphy and formation contacts are discriminated with key fossil assemblages in the measured section of Derik, Mardin Region in the field (Özkan and Altiner, 2019). Hence, while making correlation with the subsurface samples, this biostratigraphic framework created for field samples are tested. In the well samples, discrimination of the Derdere and Sabunsuyu formations is not simple as much as in the field samples.

The Derdere Formation is deposited relatively deeper-marine, anoxic conditions, and passes up into a shallowing- upward sequence consisting of lagoonal to tidal-flat carbonates. The depositional model created for the Derdere Formation is the ramp which is seperated as inner ramp (tidal flat, lagoon and shoal), proximal middle ramp, distal middle ramp and outer ramp.

One of the reasons for the selection of these seven wells is the dominant limestone lithology instead of dolomite, dolomitic limestone and calcareous dolomite. Out of the study area, intensely dolomitized successions of the Derdere Formation are commonly observed due to fracturing, faulting and hydrothermal impacts. At the contact of the Sabunsuyu and Derdere formations, the Sabunsuyu Formation is frequently as dolomitized and it is difficult to locate the contact between two formations in the wells. At the base of the Derdere Formation, limestone is the prominent lithology and thick dolomitic limestones and dolomites alternate with thin limestones. The dolomites become thicker in the wells located in the middle of the seven wells and thinner in the westernmost and easternmost wells (**Figure 20**). In the upper parts of the wells, pelagic limestones, sometimes are argillaceous, are followed by massive limestones. In the uppermost part of the Derdere Formation, dolomites, dolomitic limestones and calcareous dolomites are predominantly observed with some dissolution vugs (**Figure 20**). The upper contact is with the Sayındere Formation which composed of pelagic limestone and sometimes with argillaceous limestone deposited in deep marine environmental conditions (**Figure 20**).

In the limestone beds of the Derdere Formation diversified assemblages of benthic and planktonic foraminifers are defined in the wells; however these foraminifer assemblages are not rich and highly diversified in the succession defined in the field section of the Derik, Mardin revealed in the study of Özkan and Altiner (2019). Intense dolomitization in some parts of the wells masks most of the primary constituents. In spite of the dolomitization, the Derdere Formation is characterized by the benthic and planktonic foraminifers.The formation has diversified benthic foraminifer assemblage in the lower Cenomanian deposits and diversified

planktonic foraminifer assemblage in the lower Turonian deposits. These benthic and planktonic foraminifer assemblages are studied in order to reveal Albian-Cenomanian and Cenomanian-Turonian boundaries. *Cuneolina, Nezzazata simplex and Nezzazata isabellae* which are associated with *Cuneolina* are defined at the bottom of the Derdere Formation. At the bottom of the Cenomanian deposits of the Derdere, the benthic foraminifer assemblage is composed of *Praealveolina, Pseudolituonella, Biplanata peneropliformis, Trochospira, Dicyclina, Sellialveolina, Nezzazata conica*. Above this benthic foraminifer rich level, planktonic foraminifers including *Hedbergella, Muricohedbergella, Heterohelix* and *Macroglobigerinolloides* are scarce. Planktonic foraminifers are diversified close to Cenomanian-Turonian (C-T) boundary. The C-T boundary is located regarding to the appearance of *Whiteinella* which are accompanied by *Muricohedbergalla planispira, Muricohedbergella simplex, Archaeglobigerina cretacea, Marginotruncana (M. marianasi, M. schneegansi, M. sigali), Heterohelix globolusa, Globigerinolloides*. At the top of the Derdere Formation miliolid, textularid, *Ataxophragmidae, Belorussiella, Valvulina,* and *Coscinolina* type benthic foraminifers are identified.

The boundary between Sabunsuyu and Derdere formations is not observed in all of the studied wells due to partial penetration in production wells. Where it is possible to see, at the bottom of the Derdere Formation the inner ramp deposits of Albian are recognized with diversity and the abundance of benthic foraminifers. Descrimination of the boundary between Sabunsuyu and Derdere formations and Albian-Cenomanian boundary are not simple in the wells samples due to sample resolution and quality of cuttings. In the detailly studied K-7 well, formation boundaries and timelines are defined using benthic foraminifera whereby better sample quality and preservation of the foraminifera. The foraminiferal fauna of the Sabunsuyu Formation defined in the field section is similar to the foraminiferal assemblage of the wells and the boundary between the Derdere and Sabunsuyu formations is drawn by considering them. Orbitolinid, *Everticyclammina* and *Charentia* are the common species defined in the both field section and wells. The benthic foraminiferal fauna of the Sabunsuyu Formation also include *Cibicides*,

miliolid, *Nezzazata, Archaealveolina*, *Bolivinopsis*, *Cuneolina, Spiroloculina*, *Redmondoides lugeoni, Haplophragmoides ?*, *Protopeneroplis ?*, valvulinid, and *Trocolina.* Since the facies of the Sabunsuyu and Derdere formations are similar and inner ramp facies of these two formations are in contact in the wells of the Diyarbakır Region, the boundary between them is defined using the benthic foraminiferal assemblage.

Intense dolomitization is observed in the higher levels of Cenomanian in the field section of Derik, Mardin different from the well sections. Dolomitization is also common phenomenon in the selected well samples however it is not as highly pervasive as in the Derik.

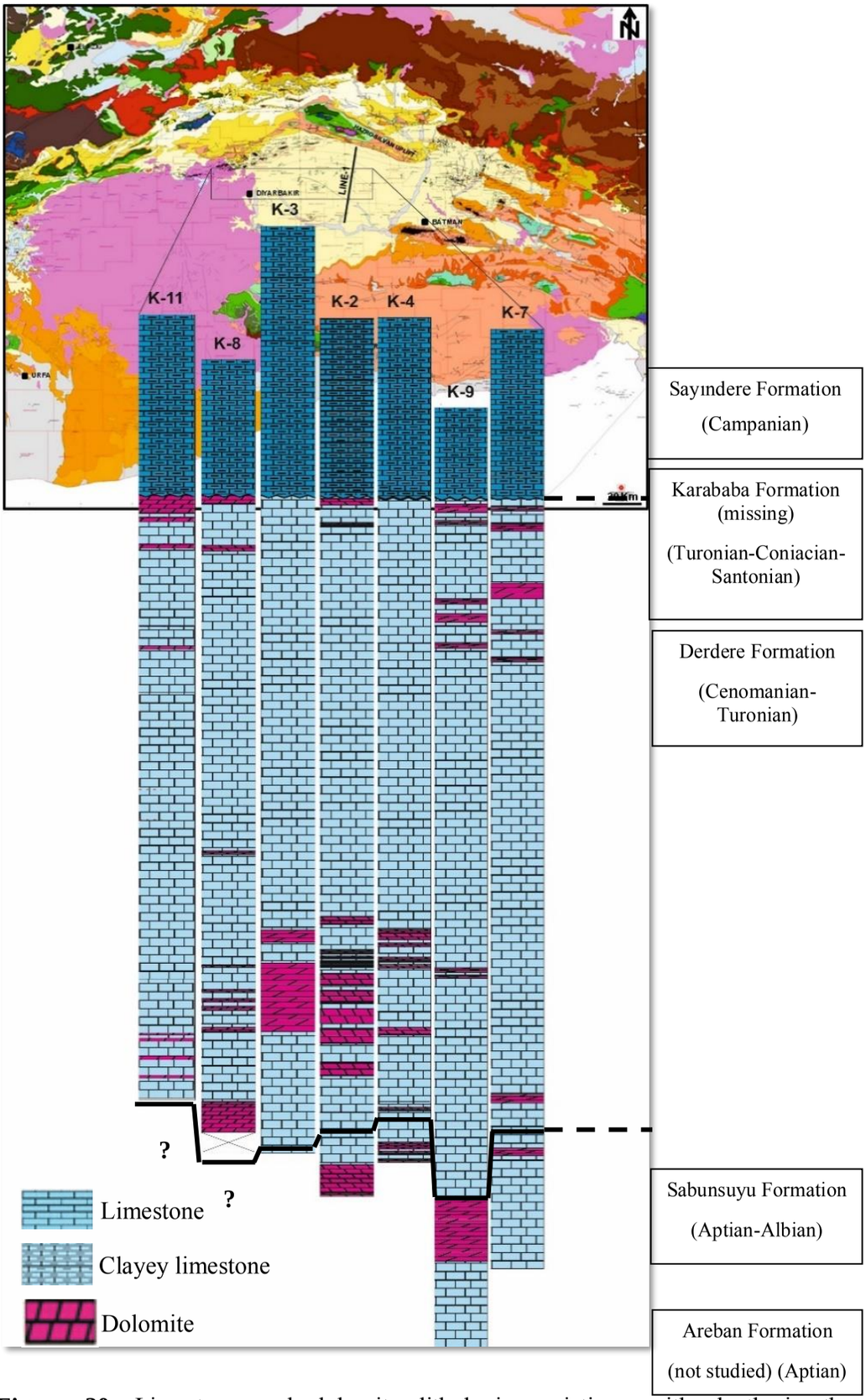


**Figure 20.** Limestone and dolomite lithologic variations with depth in the lithologically studied sections of seven wells including part of Sayındere Formation, Derdere Formation and part of Sabunsuyu Formation in some of the wells on geological map of Southeast Turkey (modified after Aydemir, 2011). Between the Derdere and Sayındere formations, Karababa Formation is missing and below the Sabunsuyu Formation, Areban Formation is missing (due to partial penetration to Mardin Group Carbonates)

# CHAPTER 3

# MICROFACIES ANALYSIS AND DEPOSITIONAL MODEL

## 3.1 PRIMARY CONSTITUENTS OF THE DERDERE FORMATION

Primary constituents including skeletal grains (bioclasts) and non-skeletal grains defined in the Derdere Formation are intraclasts, peloids, oysters (*Pycnodonteina*e), mollusk (bivalves+gastropods), brachiopods, echinoderms, sponge spicules, large benthic foraminifers, small benthic foraminifers, calcisphaerulids (*Pithonella spherica/Pithonella ovalis/Bonetocardiella conoidea*), rudists, planktic foraminifers, algae, and radiolarians (**Figure 21-23**).

The main primary constituents observed in the tidal flat part of inner ramp depositional setting is benthic foraminifers, lagoon part of inner ramp is composed of benthic foraminifers, skeletal fragments and rarely peloids and there are mainly peloids, intraclasts, benthic foraminifers, skeletal fragments (oysters, gastropods, brachiopods, rudists) and algae in shoal part of inner ramp. Proximal middle ramp depositional setting towards the inner ramp consists of skeletal fragments (transported and broken large skeletal fragments (brachiopods, echinoderms), benthic foraminifers and rarely peloids and it becomes rich in skeletal fragments and rarely benthic foraminifers towards the distal middle ramp. Distal middle ramp composed of planktonic foraminifers, calcisphaerulids (*Pithonella spherica*) and skeletal fragments. Calcisphaerulids *(Pithonella spherica/Pithonella ovalis/Bonetocardiella conoidea*), skeletal fragments (sponge spicules, thin walled mollusks (pelecypoda) and "*Saccocom*a" type echinoderms) and rarely planktonic foraminifers are commonly observed in outer ramp towards the distal ramp and it is getting rich in calcisphaerulids and skeletal fragments (sponge spicules and "*Saccocom*a" type echinoderms) towards the basin (**Figure 24** and **Figure 25)**.

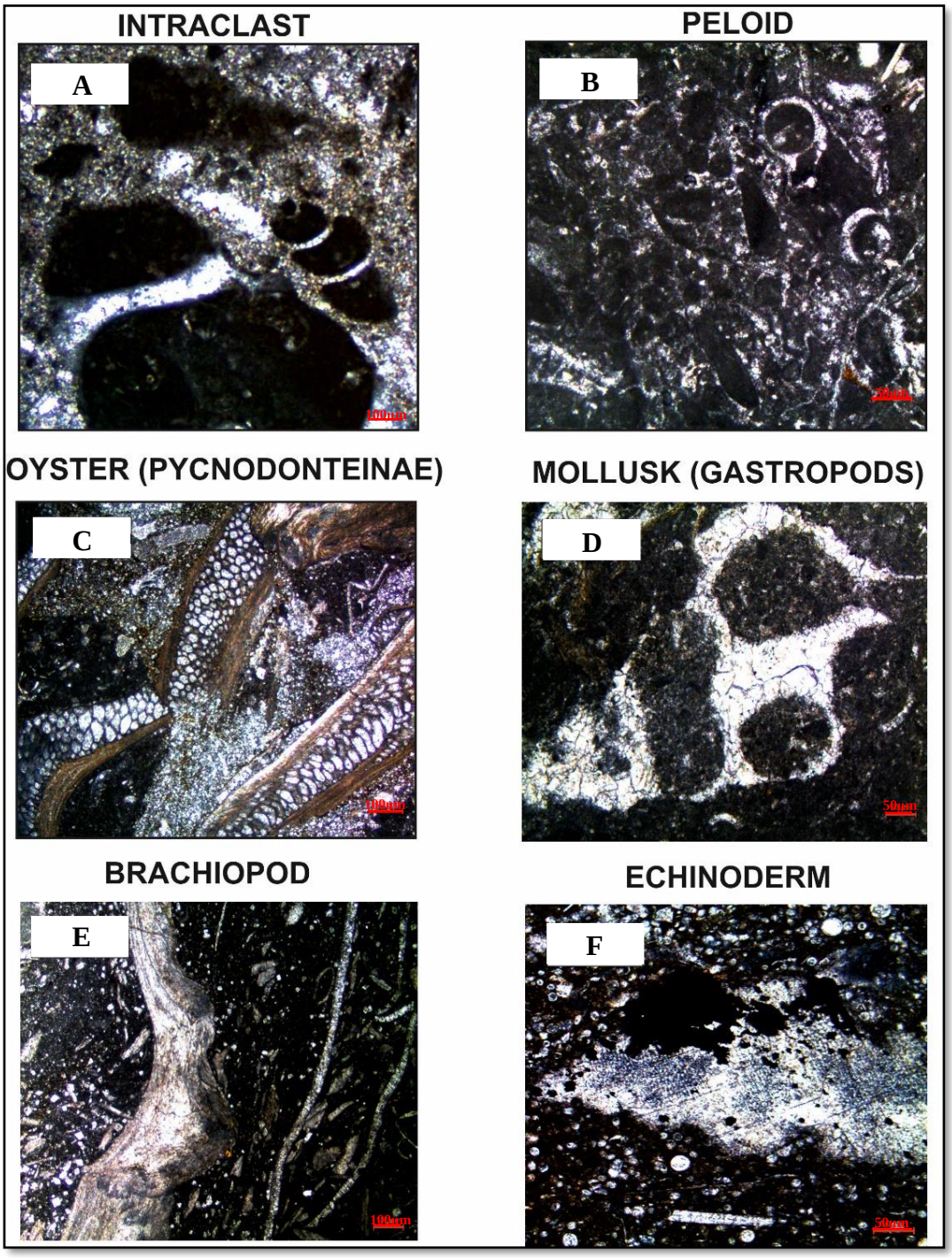


**Figure 21.** Photomicrographs, which show the primary constituents of the Derdere Formation, are from the samples of K-11 well with the scale of 50 µm (on the right) and 100µm (on the left). [Depths of samples are 1649.35 m (A), 1650.23 m (B), 1650.79 m (C), 1651.07 m (D), 1764.54 m (E), and 1722.82 (F).]

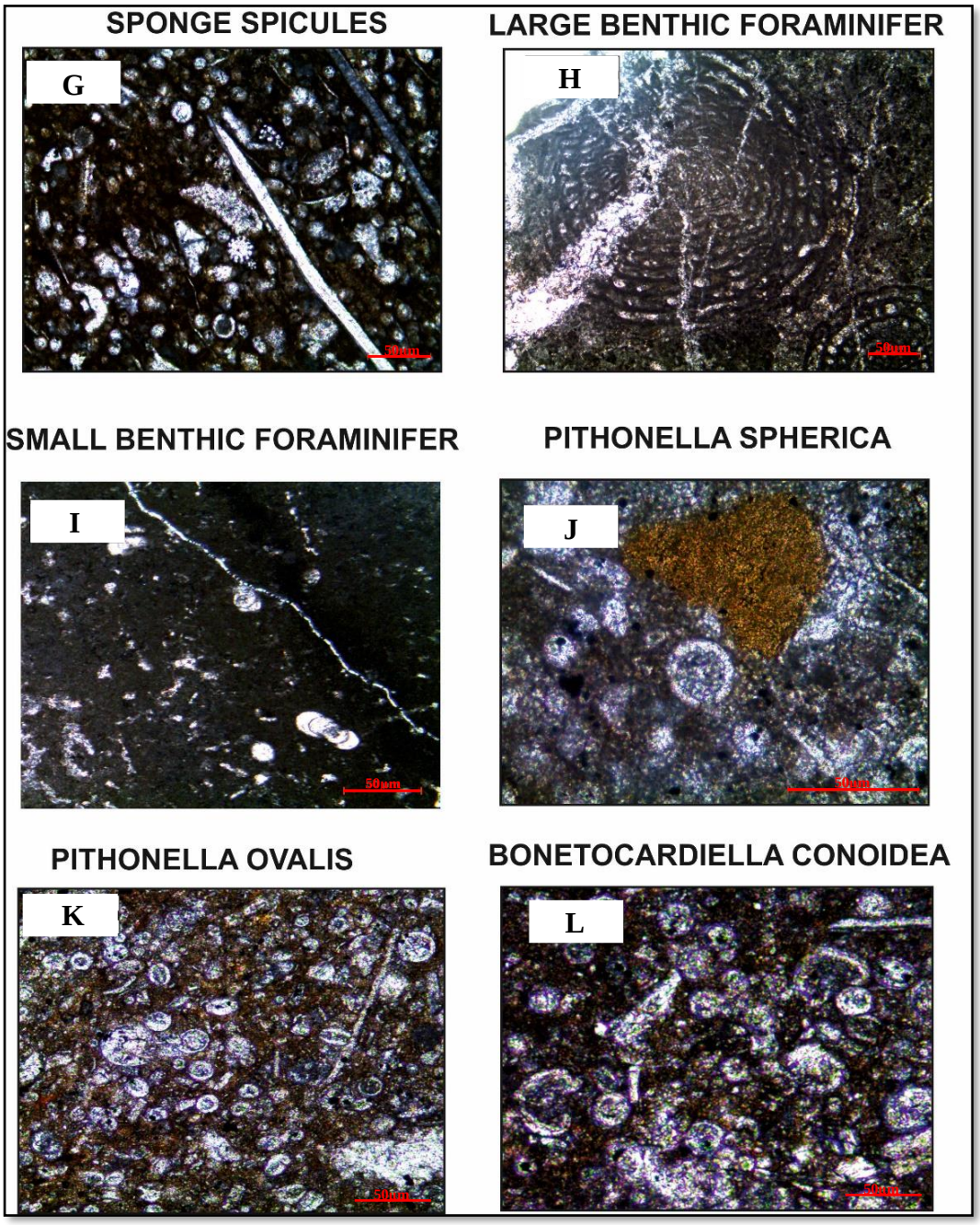


**Figure 22.** Photomicrographs, which show the primary constituents of the Derdere Formation, are from the samples of K-11 well with the scale of 50 µm.) [Depths of samples are 1721.84 m (G), 1778.04 m (H), 1778.34 m (I), 1721.84 m (J), 1722.82 m (K), and 1725.35 (L).]

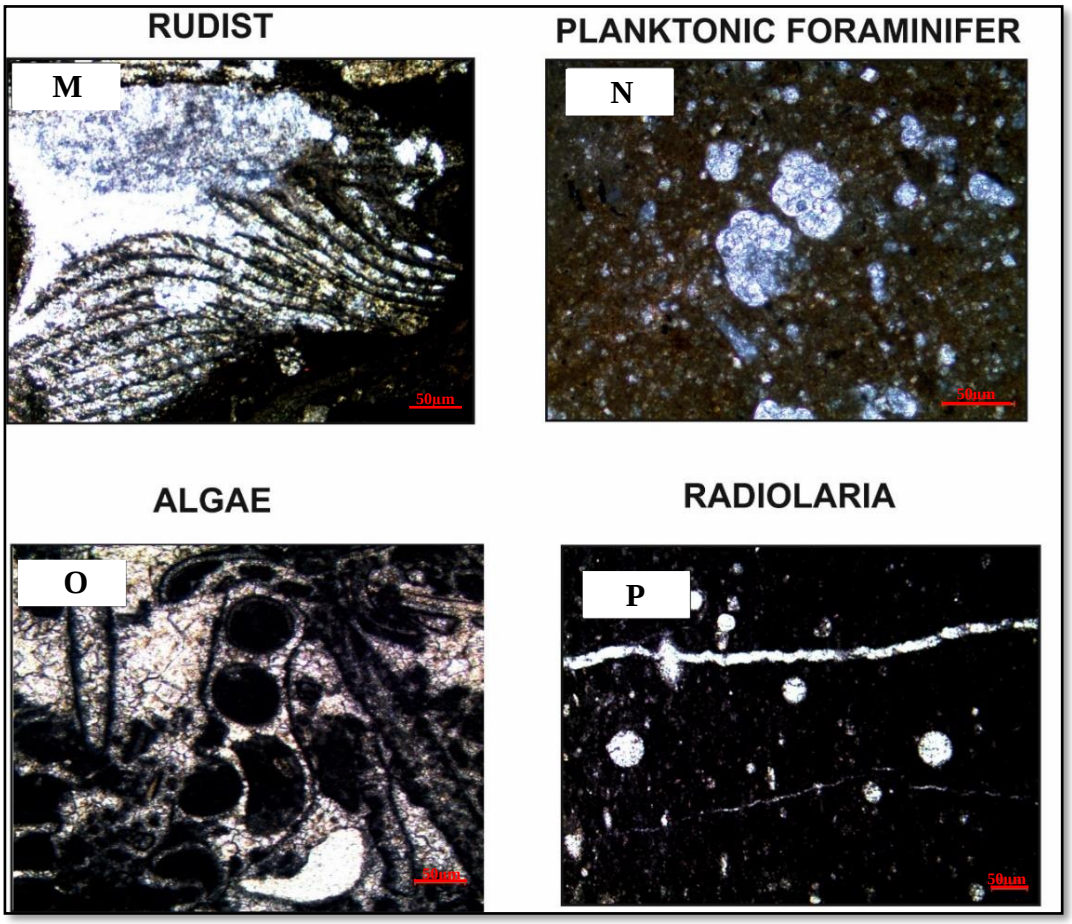


**Figure 23.** Photomicrographs, which show the primary constituents of the Derdere Formation, are from the samples of K-11 well with the scale of 50 µm.) [Depths of samples are 1781.69 m (M), 1700.03 m (N), 1650.57 m (O) and 1697.42 m (P).]

Generally speaking, some of the primary constituents are confined to some specific sequences. The large benthic foraminifers and rudist fragments are only observed at the bottom of the succession and mostly in the highstand systems tracts. In the upper parts of the succession, only few small benthic foraminifers are observed. Large benthic foraminifers are mainly found in the bottom part of the succession and their abundance is higher in the highstand systems tracts while their number is decreasing in the transgressive systems tracts. Although some algae type organisms are defined at the top of the Derdere Formation in rare amount, main reefal organisms such as corals, rudists and associated forms including large benthic foraminifers, calcareous sponges are absent. In the study of Mathey et. al. (1995), it is stated that during late Cenomanian to early Turonian reefal organisms

are not observed in Niger ramp due to unfavorable morphological conditions. These morphological conditions are associated with the absence of pronounced topographic high which is similar to the depositional conditions of the Derdere Formation. To develop model for the Derdere Formation, primary constituents and favorable environmental conditions for the deposition are considered.

Additionally, *Bonetocardiella conoidea* type calcisphaerulids and sponge spicules are characteristic for the sequences defined in the outer ramp and distal middle ramp type depositional environments and mostly in the transgressive systems tracts. On the other hand, *Pithonella spherica* and *Pithonella ovalis* are not the indicator of depositional environment or water depth. *Pithonella ovalis* is defined in the inner ramp facies of Guerrero–Morelos Basin, Southern Mexico during Cenomanian to Turonian in the study of Franco and Romao (2004). Few large *Pithonella spherica* with thick wall structure are observed together with broken skeletal fragments in the inner ramp to proximal middle ramp type of depositional environments. Even at the top of the Derdere Formation, *Pithonella spherica* can be observed. Small and thin walled *Pithonella spherica* are detected abundantly in the distal proximal ramp and outer ramp depositional environments and transgressive systems tracts of the sequences. Hence, their relative abundances, size, wall thickness and diversity are used to discriminate shoaling and deepening trends in the sequences.

Petrographical and biostratigraphical analysis reveals that benthic foraminifers do not have much variation in most of the wells. This can be related with the resolution of sampling since analyses are mainly conducted on the cutting samples of the wells. In the K-11 well, diversity of benthic foraminifers are much more higher compared to other wells, and this can be explained by higher resolution of core sampling in K-11 well. Generally speaking, when the sequences defined in the wells are compared, some benthic foraminifers are unique to some sequences, for instance *Praealveolina* rich sequences are correlatable in the wells and in the Derik Section (Özkan and Altiner, 2018).

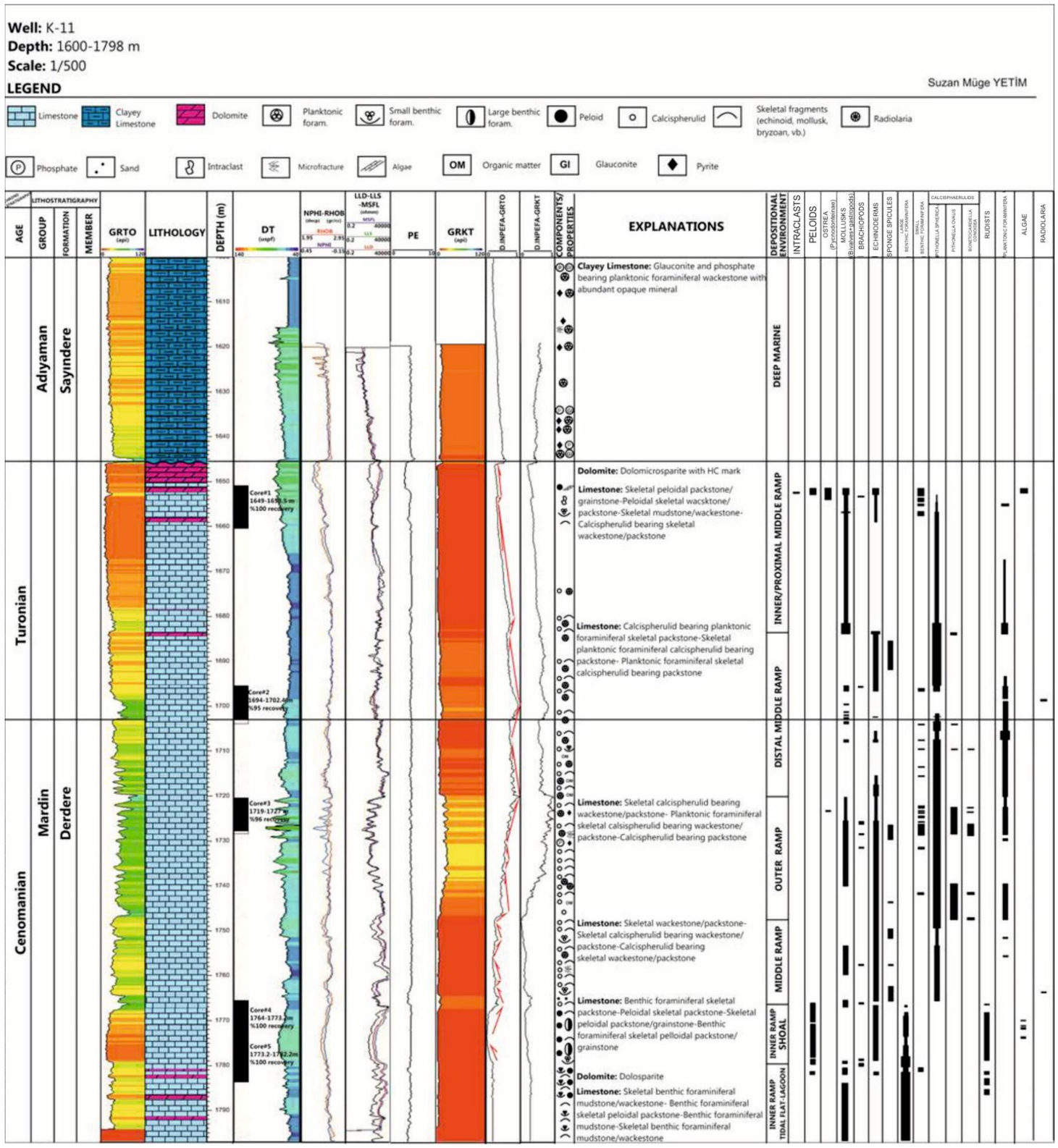


**Figure 24.** Primary constituents of the Derdere Formation defined in the K-11 well

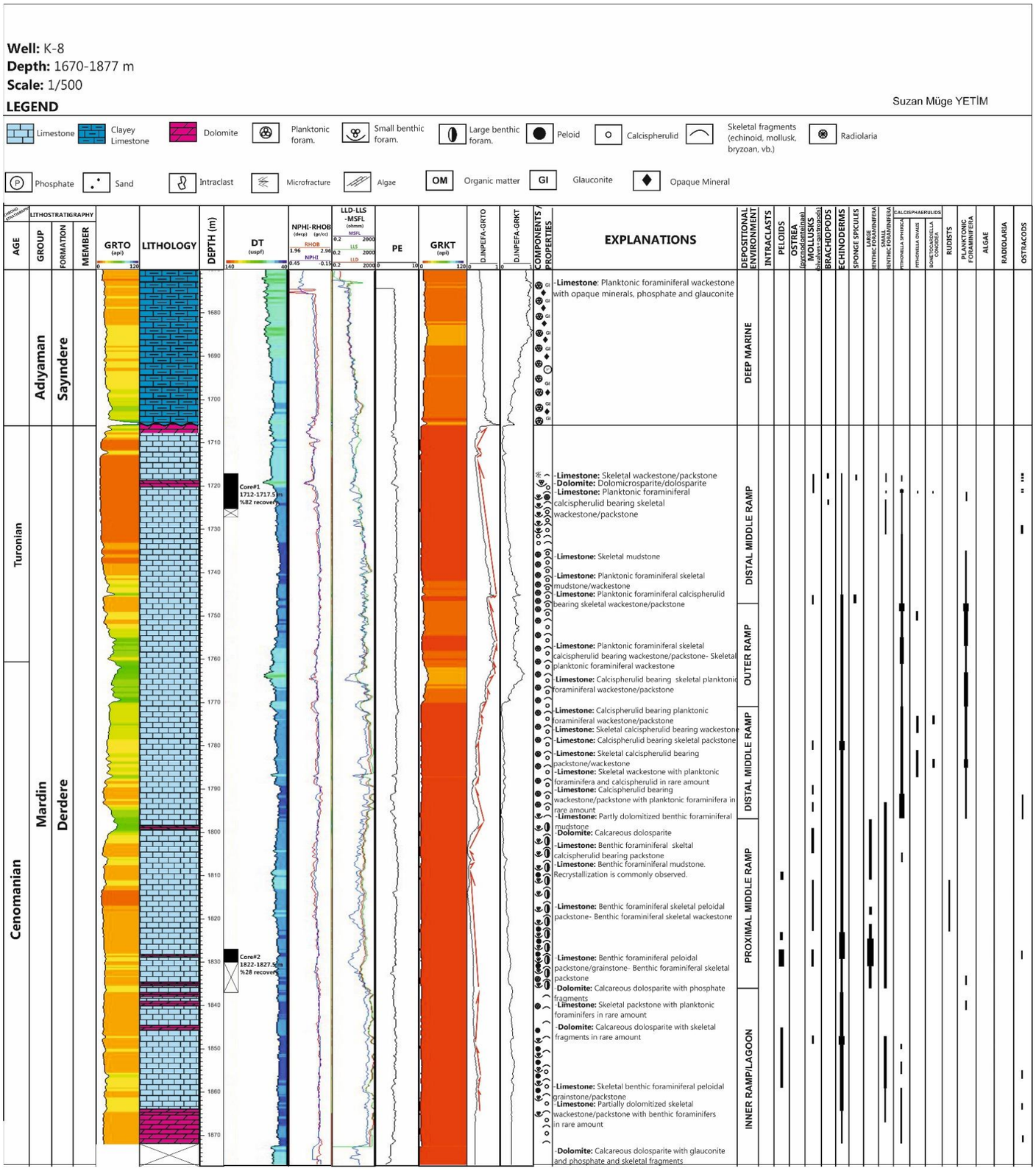


**Figure 25.** Primary constituents of the Derdere Formation defined in the K-8 well

Specific type oysters, pycnodonts, are observed at the top the Derdere Formation in the highstand systems tract of the sequences and commonly observed at this time interval globally. In this study, pycnodonte type oysters are considered as the part of the Turonian time interval. Although there are studies stating the existence of the pycnodonts, its stratigraphic position is controversial. If they are the part of Cenomanian and they become extinct after the Cenomanian-Turonian boundary (Darwish et. al., 2015). The presence of pycnodonte and Pycnodonte Event is included in the event complete Turonian succession in the Derdere Formation is supposed to be eroded since pycnodonts are at the top of the formation. On the contrary in the study of Kennedy and Cobban (1991), pycnodonte bed is reported from the lower Turonian instead of Cenomanian. To conclude, the Pycnodonte Event can be related with the sea-level rise, terrigeneous influx, environmental stress conditions and preferential preservation of shells (Wilmsen and Voigt, 2006) which differs from basin to basin in terms of timing.

## 3.2 MICROFACIES VARIATION IN THE DERDERE FORMATION

Facies, which means that textural, compositional, and structural characteristics of a sedimentary deposit resulting from accumulation and modification in a particular environment, provides the description of the genetically related vertical and lateral succession (Van Wagoner, 1988; Catuneanu, 2006). Sequence stratigraphy is used to understand how facies are related in time and space and it provides better interpretation while studying oil and gas reservoirs. This aspect of sequence stratigraphy, which links the genetically related strata with each other, provides opportunity to assess variations in the depositional trends of the Mardin Group Carbonates which have main oil and gas reservoir levels (Demirel and Guneri, 2000) in the Diyarbakir Region.

In this study, fifteen microfacies types are described according to the relative abundances of the primary constituents. The microfacies of the Derdere Formation are variable in a wide range of the depositional environment from the outer ramp to the peritidal. Four of them are deposited in the inner ramp depositional setting in

which benthic foraminifers, skeletal fragments, peloids are defined as primary constituents; two of them are the part of proximal middle ramp which can be considered as transition between inner and middle ramp settings and skeletal fragments and rarely peloids are the main primary constituents in the microfacies. Five of the defined microfacies are deposited in the distal middle ramp setting in which planktonic foraminifers, skeletal fragments, calcisphaerulids and radiolaria are found. Four of them are interpreted to be deposited in the outer ramp in which mainly calcisphaerulids are present associated with rare planktonic foraminifers and skeletal fragments. There is not a sharp contact between the distal middle ramp and the outer ramp facies since the storm wave base, which differentiates distal middle ramp and outer ramp, is considered as a zone instead of a line. In order to show the microfacies variation in the Derdere Formation numerous cores of K-11 well are studied in detail and sedimentological logs of the cores of the K-11 well are given in the scale of 1/50 (**Figure 26-30**).

This study mainly depends on the well samples. In order to prevent the problems caused by the resolution of sampling in the wells, wells with core samples are selected to study; however one of the significant obstacles of this study is the absence of or poorly recovered core samples in the study area. Although three of the studied wells have cores, recoveries of the cores are not satisfactory except for the cores of K-11 well. The reason of selecting the K-11 well as pilot well to construct detailed stratigraphic framework is the presence of complete cores.

Bottom of the Derdere Formation is not observed in all of the studied wells. Where it is possible to see, the inner ramp deposits of Albian are recognized with diversity and the abundance of benthic foraminifers. Although recognition of the boundary between Sabunsuyu and Derdere formations and Albian-Cenomanian boundary are not simple in the wells samples due to sample resolution and quality of cuttings, in the detailly studied K-7 well, boundaries are drawn using benthic foraminifera assemblages. On the other hand, in the study of Özkan and Altiner (2019) the abundance of planktonic foraminifers are recognized in the outer ramp setting of Albian deposits at the bottom part of the Derdere Formation in Derik section of Mardin. In this study, planktonic foraminifers are commonly observed in the lower

Turonian deposits while benthic foraminifers are dominant in the Cenomanian deposits in the wells drilled in the foreland area of Diyarbakır Region which are considered as similar to the results of the field study of Derik section conducted in Mardin (Özkan and Altiner, 2019). Benthic foraminifers are commonly observed in the lower Aptian and Cenomanian deposits while planktonic foraminifers are dominantly found in the Upper Albian, Turonian and Santonian deposits in the study of Özkan and Altiner (2019).

Özkan and Altiner (2019) stated that, at the lower part of the Derdere Formation, the lime mudstone and calcisphaerulid wackestone type microfacies were deposited at the outer ramp setting. Bioclastic wackestone and bioclastic packstone type microfacies, which are considered as the transition from the outer ramp to the middle ramp, are observed both at the top and at the bottom of the Derdere Formation. Bioclastic bivalve floatstone and *Praealveolin*a packstone to grainstone microfacies are characteristic for the middle ramp setting, which is above the storm wave base under the control of moderate to strong wave energy. In the upper parts of the formation characterized by the low energy lagoon type depositional environment of the inner ramp setting, there is peloidal bioclastic packstone with miliolids and gastropod floatstone microfacies. Lime mudstone with miliolids type microfacies is considered to be deposited in the peritidal environment (Özkan and Altiner, 2019).

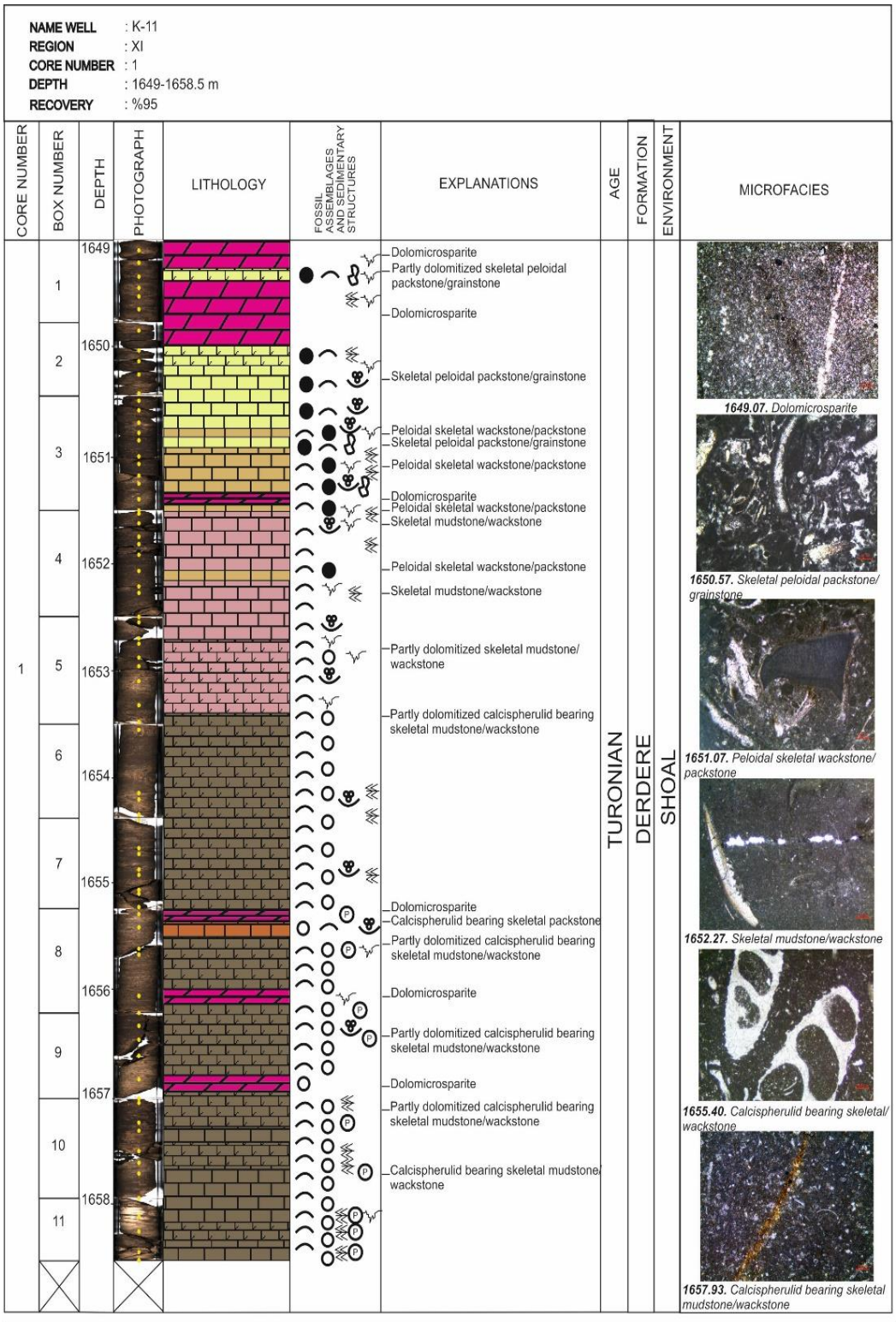


**Figure 26.** Sedimentological log of Core#1 of the K-11 Well, 1649-1658.5 m, the Derdere Formation with %100 recovery

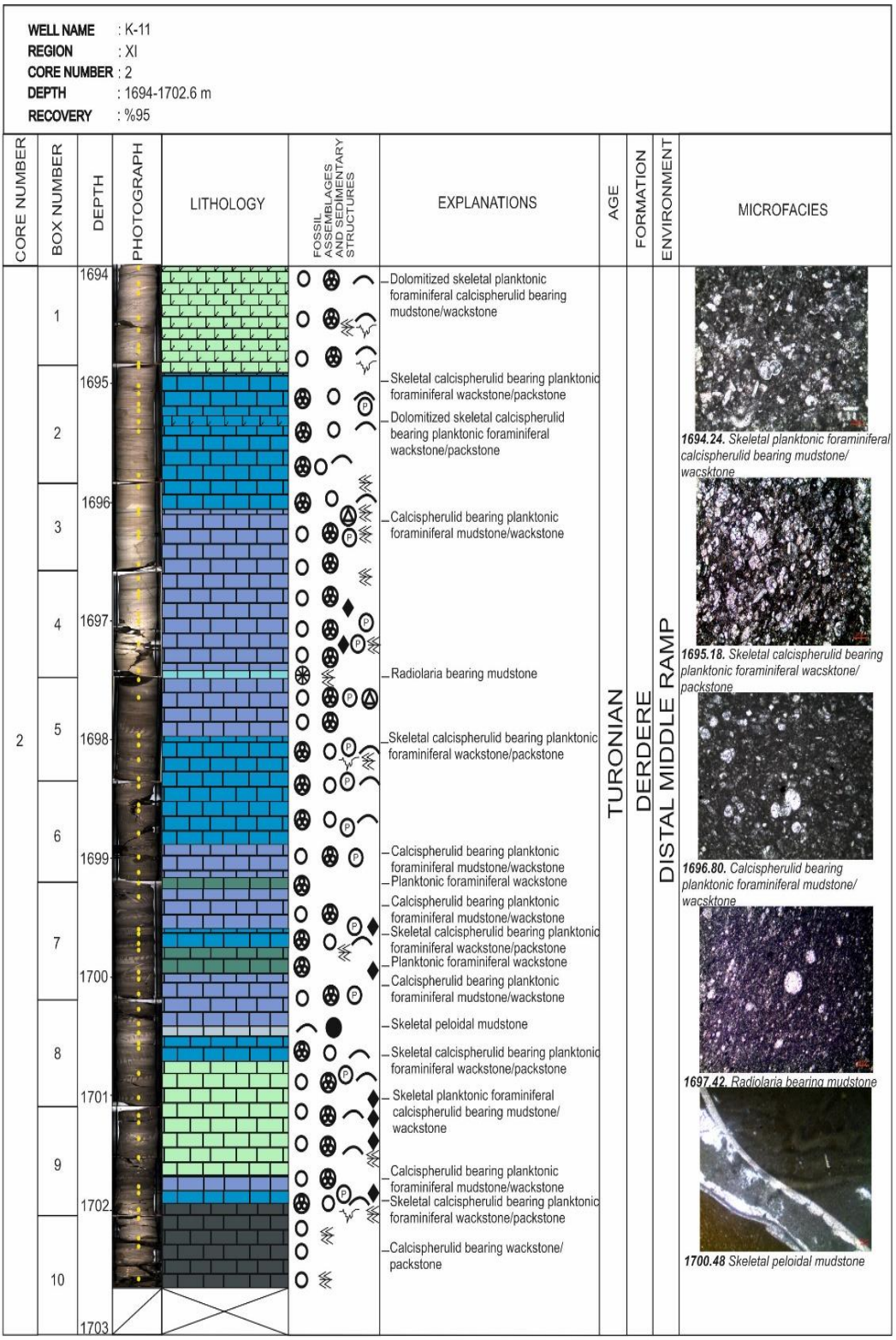


**Figure 27.** Sedimentological log of Core#2 of the K-11 well, 1694-1702.6 m, the Derdere Formation with %95 recovery

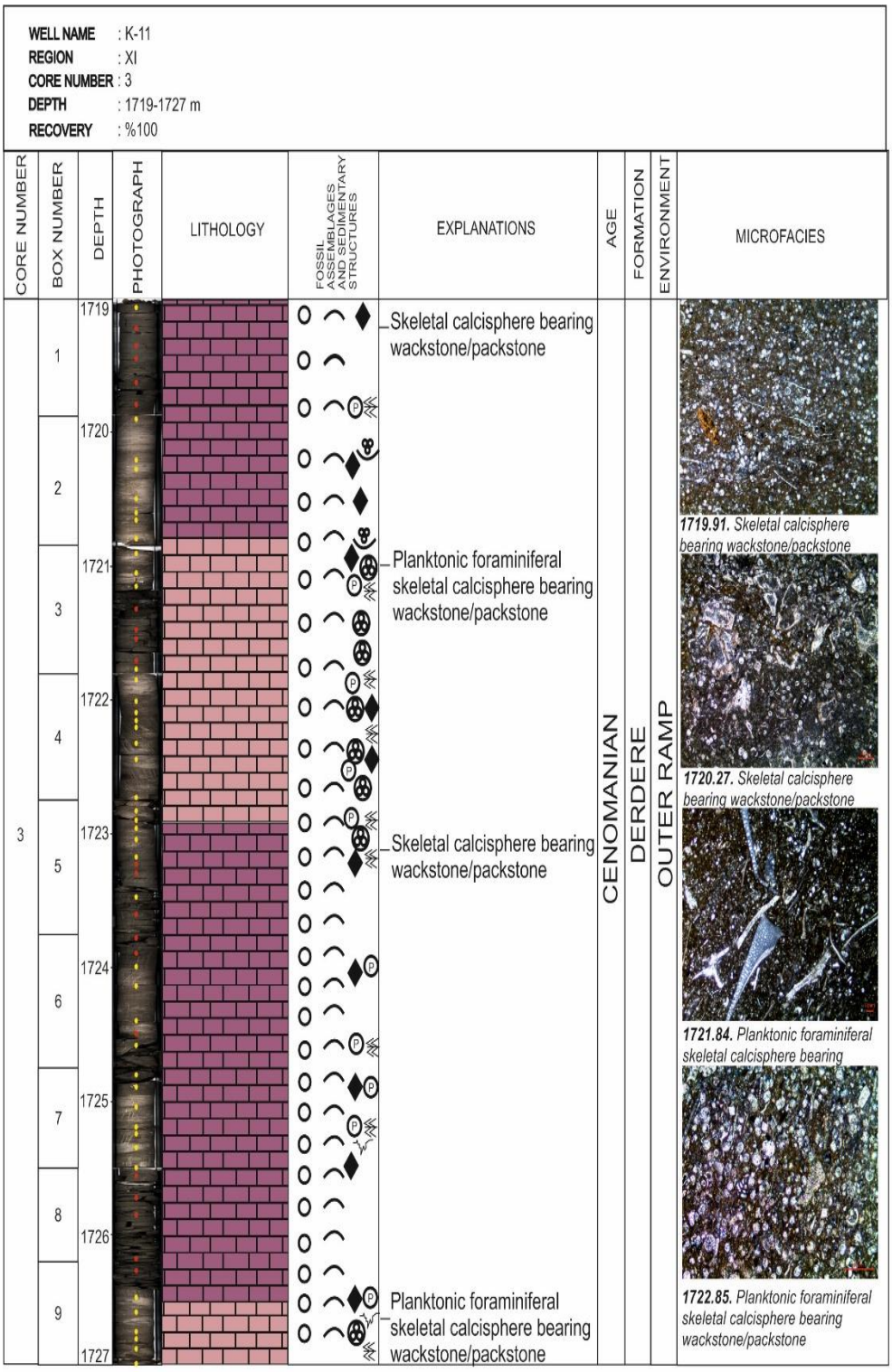


**Figure 28.** Sedimentological log of Core#3 of the K-11 well, 1719-1727 m, the Derdere Formation with %96 recovery

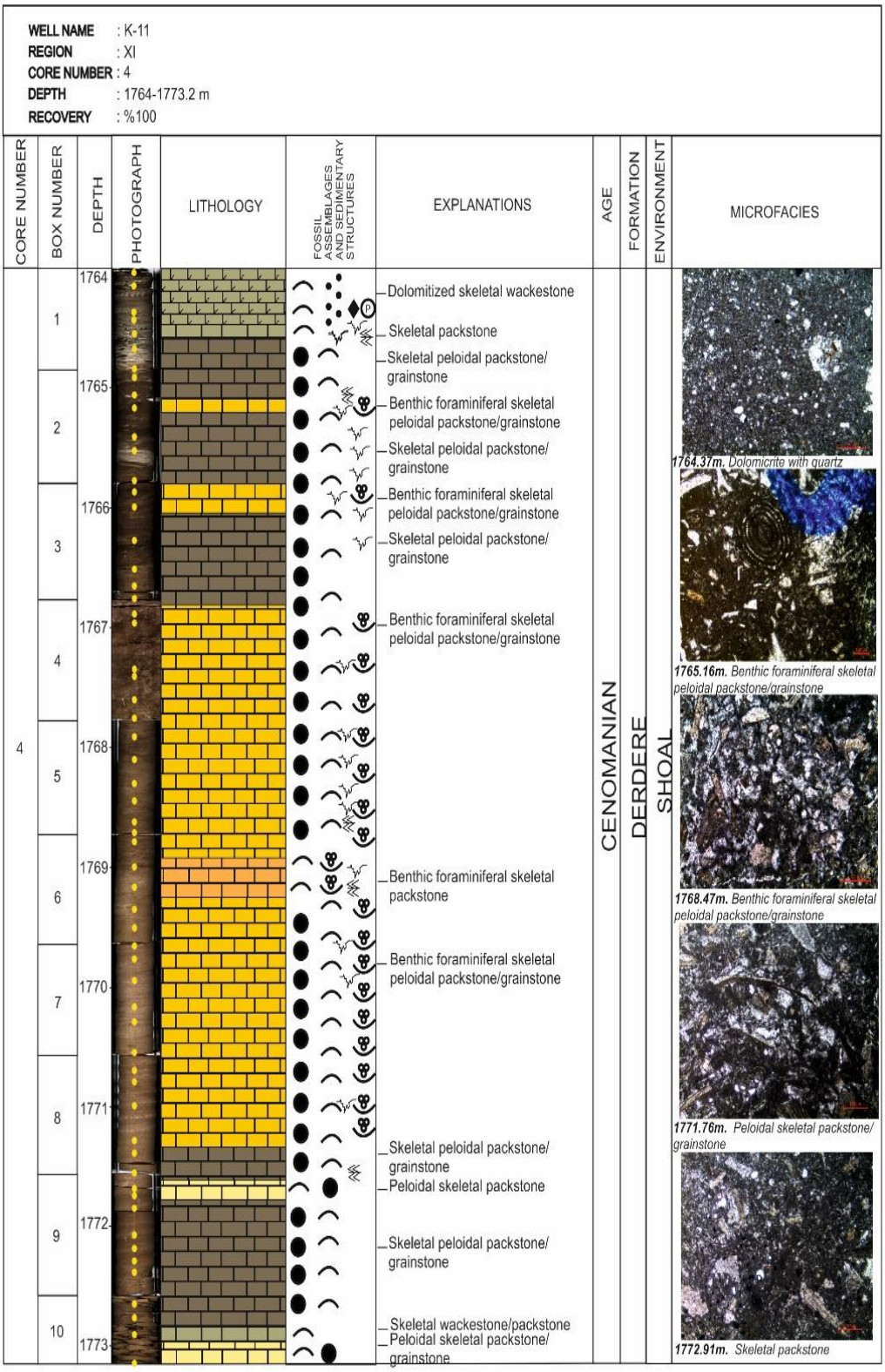


**Figure 29.** Sedimentological log of Core#4 of the K-11 well, 1764-1773.2 m, the Derdere Formation with %100 recovery

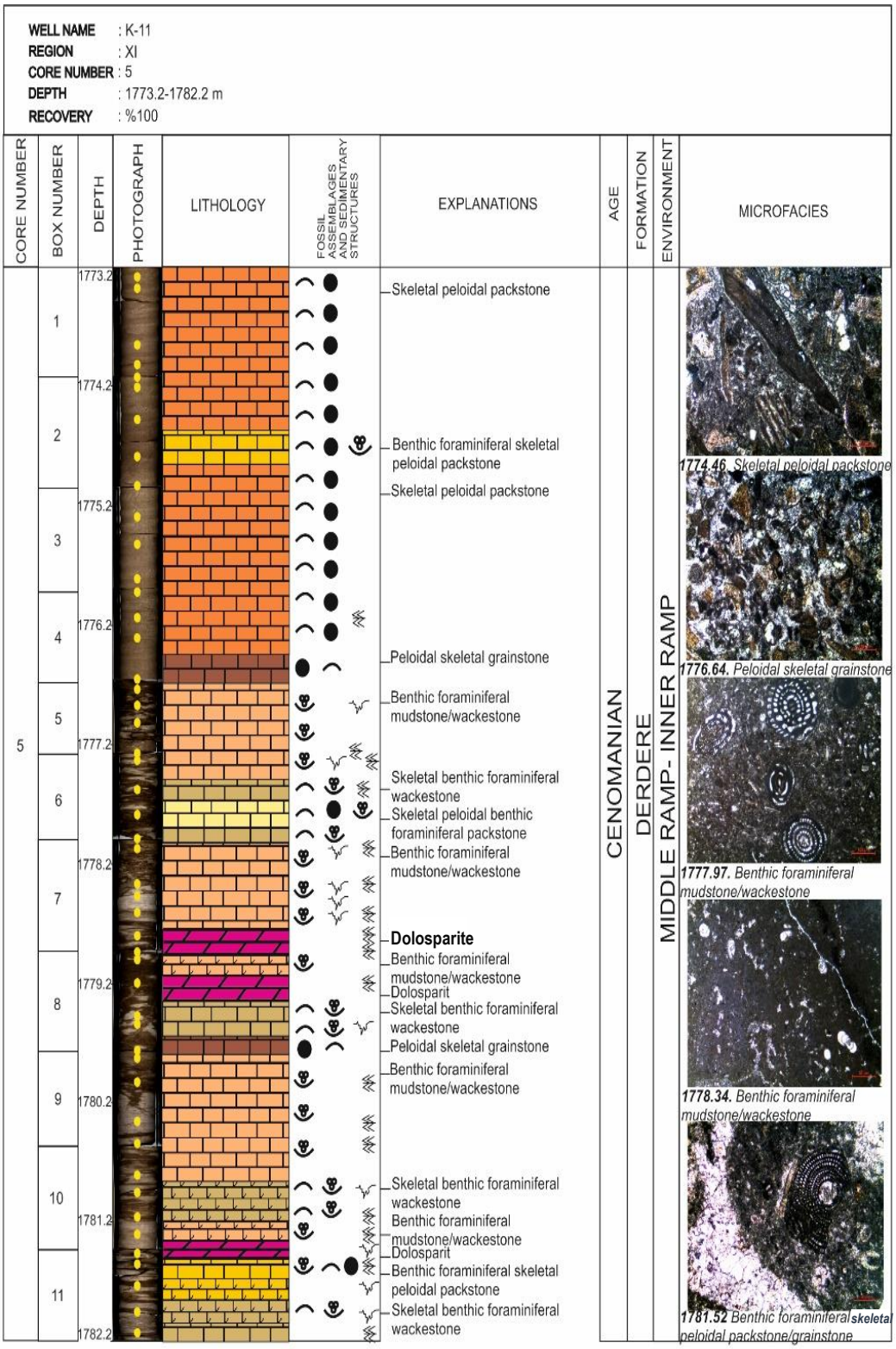


**Figure 30.** Sedimentological log of Core#5 of the K-11 well, 1773.2-1782.2 m, the Derdere Formation with %100 recovery

### 3.2.1 Ramp Facies

Primary constituents, some sedimentary structures, microfacies and depositional energy are considered together and the depositional model of the Derdere Formation is determined as a ramp model. Subdivisions of ramp model are inner ramp (between upper shoreface (beach or lagoonal shoreline) and fair-weather wave base), middle ramp (between fair-weather wave base and storm-wave base and sediment composition and textures reflect proximal-distal trends) and outer ramp (below normal storm-wave base, down to the basin plain and mud-dominated system) (Flugel, 2004) (**Figure 31**). In order to develop the depositional model of the Derdere Formation, the two most commonly used carbonate platform models proposed by Wilson (1975) and by Flugel (2004) (**Figure 32**) are considered and the microfacies defined in the Derdere Formation are evaluated as the part of this carbonate platform. Although Wilson carbonate model (1975) is composed of a barrier frame and reef bodies with boundstone type microfacies, there are not any boundstone type microfacies and reef-building organisms (except for some broken rudists and algae fragments) defined in the Derdere Formation in this study area. The primary constituents defined in the Derdere Formation can be regarded as common in the particular subdivisions of the carbonate ramp setting. Large and small benthic foraminifers, peloids, algae, intraclasts, oysters, rudists, mollusks, brachiopods are common components in the inner ramp settings. In the proximal middle ramp setting, broken shell fragments of inner ramp setting, rarely peloids and rarely calcisphaerulids are frequently observed. The most common components of distal middle ramp setting is calcisphaerulids, rare planktonic foraminifers, radiolaria and rarely broken shell fragments. In the outer ramp setting, most commonly calcisphaerulids, rare planktonic foraminifera and echinoderms are observed with some sponge spicules.

In the carbonate ramp model developed by Flugel (2004), the main grain types observed most commonly in ramp type of carbonate platforms are skeletal and non-skeletal grains including ooids, peloids and intraclasts. Smaller foraminifera, sponge spicules, bryozoans, brachiopods and mollusks and echinoderms are

frequently observed primary constituents in outer ramp depositional setting. In shallow inner ramp setting, smaller and larger benthic foraminifera, calcareous green algae, mollusks, ostracods and echinoderms are the most common constituents. In middle ramp and inner ramp settings, these shell fragments are the main components, under the affect of storm and currents. Among the non-skeletal grains, peloids are observed in inner ramp as fecal pellets and mud peloids in outer ramps. Fenestral fabric is common in the back-ramp setting of the ramp model. Packstone and grainstone type microfacies are the part of inner- and middle ramp depositional setting (Flugel, 2004).

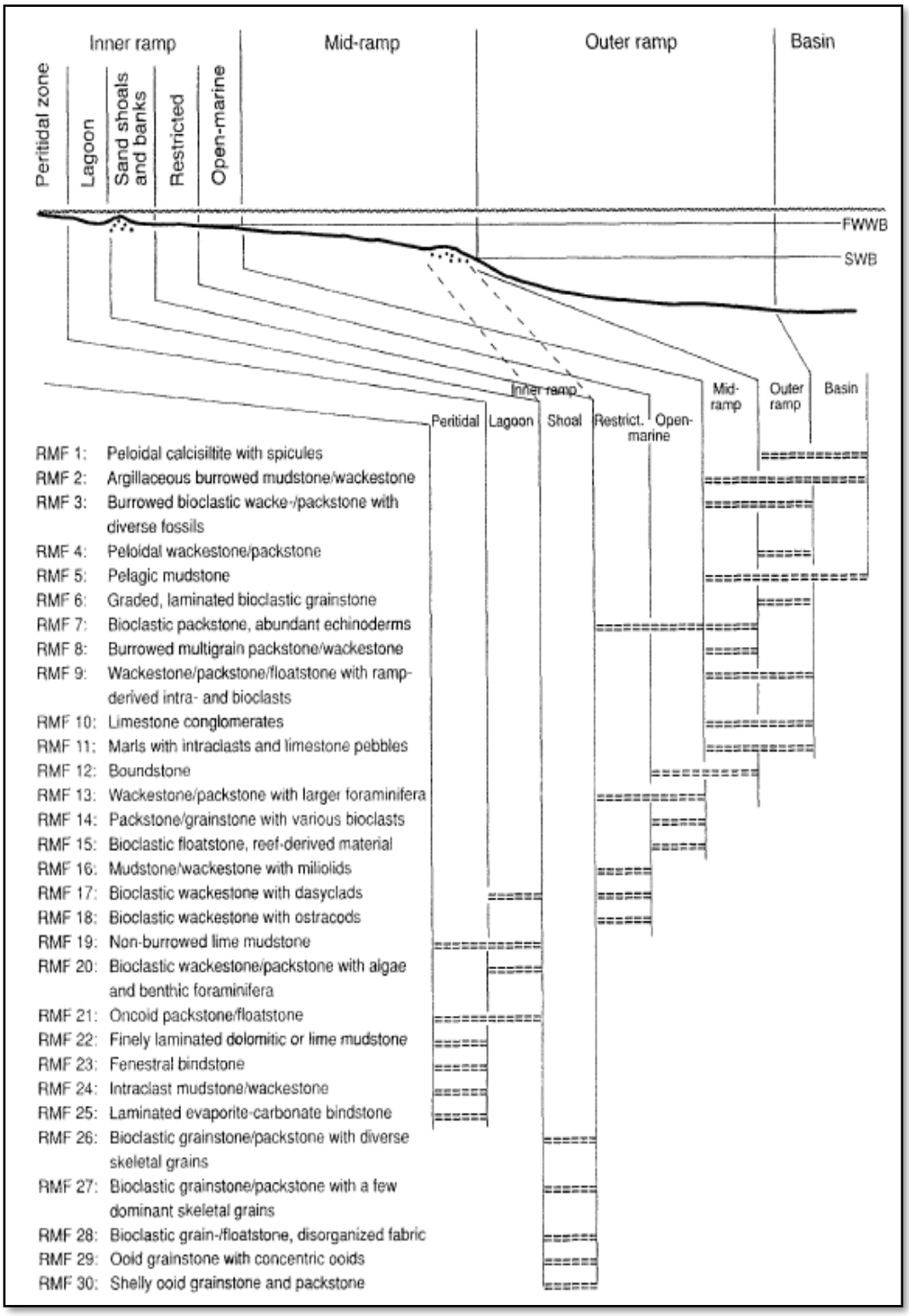


**Figure 31.** Generalized distribution of microfacies types in different parts of a homoclinal carbonate ramp (Flugel, 2004)

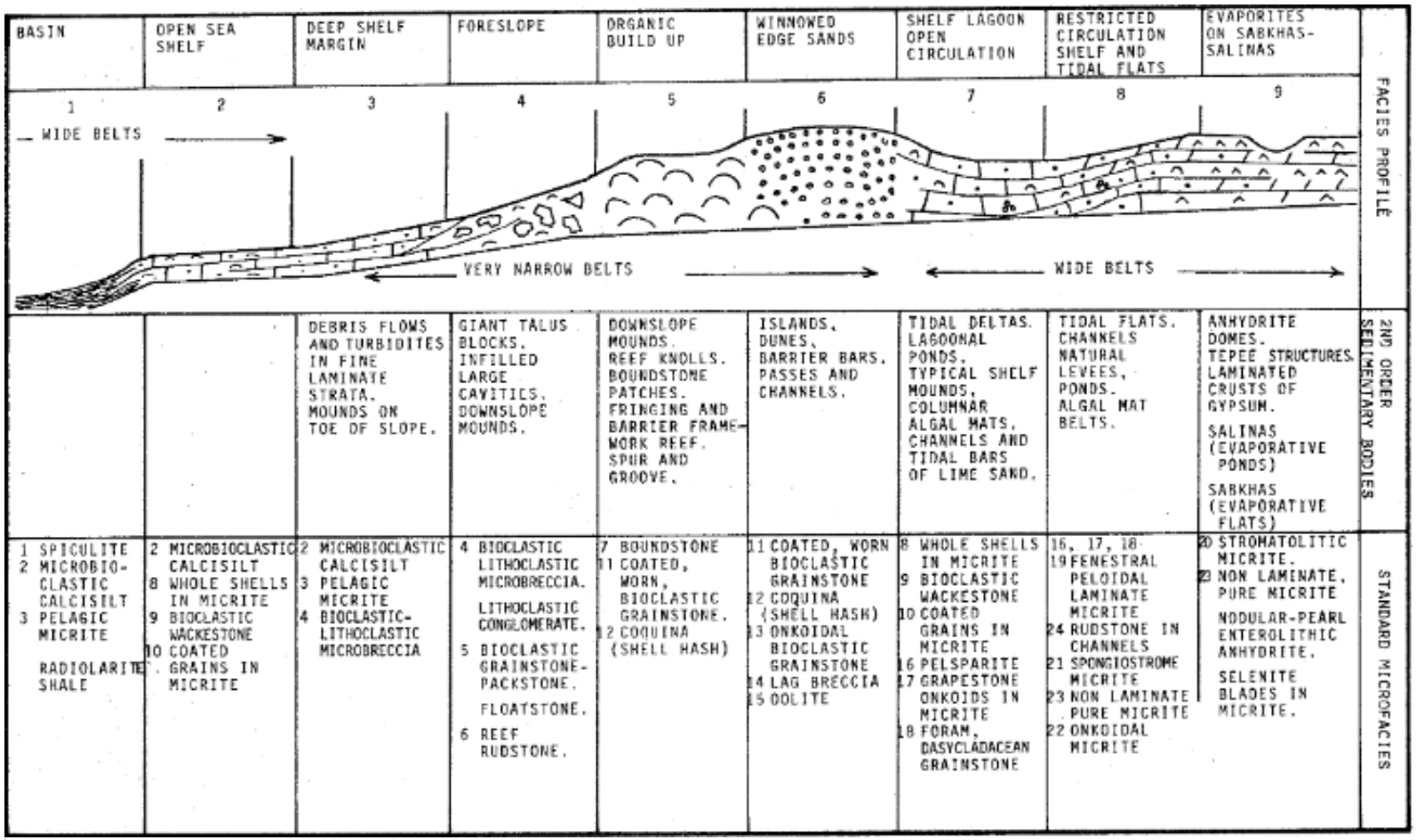


**Figure 32.** Synopsis of standard facies belts reviewing second order bodies of sediment and standard microfacies associated with each belt. After Wilson (1975).

#### 3.2.1.1 Inner Ramp Facies

##### 3.2.1.1.1 Benthic foraminiferal mudstone (MF1)

This microfacies is characterized by limited amount of allochems with bio-origin and micrites. Allochems defined in benthic foraminiferal mudstone are few large benthic foraminifera and small benthic foraminifera (*Cibicides*) and few *Thaumatoporella* type algae (**Figure 33-36**). Primary sedimentary fabrics observed on some of the thin sections are fenestral fabrics (**Figure 37-40**) indicating the deposition on a tidal flat type environment.

This microfacies corresponds to RMF 16 to RMF 23 of carbonate ramp model of Flugel (2004) and it has been interpreted that the deposition of this microfacies is in peritidal to lagoon part of inner ramp depositional setting (**Figure 31**).

In addition to depositional features of the microfacies, most commonly observed diagenetic mechanisms are also considered. One of the main diagenetic processes is partial dolomitization with some scattered rhomdohedral dolomite crystals in the micrite (**Figure 33**). Some of the dispersed rhombohedral dolomite crystals are observed with zoning. Microfractures can also be considered as common diagenetic features and they are mostly filled with calcite cement (**Figure 34** and **Figure 35**).

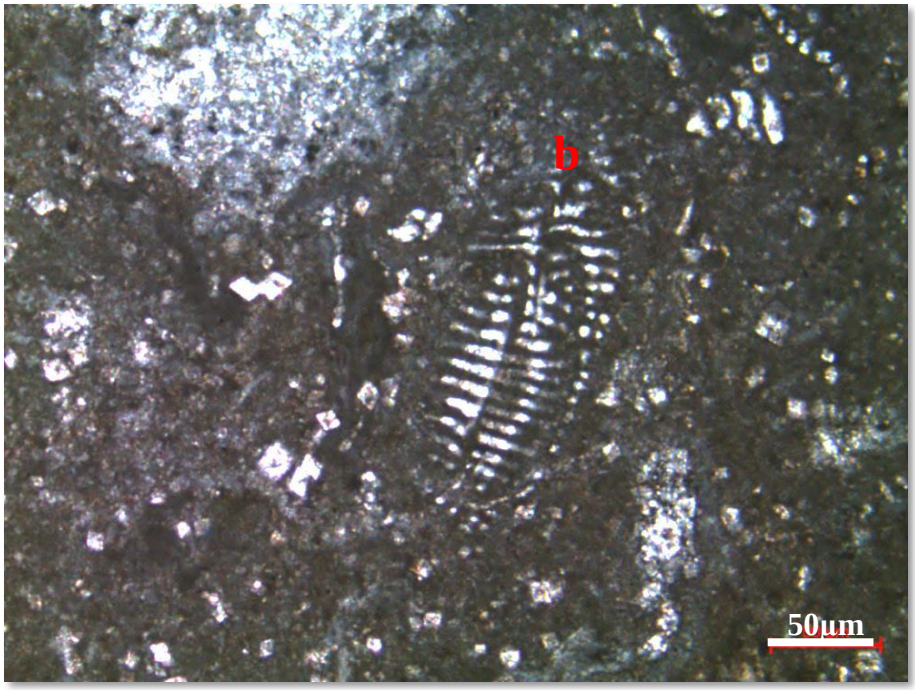


**Figure 33.** Benthic foraminiferal mudstone microfacies from the thin section at 1780.79 m of the K-11 well (b: benthic foraminifera)

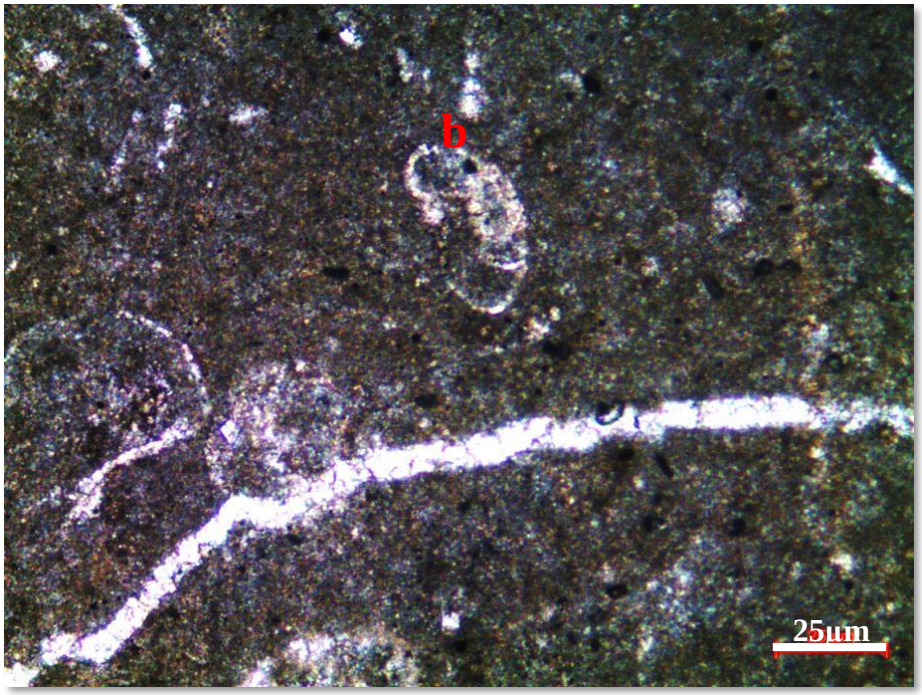


**Figure 34.** Benthic foraminiferal mudstone microfacies from the thin section at 1778.59 m of the K-11 well (b: benthic foraminifera)

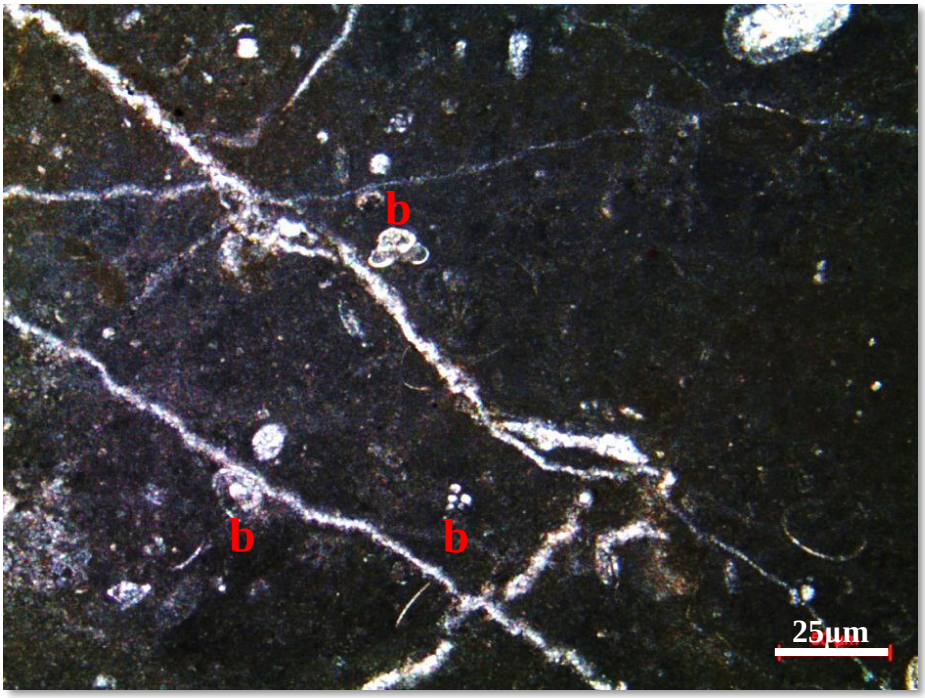


**Figure 35.** Benthic foraminiferal mudstone microfacies from the thin section at 1778.45m of the K-11 well (b: benthic foraminifera)

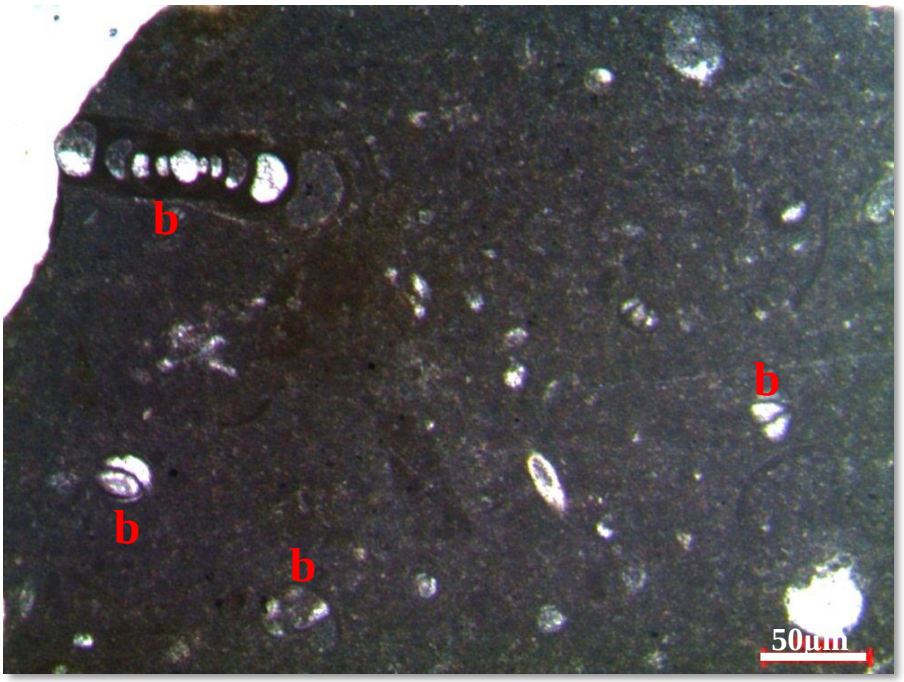


**Figure 36.** Benthic foraminiferal mudstone microfacies from the thin section at 1786 m of K-11 the well (b: benthic foraminifera)

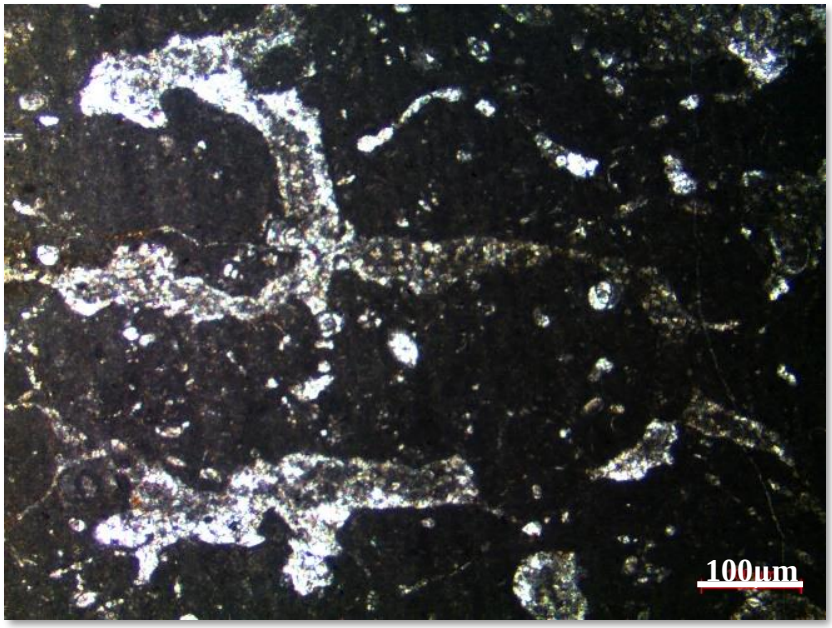


**Figure 37.** Fenestral fabric in benthic foraminiferal mudstone of the peritidal environment of inner ramp setting at 1779.80 m of the K-11 well

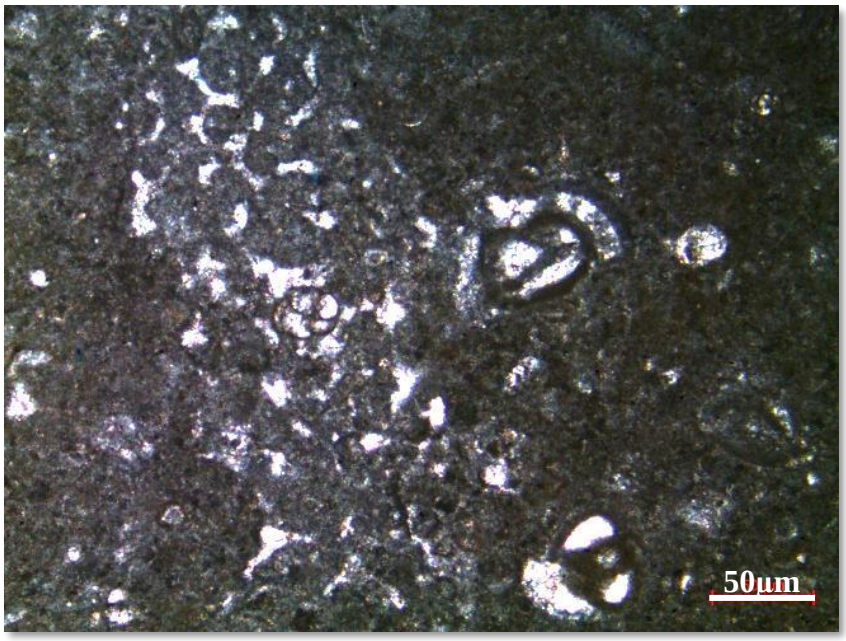


**Figure 38.** Fenestral fabric in benthic foraminiferal mudstone of peritidal environment of inner ramp setting at 1780.79 m of the K-11 well

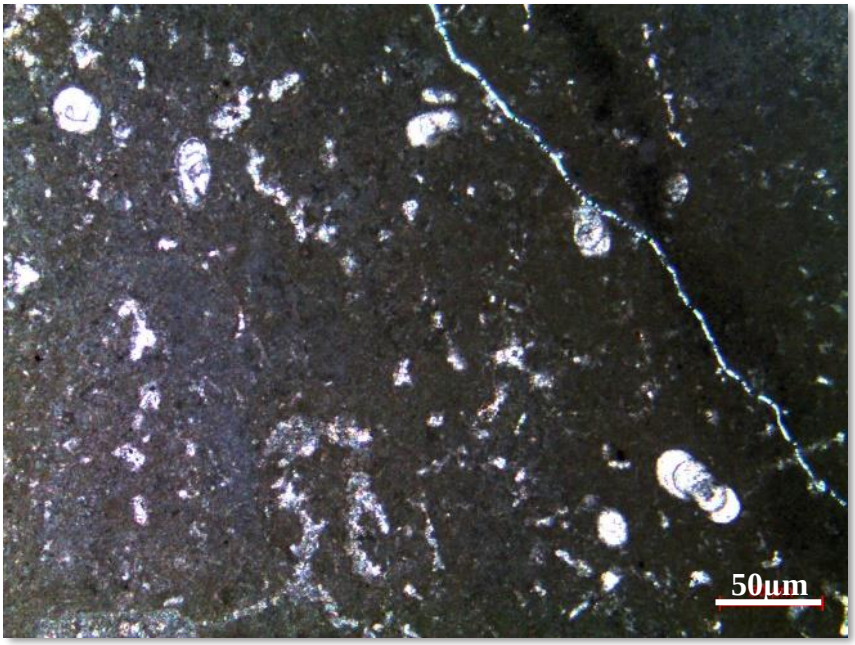


**Figure 39.** Fenestral fabric in benthic foraminiferal mudstone of the peritidal environment of inner ramp setting at 1778.45 m of the K-11 well

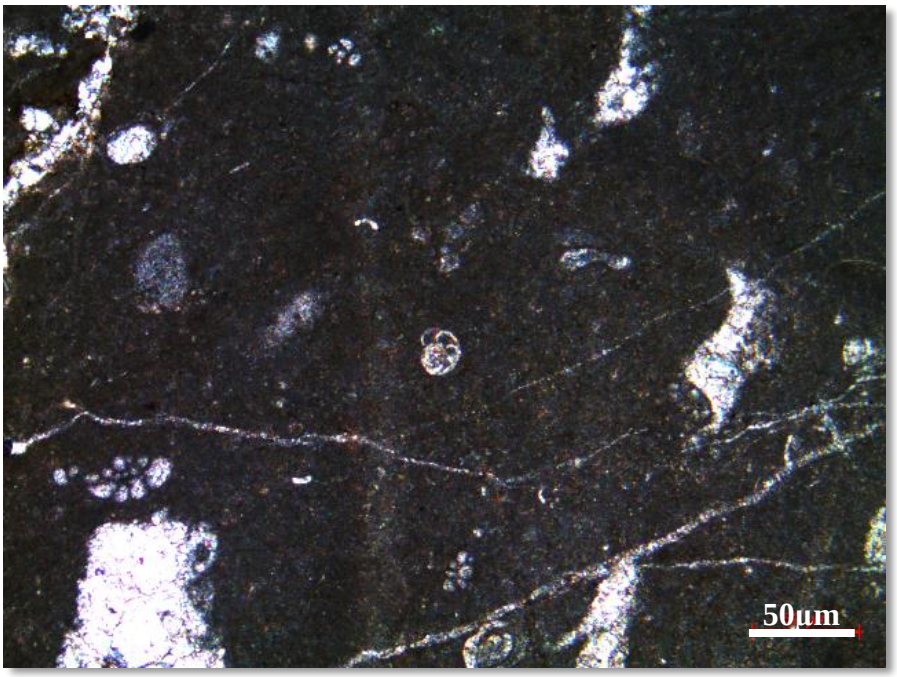


**Figure 40.** Fenestral fabric in bentic foraminiferal mudstone of the peritidal environment of inner ramp setting at 1778.34 m of the K-11 well

#### 3.2.1.1.2 Benthic foraminiferal skeletal mudstone to wackestone (MF2)

This microfacies can be recognized with the presence of benthic foraminifera and large skeletal fragments (**Figure 41** and **Figure 42**). The most common large skeletal fragments observed are rudists and mollusks, bivalves. Based on the compositional similarities it can be concluded that this microfacies corresponds to RMF 20 type microfacies of Flugel (2004) in the carbonate ramp model (**Figure 31**). Hence, benthic foraminiferal skeletal mudstone/wackestone is considered to be deposited in lagoon as a part of inner ramp setting. Additions to depositional features, diagenetic mechanisms are also evaluated. Partial dolomitization, stylolitization, recrystallization are general diagenetic processes recognized in this type of microfacies. Recrystalization observed in the soft parts of skeletal fragments composed of aragonite (**Figure 42**) and authigenic mineral enrichment on the skeletal fragments are frequently defined diagenetic mechanisms.

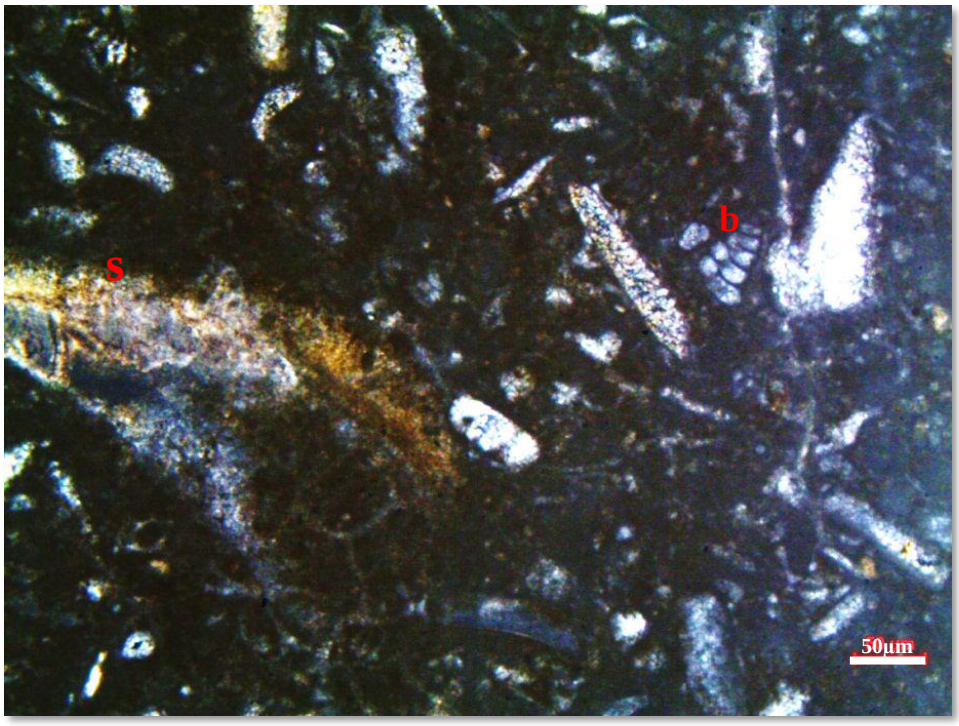


**Figure 41.** Benthic foraminiferal skeletal mudstone to wackestone microfacies from the thin section at 1650.85 m of the K-11 well [b: benthic foraminifera; s: diagenetically altered skeletal fragment (oyster)]

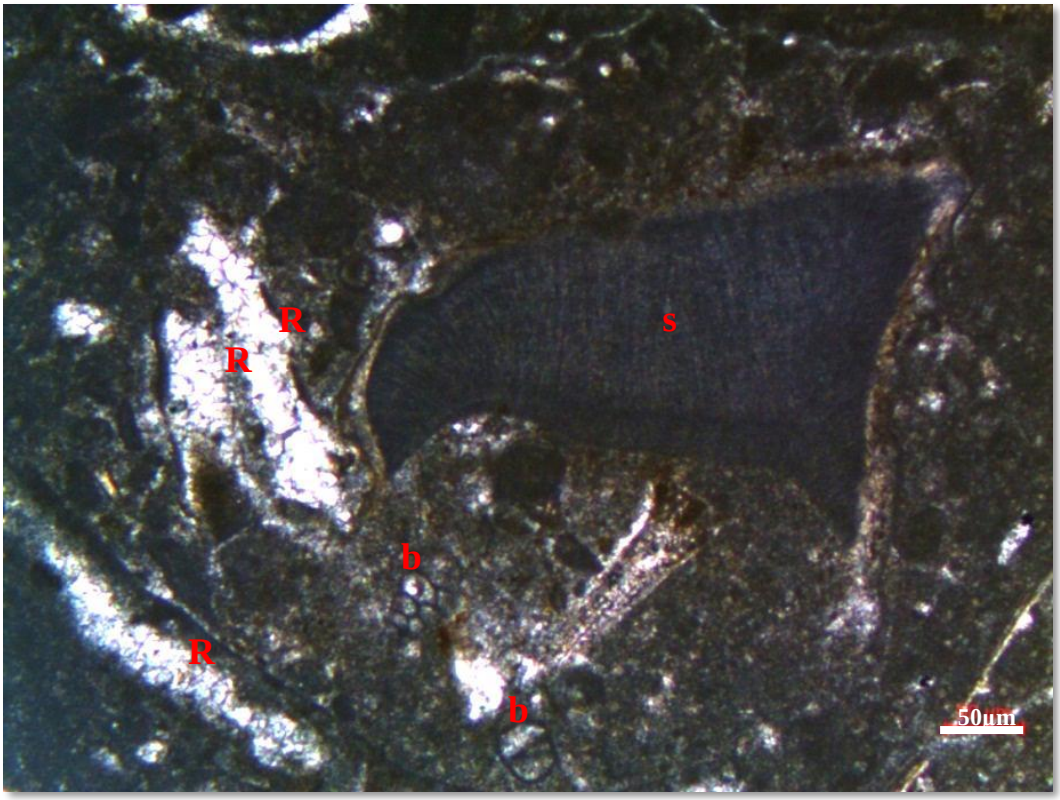


**Figure 42.** Benthic foraminiferal skeletal mudstone to wackestone microfacies from the thin section at 1651.07 m of K-11 well (b: benthic foraminifera; s: undefined skeletal fragment; R: recrystallization of the soft parts of the skeletal fragments)

#### 3.2.1.1.3 Benthic foraminiferal skeletal peloidal packstone to grainstone (MF3)

This microfacies type is characterized by the presence of both micrite and sparry calcite cement with the pronounced amount of bioclasts. The large benthic foraminifera, small benthic foraminifera and large mollusk fragments and echinoderm fragments are the most common allochems defined in the benthic foraminiferal skeletal peloidal packstone to grainstone. Peloids are the most abundant allochem in this microfacies (**Figure 43-46**).

When similar primary constituents are considered, this microfacies corresponds to RMF 14 and RMF 27 of carbonate ramp model of Flugel (2004). This microfacies

are the part of open-marine to sand shoals and banks part of inner ramp setting of homoclinal carbonate ramp of Flugel (2004) (**Figure 31**).

Local dolomitization of peloidal microfacies is observed in some samples. Recrystallization of inner parts of skeletal fragments, micritic envelope around the skeletal fragments, silicification and syntaxial cementation around echinoderm fragments are common diagenetic features identified on thin sections (**Figure 46**). Similar diagenetic processes are observed in the study of Taghavi et. al. (2006), which discusses the sequence stratigraphic control on diagenesis of the carbonate Dehluran Field, Iran.

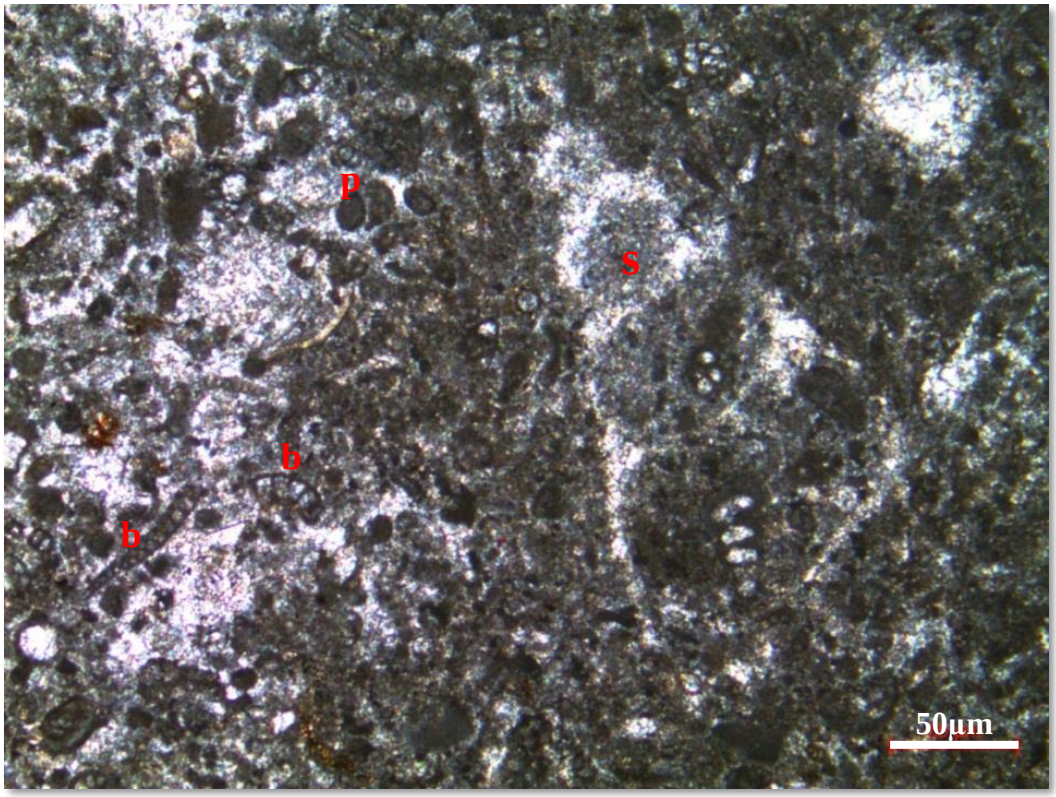


**Figure 43.** Benthic foraminiferal skeletal peloidal packstone/grainstone microfacies from the thin section at 1777.77 m of the K-11 well (b: benthic foraminifera; s: skeletal fragment (gastrod); p: peloid)

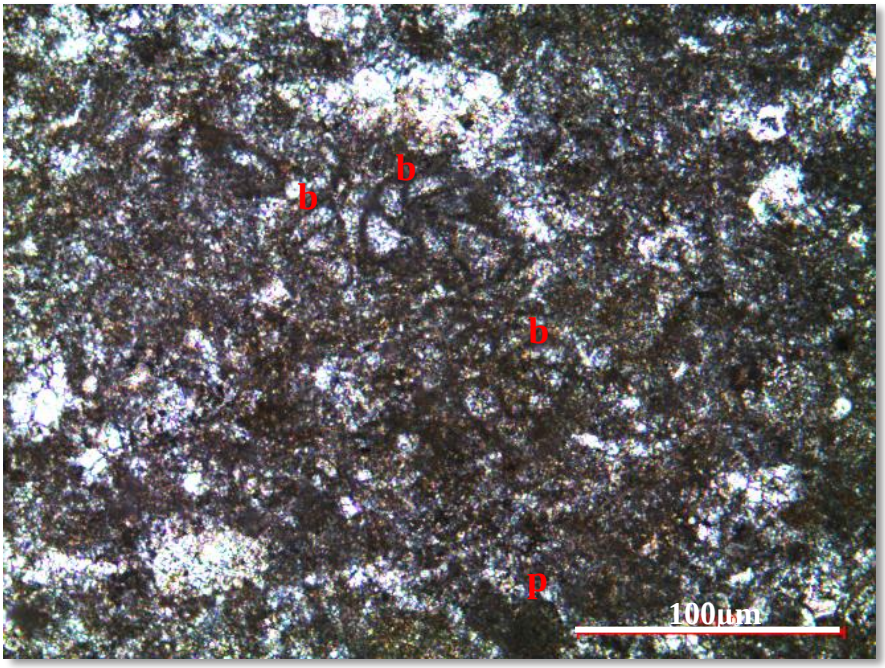


**Figure 44.** Benthic foraminiferal skeletal peloidal packstone/grainstone microfacies from the thin section at 1767.39 m of the K-11 well (b: benthic foraminifera; p: peloid)

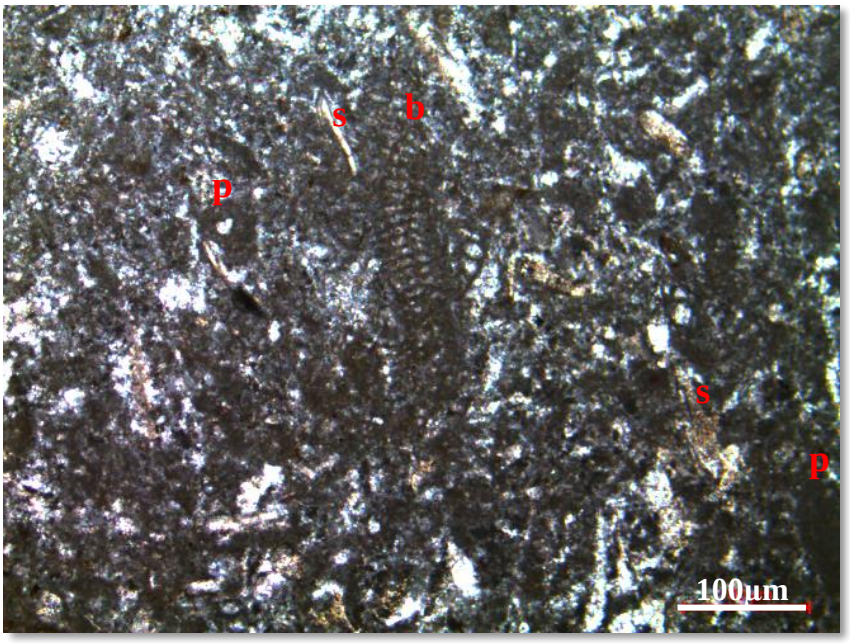


**Figure 45.** Benthic foraminiferal skeletal peloidal packstone/grainstone microfacies from the thin section at 1767.43 m of the K-11 well (b: benthic foraminifera; s: skeletal fragment; p: peloid)

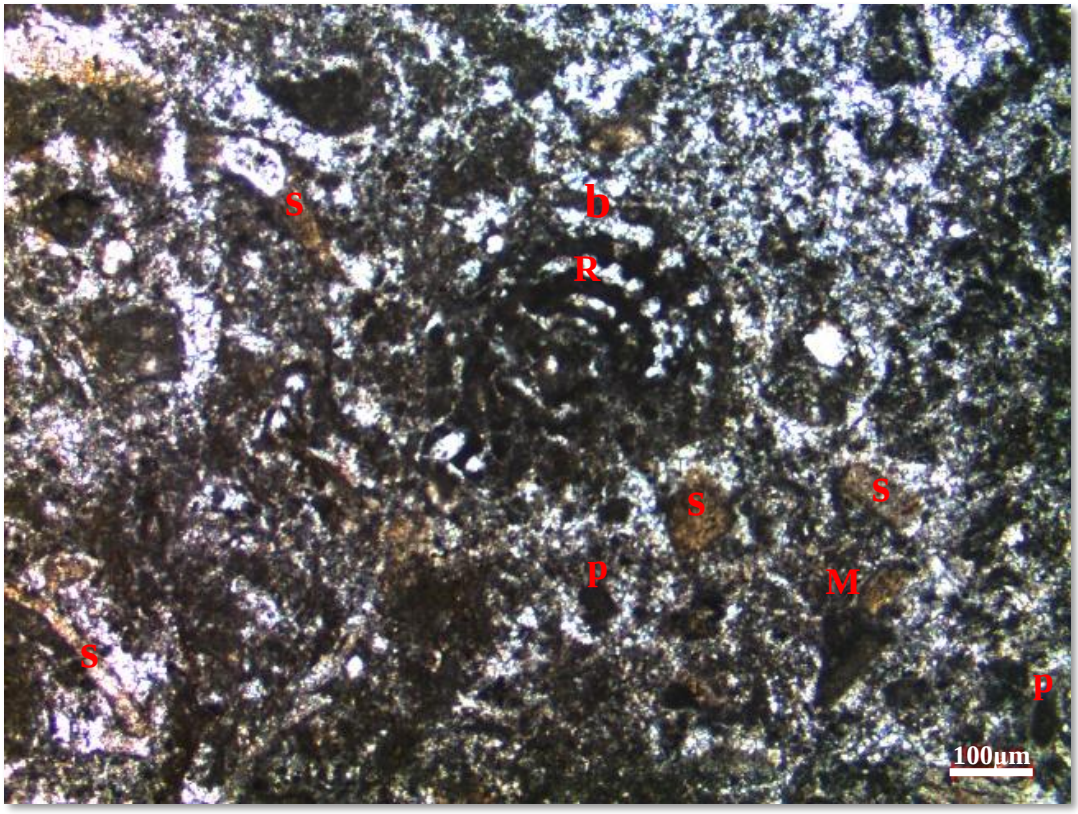


**Figure 46.** Benthic foraminiferal skeletal peloidal packstone/grainstone microfacies from the thin section at 1771.01 m of the K-11 well (b: benthic foraminifera; s: skeletal fragment; p: peloid; R: recrystallization of the soft parts; M: micritic envelope at around the skeletal fragments)

#### 3.2.1.1.4 Skeletal peloidal packstone to grainstone (MF4)

This microfacies is characterized by skeletal fragments including oyster (pycnodontinae), echinoderm, gastropods and inoceramid, abundance of peloids and micrite and sparry calcite cement. Intraclasts and benthic foraminifers are rarely identified in this type of microfacies. Benthic foraminifers are in limited amount (quantitatively one or two in a thin section) and with low diversity; that is why these allochems are not used for naming.

Based on the compositional similarities, skeletal peloidal packstone to grainstone microfacies can be considered as the equivalent of RMF 14 and RMF 26 of the model of Flugel (2004) (**Figure 31**) and they correspond to open marine to shoal part of the inner ramp setting of homoclinal carbonate ramp.

In addition to depositional features, recrystallization, fracturing, stylolization and dolomitization type diagenetic mechanisms are commonly observed. Recrystallization is intensely observed on some of the skeletal fragments. Thin fractures are mostly filled with calcite cement. Some dissolution vugs are also identified in the matrix (**Figure 47** and **Figure 48**). Due to intense recrystallization, most of the skeletal fragments remained undefined (**Figure 48**). Syntaxial cementation and micritic envelope formation at around the echinoderm fragments are also frequently observed (**Figure 49**) Taghavi et. al (2006) also states same diagenetic mechanisms in the Sarvak Formation, southwest Iran during late Albian to early Turonian.

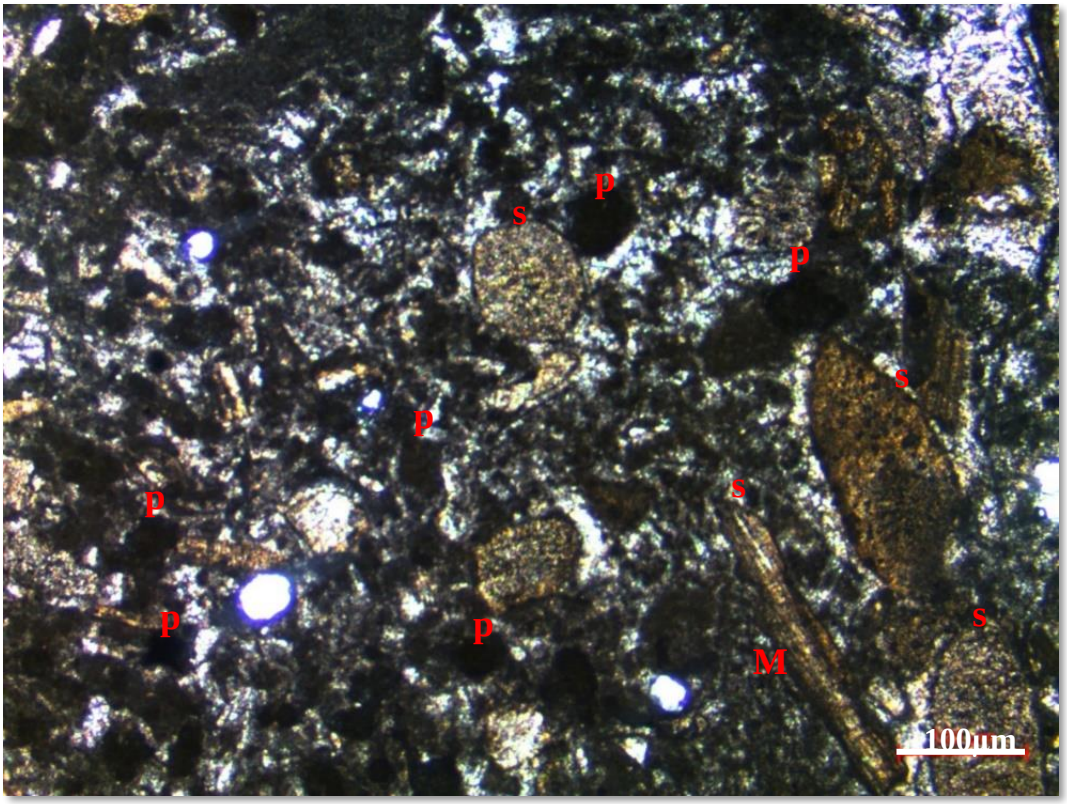


**Figure 47.** Skeletal peloidal packstone to grainstone microfacies from the thin section at 1773.35 m of the K-11 well (s: skeletal fragments; p: peloid; M: micritic envelope)

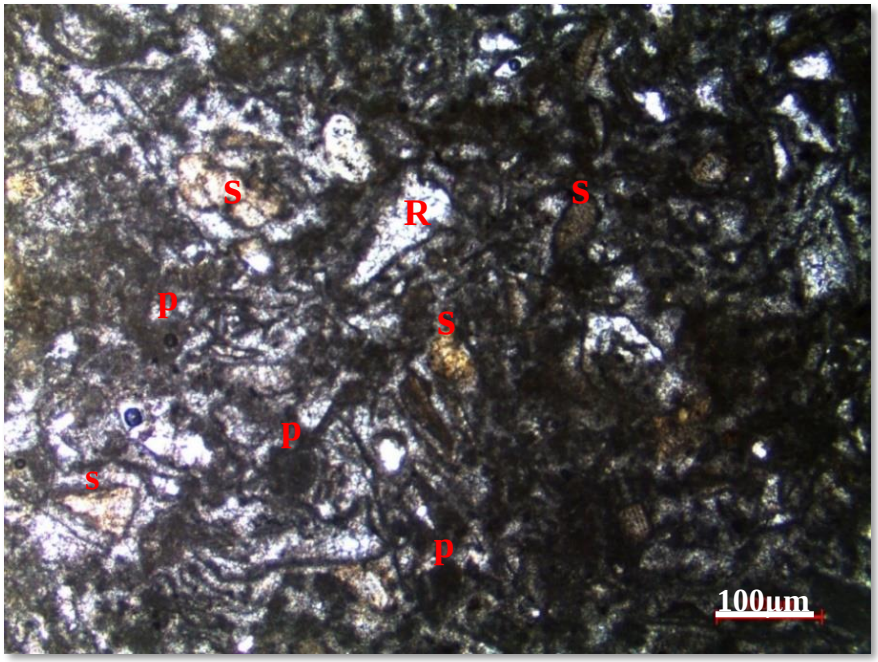


**Figure 48.** Skeletal peloidal packstone to grainstone microfacies from the thin section at 1772.17 m of the K-11 well (s: skeletal fragments; R: recrystallized skeletal fragment; p: peloid)

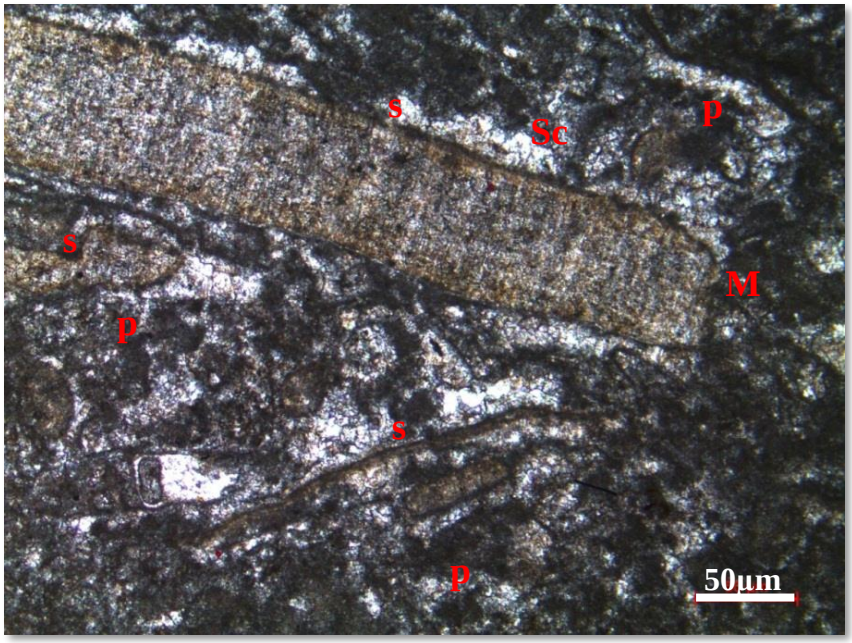


**Figure 49.** Skeletal peloidal packstone to grainstone microfacies from the thin section at 1771.65 m of the K-11 well (s: skeletal fragments; p: peloid; M: micritic envelope; Sc: syntaxial cementation).

#### 3.2.1.2 Proximal Middle Ramp Facies

##### 3.2.1.2.1 Peloidal skeletal wackestone to packstone (MF5)

This microfacies is characterized by the presence of peloids, mollusk fragments, bivalves and brachiopods as bio-allochems in the micrite dominated matrix and partially blocky calcite cement (**Figure 50-52**). In addition to these skeletal and peloid type non-skeletal fragments, rarely benthic foraminifera is identified in this type of microfacies. Mostly formation of these peloids is associated with the microbial activity or reworking of micritic carbonate grains (mud peloids) and biotic activities (fecal pellets) (Flugel, 2004).

This microfacies corresponds to RMF 9 type microfacies of Flugel (2004) and it has ben interpreted that the deposition occurs in the middle ramp depositional setting in the study of Flugel (2004) (**Figure 31**). Similarly, peloidal skeletal wacsktone to packstone is considered as the part of proximal middle ramp.

Recrystallization, cementation, fracturing, and stylolization are the most common diagenetic mechanisms observed in this type of microfacies. Blocky sparry calcite cement is recognized in the matrix (**Figure 50**). Recrystallization is intensely observed on some of the skeletal fragments (**Figure 51** and **Figure 52**). Stylolitization at around the skeletal fragment (**Figure 52**) and some unknown authigenic mineral development are also identified on the skeletal fragments. Blocky sparry calcite cement, recrystallization, stylolitization and fracturing type diagenetic mechanisms are also discussed in the Sarvak Formation which can be considered as the equivalent of the Derdere Formation (Taghavi et. al. (2006)).

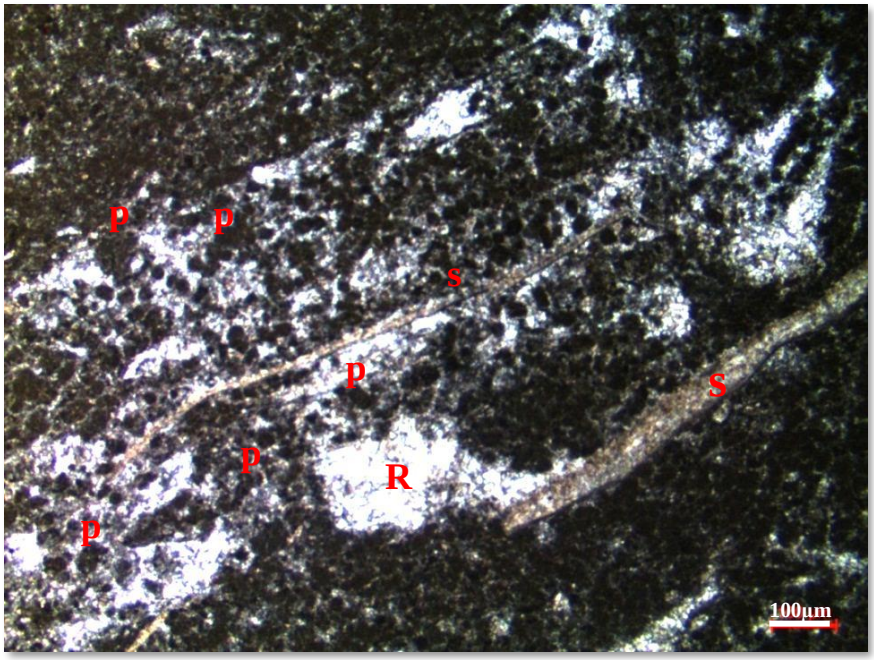


**Figure 50.** Peloidal skeletal packstone microfacies from the thin section at 1765.08 m of the K-11 well [p: peloid; s: skeletal fragments (possible brachiopod); R: Recrystallization]

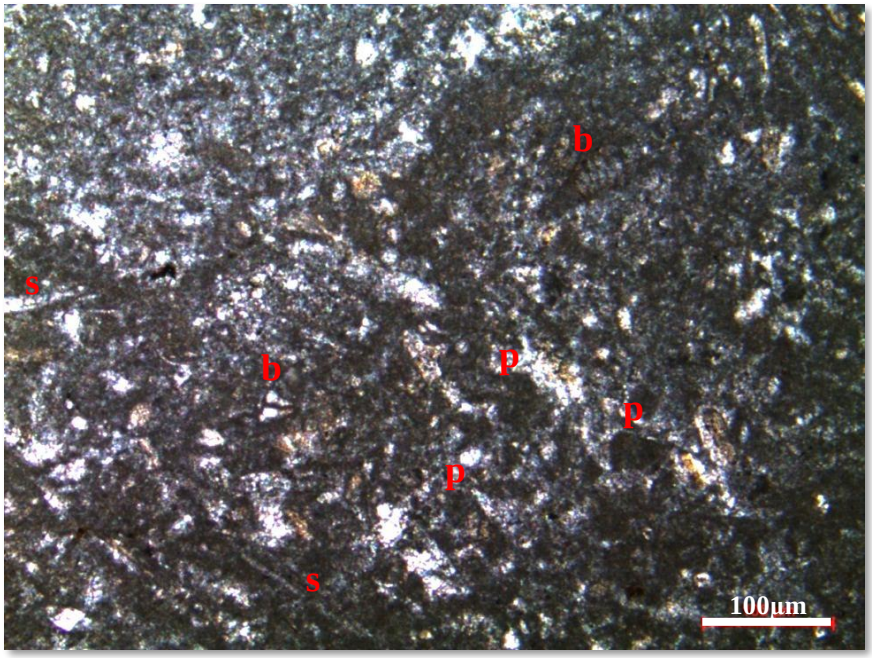


**Figure 51**. Peloidal skeletal packstone microfacies from the thin section at 1765.84 m of the K-11 well [p: peloid; s: skeletal fragments; b: benthic foraminifera (rare)]

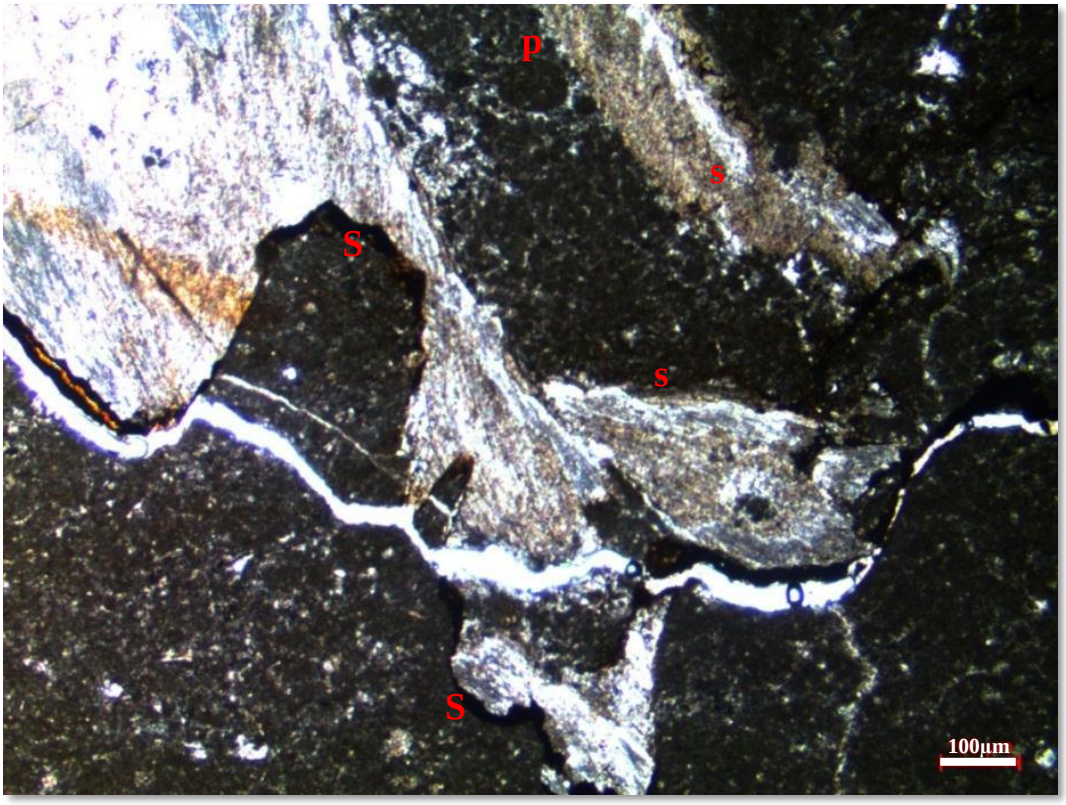


**Figure 52.** Peloidal skeletal wackestone microfacies from the thin section samples of 1764.89 m of the K-11 well [p: peloid; s: skeletal fragments (possible rudist); S: stylolitization at around skeletal fragment]

#### 3.2.1.2.2 Skeletal wackestone (MF6)

This microfacies is commonly observed with brachiopods and thin walled mollusk fragments such as bivalves (pelecypods) in the micrite dominated matrix (**Figure 53** and **Figure 54**). "*Saccocoma"*-like crinoids are other skeletal fragments recognized in thin section (**Figure 54**). Benthic foraminifera can also be identified rarely in this kind of microfacies. RMF 3 and RMF 9 of Flugel (2004) is the most similar microfacies to skeletal wackestone (MF6) defined in this study in terms of presence of bioclasts and dominance of micrite in the matrix (**Figure 31**).

RMF 3 and RMF 9 are deposited in the middle ramp setting according to Flugel (2004) similar to the depositional environment of skeletal wackestone type microfacies which is interpreted to be deposited in the proximal middle ramp setting. Thin fractures and stylolites are present on thin sections. Dispersed

euhedral dolomite crystals (**Figure 53** and **Figure 54**) are observed in the matrix between the skeletal fragments as a product of partial dolomitization and opaque mineral development are recognized around some grains.

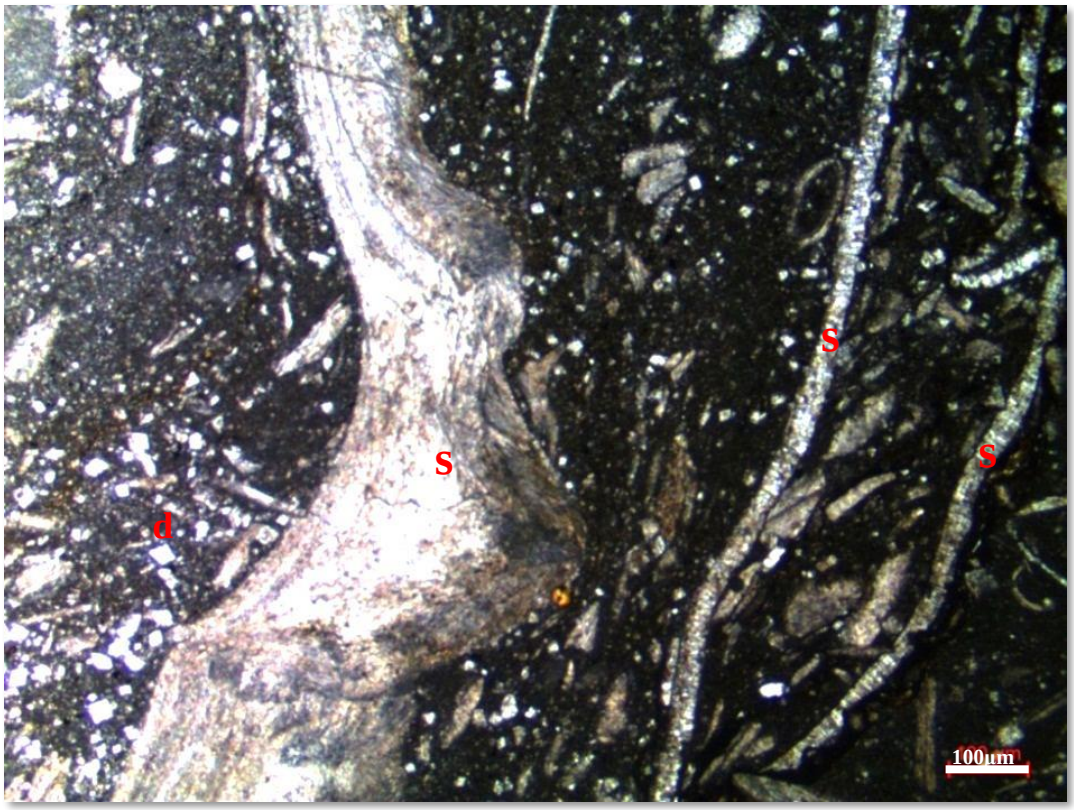


**Figure 53.** Skeletal wackestone microfacies from the thin section at 1764.54 m of the K-11 well (s: skeletal fragments (brachiopod); d: dolomite crystal)

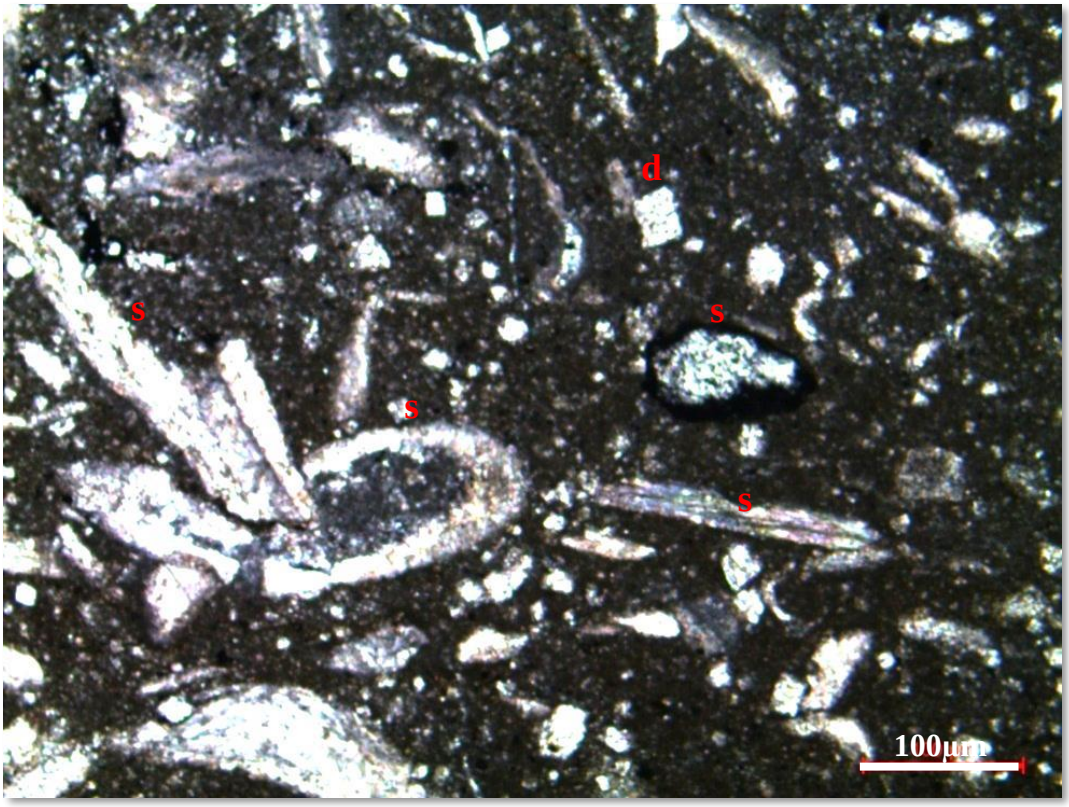


**Figure 54.** Skeletal wackestone microfacies from the thin section at 1764.57 m of the K-11 well [s: skeletal fragments (possible "*Saccocoma"*); d: dolomite crystal]

### 3.2.1.3 Distal Middle Ramp Facies

#### 3.2.1.3.1 Skeletal calcisphaerulid-bearing planktonic foraminiferal wackestone to packstone (MF7)

This microfacies is characterized by abundant bio-allochems in the micrite dominated matrix. Most of the allochems are fossil fragments including echinoderms and pelecypod-like thin walled mollusks. Planktonic foraminifera are the most common constituent of this microfacies (**Figure 55-57**). *Pithonella spherica* type calcisphaerulids are also observed (**Figure 56**). Phosphate fragments are the other constituent observed in MF7. This microfacies of the Derdere Formation is considered as pelagic.

RMF3 microfacies of Flugel (2004), which is the most similar microfacies to skeletal calcisphaerulid-bearing planktonic foraminiferal wackestone to packstone (MF7), deposited in the middle ramp setting of Flugel (2004) (**Figure 31**). The depositional environment of MF7 is also interpreted as distal part of middle ramp.

This microfacies is observed as partially dolomitized with scattered dolomite crystals in the matrix (**Figure 58**). Euhedral dolomite crystals replace planktonic foraminifera at some part of the thin sections. Cementation of thin fractures is identified mostly on thin sections. Some bivalve type mollusks are not well-preserved and they are broken due to compaction (**Figure 58**).

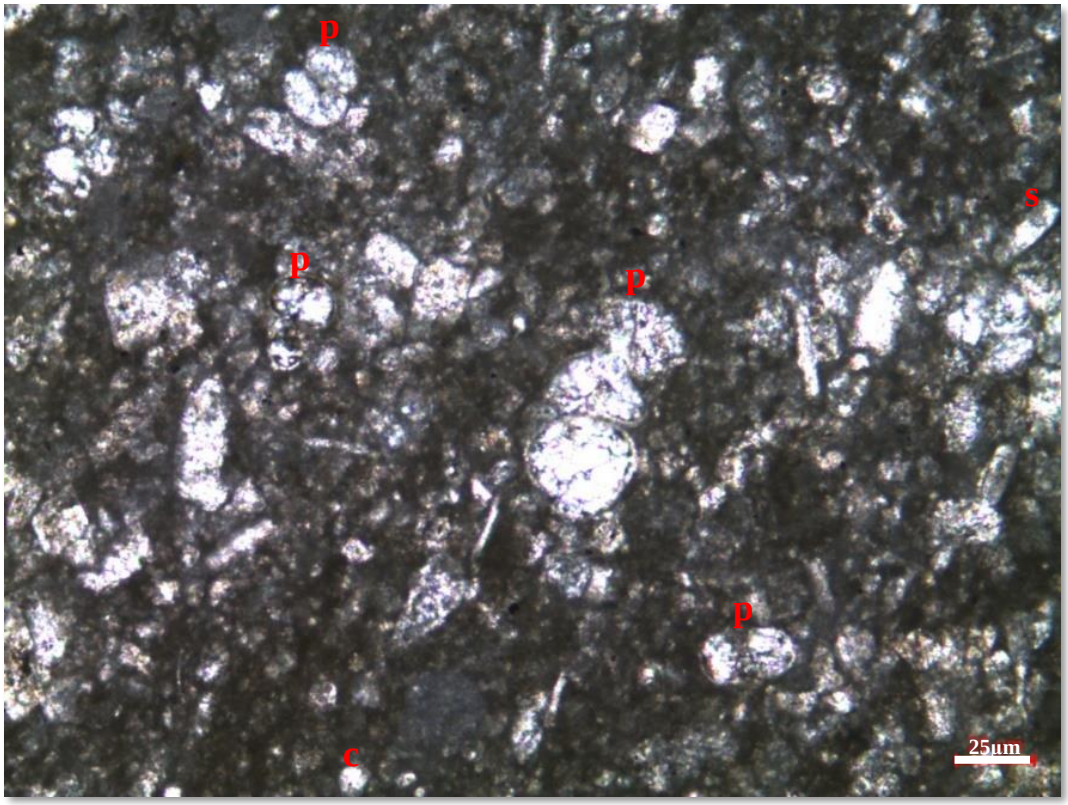


**Figure 55.** Skeletal calcisphaerulid-bearing planktonic foraminiferal wackestone/packstone microfacies from the thin section at 1694.55 m of the K-11 well (s: skeletal fragments; c: calcisphaerulid (*Pithonella spherica*); p: planktonic foraminifer)

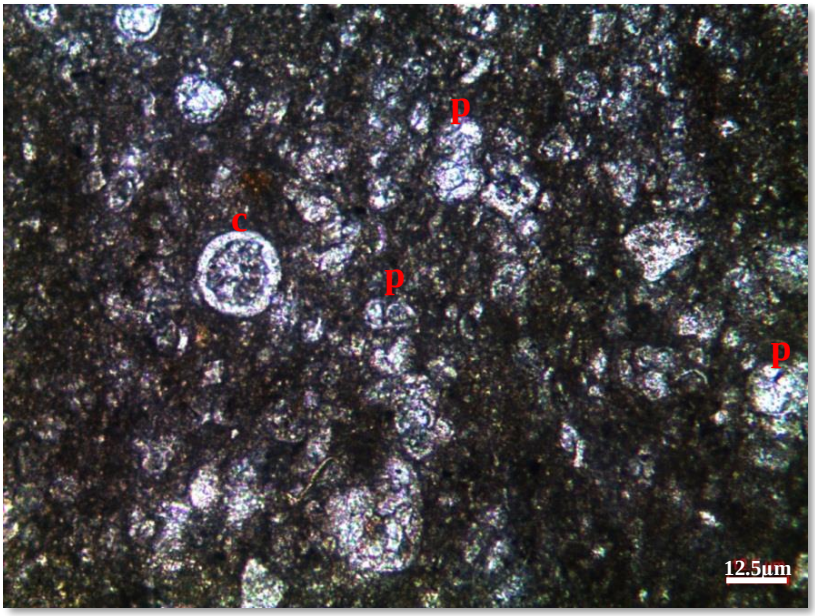


**Figure 56.** Skeletal calcisphaerulid-bearing planktonic foraminiferal wackestone to packstone microfacies from the thin section at 1695.03 m of the K-11 well (s: skeletal fragments; c: calcisphaerulid (*Pithonella spherica*); p: planktonic foraminifer)

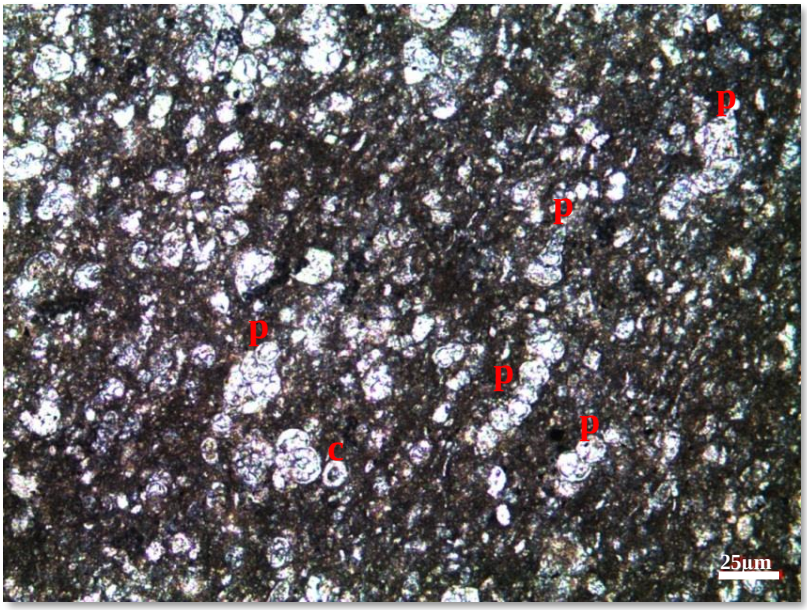


**Figure 57.** Skeletal calcisphaerulid-bearing planktonic foraminiferal wackestone to packstone microfacies from the thin section at 1695.09 m of the K-11 well (c: calcisphaerulid (partially compacted *Pithonella spherica*; p: planktonic foraminifer)

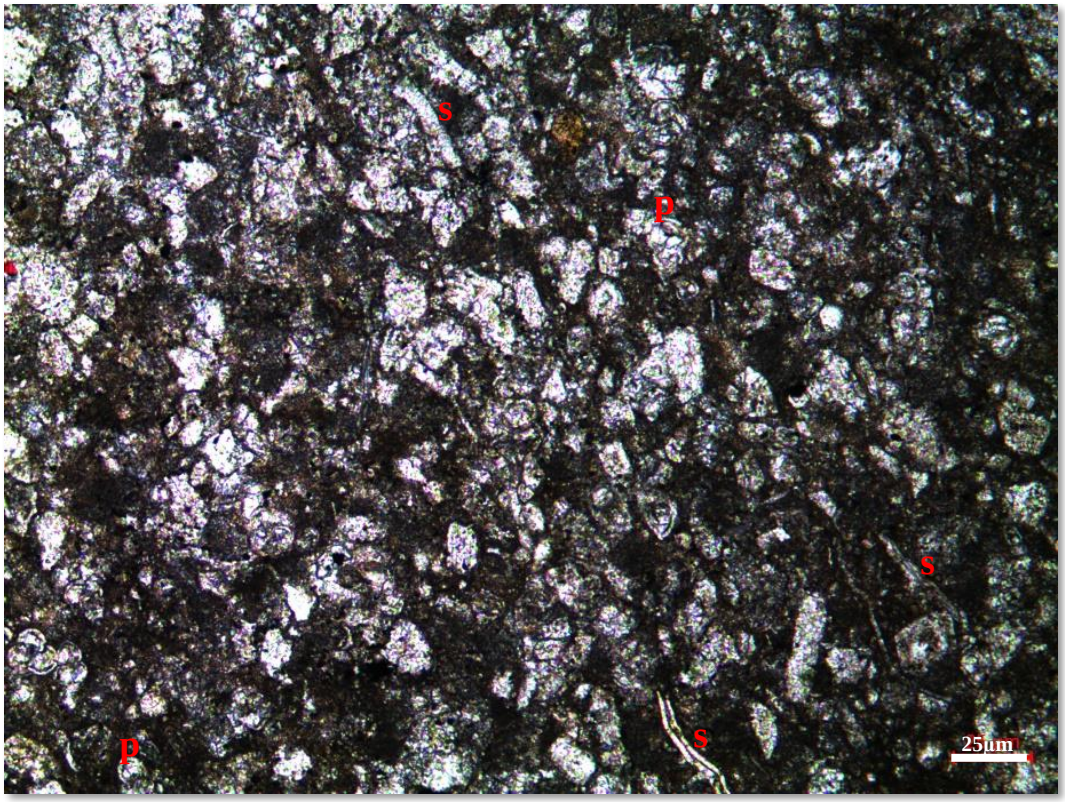


**Figure 58.** Skeletal calcisphaerulid-bearing planktonic foraminiferal wackestone to packstone microfacies from the thin section at 1695.09 m of the K-11 Well (s: skeletal fragment (broken pelecypod due to compaction); p: planktonic foraminifer)

#### 3.2.1.3.2 Skeletal planktonic foraminiferal calcisphaerulid-bearing wackestone to packstone (MF8)

This microfacies can be recognized with abundant calcisphaerulids, presence of planktonic foraminifera and rarely echinoderms, mollusks, and few brachiopods type skeletal fragments as bioclastic content in micritic background (**Figure 59-61**). Among the calcisphaerulids, the most frequently *Pithonella spherica* (**Figure 59**) and sometimes *Pithonella ovalis* (**Figure 60**) are identified. Some phosphate fragments, which can be fish teeth/bone, are also recognized in the sections (**Figure 61**). This microfacies of the Derdere Formation is also pelagic and the difference between MF7 and MF8 is the relative abundances of calcisphaerulids and planktonic foraminifera. Based on the compositional similarities it can be

interpreted that microfacies is quite similar to RMF3 of Flugel (2004) which is considered to be deposited in the middle ramp setting of carbonate ramp model of Flugel (2004) (**Figure 31**). The depositional environment of MF8 is defined as the most distal part of the middle ramp setting.

This microfacies is partially dolomitized in some levels of the core. Some stylolites and thin fractures are other diagenetic features identified in thin sections. Thin fractures are mostly filled with calcite cement. Bivalves are mostly broken due to physical diagenesis (compaction) (**Figure 60**). Opaque mineral enrichment is commonly observed in the matrix and inside the pore spaces of calcisphaerulids and planktonic foraminifera as cement (**Figure 59**).

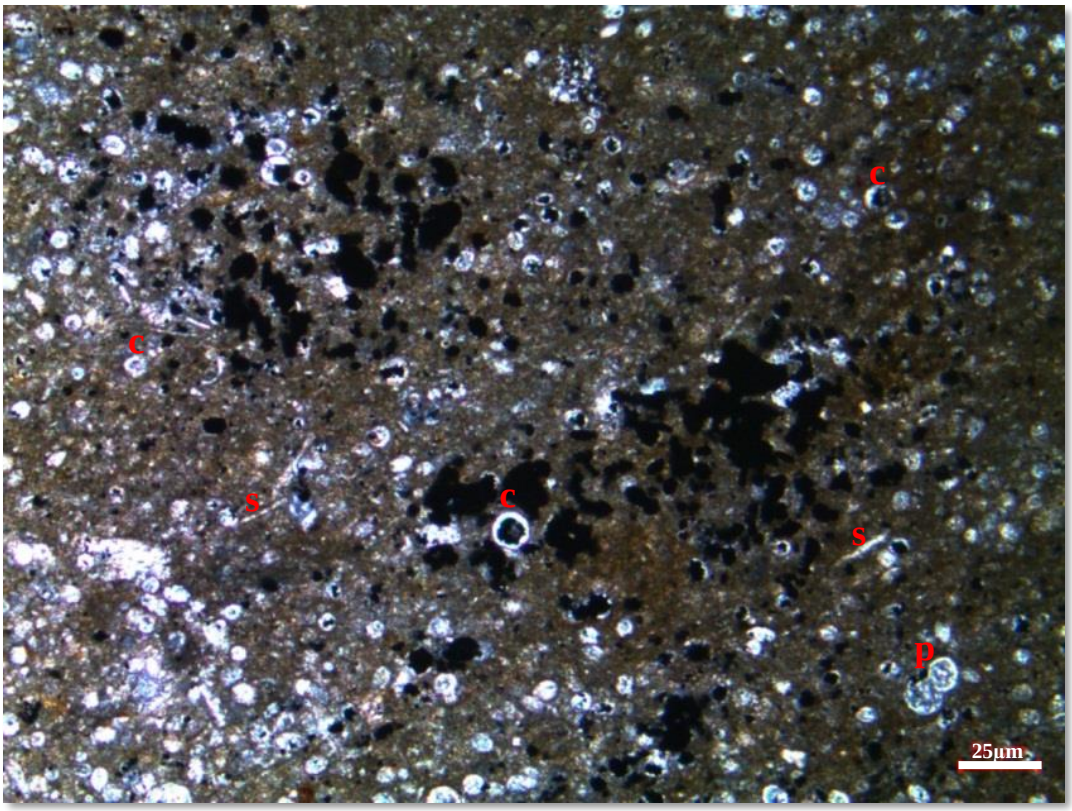


**Figure 59.** Skeletal planktonic foraminiferal calcisphaerulid-bearing wackestone to packstone microfacies from the thin section at 1719.06 m of the K-11 well [s: skeletal fragments; p: planktonic foraminifers; c: calcisphaerulid (*Pithonella spherica*)]

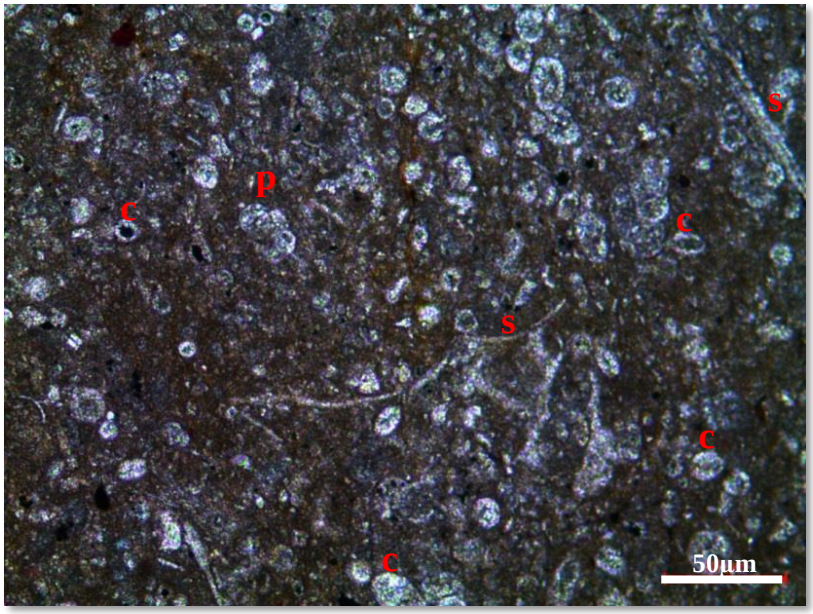


**Figure 60.** Skeletal planktonic foraminiferal calcisphaerulid-bearing wackestone to packstone microfacies from the thin section at 1721.05 m of the K-11 well [s: skeletal fragments (broken bivalves); p: planktonic foraminifers; c: calcisphaerulids (*Pithonella ovalis)*]

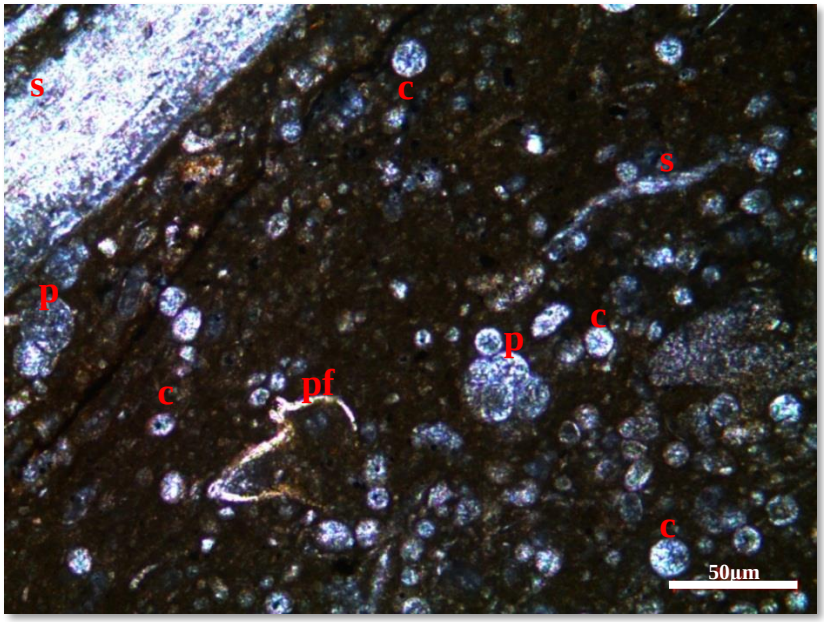


**Figure 61**. Skeletal planktonic foraminiferal calcisphaerulid-bearing wackestone to packstone microfacies from the thin section at 1721.16 m of the K-11 well (pf: phosphate fragment; s: skeletal fragments; p: planktonic foraminifers; c: calcisphaerulids (*Pithonella spherica*)

#### 3.2.1.3.3 Calcisphaerulid-bearing skeletal wackestone to packstone (MF9)

This microfacies is characterized commonly by abundant bioclast content in the micrite matrix. Sponge spicules and "*Saccocoma"*-like crinoids, mostly *Pithonella spherica* and *Pithonella ovalis* type calcisphaerulids are the fossil allochems and they are the indicator of open water depositional setting (**Figure 62-64**) in this study. "*Saccocoma"* is the planktonic crinoids and sometimes rock-forming constituents of pelagic carbonates (Flugel, 2004). The microfacies with "*Saccocoma"* type crinoids are characteristic for late transgressive system tract and highstand deposits and it is common in deep-marine basinal sequences (Matyszkiewicz, 1996; Flugel, 2004). Small benthic foraminifera are another component observed rarely in this microfacies.

RMF2 and RMF3 of carbonate ramp model of Flugel (2004) are considered as the most similar microfacies to MF9 in terms of compositional similarities. In the model of Flugel (2004), RMF2 and RMF3 type of microfacies has been deposited in the middle ramp to outer ramp depositional setting (**Figure 31**). The depositional environment of this type of microfacies is interpreted as distal part of middle ramp.

Recrystallization of "*Saccocom*a"-like skeletal fragments, fracturing, stylolization and dolomitization are the most commonly observed diagenetic mechanisms. Thin fractures, which are mostly filled with calcite cement, and some stylolites are also other diagenetic features. Local dolomitization is also observed as dispersed euhedral rhombohedral dolomite crystals [idiotopic (Flugel, 2004)].

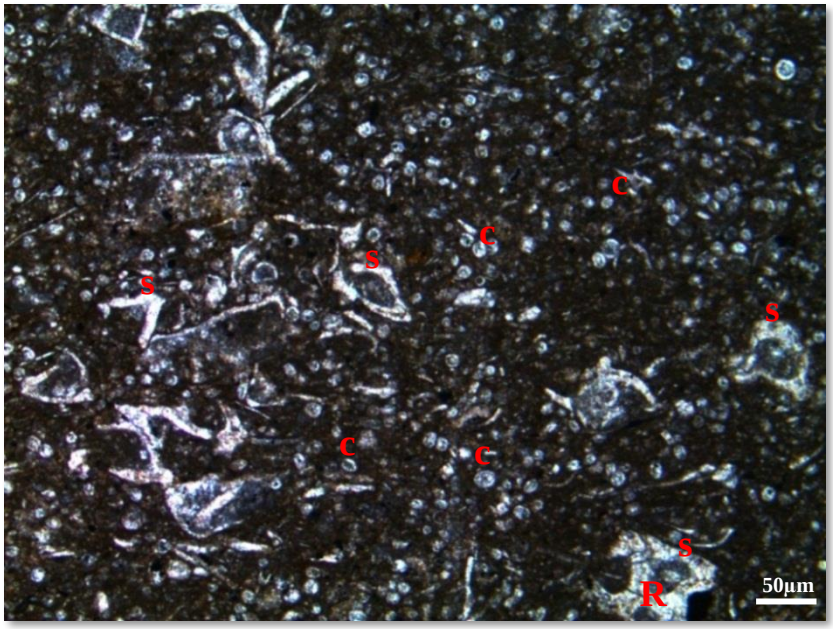


**Figure 62.** Calcisphaerulid-bearing skeletal wackestone/packstone microfacies from the thin section samples of 1720.21 m of K-11 well (c: calcisphaerulid (*Pithonella spherica*; s: skeletal fragments (*Saccocoma*); R: Recrystallization)

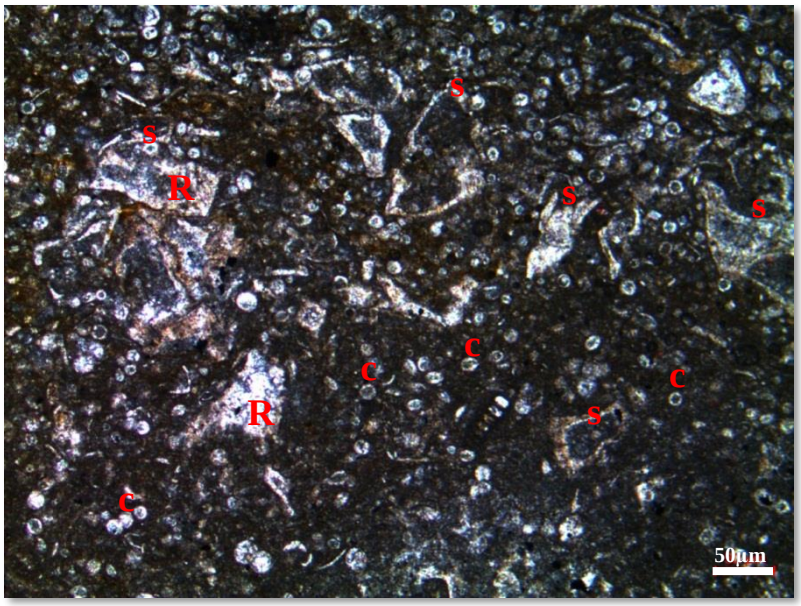


**Figure 63.** Calcisphaerulid-bearing skeletal wackestone to packstone microfacies from the thin section at 1720.27 m of the K-11 well [c: calcisphaerulid (*Pithonella spherica*); s: skeletal fragments (*Saccocoma*); R: recrystallization]

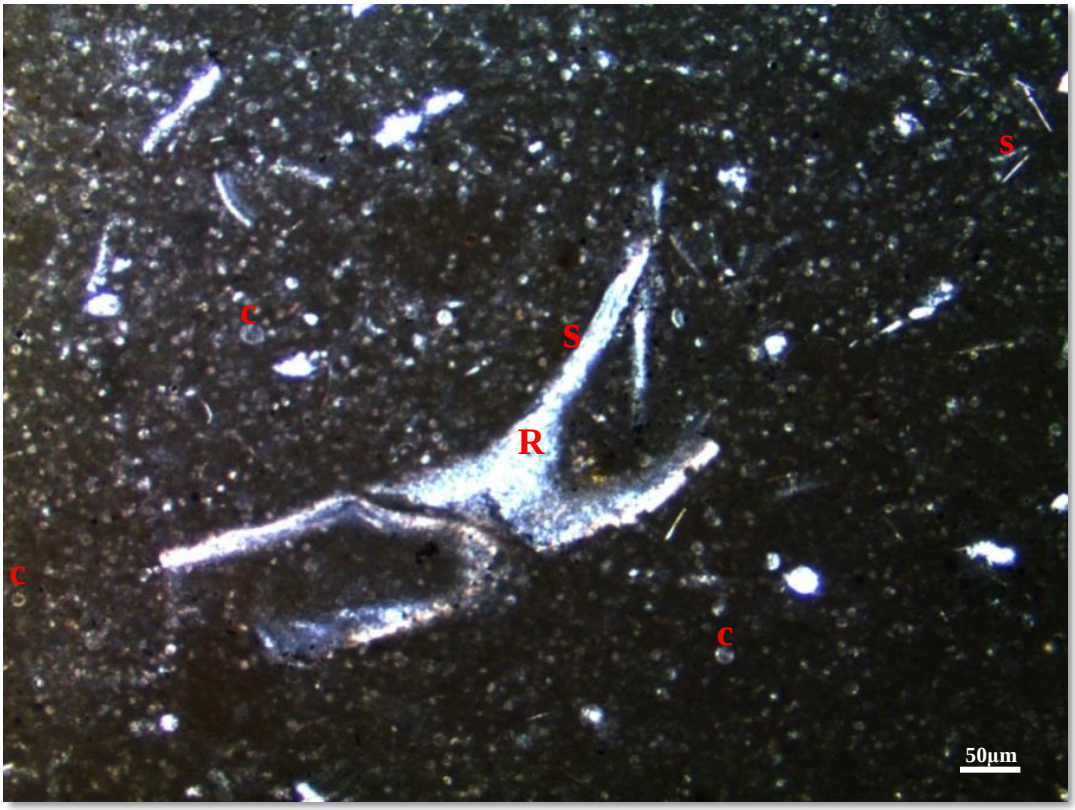


**Figure 64.** Calcisphaerulid-bearing skeletal wackestone to packstone microfacies from the thin section at 1720.81 m of the K-11 well [c: calcisphaerulid (*Pithonella spherica*); s: skeletal fragments; R: recrystallization]

#### 3.2.1.3.4 Calcisphaerulid-bearing planktonic foraminiferal mudstone to wackestone (MF10)

This microfacies (**Figure 65-68**) is characterized by an increase in the amount of micrite and decrease in the size and abundance of the allochems. The most frequently observed bio-allochems are planktonic foraminifera and infrequently *Pithonella spherica* type calcisphaerulids. Phosphate fragments (fish bone or teeth) are also common (**Figure 66**). This microfacies of the Derdere Formation is considered as pelagic microfacies.

RMF5 of Flugel (2004) which is pelagic mudstone can be interpreted as compositionally the most similar microfacies to MF10 (**Figure 31**). It has been concluded that the deposition of this microfacies is in middle ramp to outer ramp to

basin. Similarly, the depositional environment of MF10 is the most distal part of the middle ramp.

Local dolomitization, phosphatization of carbonate grains (**Figure 66**) especially pelagic organisms and opaque mineral development are the main diagenetic processes observed petrographically. Phosphatic grains are the indicator of strong upwelling regime associated with oxygen minimum layer and the absence of pronounced topographic high during the deposition of the Derdere Formation allows the entrance of phosphate-rich waters and phosphatization, which is also suggested in the study of Mohseni and Al-Aasm (2004). Euhedral dolomite crystals are dispersed in the matrix during partial dolomitization (**Figure 65**, **Figure 67** and **Figure 68**). Mostly filled thin fractures are identified in thin sections.

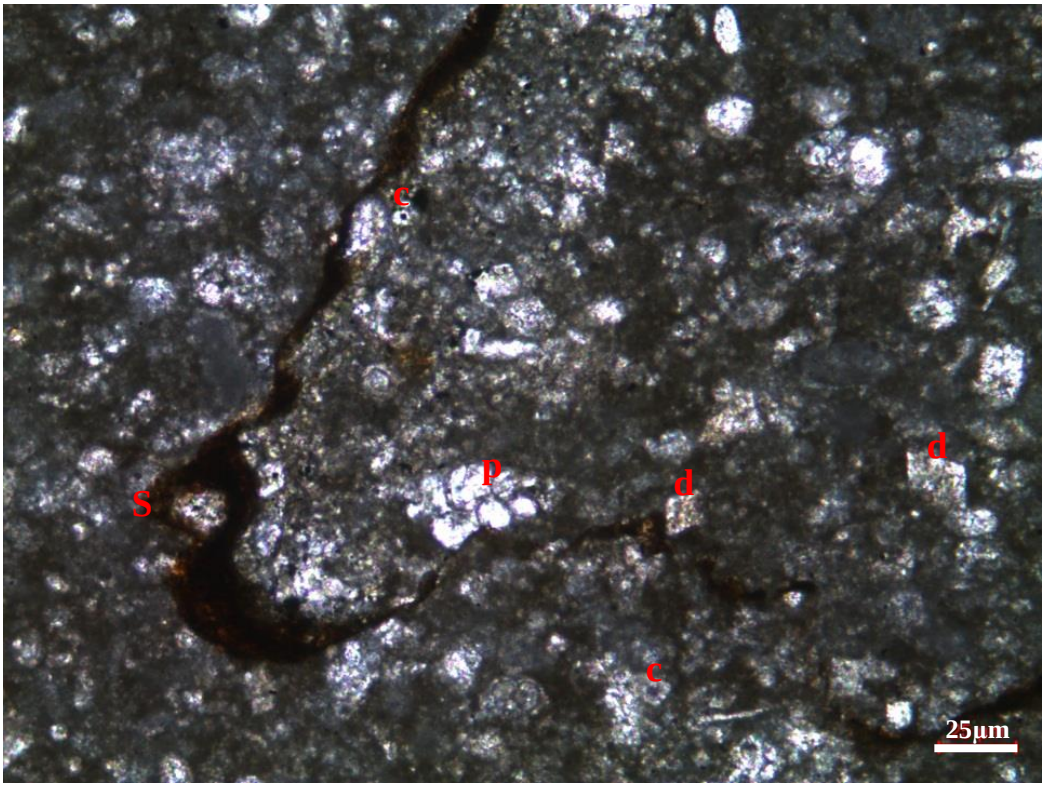


**Figure 65**. Calcisphaerulid-bearing planktonic foraminiferal mudstone to wackestone microfacies from the thin section at 1694.46 m of the K-11 well [d: dolomite; p: planktonic foraminifer; c: calcisphaerulid (*Pithonella spherica*); S: stylolitization]

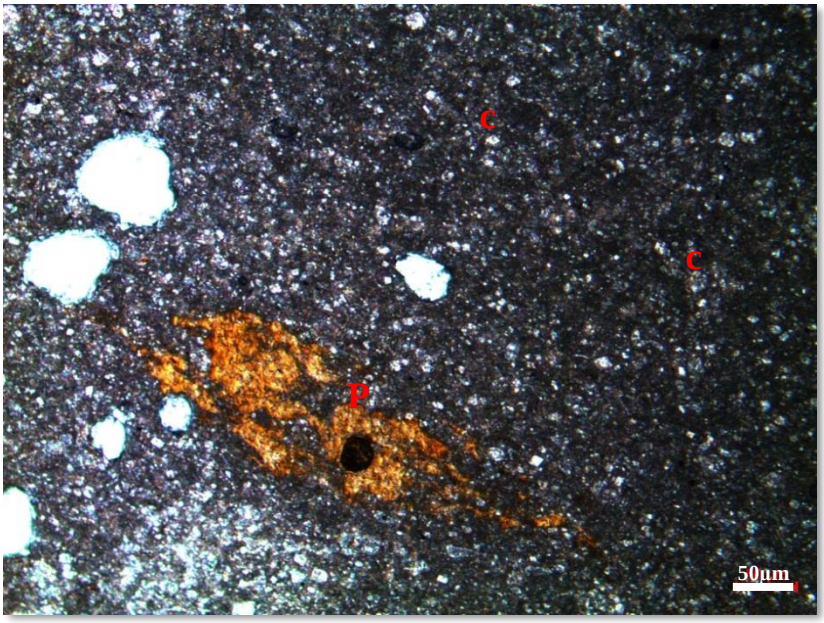


**Figure 66.** Calcisphaerulid-bearing planktonic foraminiferal mudstone to wackestone microfacies from the thin section at 1697.20 m of the K-11 well [c: calcisphaerulid (*Pithonella spherica*); P: phosphatization]

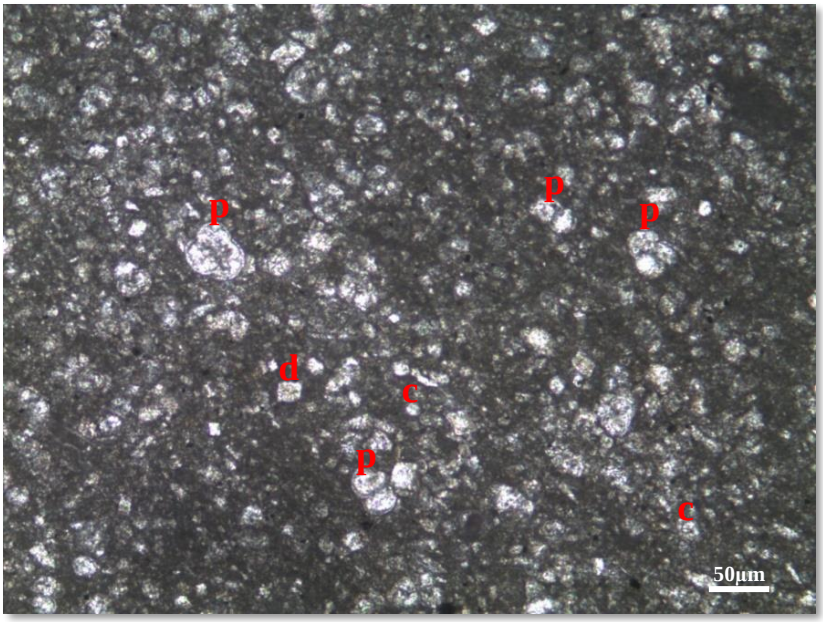


**Figure 67.** Calcisphaerulid-bearing planktonic foraminiferal mudstone to wackestone microfacies from the thin section at 1696.53 m of the K-11 well [c: calcisphaerulid (*Pithonella spherica*); p: planktonic foraminifer; d: dolomite]

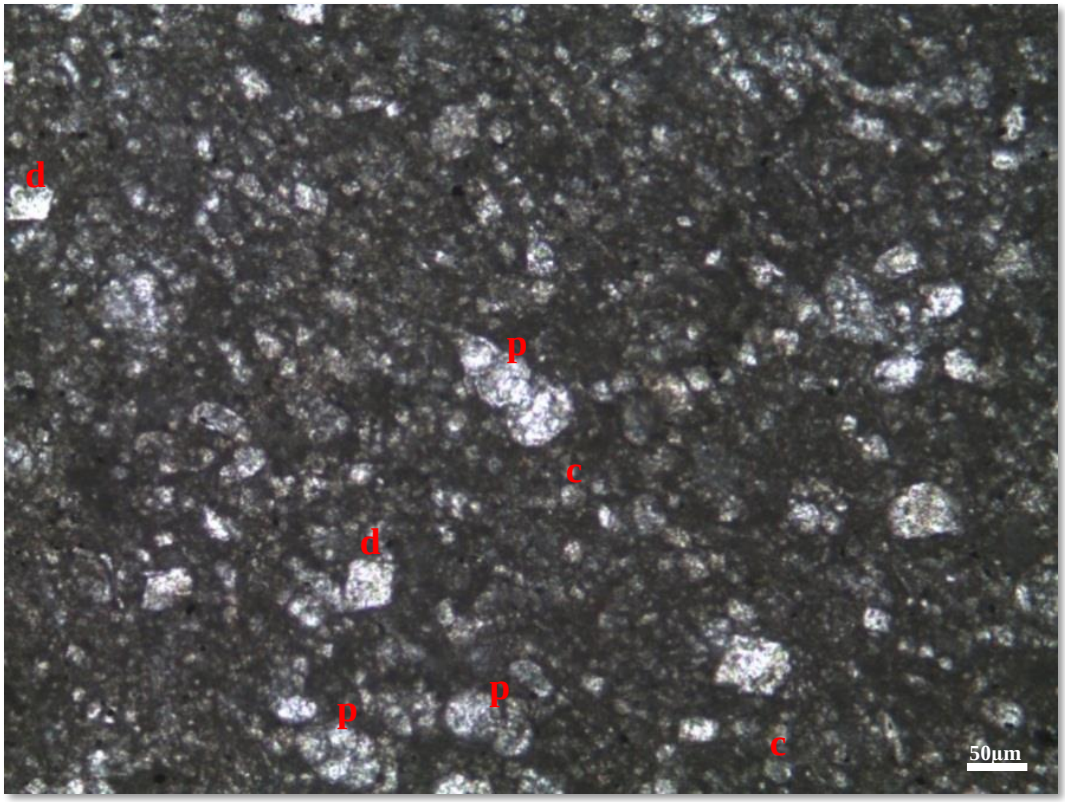


**Figure 68.** Calcisphaerulid-bearing planktonic foraminiferal mudstone to wackestone microfacies from the thin section at 1696.75 m of the K-11 well [c: calcisphaerulid (*Pithonella spherica*); p: planktonic foraminifer; d: dolomite]

#### 3.2.1.3.5 Radiolaria-bearing mudstone (MF11)

This microfacies is mainly composed of radiolaria type allochems and micrite matrix. Radiolaria-bearing mudstone is defined petrographically by using light microscope and they are differentiated from calcisphaerulids by their some spine-like extensions (**Figure 69**). This microfacies of the Derdere Formation is considered as pelagic microfacies. The existence of radiolaria is associated with Oceanic Anoxic Event (OAE2) (Bragina and Bragin, 2010) during the deposition of the Derdere Formation.

The plankton extinctions at around the Cenomanian-Turonian boundary are caused by the expansion of oxygen minimum zone. The evolution of the mid-Cretaceous radiolarian has a strong relationship with the sea-level changes. The transgressive

periods suggest the high productivity, expansion of oxygen minimum zone and low diversities of radiolarian and organic matter enrichments (Erbacher et. al., 1996). In the sections of Italy and Spain enrichment of radiolarian assemblages occur in the earliest Turonian similar to the Derdere Formation (O'Dogherty, 1994).

This microfacies corresponds to RMF5 of Flugel (2004) and it has been interpreted to be deposited in middle ramp to outer ramp to basin in the model of Flugel (2004) (**Figure 31**). The depositional environment of MF11 is also defined as the most distal part of middle ramp and outer ramp in this study.

The main diagenetic mechanism observed in this type of microfacies is replacement. Although radiolarians are composed of silica originally, they are totally replaced by calcite. Due to spheroid shape, unpreserved spines, and mineralogy of organisms, it is not easy to differentiate calcisphaerulid from the radiolarian after the replacement. Revealing the existence of radiolaria is going to be proved with the light microscope based cathodoluminescence. Mostly filled thin fractures are identified on thin sections, as well.

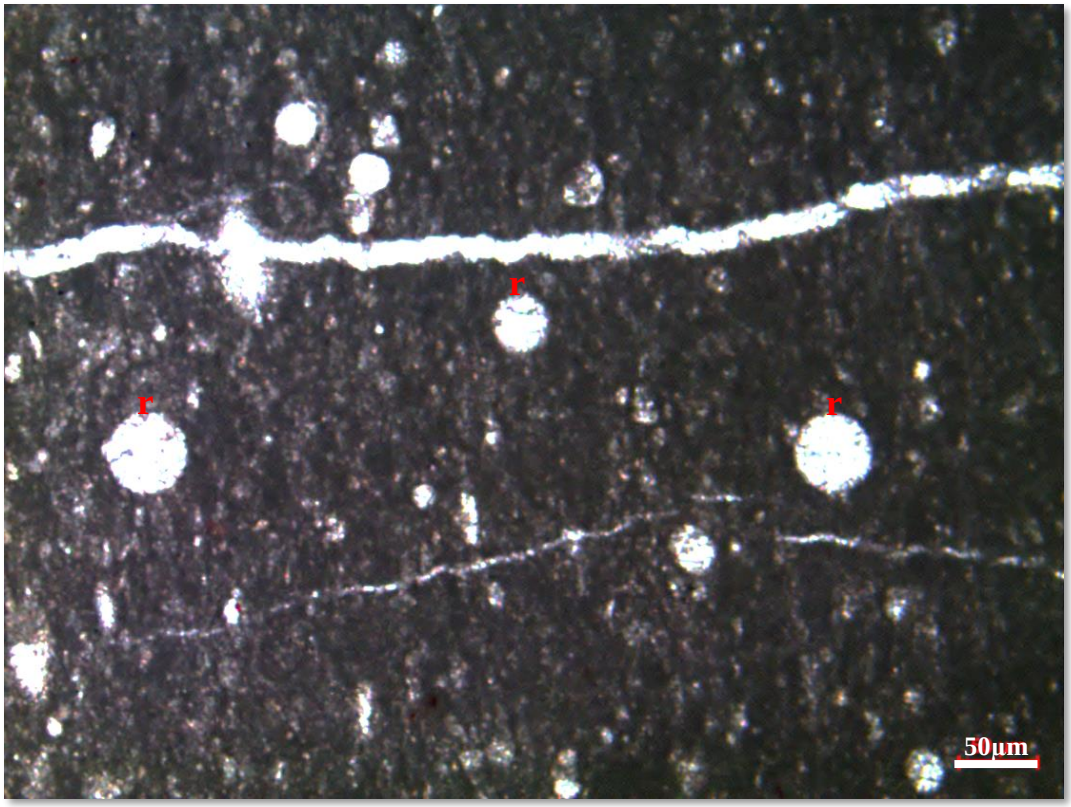


**Figure 69.** Radiolaria-bearing mudstone microfacies from the thin section at 1697.42 m of the K-11 well (r: calcified radiolaria)

#### 3.2.1.4 Outer Ramp Facies

##### 3.2.1.4.1 Planktonic foraminiferal wackestone (MF12)

This microfacies (**Figure 70-72**) is characterized by the presence of planktonic foraminifera, organic matter, laminations, and carbonate aggregates.

Carbonate aggregates are composed of suspended very fine grained particles and they are common in Upper Cretaceous chalk formations worldwide (Hattin, 1981; Pollastro, 2009) (**Figure 70**). In order to see whether these carbonate aggregates have calcareous nannofossils, SEM study is conducted and nannofossils less than 30 microns in diameter are observed.

This pelagic microfacies can be considered as similar to RMF2 and RMF5 of the carbonate model of Flugel (2004) in terms of compositional and textural

similarities (**Figure 31**). They are evaluated to be deposited in the outer ramp to basin depositional setting in the study of Flugel (2004), which is also similar to the depositional environment of MF12.

Phosphate fragments and opaque minerals are observed frequently in thin sections.

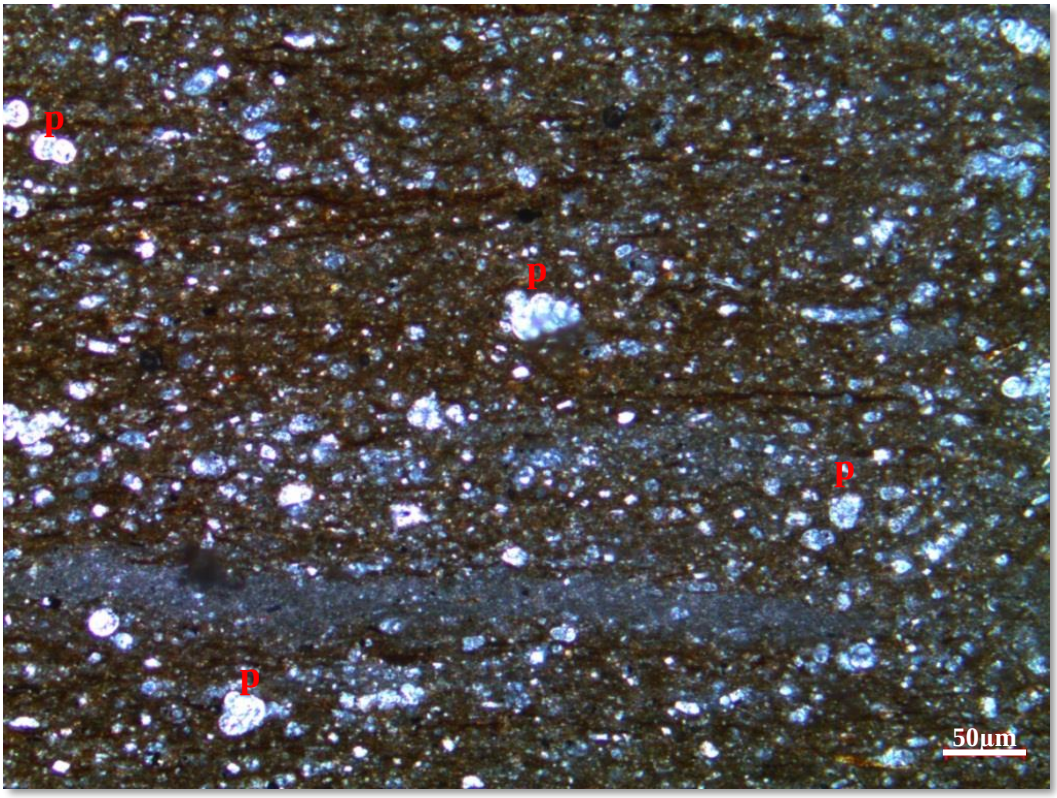


**Figure 70.** Planktonic foraminiferal wackestone microfacies from the thin section at the K-11 well (p: planktonic foraminifer)

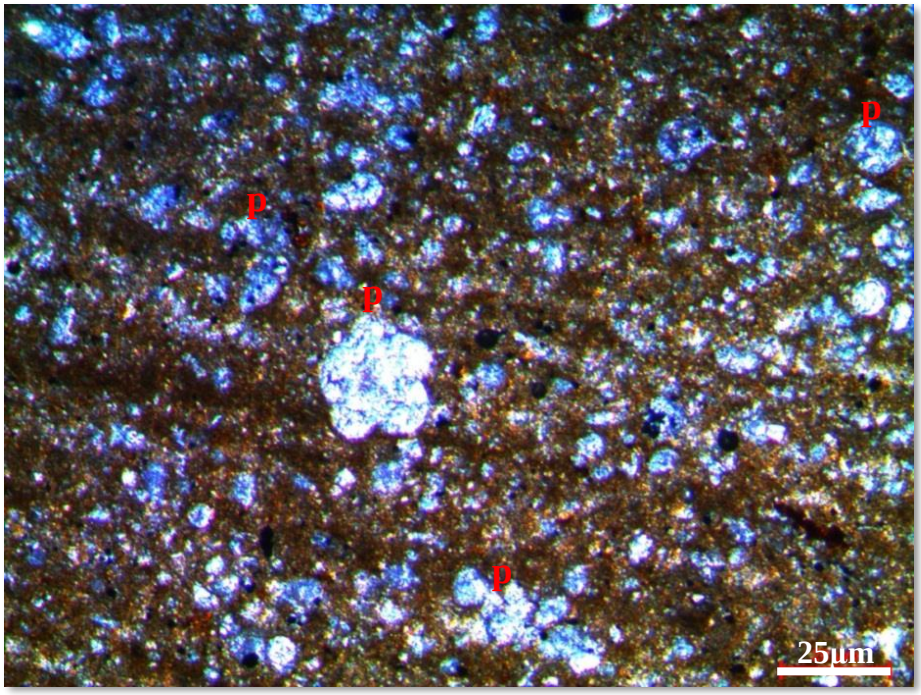


**Figure 71.** Planktonic foraminiferal wackestone microfacies from the thin section at 1704 m of the K-11 well (p: planktonic foraminifer)

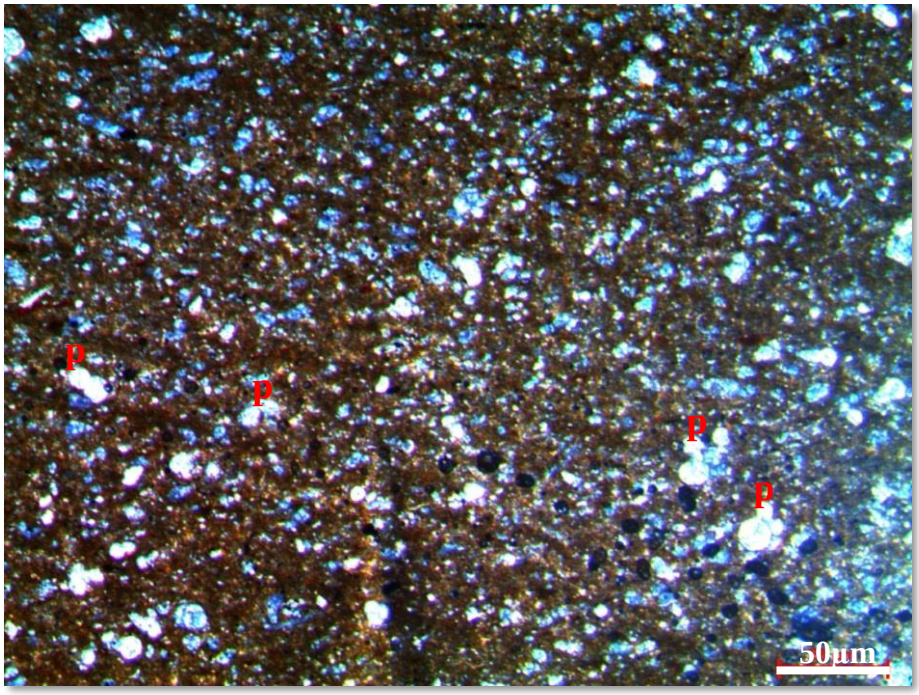


**Figure 72.** Planktonic foraminiferal wackestone microfacies from the thin section at 1704 m of the K-11 well (p: planktonic foraminifer)

#### 3.2.1.4.2 Calcisphaerulid-bearing wackestone to packstone (MF13)

This microfacies (**Figure 73** and **Figure 74**) is represented with a calcisphaerulid bloom (domination of calcareous nannofossils) is associated with rare benthic foraminifera (one or two in a thin section) in micrite dominated matrix. These calcareous nannofosils are also recognized on (SEM) (**Figure 75**). Calcisphaerulid-bearing wackestone to packstone is commonly observed with the enrichment of organic matter.

This pelagic microfacies is interpreted as associated with the RMF2 of Flugel (2004) which is the part of outer ramp to basin depositional setting (**Figure 31**). Likely to RMF2 microfacies, the depositional environment of MF13 is considered to be deposited in the outer ramp and they are commonly observed in the distal middle ramp to outer ramp depositional setting of Guerrero–Morelos Basin, Southern Mexico during Cenomanian to Turonian in the study of Franco and Romano (2004) and in the study of (Dias-Brito, 2000).

Thin fractures and stylolites are main diagenetic features observed petrographically. Fractures are mostly filled with calcite cement whereas; stylolites are commonly cemented with clay and/or organic matter.

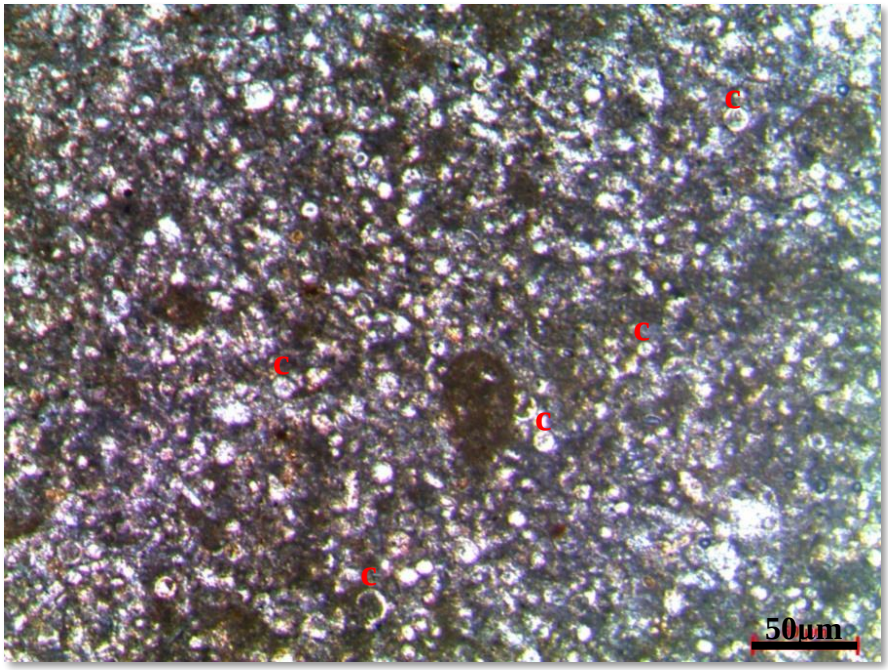


**Figure 73.** Calcisphaerulid-bearing packstone microfacies from the thin section at 1712 m of the K-11 well (c: calcisphaerulid (*Pithonella spherica*))

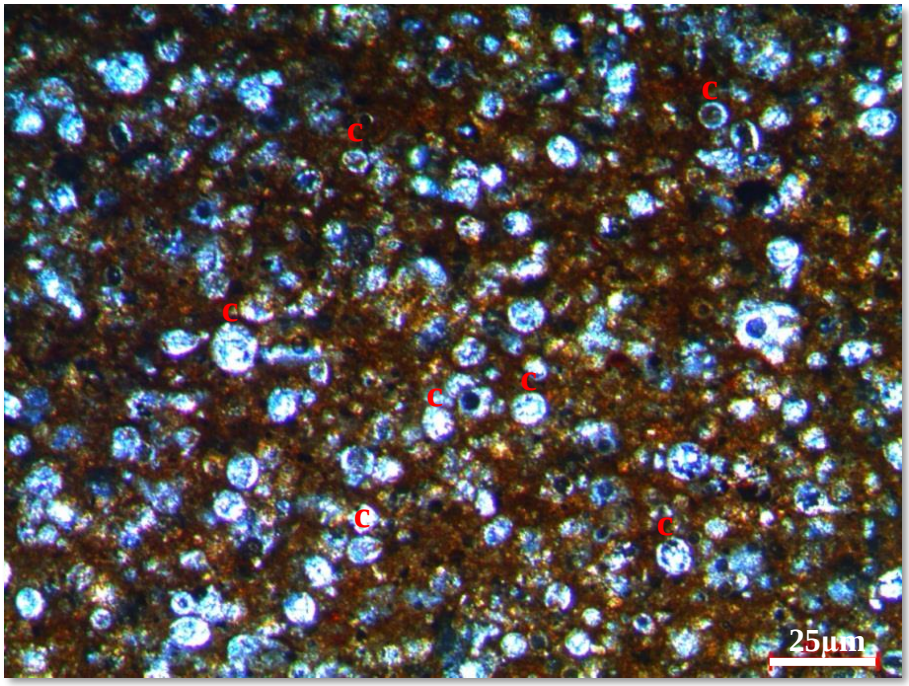


**Figure 74.** Calcisphaerulid-bearing wackestone to packstone microfacies from the thin section at 1718 m of the K-11 well (c: calcisphaerulid (*Pithonella spherica*)

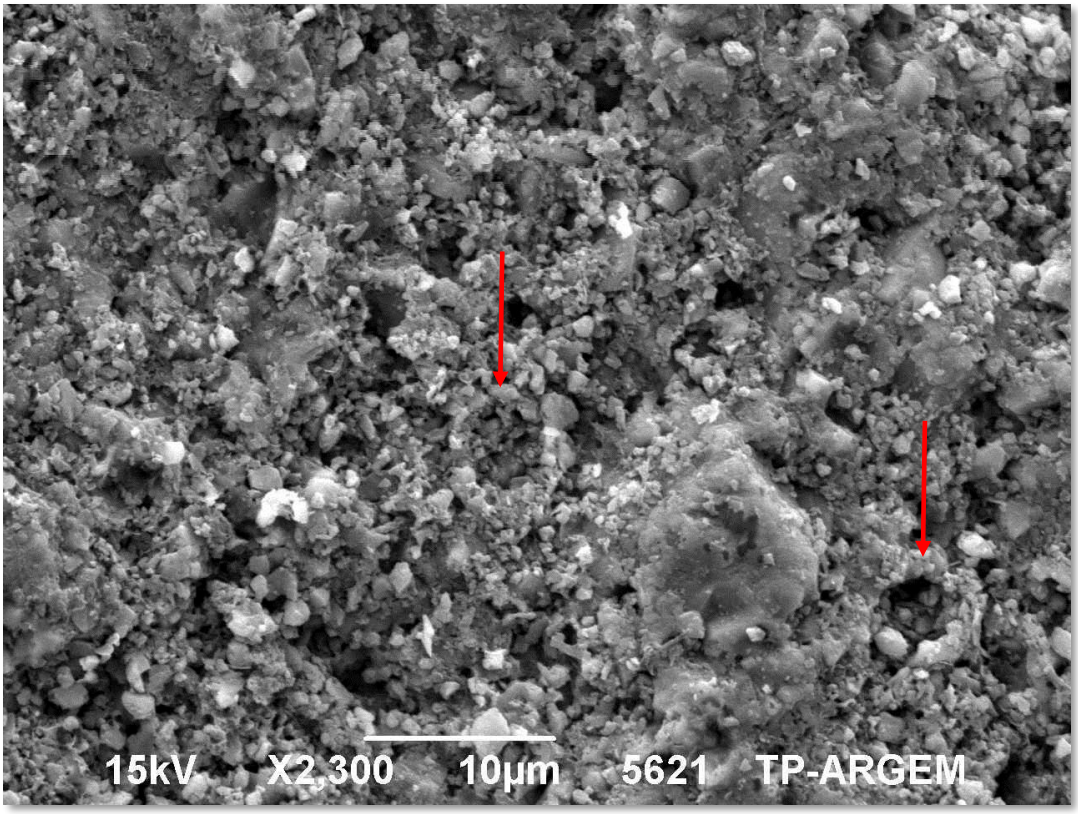


**Figure 75.** Possible calcareous nannofossils (indicated with red arrows) are shown on the SEM photomicrograph. Thin section is from 1699.21 m

#### 3.2.1.4.3 Planktonic foraminiferal skeletal calcisphaerulid-bearing wackestone to packstone (MF14)

This microfacies (**Figure 76** and **Figure 77**) consists of planktonic foraminifera, "*Saccocoma"*-like crinoids and thin walled mollusk type bio-allochems and the most commonly *Pithonella spherica, Pithonella ovalis* and *Bonetocardiella conoidea* type calcisphaerulids and micritix matrix. Additionally, few benthic foraminifera (**Figure 76**) are identified in the thin sections. Presence of organic matter, phosphate fragments and enrichment of opaque minerals are other descriptive characteristics of this microfacies.

The most appropriate microfacies to the MF14 based on the compositional similaries defined in the model of Flugel (2004) are RMF2 and RMF3 (**Figure 31**). They are interpreted to be deposited in the middle ramp to outer ramp setting

similar to the depositional environment of MF14. Drawing the sharp line between distal middle to outer ramp depositional setting and deposited microfacies are problematic due to unsteady storm weather wave base; hence even in the model of Flugel (2004), some of the microfacies types are mutual in both middle and outer ramp settings. Similar facies, which is "Calcisphaerulid – roveacrinid – whiteinellids nodular limestones" composing of calcisphaerulids, planktonic foraminifers and thin bivalve shells, are identified in the Cenomanian–Turonian facies succession of the Guerrero–Morelos Basin, Southern Mexico (Franco and Romano, 2004). It is also considered as outer ramp deposits in their study.

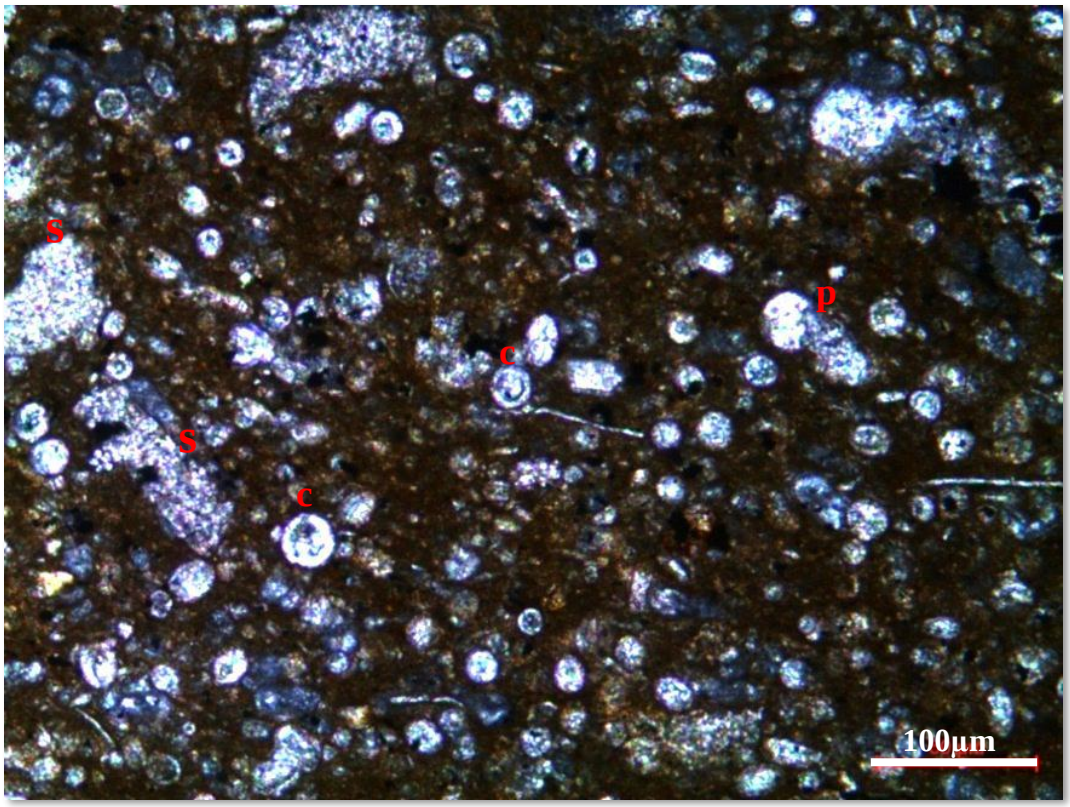


**Figure 76.** Planktonic foraminiferal skeletal calcisphaerulid-bearing wackestone to packstone microfacies from the thin section at 1722.96 m of the K-11 well (p: planktonic foraminifer; s: skeletal fragment (echinoderm); c: calcisphaerulid (*Pithonella spherica*)

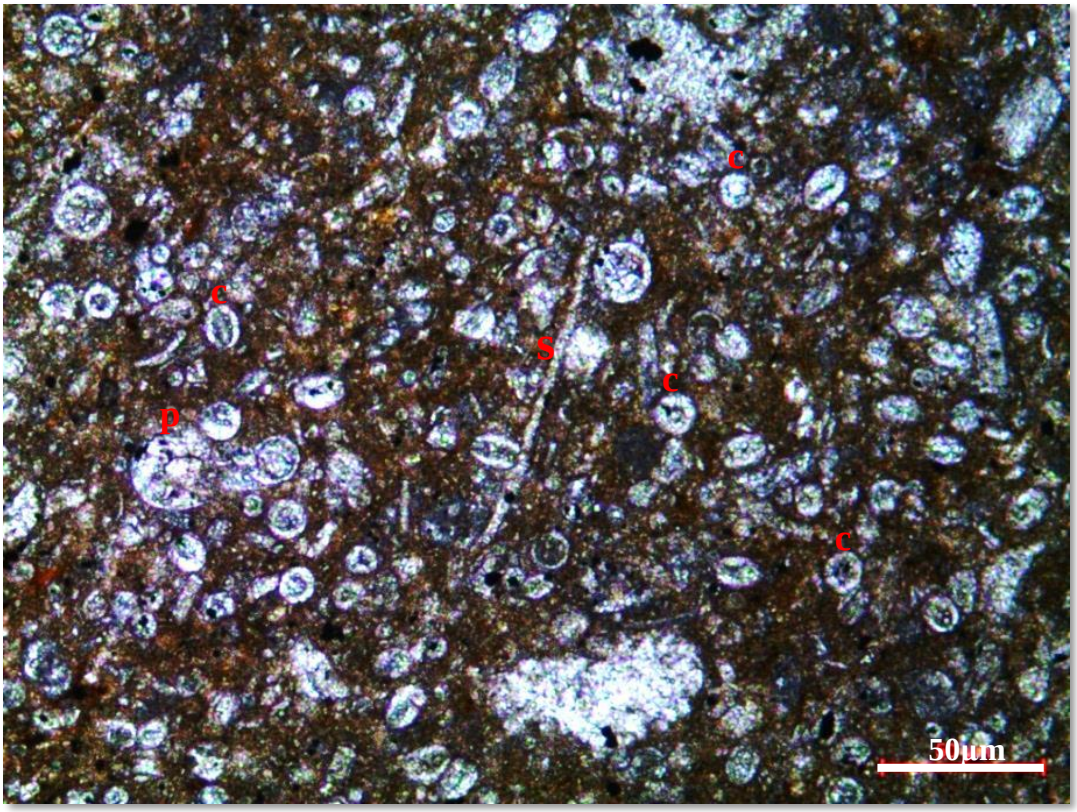


**Figure 77.** Planktonic foraminiferal skeletal calcisphaerulid-bearing wackestone to packstone microfacies from the thin section at 1722.82 m of the K-11 well (p: planktonic foraminifer; s: skeletal fragments (thin walled mollusk (pelecypod)); c: calcisphaerulid (*Pithonella spherica* and *Pithonella ovalis*)

#### 3.2.1.4.4 Skeletal calcisphaerulid-bearing wackestone to packstone (MF15)

This microfacies (**Figure 78-81**) is mainly composed of thin walled mollusk fragments (pelecypods) (thin-bivalve shells), "*Saccocoma"*-like crinoids and dominated with the abundance of calcisphaerulids as a bloom including the main types of *Pithonella spherica*, *Pithonella ovalis* and *Bonetocardiella conoidea* in micritic matrix. Generally, outer ramp microfacies do not have the variety of bio-allochems. Planktonic and benthic foraminifers are identified rarely in thin sections.

Presence of organic matter, phosphate fragments (**Figure 79**) and enrichment of opaque minerals on the skeletal fragments (**Figure 81**) are the other descriptive properties of MF15 similar to other outer ramp microfacies. This pelagic

microfacies is similar to the RMF2 and RMF3 of Flugel (2004) in terms of composition (**Figure 31**). In the model of Flugel (2004), the depositional environments are interpreted to be middle to outer ramp. It has been concluded that deposition of MF15 is in the outer ramp below the storm weather wave base. "Calcisphaerulid-roveacrinid-thin-bivalve shells packstone to wackestone" facies, which is composed of calcisphaerulids, echinoderms and thin bivalve shells, is described in the study of Franco and Romano (2004). This facies is interpreted as outer ramp deposits of the Cenomanian-Turonian succession of Guerro-Morelos Basin (Franco and Romano, 2004).

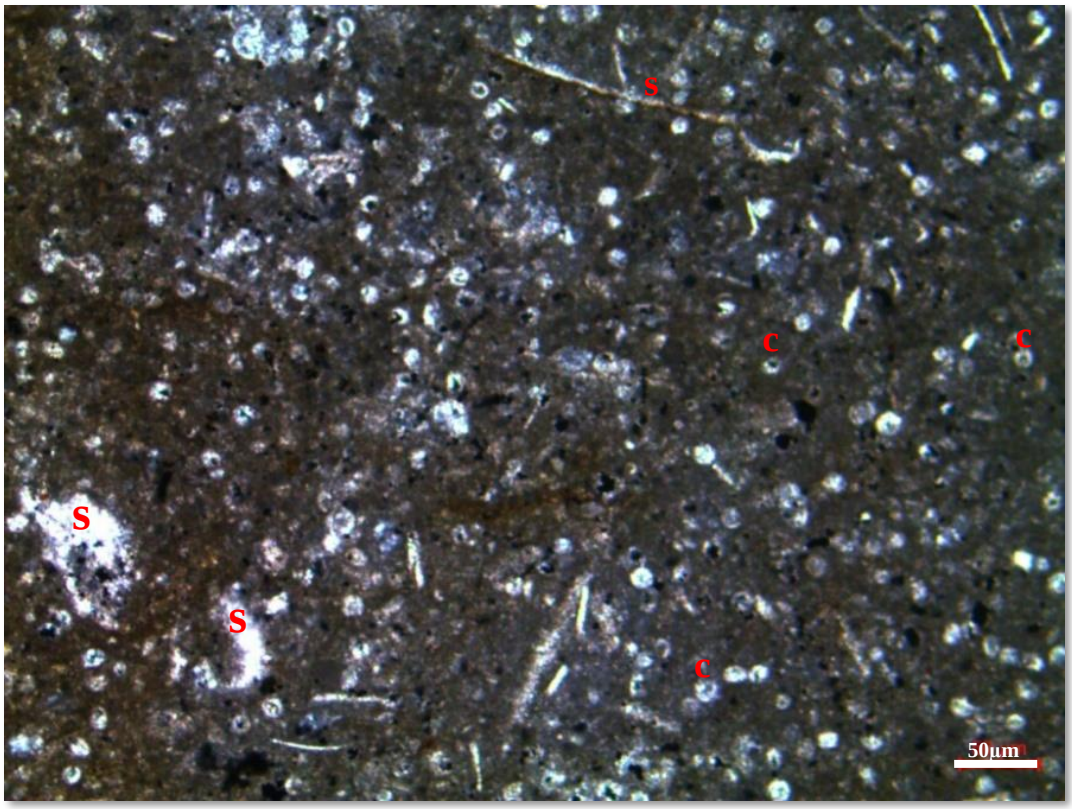


**Figure 78**. Skeletal calcisphaerulid-bearing wackestone to packstone microfacies from the thin section at 1719.06 m of the K-11 well [s: skeletal fragments (thin walled mollusk (pelecypod) and "*Saccocoma*"; c: calcisphaerulid (*Pithonella spherica*)]

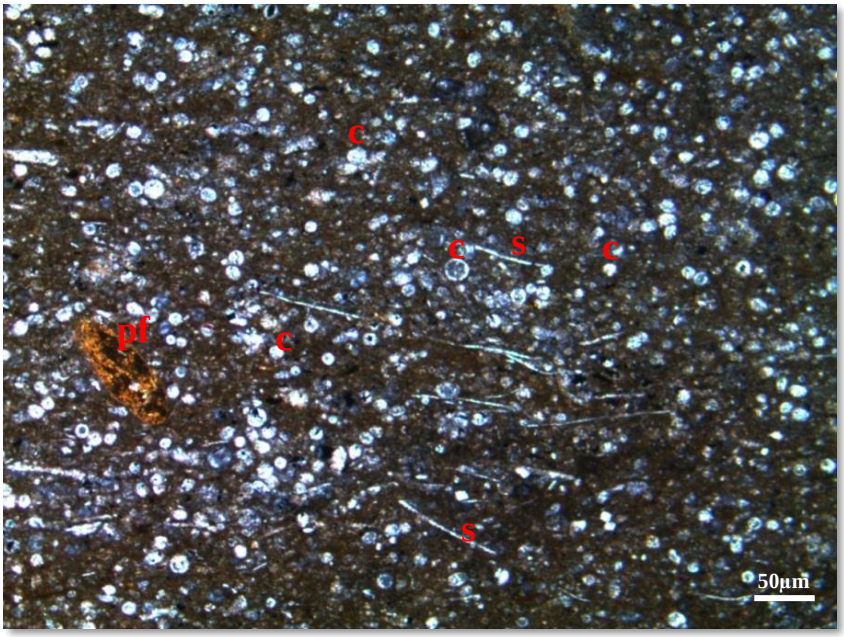


**Figure 79.** Skeletal calcisphaerulid-bearing wackestone to packstone microfacies from the thin section at 1719.91 m of the K-11 well [pf: phosphate fragments; s: skeletal fragments (thin walled mollusk (pelecypod)); c: calcisphaerulids (*Pithonella spherica*)]

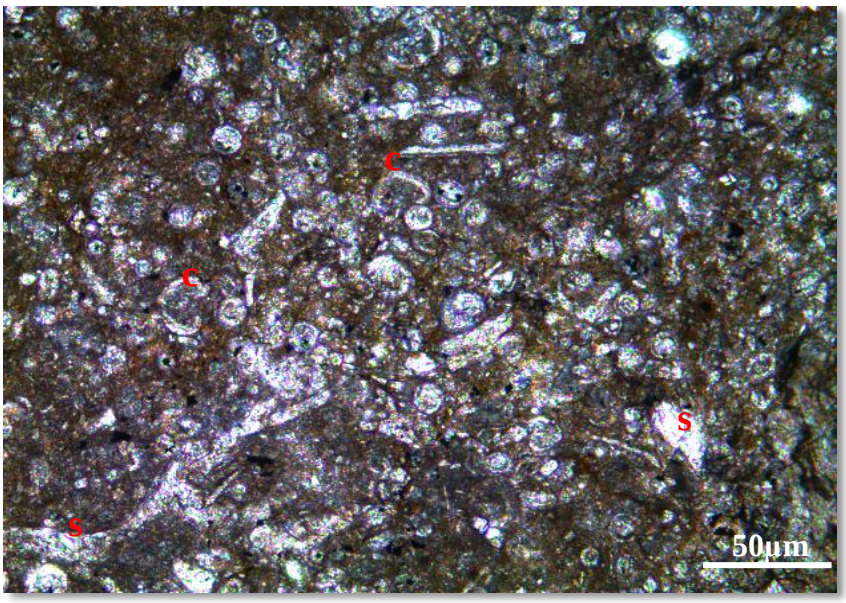


**Figure 80**. Skeletal calcisphaerulid-bearing wackestone to packstone microfacies from the thin section at 1725.35 m of the K-11 well (s: skeletal fragments (broken thin bivalve shells; c: calcisphaerulids (*Bonetocardiella conoidea*))

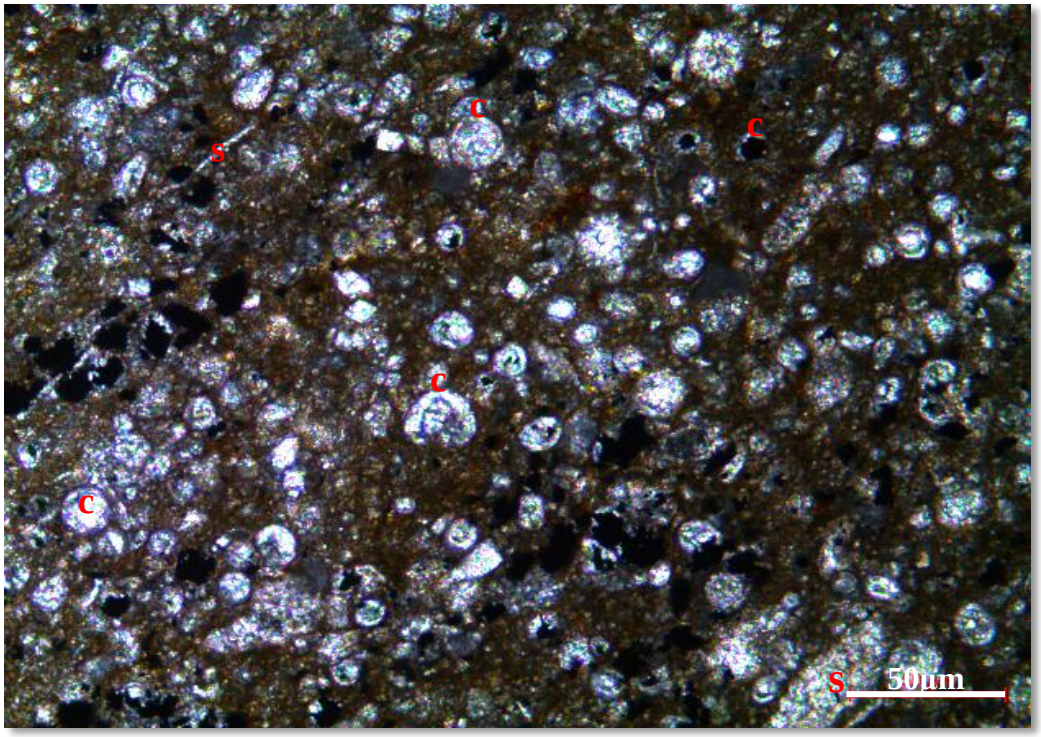


**Figure 81.** Skeletal calcisphaerulid-bearing wackestone to packstone microfacies from the thin section at 1726.99 m of the K-11 well (s: skeletal fragments; c: calcisphaerulids (*Pithonella spherica* and *Bonetocardiella conoidea*))

## 3.3 DEPOSITIONAL MODEL

This study states that the depositional environment of the Derdere Formation evolves from ramp system to intra-shelf type system with the increasing rate of sea level (early slow transgression to late fast transgression) during the deposition of the Derdere Formation since changing accommodation space with the variable rates of sea level has the significant impact on the morphology of the depositional profile.

The depositional model created for the Derdere Formation is based on the model developed by Flugel (2004) and Wilson carbonate model (1975). The ramp is divided as inner ramp (tidal flat, lagoon and shoal), proximal middle ramp, distal middle ramp and outer ramp by the detailed classification of microfacies.

Microfacies defined at the top of the Derdere Formation is shoal to lagoon facies and the depositional environment is interpreted as inner ramp with grainstone to packstone microfacies with large and small benthic foraminifera, green algae, peloid, various skeletal fragments (brachiopods, rudists, echinoderms, oysters, mollusks) and rarely intraclasts. The main constituents in the proximal middle ramp are algae, peloids, benthic foraminifera and skeletal fragments. In the distal middle ramp, benthic foraminifera still continues to be rarely observed with mainly skeletal fragments towards the land and microfacies become more pelagic and calcisphaerulids are observed with skeletal fragments towards the basin. Planktonic foraminifera enter to the pelagic system and calcisphaerulids and skeletal fragments are still the constituents in the distal middle part towards basinward. The microfacies identified in the distal part of middle ramp are mainly represented by wackestones due to the lesser amount of constituents. Just below the storm wavebase, in the outer ramp part of depositional model calcisphaerulids become much more abundant as a bloom and microfacies are classified according to variable abundance of planktonic foraminifera and skeletal fragments.

MF1 (benthic foraminiferal mudstone), MF2 (Benthic foraminiferal skeletal mudstone to wackestone), MF3 (Benthic foraminiferal skeletal peloidal packstone to grainstone) and MF4 (Skeletal peloidal packestone to grainstone) microfacies are deposited in the inner ramp depositional setting of the Derdere Formation. The microfacies MF5 (Peloidal skeletal wackestone to packstone) and MF6 (Skeletal wackestone) constitute the transition between the inner ramp and proximal middle ramp are. In the model of homoclinal carbonate ramp model of Flugel (2004), this proximal middle ramp can be considered as the part of inner ramp including restricted and open marine settings. This depositional setting contains ramp derived intra- and bioclasts. Toward the basin, until the storm wavebase (SWB), in the distal part of middle ramp, the microfacies MF7 (Skeletal calcisphaerulid-bearing planktonic foraminiferal wackestone to packstone), MF8 (Skeletal planktonic foraminiferal calcisphaerulid-bearing wackestone to packstone), MF9 (Calcisphaerulid-bearing skeletal wackestone to packstone), MF10 (Calcisphaerulid-bearing planktonic foraminiferal mudstone to wackestone), and

MF11 (Radiolaria-bearing mudstone) are identified. Below the storm wavebase, in the outer part of ramp, only pelagic microfacies with greater abundance of planktonic foraminifera, mainly calcisphaerulids and rarely skeletal fragments are observed. These outer ramp microfacies are MF12 (Planktonic foraminiferal wackestone), MF13 (Calcisphaerulid-bearing wackestone to packstone), MF14 (Planktonic foraminiferal skeletal calcisphaerulid-bearing wackestone to packstone), and MF15 (Skeletal calcisphaerulid-bearing wackestone to packstone) (**Table 6** and **Figure 82**).

In the study of Özkan and Altıner (2019), microfacies defined in the Mardin Group Carbonates are variable from the outer ramp to the peritidal depositional environment similar to this study. The inner ramp facies defined in their study are the orbitolinid wackestone to packstone, the peloidal bioclastic packstone with miliolids, the gastropod floatstone and *Salpingoporella dinarica* mudstone characterizing the low energy lagoonal environment. The other facies are lime mudstone with miliolids and dolomitic peloidal bindstone which are considered to be deposited in the peritidal environment. These inner ramp facies are similar to the facies defined in this study. The benthic foraminiferal mudstone (MF1) defined in this study corresponds to lime mudstone with miliolids. The benthic foraminiferal skeletal mudstone to wackestone (MF2) and the skeletal wackestone (MF6) are associated with gastropod floatstone. The benthic foraminiferal skeletal peloidal packstone to grainstone (MF3) and the skeletal peloidal packstone to grainstone (MF4) facies correspond to dolomitic peloidal bindstone facies defined in the study of Özkan and Altiner (2019). The peloidal skeletal wackestone and packstone (MF5) facies is associated with peloidal bioclastic packstone with miliolids. The orbitolinid wackestone to packstone and *Salpingoporella dinarica* mudstone type facies does not have direct equivalent; however the benthic foraminieral mudstone facies can be considered as similar to these facies in terms of the large benthic foraminifera and algae content.

**Table 6.** Microfacies and depositional environments defined in the studied wells

| Depositional Environment | Microfacies No | Microfacies | Main Components |
|---|---|---|---|
| Inner Ramp | MF1 | Benthic foraminiferal mudstone | Large benthic foraminifera, small benthic foraminifera (*Cibicides*), *Thaumatoporella* type algae |
| | MF2 | Benthic foraminiferal skeletal mudstone to wackestone | Benthic foraminifera and large skeletal fragments (rudists and mollusks, bivalves) |
| | MF3 | Benthic foraminiferal skeletal peloidal packstone to grainstone | Large benthic foraminifera, small benthic foraminifera and large mollusk fragments, echinoderm fragments, peloids |
| | MF4 | Skeletal peloidal packestone to grainstone | Oyster (pycnodontinae), echinoderm, gastropods and inoceramid, peloids, intraclasts and benthic foraminifera, benthic foraminifera |
| Proximal Middle Ramp | MF5 | Peloidal skeletal wackestone to packstone | Peloids, mollusk fragments, bivalves and brachiopods, benthic foraminifera |
| | MF6 | Skeletal wackestone | Brachiopods, thin walled mollusk fragments such as bivalves (pelecypods), *Saccocoma*-like crinoids, benthic foraminifera |
| Distal Middle Ramp | MF7 | Skeletal calcisphaerulid-bearing planktonic foraminiferal wackestone to packstone | Echinoderms and pelecypod-like thin walled mollusks, *Pithonella spherica* type calcisphaerulids, planktonic foraminifera |
| | MF8 | Skeletal planktonic foraminiferal calcisphaerulid-bearing wackestone to packstone | Planktonic foraminifera, echinoderms, mollusks, brachiopods, *Pithonella spherica* and *Pithonella ovalis* type calcisphaerulids,fish teeth/bone |
| | MF9 | Calcisphaerulid-bearing skeletal wackestone to packstone | Sponge spicules and *Saccocoma*-like crinoids, mostly *Pithonella spherica* and *Pithonella ovalis* type calcisphaerulids, small benthic foraminifera |
| | MF10 | Calcisphaerulid-bearing planktonic foraminiferal mudstone to wackestone | Planktonic foraminifera, *Pithonella spherica* type calcisphaerulids, fish bone/teeth |
| | MF11 | Radiolaria-bearing mudstone | Radiolaria |
| Outer Ramp | MF12 | Planktonic foraminiferal wackestone | Planktonic foraminifera and carbonate aggregates calcareous nannofossils |
| | MF13 | Calcisphaerulid-bearing wackestone to packstone | Calcisphaerulids and benthic foraminifera |
| | MF14 | Planktonic foraminiferal skeletal calcisphaerulid-bearing wackestone to packstone | Planktonic foraminifera, *Saccocoma*-like crinoids, thin walled mollusk, *Pithonella spherica, Pithonella ovalis* and *Bonetocardiella conoidea* type calcisphaerulids |
| | MF15 | Skeletal calcisphaerulid-bearing wackestone to packstone | Thin walled mollusk fragments (pelecypods), *Saccocoma*-like crinoids,*Pithonella spherica*, *Pithonella ovalis* and *Bonetocardiella conoidea* type calcisphaerulids, planktonic and benthic foraminifers |

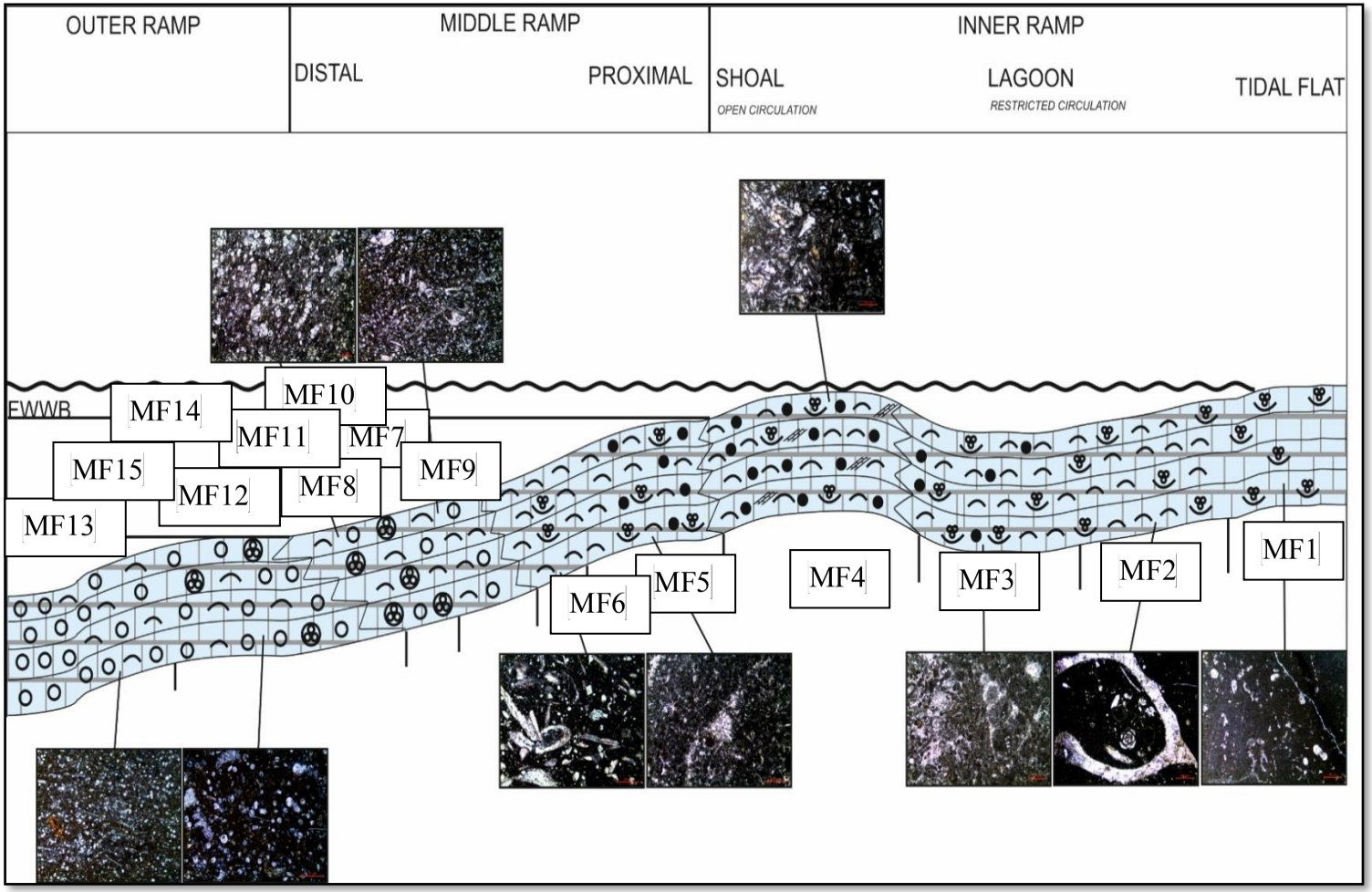


**Figure 82.** Depositional model of the Derdere Formation developed using microfacies (plotted on to the carbonate model of Wilson (1975))

Another significant point is the inner ramp facies defined in the study of Özkan and Altiner (2019) includes both inner ramp and proximal middle ramp facies of this study. The proximal middle ramp facies defined in this study corresponds to the middle ramp and to the transition of the middle ramp to the outer ramp facies of Özkan and Altiner (2019). The peloidal skeletal wackestone to packstone (MF5) can be considered as similar to the bioclastic wackestone, the biocastic packstone and the echinoderm packstone facies of the study of Özkan and Altiner (2019). Skeletal wackestone (MF6) is the equivalent of bioclastic bivalve floatstone.

In both studies bioclasts are considered as derived from the shallow water environment and transported to deeper environments; however in the study of Özkan and Altiner (2019), wackestones and packstones are interpreted as the transitional facies to the outer ramp setting whereas floatstone is supposed to be deposited in the middle ramp setting. In this study, although some large reworked bioclasts are described, they are not in pronounced amount and most of them are observed as broken due to transportation. Hence, the equivalents of these facies are interpreted as the deposits of the middle ramp without making any discrimination. The reason could be related to the sampling which is the working difference with the field and the cutting samples. Another important point is the facies defined in the wells of Diyarbakır Region are deeper compared to facies of field section of Derik, Mardin which makes the middle ramp facies of this study the transition to the outer ramp in the study of Özkan and Altiner (2019). The *Praealveolina* packstone to grainstone facies of Özkan and Altiner (2019) does not have direct equivalent in this study; although there are some levels with *Praealveolin*a.

The lime mudstone facies of Özkan and Altiner (2019) can be considered to be the equivalent of the radiolaria-bearing mudstone (MF11) and the calcisphaerulid-bearing planktonic foraminiferal mudstone to wackestone (MF10) facies of this study. The sponge spicule wackestone to packstone corresponds to the calcisphaerulid-bearing skeletal wackestone to packstone (MF9). The calcisphaerulid wackestone is the equivalent of calcisphaerulid-bearing wackestone to packstone (MF13). The keeled planktonic foraminiferal wackestone to packstone facies corresponds to the planktonic foraminiferal wackestone (MF12) and similar

to the skeletal calcisphaerulid-bearing planktonic foraminiferal wackestone to packstone (MF7). The outer ramp facies of Özkan and Altiner (2019) partly overlaps with the distal middle ramp to the outer ramp facies of this study, since the distal middle ramp and the outer ramp facies are transitional.

Primary consitituents, which are defined the field section of Derik, Mardin and wells of Diyarbakır Region are associated, although there are some varieties in the facies. The main difference between the field descriptions and the studied wells is the diversity of primary constituents and facies deposited in the shallow water environment.

In the study of Spadini et al. (1988), carbonate ramp depositional model of Macae Formation, Campos Basin in Brazil is divided into three lithofacies, high energy shoal system, shelf environment and basinal environment. The shoal system is composed of lithofacies rich in oncolites, peloids and ooids with rare amount of bioclasts. The peloidal grainstones include mostly echinoderm fragments, gastropods, some textularids, miliolids and limited amount of planktonic foraminifera. This part of the carbonate ramp is interpreted as the highest depositional energy of the system. In the depositional model of the Derdere Formation, microfacies defined at the uppermost part consisting of skeletal peloidal packstone to grainstone and peloidal skeletal packstone facies, can be interpreted as high-energy shoal system. In the study of Spadini et. al. (1988), relatively low energy shelf environment is characterized by the deposition of the fine grained limestones. These microfacies have up to %5 of bioclasts (foraminifera and small echinoderm fragments, rarely micromollusks, ostracods and calcisphaerulids (including the species of *Pithonella spherica* and *Pithonella ovalis* reaching up to 5%). In the inner parts of the shelf, the matrix of the fine-grained limestones is peloidal. In the depositional model of the Derdere Formation, the skeletal mudstone to wackestone, the calcisphaerulid-bearing skeletal mudstone to wackestone, and the planktonic foraminiferal, skeletal, calcisphaerulid-bearing wackestone, and the skeletal, calcisphaerulid-bearing planktonic foraminiferal wackestone can be interpreted as deposits of outer shelf environment. Similarly to the model of

Spadini (1988), mudstone and wackestone, in which percentages of the bioclasts is approximately %10, is the most commonly observed microfacies.

The third depositional environment identified in the upper section of Macae Formation according to Spadini et. al. (1988) is the basinal environment, which is a deep-water, the outermost ramp depositional environment. It is mainly characterized by the fine-grained limestones, rich in planktonic foraminifera and calcisphaerulids. In depositional model of the Derdere Formation, the calcisphaerulid-bearing planktonic foraminiferal packstone and the calcisphaerulid-bearing packstone can be considered as the deposits of the basinal environment beyond the limit of fairweather wave base.

In the paper of Wilmsen (2003), the Cenomanian stage in the northern Germany in terms of the depositional environments and sequence stratigraphy is studied. The depositional model is developed according to fairweather and storm wave bases. The depositional environment, which is above the fairweather wave base is described as inner shelf and characterized by high terrigenous input. Middle shelf is divided into two zones: proximal middle shelf above the average storm wave base and distal middle shelf below the average storm wave base and above major storm wave base. Inoceramids, sponges and gastropods are the main constituents of proximal middle shelf while distal middle shelf is characterized by calcisphaerulids, inoceramids, bivalves, gastropods, brachiopods, and echinoderm. Outer shelf/ basin is described by the deposition of pelagic carbonate muds below the major storm wave base. Coccolithophorids as pelagic carbonate mud producers and echinoderms and bivalves are dominant in this part of the depositional model (Wilmsen, 2003).

In the study of Riktegarzadeh et. al., (2016), depositional model is created for the Cenomanian-Turonian Sarvak Formation in Bi Hakimeh oil field by the description of microfacies similar on the basis of petrographic analysis. Four major depositional environments including shelf lagoon, platform margin, slope and basin environments are identified as a part of carbonate shelf model without a pronounced barrier. Outer shelf microfacies includes planktonic foraminifera and oligosteginid type calcisphaerulids, echinoids and bivalves, few benthic

foraminifera, middle shelf microfacies include rudist and bioclast debris, peloids, bivalves, echinoids and benthic foraminifera and inner shelf microfacies include alveolinids, miliolids and orbitolinids type benthic foraminifera, peloids, rudist and echinoids and bivalves.

The Cenomanian–Turonian succession of Guerrero–Morelos Basin, Southern Mexico is studied in the paper of Franco and Romano (2004) and it is characterized by the depositional facies from shallow marine to pelagic facies, whose depositional setting is defined as carbonate ramp similar to the Derdere Formation. The inner ramp is represented by the peloidal benthic foraminiferal grainstone, calcareous red and green algae, rudists and minor solitary corals. The main primary constituents defined in the middle ramp are diverse assemblage of echinoderms, green and red algae, bryozoan, rudists, solitary corals, roveacrinids, calcisphaerulids, and planktonic foraminifers. The facies identified in the outer ramp are argillaceous wackestone to packstone with calcisphaerulids, roveacrinids, and planktonic foraminifers.

In the study of Dias-Brito (1985), calcisphaerulids of the fine-grained limestones are divided into two biozones including *Pithonella spherica* and *Pithonella spherica/Pithonella ovalis/Bonetocardiella conoidea* zones. The depositional environment, where calcisphaerulids are abundant, is considered as deep neritic environment with warm/dry climatic conditions and calcisphaerulids are related with fine-grained carbonates, which are deposited in deep shelf to shallow bathyal environments (Dias-Brito, 2000). These accumulations are directly associated with the variations in water conditions and relative sea level. Among the calcisphaerulid types mentioned above, *Bonetocardiella conoidea* and *Pithonella ovalis* are more stenotopic taxa and become more abundant in more nutritive waters of the outer neritic-oceanic transitional zone. *Pithonella spherica* is more opportunistic of all the pithonellid species and can tolerate the higher stress conditions and variable levels of nutrients and can be found in shallower and internal sections of the neritic environment (Dias-Brito, 2000). Therefore, calcisphaerulids, which are classified as *Pithonella spherica, Pithonella ovalis* and *Bonetocardiella conoidea,* are considered to reveal shoaling upward sequences in the Derdere succession.

To conclude, primary constituents, facies and depositional model of the Derdere Formation defined in the wells is compared with the Derdere Formation defined in the field and other Cenomanian-Turonian carbonate platforms worldwide. Although there are some differences in the facies, main primary constituents defined in the different parts of the ramp models are similar. The inner ramp facies of field section contains both the inner ramp and proximal middle ramp facies of this study. Similarly, the outer ramp facies of field section partly overlaps with the distal middle ramp to the outer ramp facies of this study, due to the fact that the distal middle ramp and the outer ramp facies are transitional. The main difference between the field and the well descriptions of the Derdere Formation is the highly variable primary constituents and facies deposited in the shallow water environment of Derik field section. The Macae Formation, Campos Basin in Brazil, the Cenomanian stage of the northern Germany, the Cenomanian-Turonian Sarvak Formation in Bi Hakimeh oil field, and the Cenomanian–Turonian succession of Guerrero–Morelos Basin, Southern Mexico are compared with the Cenomanian-Turonian Derdere Formation of Diyarbakır Region, southeastern Turkey. Peloids, intraclasts, benthic foraminifera, echinoderms, rudists, gastropods and algae are common constituents of inner ramp depositional setting defined in different formations of Cenomanian-Turonian worldwide. Peloids, benthic foraminifera and bioclast debris including variable skeletal fragments are the components of proximal middle ramp and planktonic foraminifera, calcisphaerulids and skeletal fragments (bivalves and crinoids) are defined in all of the Cenomanian-Turonian successions mentioned. The outer ramp depositional settings of the carbonate ramp platforms worldwide are dominated by calcisphaerulids, planktonic foraminifera, bivalve and crinoids during Cenomanian-Turonian.

# CHAPTER 4

# SEQUENCE STRATIGRAPHY

The main purpose of this study is to reveal sequence stratigraphic framework of the Derdere Formation in the well samples as an alternative to lithostratigraphy. The reason of studying sequence stratigraphy is to show whether there is a direct relationship with the global eustatic signals and facies change during the depositional time interval of Derdere Formation and upgrading the studies related with the Derdere Formation from lithostratigraphy to chronostratigraphy and eventually provide a relation to the reservoir quality development in terms of petroleum exploration. The most challenging part of this study is dealing with dolomites observed in some levels of the well sequences which prevent us to describe genetically related depositional sequences during sea level changes since dolomitization causes depositional features disappear. The other challenging point is studying with wells samples instead of field samples due to problems related with sample resolution and impossibility of observing bedding and bed thickness in the well samples. Among the studied well, the K-11 well has been selected for the sequence stratigraphic study with numerous and well recovered core samples in order to prevent problems related with sample resolution.

Eustatic signals recorded in the deposition of the Derdere Formation are detected with the sequence stratigraphic study and the correlation of global sea level chart of Haq (2014) from the late Albian to early Turonian. Hence, with the integrated study of microfacies analysis and log studies, nine depositional sequences are identified within the complete Cenomanian to early Turonian time interval which corresponds to the Derdere Formation. In the Derik section of Mardin which triggers this study a total of twelve depositional sequences are observed in the Derdere Formation (Özkan and Altiner, 2019).

The reason of different number of depositional sequences in K-11 pilot well and in the Derik section is the missing part at the base of the Derdere in the studied wells and due to time transgressive deposition of the Derdere Formation. The number of depositional sequences in early Turonian time is the same in the studied wells and field section. Among the wells which do not have entire penetration to the Derdere Formation, the number of sedimentary packages is less than the number of sedimentary packages where whole succession of the Derdere is penetrated.

## 4.1 SEQUENCES IN DERDERE FORMATION

In sequence stratigraphy, cyclicity can be detected at different scales. At this different hierarchical levels sequence stratigraphic framework is developed by sequences, system tracts and depositional systems; for instance at the smallest scales, beds and bedsets type of sedimentological cycles can be discriminated. “Sequences” are lower rank stratigraphic cyles and they can be developed at any larger scale system tracts and depositional systems (Catuneau, 2019). ‘Megasequence’ and ‘supersequence’ nomenclature is developed by Krapez (1996). Fourth-order and lower rank sequences are also termed ‘cyclothems’ (Wanless and Weller 1932), ‘cycles’ (Heckel, 1986) or ‘simple sequences’ (Vail, 1991; Schlager, 2010); Third-order sequences are also termed ‘mesothems’ (Ramsbottom, 1979), ‘megacyclothems’ (Heckel, 1986) or ‘standard sequences’ (Vail, 1991; Schlager, 2010); Second-order sequences are also termed ‘composite sequences’ (Abreu et al., 2010) (**Figure 83**).

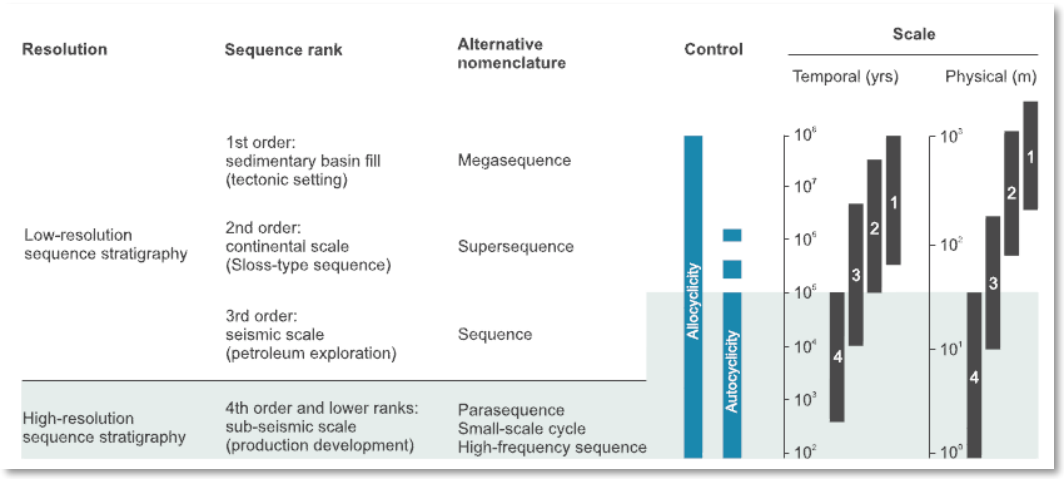


**Figure 83.** Classification of stratigraphic sequences including temporal and physical scales compiled from the study of Vail et. al. (1977), Vail (1991), Williams (1988) Van Wagoner et. al. (1990) Carter et. al. (1991), Einsele et. al. (1991), Reid and Dorobek (1993), Duval et. al. (1998), Lehrmann and Goldhammer (1999), Schkager (2004, 2010), Miall (2010), Catuneanu (2019)

In this study, mainly 3rd order sequences are detected regarding eustatic control on the variations of microfacies (shoaling and deepening upward sedimentary packages). The resolution of the 3rd order sequences are considered as suitable for the purpose of this study. As mentioned above, the thicknesses of the sequences vary between 5 meters to 50 meters. According to the classification chart of stratigraphic sequences, physical scale for the 3rd order sequences is between 10-100 meters (**Figure 83**). The resolution of sampling for cutting samples is 2 meters which is not suitable to study high resolution sequence stratigraphy including the 4th and 5th order parasequences the reason why, the study is based on the 3rd order sequences. Although there have been some sequences which are less than 10 meters in thickness, the number of these type of sequences are less. Using INPEFA log data, interpreting relative sea level changes and describing microfacies petrographically, eight and a half 3rd order sequences are defined in K-11 well which do not have entire penetration to the Derdere Formation. In the other wells, totally nine 3rd order sequences are recognized.

With the description of the upward shoaling and deepening packages, maximum flooding surfaces (MFS) and sequence boundaries (SB) are defined and

sequentially important key surfaces including SBs and MFSs are correlated with the turning points defined on the INPEFA log (**Figure 84** and **Figure 85**).

Main primary constituents defined in highstand systems tracts (HSTs) are peloids, mollusks (bivalve and gastropods), large benthic foraminifers, echinoderms, rudists, intraclasts, and oyster which become more abundant at the top of HST. In transgressive systems tracts (TSTs), the main primary constituents are rare large benthic foraminifers, small benthic foraminifers and rare mollusks, planktonic foraminifers, calcisphaerulids including *Pithonella spherica*, *Pithonella ovalis* and *Bonetocardiella conoidea*, sponge spicules frequently and rare radiolaria at the top of TST. As another observation in HSTs, shallower microfacies, wall type of calcisphaerulids differs from wall type of calcisphaerulids observed commonly in TSTs, deeper microfacies. In shallower microfacies, thin walled *Pithonella spherica* and *Pithonella ovalis* type calcisphaerulids are observed while in deeper microfacies, thick walled calcisphaerulids including *Pithonella spherica*, *Pithonella ovalis* and *Bonetocardiella conoidea* are recorded as mentioned in the study of Dias-Brito (2000).

INPEFA curves show general trends recording turning points that can be interpreted as they are related with significant events as mentioned in previous sections. Lithology sensitive logs can be a good indicator for the effects of Milankovitch cycle recorded in sedimentary strata. From the sequence stratigraphic point of view, key bounding surfaces including sequence boundaries and maximum flooding surfaces, which have time significance, can be distinctive on INPEFA logs although it is not easy to differentiate seismically defined sequence boundaries and maximum flooding surfaces on other well logs (**Figure 84** and **Figure 85**).

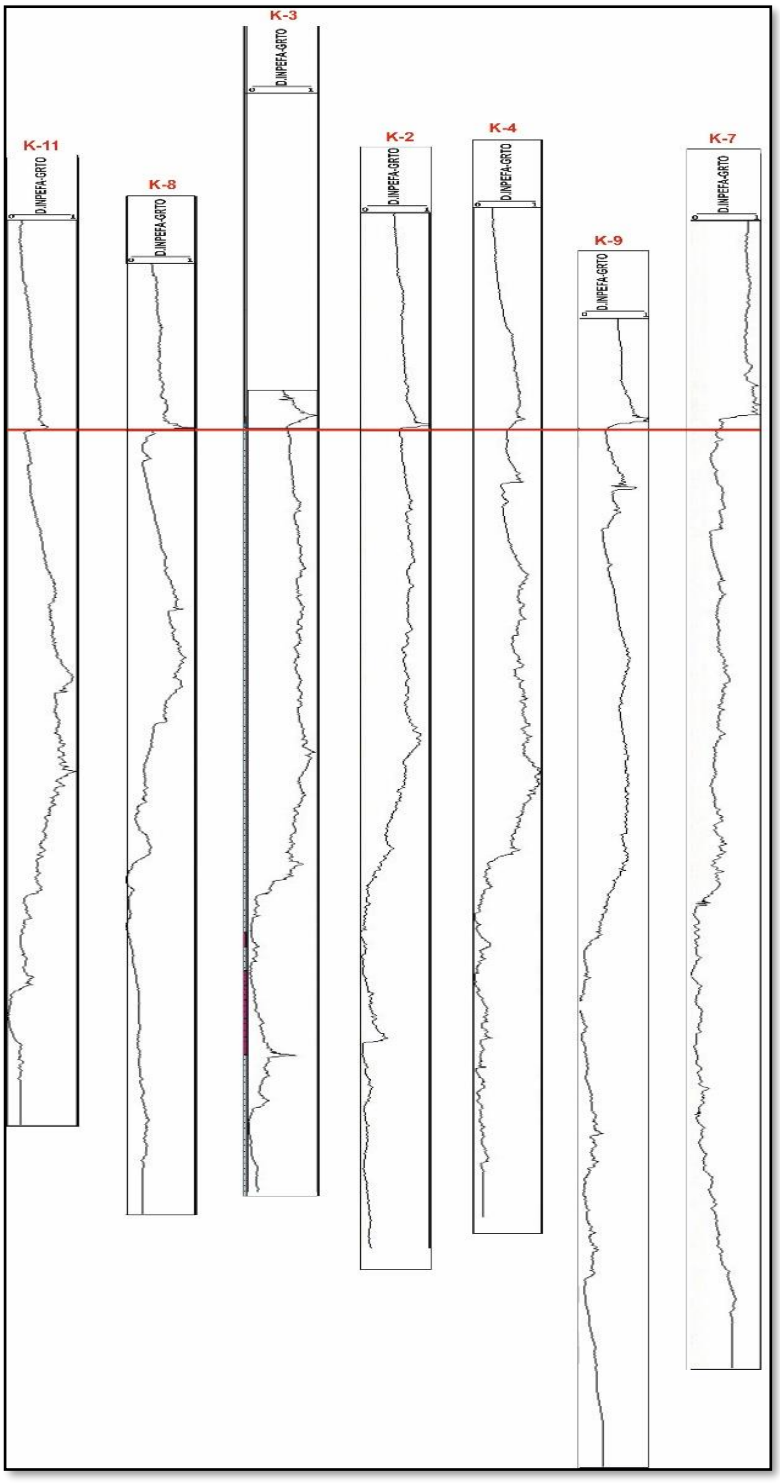


**Figure 84.** From west to east INPEFA log responses without interpretation (K-11, K-8, K-3, K-2, K-4, K-9, and K-7) (Red line shows the boundary between Derdere and Sayındere formations.)

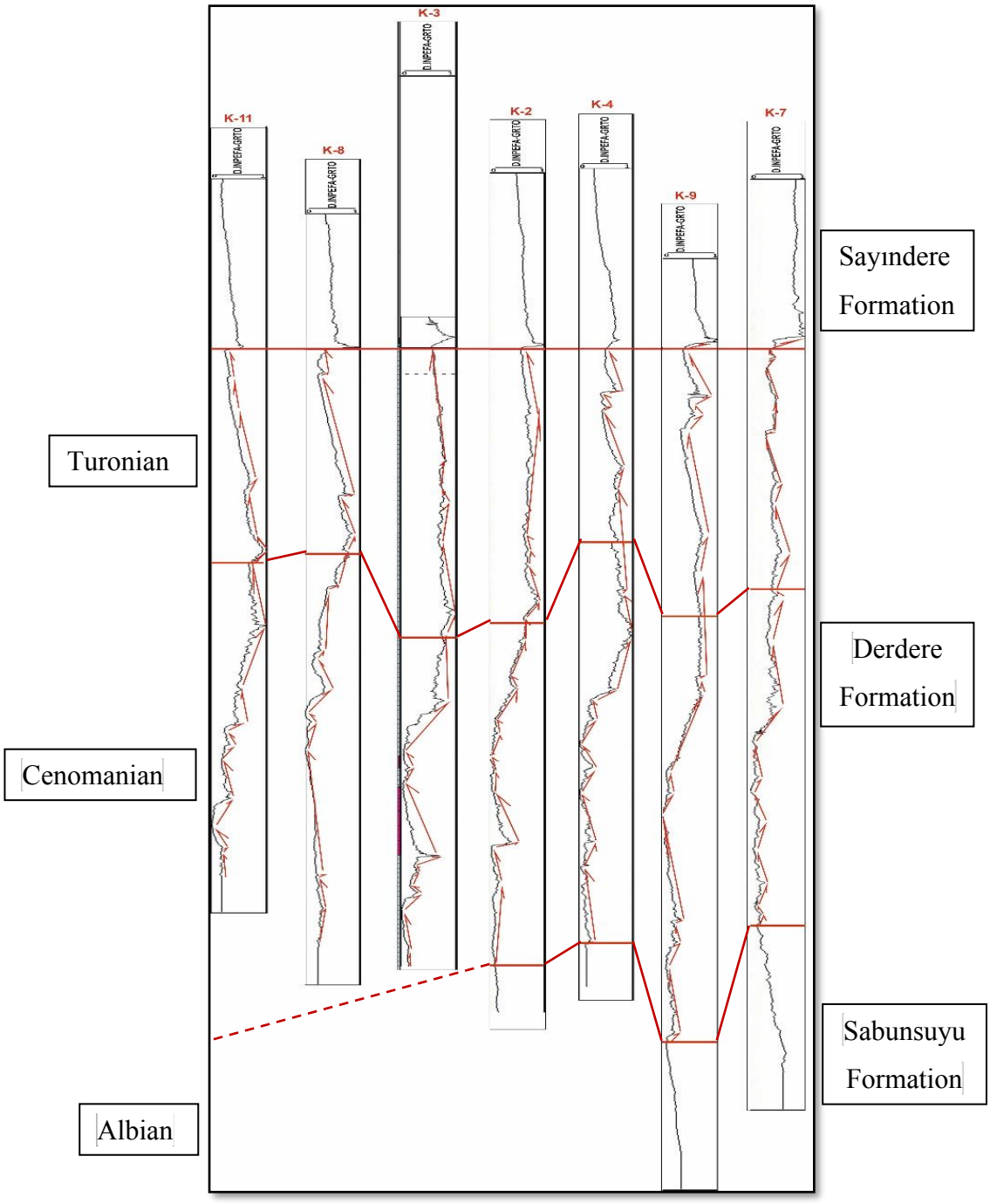


**Figure 85.** From west to east INPEFA log responses with interpretation (K-11, K-8, K-3, K-2, K-4, K-9, and K-7) (The direction of red arrows shows shoaling upward and deepening upward packages in the sequences. Going through right means deepening, going through left means shoaling. Red lines show timelines including Albian-Cenomanian and Cenomanian-Turonian boundaries.)

Where seismic sections are not available to use for sequence stratigraphic interperations, INPEFA log provides high-resolution divisions between time significant units instead of seismic (Nio et. al., 2005). It is commonly used in other sequence stratigraphic studies in terms of providing insights to sea level fluctuations including regression and transgression of sea level (Soua, 2012; Soleimani, 2013).

In this study INPEFA logs are created by using GRTO and GRKT where it is available, which are considered as lithofacies sensitive logs, and turning points observed on the curves interpreted as they are associated with sea level change. Since INPEFA log is obtained by using gamma ray log, it has same working principle with the gamma ray log in terms of lithofacies. Scale of INPEFA log defined in this study is between zero (on the left) and one (on the right). If trend of the curve is going through one (to right), deeper lithofacies is supposed to be recorded due to the working principle of gamma ray well log which is deeper lithofacies shows higher gamma ray values and vice versa. In other words, if turning point identified on the INPEFA curve is tending move right, transgressive systems tract is drawn and if turning point goes to left, highstand systems tract is drawn. Where TSTs change to HSTs, and HSTs evolve to TSTs on INPEFA log curves, change in lithofacies is also observed petrographically. To locate sequence boundaries and maximum flooding surfaces exactly on the sedimentological log, depth of drilling and depth of logging should be calibrated. In order to use logs drilling depths and logging depths should be correlated. For instance; if the total depth according to drilling is 1872 m while according to logging 1877 m as in K-8 well, cuttings and core samples should be located 5 meters above the actual depths while drawing sedimentological logs. Change in lithofacies and the turning points on INPEFA log are evaluated together to define the 3$^{rd}$ order sequences on the whole section.

Microfacies descriptions, INPEFA logs, biostratigraphic analysis and stable isotope data are used to define the 3$^{rd}$ order sequences in each well sepearately (**Figure 86** and **Figure 87**). From bottom to top, totally nine sequences are numbered in order to follow the descriptions.

In the first sequences at the bottom of the Derdere succession, inner ramp (tidal flat to lagoon) depositional conditions are prevailing and deepening upward (TST) package of first sequence is observed as dolomitized (**Figure 87**) and partially dolomitized benthic foraminiferal skeletal wackestone to packstone (MF2) is observed petrographically. In the shoaling upward (HST) package, skeletal benthic foraminiferal peloidal grainstone to packstone, benthic foraminiferal skeletal peloidal packstone (MF3) and benthic foraminiferal mudstone (MF1) is described and in some wells, at the top of this sequence, dolosparite is identified (**Figure 86**). In the K-11 well, TST package of the sequence is absent due to the partial penetration in the Derdere Formation.

In the second sequences, inner ramp to proximal middle ramp environmental conditions are still dominant and mostly thickness of TST in this sequence is a few meters whereas HSTs are thicker and reach up to 30 meters (**Figure 87**). In the bottom and middle part of HST package, thin calcareous dolosparite with some preserved allochems are noted (**Figure 87**) and benthic foraminiferal skeletal peloidal packstone to grainstone (MF3) and peloidal packstone to grainstone (MF4) are remarkable microfacies at the top of this sequence (**Figure 86** and **Figure 87**).

In the third sequences, microfacies are interpreted as the deposits of middle ramp depositional setting. In the deepening upward package (TST) of the sequence, calcisphaerulids enter to the system and skeletal calcisphaerulid-bearing packstone wackestone to packstone and in the shoaling upward package (HST) of the sequence, calcisphaerulid-bearing skeletal wackestone to packstone (MF9) is observed. In some sequences, although components of the microfacies do not have pronounced difference, with the relative increase in the abundance of the skeletal fragments, TSTs are discriminated from HSTs.

In the fourth sequence, still middle ramp conditions are prevailing and even distal middle ramp conditions are more dominant compared to proximal middle ramp. In the middle part of the Cenomanian, thicknesses of the sequences decrease (**Figure 87**). In the TST part, calcareous dolosparite and skeletal calcisphaerulid-bearing packstone with rare benthic foraminifera are described. In the HST package,

skeletal wackestone to packstone (MF6) with planktonic foraminifera and rare calcisphaerulid is identified. Similar to third 3rd order sequence, the main difference between deepening and shoaling upward packages are relative abundance of skeletal fragments. In the distal part of middle ramp and outer ramp microfacies, identification of the packages is problematic.

In the fifth sequence, distal middle ramp to outer ramp microfacies are frequently observed. The deepening upward package (TST) is a few meters in this sequence with the abundance of calcisphaerulids and sometimes organic matter, whereas shoaling upward package is thicker with the presence of planktonic foraminifera and skeletal fragments.

In the sixth sequence which is located just below the Cenomanian-Turonian boundary, thicknesses of the packages increase with the increasing rate of relative sea level change and incrasing accommodation space in some of the studied wells (**Figure 86**). During this time interval, still distal middle ramp to the outer ramp depositional conditions are prevailing for the deposition of microfacies. In the TST, outer ramp microfacies including calcisphaerulid-bearing packstone (MF13), and skeletal calcisphaerulid-bearing wackestone to packstone (MF15) are observed, in the HST, skeletal planktonic foraminiferal wackestone and planktonic foraminiferal skeletal calcisphaerulid-bearing packstone (MF14) are observed.

In the seventh sequence, distal middle ramp to outer ramp conditions constitute the microfacies defined in this time interval. This sequence is located in the bottom part of the Turonian succession (**Figure 86** and **Figure 87**). In the TST package of the sequence, among the pelagic microfacies, planktonic foraminiferal wackestone (MF12) and radiolaria-bearing mudstone (MF11), in the HST package, calcisphaerulid-bearing skeletal wackestone to packstone (MF9) with planktonic foraminifera in rare amount are idenitified.

The eighth sequence is thicker in most of the studied wells and thickness of it reaches approximately 30 meters (**Figure 86** and **Figure 87**) with thin TST and thick HST packages. This sequence is characterized by the middle ramp to inner ramp deposits. In the deepening upward part of the sequence, planktonic

foraminiferal skeletal mudstone to wackestone microfacies, in the shoaling part of it is composed of skeletal wackestone to mudstone (MF6), skeletal peloidal packstone to grainstone (MF4), peloidal skeletal wackestone to packstone (MF5) are identified. In the upper part of the HST, a few meter thick dolomicrosparite to dolosparites are observed (**Figure 86** and **Figure 87**).

In the nineth sequence which is the top of the Derdere Formation, a few meters thick TST is described and HST package is mostly observed as totally or partially dolomitized consisting of dolomicrosparite to dolosparite according to the size of primary depositional features in this sequence (**Figure 86** and **Figure 87**). If depositional constituents are small in size and in lesser amount (wackestone to mudstone in pelagic facies), dolomite texture tends to be dolomicrite to dolomicrosparite. If the facies are grain dominated, dolomite texture tends to be dolosparite.

Thin sections selected from the seven wells are studied biostratigraphically and petrographically to reveal the main components of the microfacies, depositional age of the Derdere Formation and significant biostratigraphic events during the deposition of the Derdere Formation, mainly the Cenomanian-Turonian boundary.

In order to show the planktonic and benthic foraminiferal assemblages, two of the seven wells are selected. The reason of selecting these two wells are the diversity of planktonic and benthic foraminifers compared to the other studied wells (**Figure 88** and **Figure 89**). Five of the seven wells have entire penetration of the Derdere Formation above the Sabunsuyu Formation. The Derdere Formation is rich in benthic and planktonic foraminifer assemblages where the bioclasts are not masked due to the intense dolomitization.

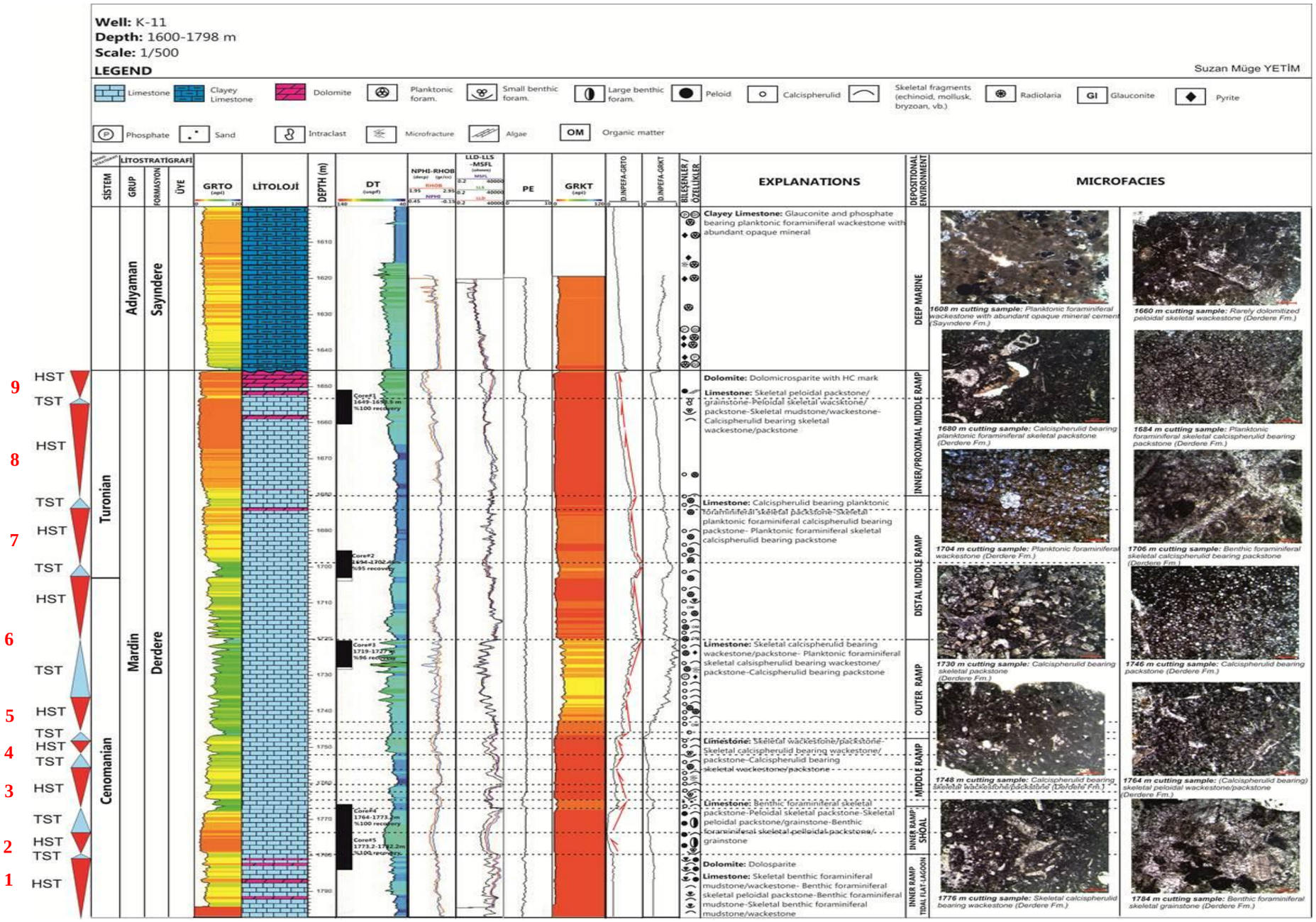


**Figure 86.** Sedimentological log and sequences of the Derdere Formation in the K-11 well (1600-1798m)

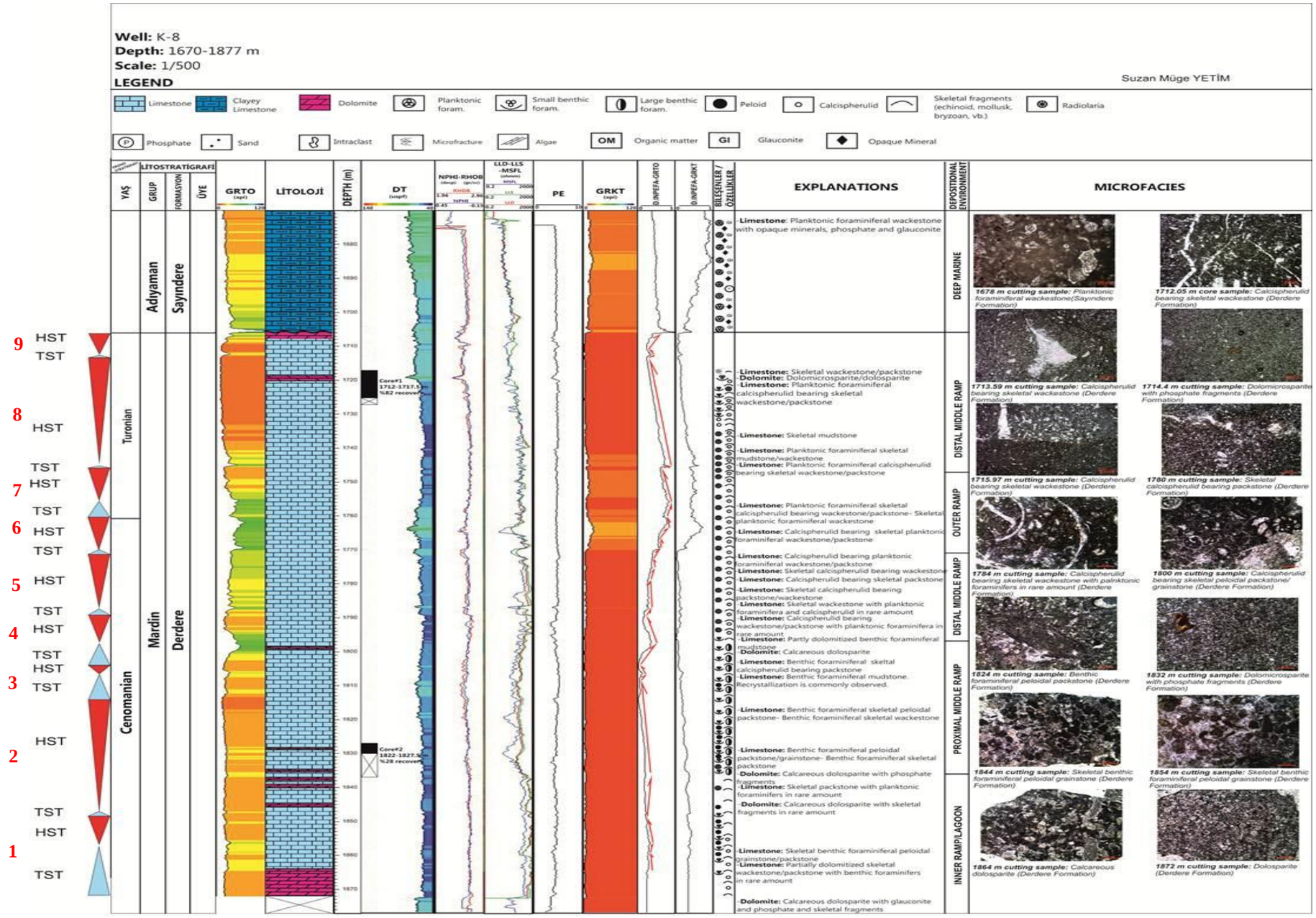


**Figure 87.** Sedimentological log and sequences of the Derdere Formation in the K-8 well (1670-1877m)

The formation has diversified benthic foraminifer assemblage in the lower Cenomanian deposits and diversified planktonic foraminifer assemblage in the lower Turonian deposits. The first appearance of *Cuneolina pavonia* d'Orbigny is firstly observed in the Albian (Vanneau and Sliter, 1995; Husinec and Sokoć, 2006; Velić, 2007; Ghanem and Kuss, 2013; Özkan and Altiner, 2019) and other benthic foraminifers *Praechrysalidina infracretacea* whose last appearance is also defined as late Albian (Vanneau and Silva, 1995; Velić, 2007; Ghanem and Kuss, 2013; Özkan and Altiner, 2019), *Nezzazata simplex and Nezzazata isabellae* (Özkan and Altiner, 2019) are associated with *Cuneolina*. In the section of K-11 well, benthic and planktonic foraminifers are studied in detail in order to reveal Cenomanian-Turonian boundary and Cenomanian-Albian boundary whether there is Albian or not. The significant distribution of the significant benthic species, *Hensonina lenticularis* is limited to late Albian (Castro et al., 2001; Ghanem and Kuss, 2013; Özkan and Altiner, 2019) and the last occurance of this type of benthic species is nearby Albian-Cenomanian boundary (Özkan and Altiner, 2019). In the section of K-7 Well, *Hensonina lenticularis* type benthic foraminifer is recognized where Albian-Cenomanian boundary is located at 2948 meters (**Figure 89**).

At the bottom of Cenomanian deposits, the benthic foraminifer assemblage is composed of *Praealveolina, Pseudolituonella, Biplanata peneropliformis, Trochospira, Dicyclina, Sellialveolina, Nezzazata conica* in K-11 well (**Figure 88**). Above this level which is rich and diversified in terms of benthic foraminifers, planktonic foraminifers including *Hedbergella, Muricohedbergella, Heterohelix* and *Macroglobigerinolloides* are observed. Planktonic foraminifers become more abundant close to Cenomanian-Turonian boundary. The boundary between the Cenomanian-Turonian is located regarding to the appearance of *Whiteinella* which is accompanied by *Muricohedbergalla planispira, Muricohedbergella simplex, Archaeglobigerina cretacea, Marginotruncana (M. marianasi, M. schneegansi, M. sigali), Heterohelix globolusa, Globigerinolloides*. *Whiteinella* species are recorded in the cores of K-11 Well and they are described as *Whiteinella baltica, Whiteinella praehelvetica, Whiteinella britonensis, Whiteinella paradubia, Whiteinella archaecretacea, Whiteinella inornata* (**Figure 88**). At the top of the Derdere Formation benthic foraminifer assemblage consists of miliolid, textularid, *Ataxophragmidae, Belorussiella, Valvulina and Coscinolina*.

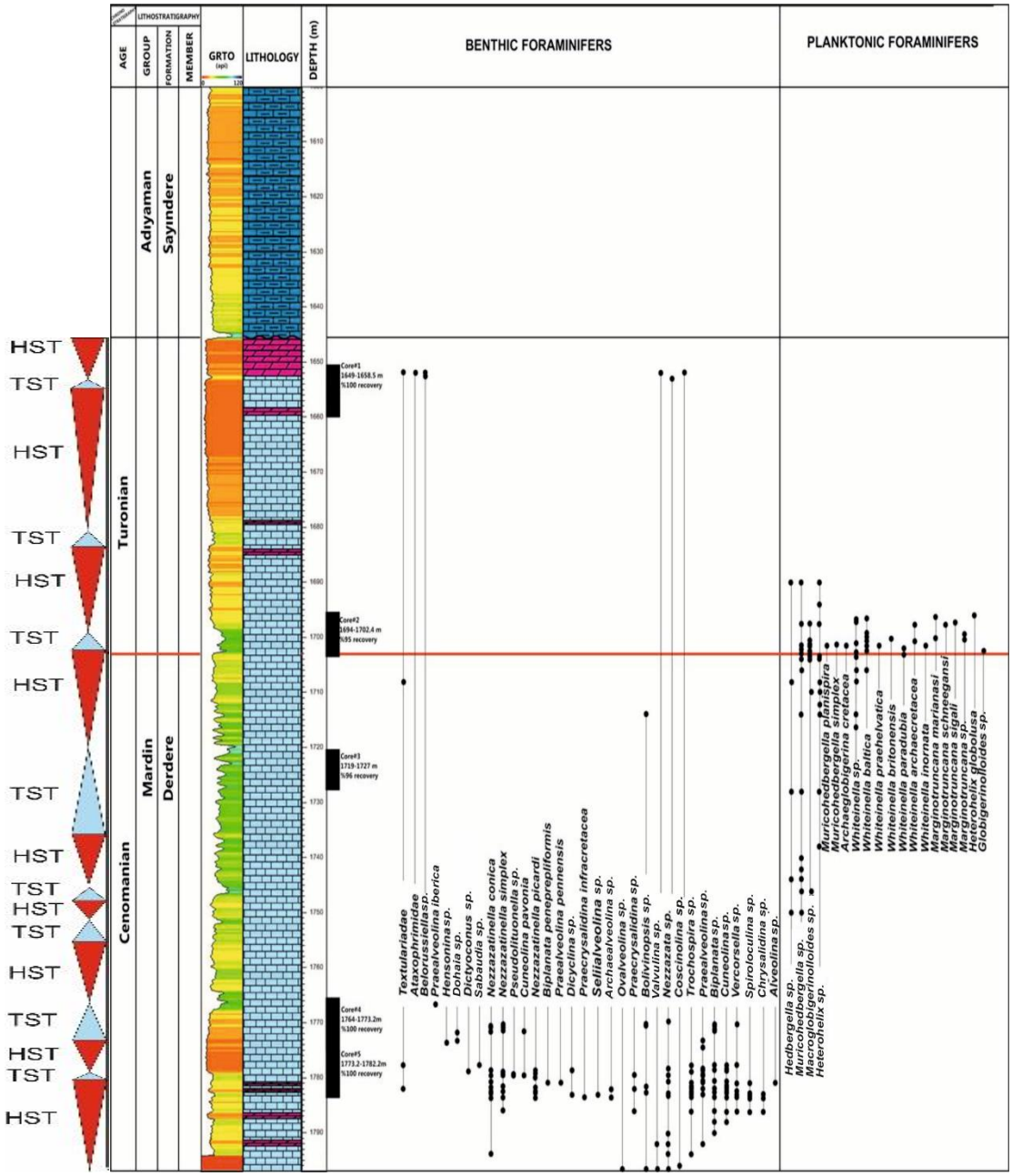


**Figure 88.** Benthic and planktonic foraminifer assemblage of the Derdere Formation observed in the K-11 well (Red line shows the Cenomanian-Turonian boundary.)

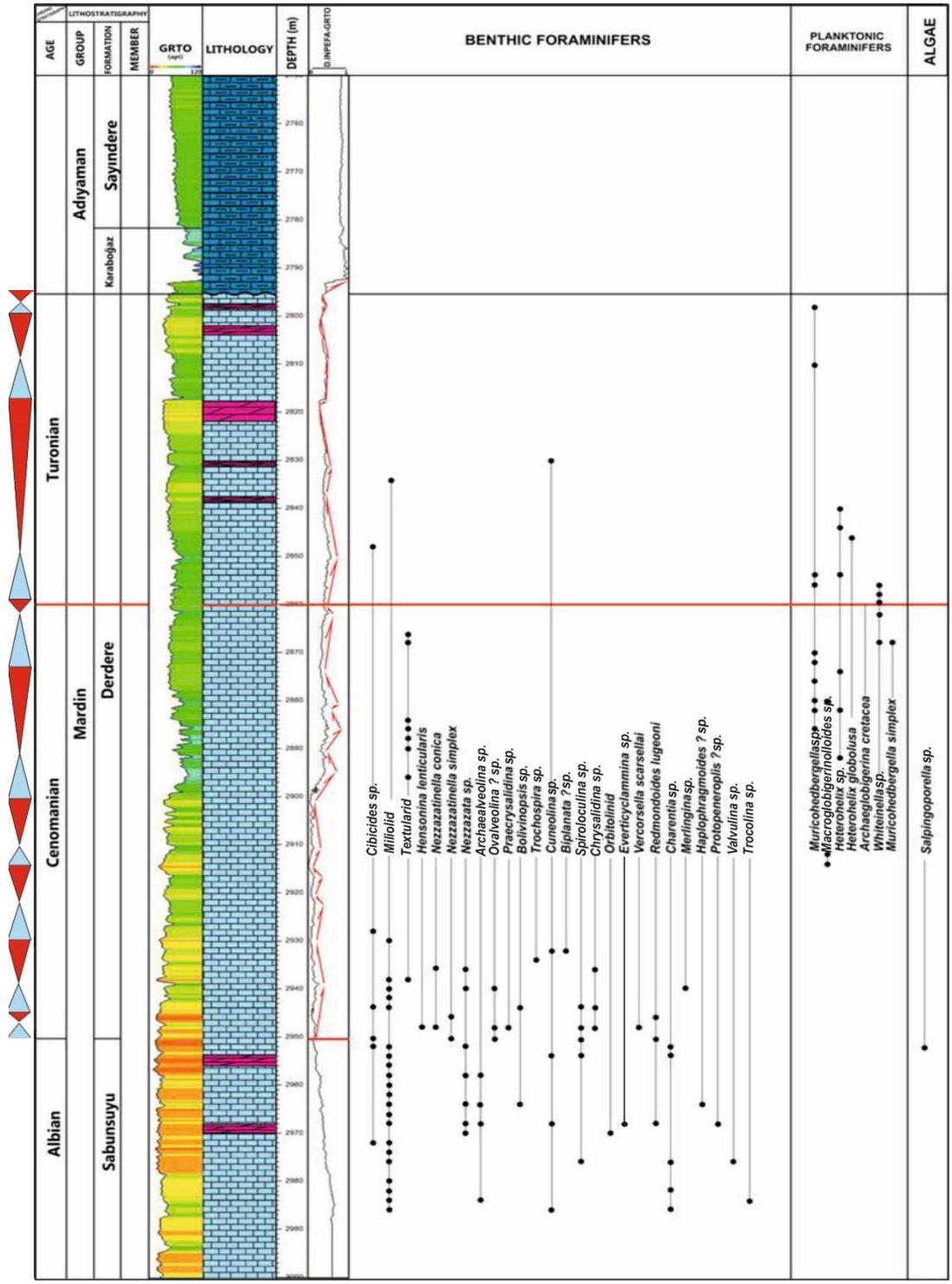


**Figure 89.** Benthic and planktonic foraminifer assemblage of the Derdere Formation observed in the K-7 well (Red line shows the Cenomanian-Turonian boundary.)

### 4.1.1 Sequence Stratigraphic Correlation between the Wells of the Study Area

Totally seven wells including K-11, K-8, K-3, K-2, K-4, K-9 and K-7 wells are studied in order to discriminate 3rd order sequences from west to east in the studied region (**Figure 90**). Benthic and plantonic foraminifer assemblages are more or less similar in the same time intervals of the studied wells and by taking into consideration of these assemblages microfacies are described (**Figure 90**).

INPEFA log, which reveals trends and other patterns that are not generally apparent from the original log data, is evaluated together with the microfacies descriptions and biostratigraphic data in order to reveal eustatic signals. All INPEFA logs based on gamma ray logs are hanged from the top of Derdere Formation using the same left shift on INPEFA log (**Figure 90**) where the unconformable boundary between Sayındere and Derdere formations and Karaboğaz and Derdere formations in K-7 Well. Correlation with lithofacies provides the definite sequence stratigraphic key surfaces (sequence boundaries and maximum flooding surfaces) and they become correlative throughout the basin.

The numbers of sequences defined in the wells are the same except for the westernmost K-11 well which does not have entire penetration to the Derdere Formation. In the K-11 well, eight and a half sequences are detected and half more sequence should have been in the Derdere Formation if drilling would have been continued before the Sabunsuyu Formation is reached. The omission from the top of the Derdere Formation is not taken into consideration due to the same number of sequences in Turonian time interval where Derdere and Karababa formations have contact in the field section. In Turonian section, there are three and a half sequences in the Derik section of Mardin.

The thicknesses of depositional sequences defined in the well sections are variable (**Figure 90**). There are some sequences whose thicknesses are about 5 meters and they are mostly distinguished with the use of shifts observed on the wireline logs (INPEFA log) which are interpreted to be related to sea level changes. The thicknesses of depositional sequences reach at about 50 meters in some parts of the sections which can be interpreted as related with the accommodation space.

The C-T boundary sequences are generally getting thicker with the increasing accommodation space and increasing rate of sea level, recognized and explained also in the study of Özkan and Altiner (2019). Another consequence of this study which is also supported by the study of Özkan and Altiner (2019) is that the meteoric diaganesis is related with the subaerial exposure on the top of highstand systems tract deposit and the dolomitization is related with the relative sea level fall (Morad et. al, 2012). Dolomitic peloidal bindstone facies which is observed in the highstand system tract deposit is capped by and a hematic crust interpreted as the indicator of subaerial exposue in the study of Özkan and Altiner (2019). If there is subaerial exposure and entrance of meteoric water, it is believed that it should be in the tidal flat/shoal and inner ramp type of depositional environments of the Derdere Formation rather than at the top of each highstand systems tracts.

Another observation on the sequences is thin transgressive systems tract deposits, which is also recognized in the Derik Section by Özkan and Altiner (2019), due to the slower rate of deposition or late onlap on the highstand systems tracts after the nondepositional hiatus (Özkan and Altiner, 2109).

In the studied sections of the wells, there is carbonate rock dominance (including limestone, dolomite and dolomitic limestone) which are considered as shoaling and deepening in order to describe genetically related depositional sequences. Siliciclastic contribution to the carbonate successions is only observed in one thin section of the K-11 well. In the thin sections obtained from the core sample at 1764.37 m (top of Core#4), silt and sand size quartz particles are observed as a siliciclastic contribution to the carbonate facies which can be interpreted as “catch-up” phase which is at the bottom of transgressive system tract deposits due to slow rate of accumulation during the early Cenomanian time of the Derdere deposition. In the Derik section the siliciclastic deposition of Aptian age was considered as lowstand systems tract deposits in the Sabunsuyu Formation (Özkan and Altiner, 2019). With the acceleration of the rate of sea level rise, carbonates could not keep pace with the rising sea level and thin carbonate successions especially were deposited in the transgressive systems tracts. As a general principle of sequence stratigraphy, the rates of carbonate deposition keep pace with the changing rates of accommodation space and start to fill accommodation spaces and the thickness of

depositional sequences during highstand systems tract deposits start to increase (Özkan and Altiner, 2019).

As a general observation in the studied sections of the wells, transgressive systems tracts of the depositional sequences correspond to the outer ramp to distal middle ramp facies and are thin to medium; however highstand systems tracts of sedimentary packages are thicker in inner ramp/shoal and tidal flat facies (**Figure 90**).

C-T boundary is defined biostratigraphically in the wells and it is correlated throughout the basin (**Figure 90**). When biostratigraphically defined C-T boundary is drawn on the GR and INPEFA logs, wireline log trend of the C-T boundary could be generalized. On the INPEFA logs, there are two levels where the sea level is at its highest position and the biostratigraphically defined C-T boundary is between these two highest sea levels according to INPEFA log. By using this method based on the INPEFA logs, the C-T boundary can be drawn where cutting and core samples are insufficient. Between the highest sea levels on the INPEFA log, the C-T boundary is located somewhere in the highstand systems tract of the sixth sequence. According to GR log similar to INPEFA, where first shoaling is observed after the highest sea level in the Derdere succession, C-T boundary can be drawn (**Figure 90**).

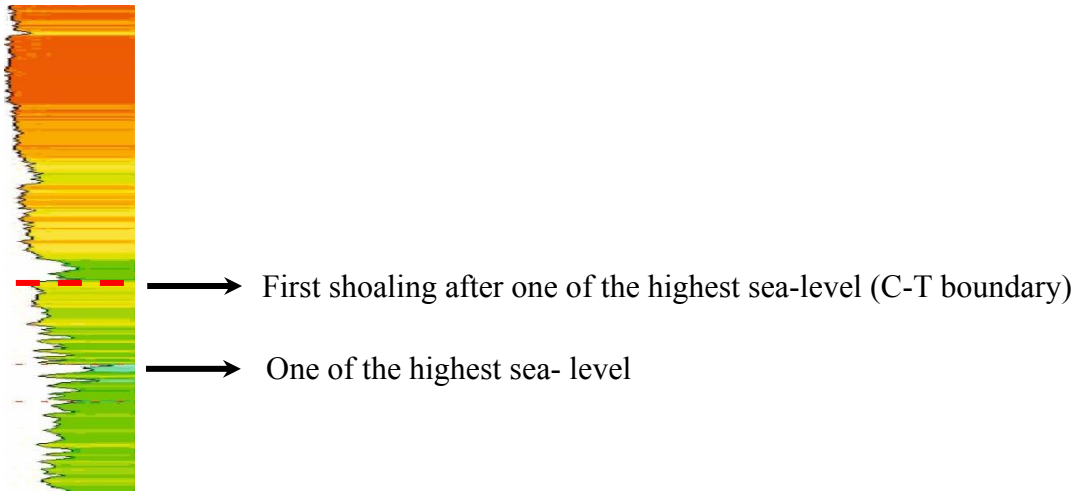

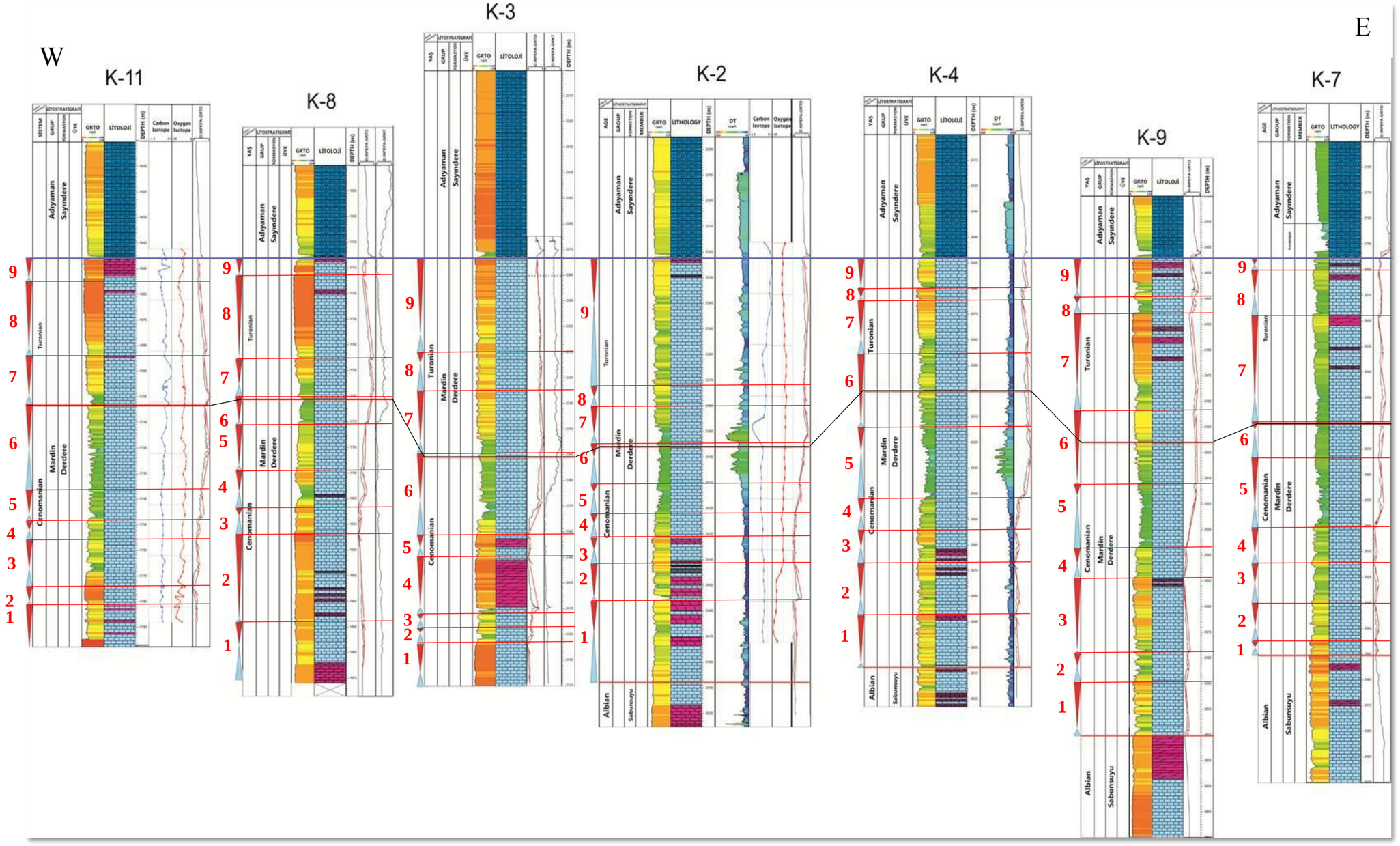


**Figure 90.** 3rd order sequence correlation between the wells of the study area from west to east (K-11, K-8, K-3, K-2, K-4, K-9, and K-7) (Red lines show sequence boundaries, black line shows C-T boundary and blue boundary shows the boundary between Derdere and Sayındere formations)

### 4.1.2 Sequence Stratigraphic Correlation between the Wells of the Study Area and the Derik Field Section

In the field study of Mardin Group Carbonates including Areban, Sabunsuyu and Derdere Formations, totally twenty-one 3rd order sequences are defined within the earliest Aptian to late middle Turonian time interval in the Derik Section (Özkan and Altiner, 2019) (**Figure 91**). In the Derik Section, the Derdere Formation starts from 10th sequence and continues up to 21st sequence, where totally twelve 3rd order sequences are defined (**Figure 91**). Thicknesses of the sequences defined in the Derik Section are variable which can be considered as similar to the sequences defined in the studied wells. Deposition of the Derdere Formation starts from mid-Albian and ends in Turonian time interval (**Figure 91**). In the Derik Section where the C-T boundary is defined, there are three and a half 3rd order sequences in the uppermost part of the Derdere Formation numbered as 18th 19th, 20th and 21st sequences (**Figure 91**). In the studied wells, where the Cenomanian-Turonian boundary is defined, there are three and a half 3rd order sequences in the uppermost part of the Derdere Formation. In the Derik Section, the Derdere Formation directly underlies the Karababa Formation while the Derdere Formation unconformably underlies the Sayındere Formation in the wells. Whether there is erosion it is supposed to be in a minor degree which does not change the number of sequences at the topmost part of the Derdere Formation. The same number of sequences in the Turonian time interval detected in the Derdere Formation suggests that the gap between the Derdere and Sayındere formations correspond to a non-deposition rather than erosion.

In the field section, Albian deposits are represented by a rich and partially diversified planktonic foraminifer assemblage, which is also associated with abundant calcisphaerulids. The boundary between Derdere and Sabunsuyu Formations is located by considering the pelagic facies in the Derdere Formation. Some rarely observed benthic foraminifera including *Hensonina lenticularis* are used to define late-middle Albian (Özkan and Altiner, 2019).

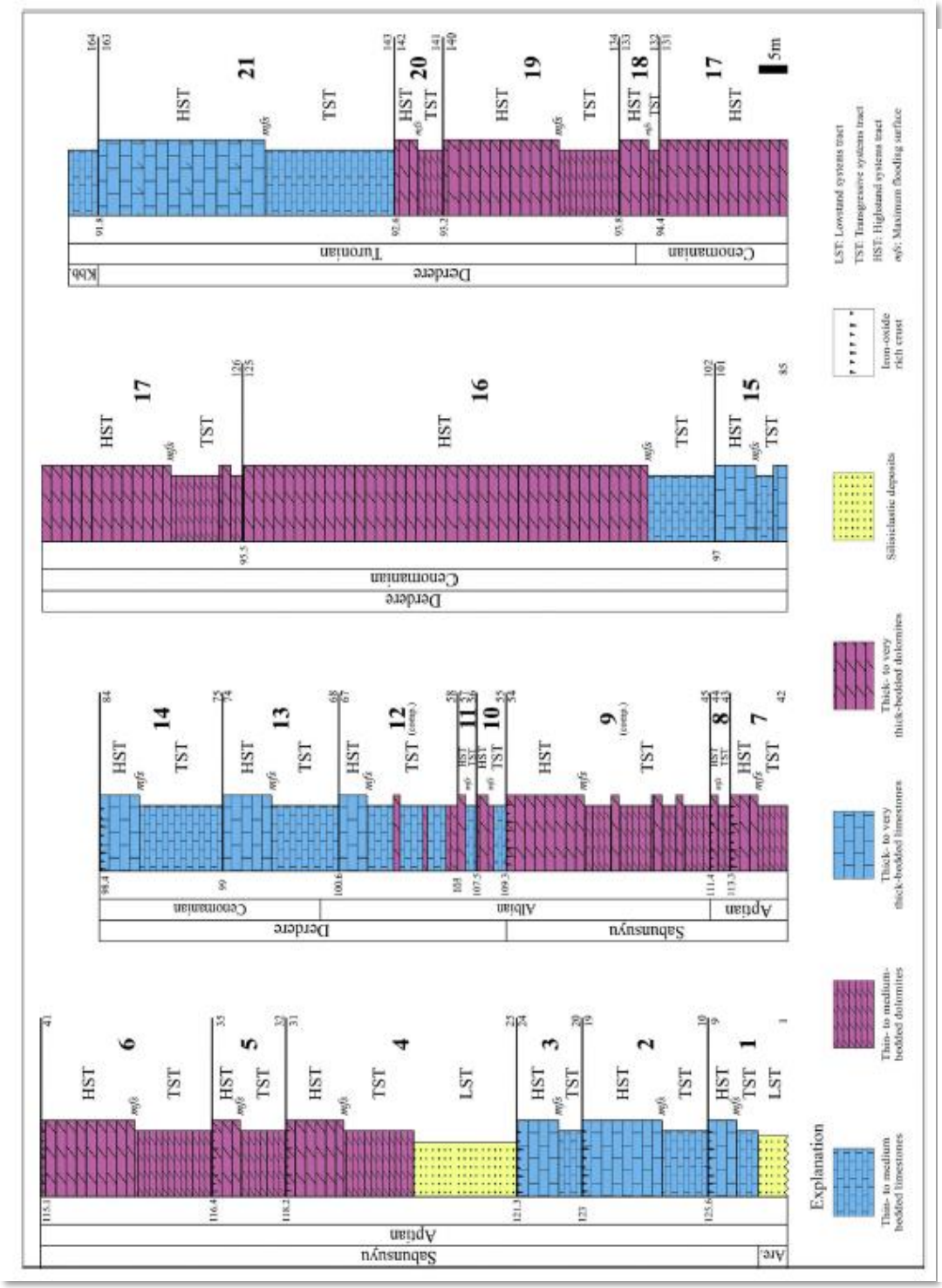


**Figure 91.** Sequence stratigraphy of the Areban, Sabunsuyu and Derdere formations of the Mardin Group in the Derik section, Mardin (Özkan and Altiner, 2019)

The lithologic separation of Derdere and Sabunsuyu formations based on the existence of pelagic facies including planktonic foraminifers and calcisperulids according to the study of Özkan and Altiner (2019). In this study, benthic foraminifera are dominant instead of

planktonic foraminifera in the Albian and pelagic facies are observed in the upper levels of the Derdere Formation. In other words, planktonic foraminifers and calcisphaerulids are found in the Turonian different from the field study. Hence, shallow-water facies are defined in the Albian of the well samples and the deposition age of the Derdere Formation is restricted to Cenomanian to Turonian. Since the deposition of the Derdere Formation started in late-middle Albian in the Derik section of Mardin whereas the deposition of the Derdere Formation started in the Cenomian in the wells of foreland area of the Diyarbakır Region, the deposition of the Derdere Formation is considered as time-transgressive.

When the well samples are compared with the field samples in terms of skeletal and non-skeletal fragments, it is obvious that components of well samples are not as diverse as field samples. This can be explained by sample resolution of cuttings in the wells. Another difference between the field section and the well sections is the presence of *Marginotruncana*-type planktonic foraminifers in different sequences and during different time intervals. In the thin sections of the K-11 well, *Marginotruncana* species are identified just above the the Cenomanian-Turonian boundary while this type of planktonic foraminifera is recognized in the Karababa Formation during Turonian in the field section.

Similarly *Praealveolina* type benthic foraminifers are described in the 14$^{th}$ sequence of field section and there are four more sequences until the bottom of Derdere Formation; however *Praealveolina* rich zone is observed at the bottom of the Derdere Formation in the studied wells. When the Derik field section is correlated with the studied wells, 14$^{th}$ of the *Praealveolina* rich sequence of field section correspond to 2$^{nd}$ sequence of the studied wells (**Figure 92**).

In the study of Özkan and Altiner (2019), 5 types of sequence boundaries are described in the field section of Derik, Mardin. If there is subaerial exposure at the top of highstand systems tract, they mentioned the existence of hematic crust at the cycle top or iron oxide rich mottled limestone. Another type of sequence boundary is dolomitized surface with dissolution vugs or bedding parallel irregular erosional surface. The other type is not easy to detect at the field due to less effective or lack of subaerial exposure and this type of sequence boundaries can be discriminated with the sharp contact between highstand systems tract and transgressive systems tract deposits.

In the sequence stratigraphic study of the well samples, it is not easy to distinguish the sequence boundaries since evidences of sequence boundaries are challenging to observe lithologically on cutting samples unless there are not core samples. Among these sequence boundary types and evidences, the boundary between highstand systems tract and transgressive systems tracts are used commonly to detect sequence boundaries. Dolomitized surfaces with the dissolution vugs are observed in thin sections of the core samples of the K-11 well which has been considered as a significant evidence of sequence boundaries. In order to define sequence boundaries in the other studied wells, these dissolution vugs are tried to be detected petrographically and correlated with the shifts on INPEFA logs.

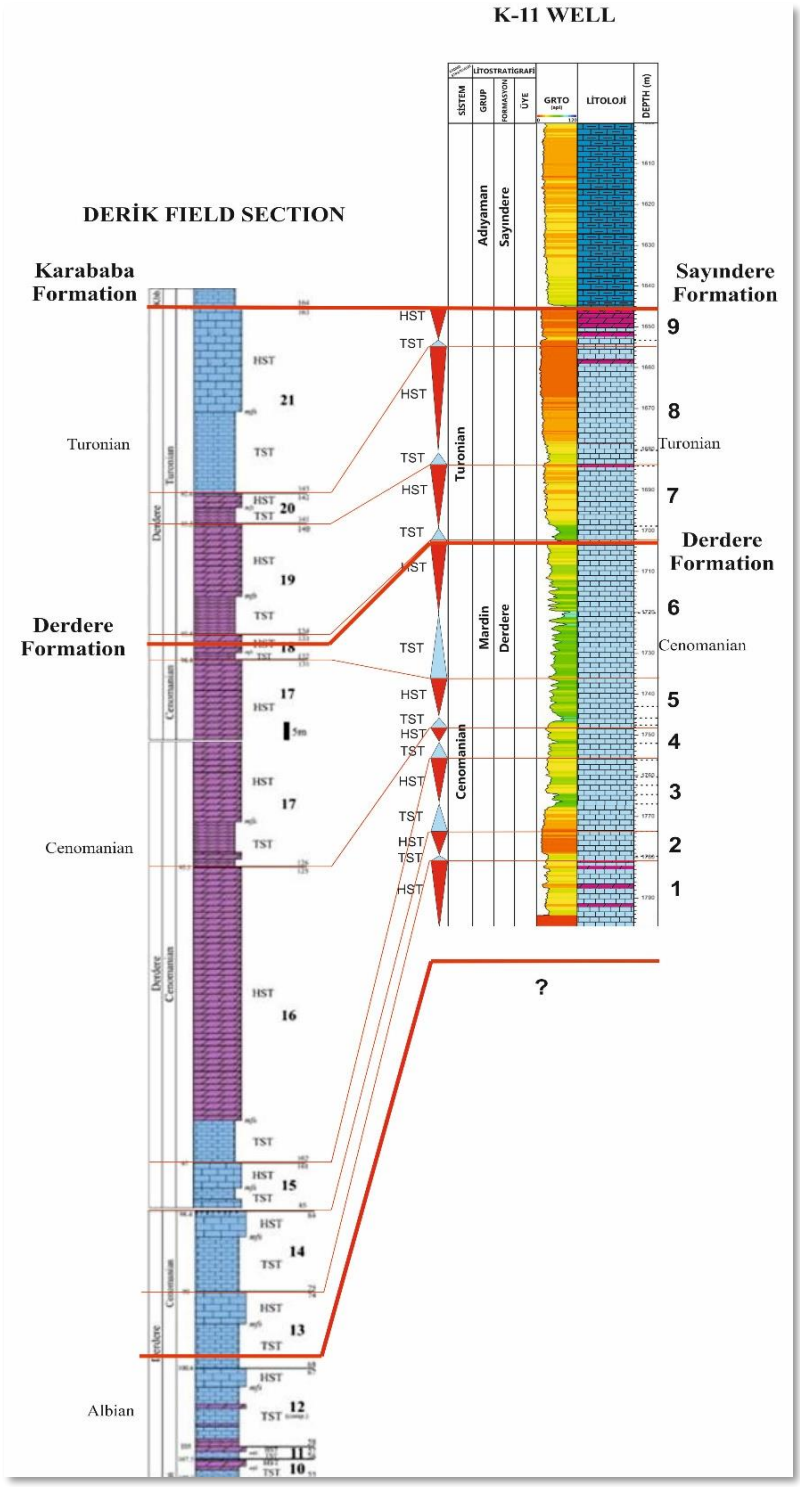


**Figure 92.** Sequence stratigraphic correlation between the K-11 Well and the Derik field section [Sequences defined in the Derik field section is modified from the study of Özkan and Altıner (2019)]

### 4.1.3 Sequence Correlation with the Global Cycle Chart of Haq, 2014

In this study, 3rd order sequences are defined using both microfacies data and INPEFA logs due to the restriction related with working on cutting samples and sample resolution. Working principle of INPEFA logs depend on relative sea level changes and shifts on INPEFA logs reveal the changes, which can also be detected on microfacies. Hence, relative sea level shifts defined on the sea level curve of Haq (2014) between the time interval of Cenomanian to Turonian should be correlated with the shifts detected on INPEFA logs based on both GRTO and GRKT. On Haq curve (2014) going through left side shows higher sea levels while going through right side shows lower sea levels. On INPEFA log where sea level is at its highest level where maximum flooding surfaces are picked up, sea level also should show highest meters which is around 250 meters on Haq curve and away from this highest levels of sea level, sea level starts to decrease on both INPEFA log and Haq curve (2014) (**Figure 93**).

Raw INPEFA log data is interpreted using red arrows in order to define shoaling and deepening upward sequences (**Figure 94**). In the study of Haq (2014) five sequence boundaries are detected in the Cenomanian time, which are associated with the KCe1, KCe2, KCe3, KCe4, and KCe5 eustatic signals (**Figure 94**). According to Haq (2014), there are five sequence boundaries in the Turonian time interval which corresponds to KTu1, KTu2, KTu3, KTu4 and Ktu5 eustatic signals.

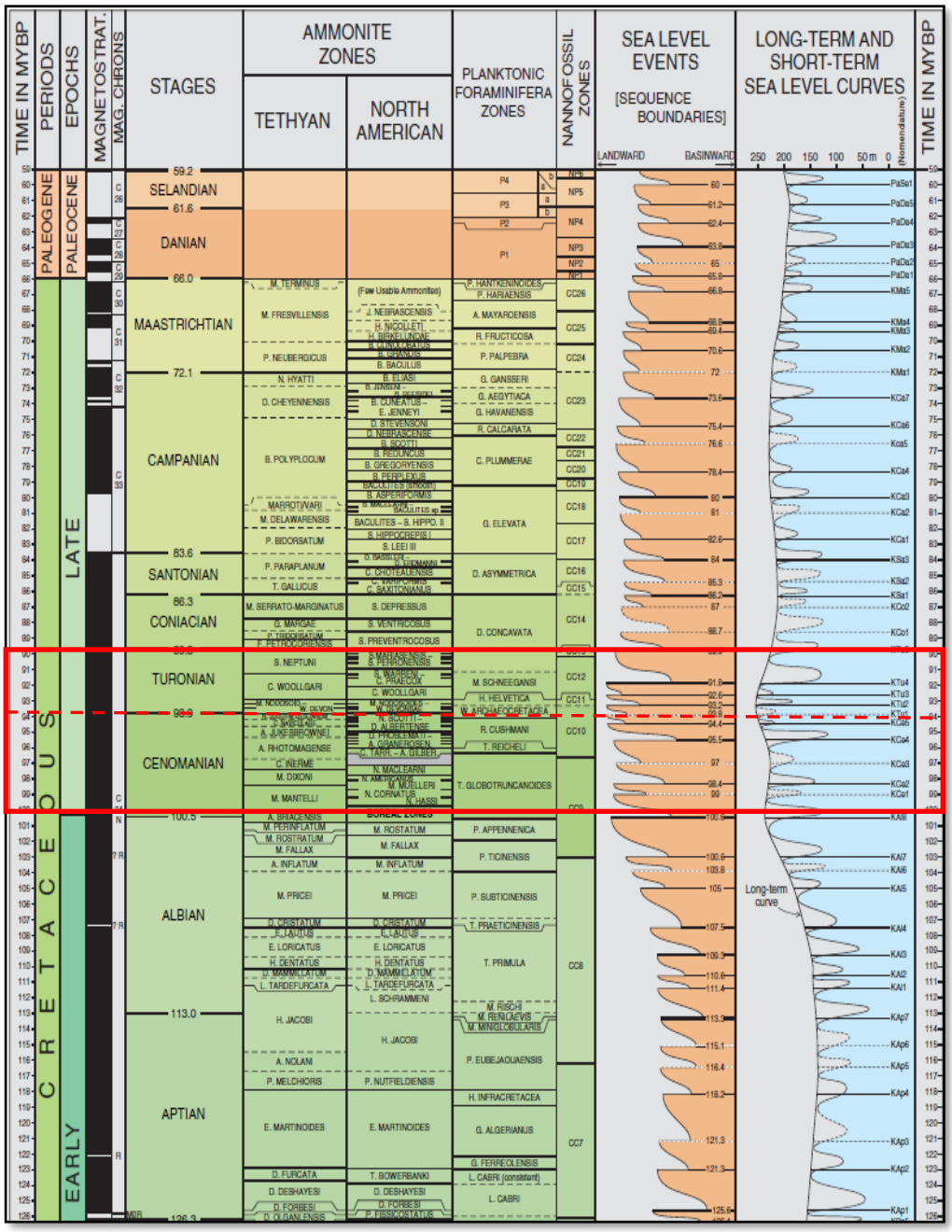


**Figure 93.** Cretaceous-Paleocene Eustatic Cycle Chart with the correlation of biozones after Hardenbol et al. (1998) and Ogg and Hinnov (2012) (modified after Haq, 2014) (Red rectangle shows the Cenomanian-Turonian time interval and red dotted line shows Cenomanian-Turonian boundary.)

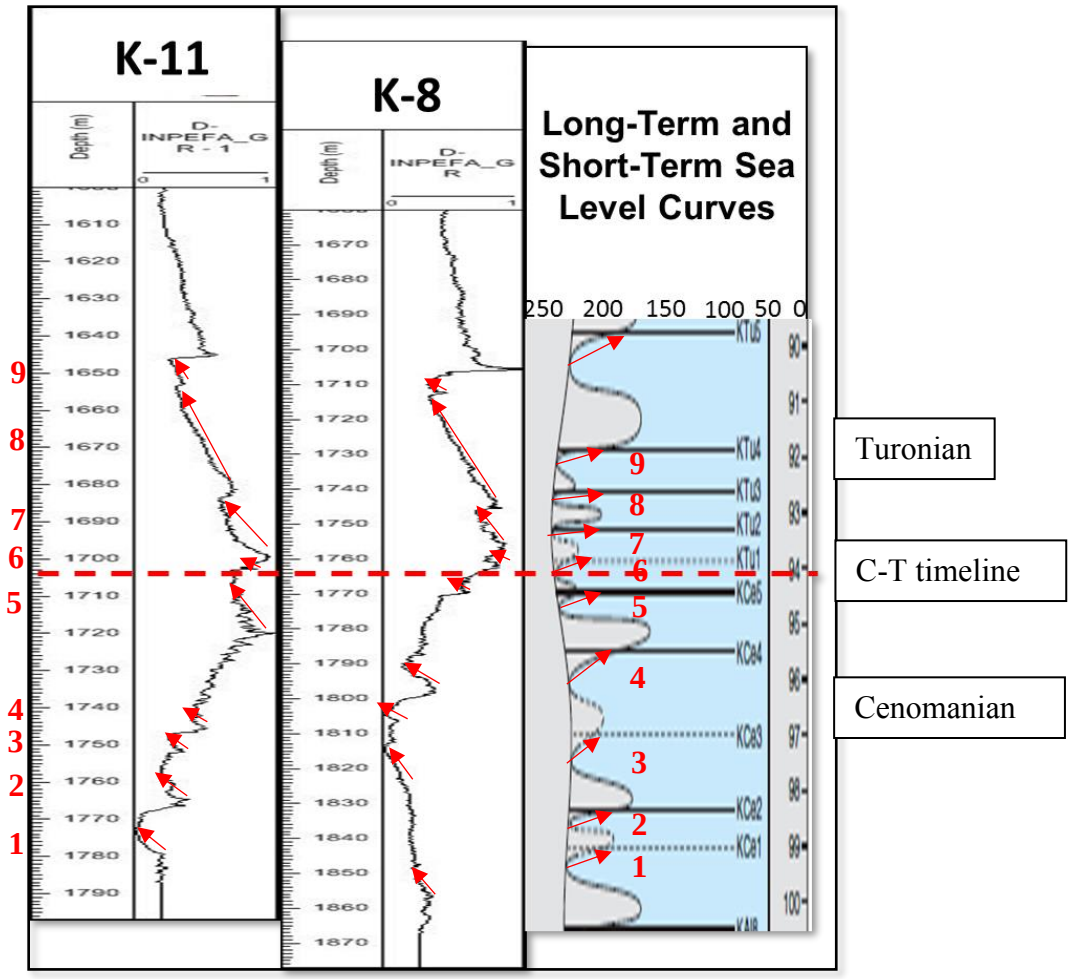


**Figure 94.** Raw INPEFA log data of K-11(on the left), K-8 wells (on the right) on the scale of 1/1000 and long term and short term sea level curves belongs to the Cenomanian-Turonian time interval of Haq (2014) [Red line shows Cenomanian-Turonian boundary, red arrows show the locations of sequence boundaries on the INPEFA logs and sea-level curve of Haq (2014), and red numbers show the number of the sequences defined in the wells and correlated sequences on the sea-level curve of Haq (2014)]

INPEFA log data is interpreted using the shifts on the curve. Shoaling and deepening upward sequences, maximum flooding surfaces and sequence boundaries by using these shifts. Shifts through left show the sequence boundaries and shifts through right show the maximum flooding surfaces (**Figure 94**). Red triangles show shoaling upward and blue triangles show deepening upward packages and at the topmost part of shoaling upward packages, sequence boundaries are supposed to be located (**Figure 95**). There are three sequence boundaries recorded in the Turonian of the studied wells (**Figure 95**) although

five sequence boundaries are identified in the Turonian time interval of sea-level curve of Haq (2014) (**Figure 94**). This can be explained by the absence of one of the sequences at the topmost part of the Derdere Formation in the study area.

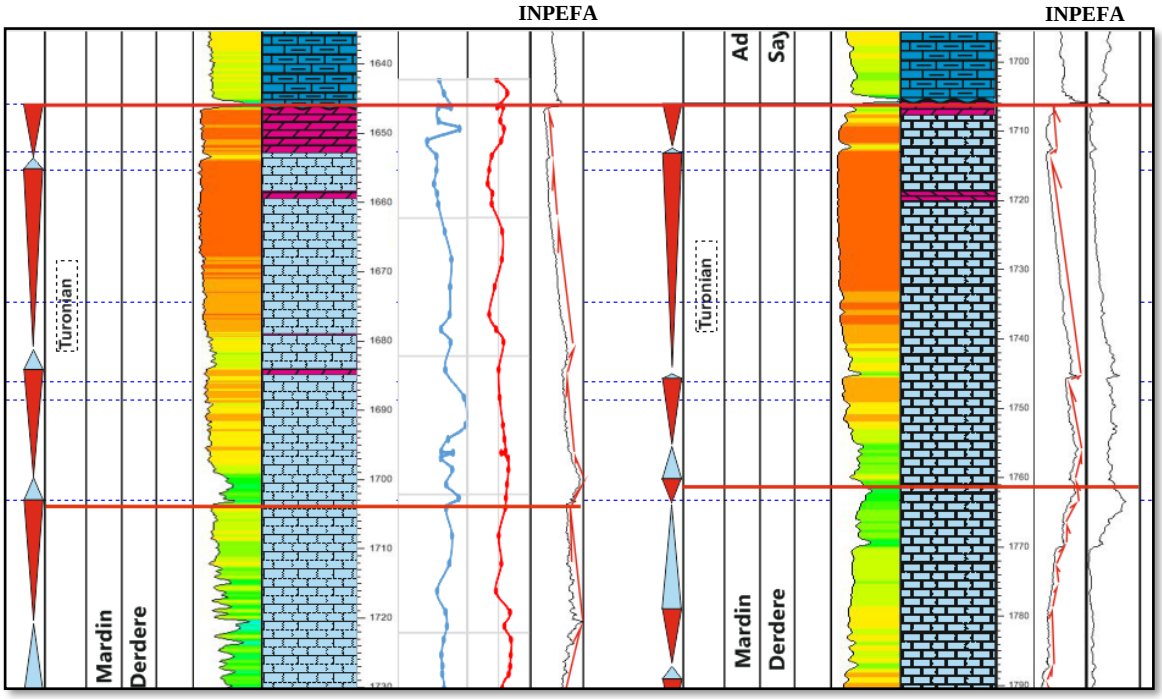


**Figure 95.** Number of sequences and sequence boundaries of K-11 well (on the left) and K-8 well (on the right) on the scale of 1/500 defined in Turonian time interval which is correlated with global cycle chart of Haq (2014) (Red lines shows the top of Turonian (top of the Derdere Formation) and Cenomanian-Turonian boundary and red arrows show the interpreted shifts on INPEFA log)

One of the important purposes of this study is to compare the sequences of this study with the other sequence stratigraphic studies worldwide. Hence, the sequences defined in the wells of the Diyarbakır Region are correlated with the other carbonate platforms in neighbouring areas deposited during the Cenomanian-Turonian time and the sequences defined in the other Derdere studies (**Figure 96**). In the study of Schulze et. al., three sequence boundaries and four sequence boundaries are described in the Turonian time and in the Cenomanian time, respectively. The number of the sequences and the thickness of the sequences of the Jordan section are similar to the sequences of the Derdere Formation in this study (**Figure 96**). The number of the sequences defined in the other studies of Sherland et al. (2004), Saber et. al. (2009) and Razin et. al. (2010) are different from the number of the sequences in this study. However the locations of the some sequence

boundaries on the successions from worldwide correspond to the locations of the sequence boundaries of the Derdere succession in this study (**Figure 96**). Although the number of the sequences differs in the Derdere succession defined in the study of Mülayim et. al. (2020) and this study, sequence boundary 1 (Sb1) stated in the study of Mülayim et. al. corresponds to Ce 2 of this study in K-11 pilot well and sequence boundary 3 (Sb3) corresponds to the Tu 2 of the present study (**Figure 96**).

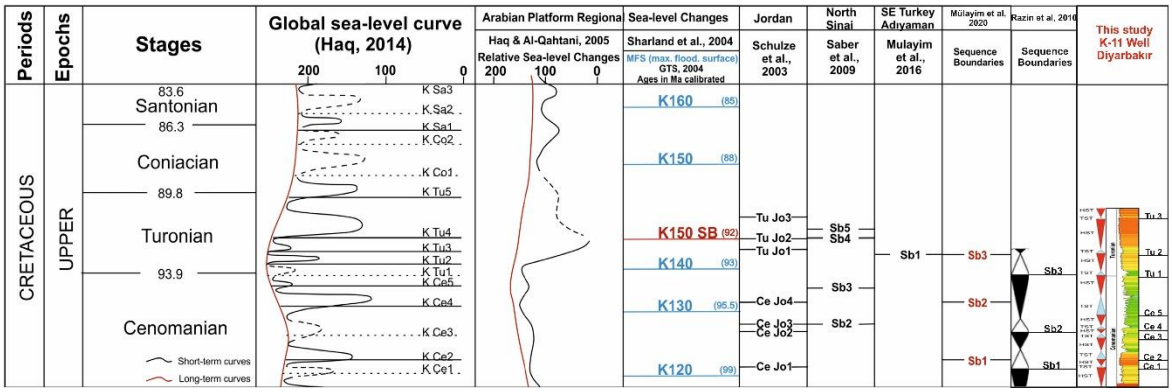


**Figure 96.** Comparison between the sequence boundaries of the present study with the other Cenomanian-Turonian carbonate platforms in neighbouring areas and with the global eustatic scheme of Haq (2014) (modified from Mülayim et. al., 2020)

### 4.1.4 Sequence Correlation of Global Events Using Isotope Data

#### 4.1.4.1 Cenomanian-Turonian Boundary Event and Oceanic Anoxic Event-2 (OAE-2)

During the time interval of the deposition of the Derdere Formation there are some significant events which can be detected using biostratigraphic data, microfacies descriptions, electric logs and isotope studies. The events which are called as “Oceanic Anoxic Events (OAEs)” are firstly described in the study of Schlanger and Jenkyns (2007). As a consequence of these OAEs, deposition of organic-rich fine grained sediments in the oxygen depleted zones of the oceans can be recorded globally since global geologic and climatic factors control these events. The deposition of the Derdere Formation is in the interval of Albian to Turonian time, and the global oceanic anoxic events, recorded

woldwide and corresponding to this time interval, should have left traces in the deposits of the Derdere Formation (Scholle and Arthur, 1980; Jenkyns, 1985; Jarvis et. al., 1988).

Oceanic Anoxic Event-2 (OAE-2) corresponds to one of the major eustatic transgressive pulses of late Cenomanian time. Due to the upwelling events observed in the oceans, ocean surface productivity increased and it caused oxygen minimum zone in the water column in the ocean margin settings. As a consequence of this zonation, the amount of burial of marine organic matter increased and seawater and carbonate sediments became enriched in $^{13}C$ concentrations. At the end of the Cenomanian due to annihilation of the upwelling currents, oxygen minimum zonation in the water column started to shrink gradually and marine conditions returned back to normal by the early Turonian (Jarvis et. al., 1988). Since it started before the end of Cenomanian and continues up to the early Turonian, OAE-2 recorded the C-T boundary. As a result of anoxic conditions, the extinction rates increased during the latest Cenomanian and with the evolution of new species in the early Turonian, a rather big faunal turnover occurred at the C-T boundary (Jarvis et. al., 1988). In the study of Scholle and Arthur (1980), it is stated that $\delta^{18}O$ value shows depletion at or near the C-T boundary where $\delta^{13}C$ has higher values as mentioned above. Deposition of organic carbon-rich sediments can be detected as positive carbon isotope excursions nearby the Cenomanian-Turonian boundary which is associated with OAE-2 (Jenkyns 1980; Arthur et al. 1988). During the deposition of the Derdere Formation OAE-2 is detected lithologically, petrographically, geochemically by using isotope data. As a result of lithologic and petrographic analyses, organic matter enrichments, abundances of opaque minerals, phosphate fragments and argillaceous material and the change in the biota with the presence of radiolaria, abundance of calcisphaerulids are the evidences of OAE-2 during the deposition of the Derdere Formation. It can also be recorded in the carbon isotope studies due to the increase in the amount of organic carbon.

#### 4.1.4.2 Isotope Data Interpretation

Generally, carbon and oxygen isotopes of carbonate rocks are affected from the global sea level changes and they are the indicators of relative rise and fall of global sea level. Heavier carbon isotopes and lighter oxygen isotope values can be considered as the reflection of relative change of global sea level (Zhao et. al., 2017). Carbon isotope values are more reliable than oxygen isotope values to make interpretation of relative fluctuations on the global sea level curve for the carbonate rocks deposited before Tertiary (Zhao et. al., 2017). Carbon isotopic signals are mostly considered as the indicator of the Cenomanian-Turonian Boundary Event (93.9 Ma), mid-Cenomanian event and Oceanic Anoxic Event-2 (OAE-2) (~94 Ma) (Jarvis et. al., 2001).

When oxygen isotope curves and INPEFA logs are studied together, it is observed that general trends on the oxygen isotope curve are similar to turning points defined on INPEFA logs which show that oxygen isotope values are affected by sea level changes. Hence, in order to define 3$^{rd}$ order sequences in the wells oxygen isotope curves are also used for these two wells in addition to data obtained from microfacies studies and INPEFA logs. Although oxygen isotope values of carbonate rocks are affected by the diagenesis, depositional sequences defined in the Derdere Formation is compared with the oxygen isotope data. Generally, negative excursions on the oxygen isotope curves correspond to TSTs and maximum flooding surfaces and positive excursions on the oxygen isotope curve coincides with the HSTs and sequence boundaries which can be explained by the early diagenesis and low degree dolomitization of the samples of K-2 and K-11 wells.

Oxygen isotope studies are also important tool while studying diagenesis. The $\delta^{18}O$ values are under the control of fluid composition, temperature and water/rock ratios (Brand and Veizer, 1981) hence oxygen isotope values are affected by diagenesis. Drusy mosaic calcite cements (product of early diagenesis), carbonate matrix and rudist shell fragments show similar isotopic compositions. The $\delta^{18}O$ values of blocky calcite cement which is considered as late diagenetic cement are lower compared to $\delta^{18}O$ values of matrix and cement formed during early diaganesis. Hence, presence of blocky cement shows entrance of meteoric water to the system, high temperatures due to burial depth or combination of

them (Hajikazemi et. al. 2010). Both $\delta^{13}C$ and $\delta^{18}O$ values become more negative if there is meteoric diaganesis of marine carbonates (Al-Aasm and Veizer 1986; Hajikazemi et. al. 2010). Since meteoric waters are isotopically lighter, meteoric water entrance to the system will deplete $\delta^{18}O$ values similar to carbon isotope values. Petrographical observations are also supposed to support this interaction with meteoric water.

Carbon isotope studies are crucial while studying diagenetic environments. At around the subaerial exposure surface $\delta^{13}C$ values are more negative than values compared to $\delta^{13}C$ values several meters below the subaerial exposure surface (Allan and Matthews, 1982). Similarly $\delta^{13}C$ values become also more negative at around unconformities (Allan and Matthews, 1982; Hajikazemi et. al., 2010). Although diagenetic phases of carbon isotope values are affected by the isotopic composition of the host rock (Brand and Veizer, 1981), $\delta^{13}C$ values is under the control of the duration of meteoric diaganesis and extent of water rock interaction (James and Choquette, 1990; Hajikazemi et. al., 2010).

In terms of carbon isotope studies the Cenomanian-Turonian (C-T) boundary event is mostly detected by the positive carbon isotope excursion due to increase in the rate of burial organic carbon which have a significant effect on $CO_2$ and $O_2$ concentrations in the ocean and the atmosphere, global climate and sedimentary facies (Arthur et. al. 1988) (**Table 7** and **Table 8**) and (**Figure 97** and **Figure 98**).

Isotope studies can give an opportunity to detect Oceanic Anoxic Events (OAEs) which is at around the C-T boundary event and detected in the time interval of deposition of the Derdere Formation. Biostratigraphic data which gives the C-T boundary by the use of planktonic foraminifer assemblage and positive carbon isotope excursions correspond to C-T boundary event provides an opportunity to make correlation. To make biostratigraphic correlation, these positive excursions appear to correspond to times of large sea level regressions in global sequence stratigraphic sea-level curves during C-T time interval (Stoll and Schrag, 2000).

**Table 7.** Carbon isotope and oxygen isotope values of cutting samples of K-2 well

| Depth | Carbon Isotope | | Oxygen Isotope | |
|---|---|---|---|---|
| | | std | | std |
| **2316** | 1,73 | 0,01 | -3,95 | 0,05 |
| **2320** | 3,11 | 0,02 | -5,25 | 0,06 |
| **2324** | 3,40 | 0,02 | -4,92 | 0,07 |
| **2328** | 3,44 | 0,03 | -5,29 | 0,03 |
| **2332** | 3,02 | 0,02 | -5,31 | 0,05 |
| **2336** | 2,93 | 0,02 | -5,19 | 0,03 |
| **2340** | 3,30 | 0,05 | -4,50 | 0,09 |
| **2344** | 2,87 | 0,02 | -4,69 | 0,06 |
| **2348** | 2,41 | 0,02 | -4,23 | 0,06 |
| **2352** | 2,28 | 0,02 | -4,14 | 0,04 |
| **2356** | 2,21 | 0,02 | -4,35 | 0,06 |
| **2360** | 1,33 | 0,04 | -3,33 | 0,08 |
| **2364** | 1,45 | 0,02 | -3,36 | 0,02 |
| **2368** | 1,85 | 0,02 | -3,44 | 0,05 |
| **2372** | 2,01 | 0,02 | -4,10 | 0,08 |
| **2376** | 2,04 | 0,02 | -3,23 | 0,04 |
| **2380** | 1,92 | 0,02 | -3,59 | 0,04 |
| **2384** | 1,68 | 0,02 | -3,69 | 0,04 |
| **2388** | -1,01 | 0,01 | -3,66 | 0,04 |
| **2396** | 1,42 | 0,01 | -3,96 | 0,03 |
| **2400** | 1,37 | 0,01 | -4,26 | 0,07 |
| **2404** | 0,99 | 0,02 | -3,94 | 0,04 |
| **2408** | 1,15 | 0,03 | -4,12 | 0,05 |
| **2412** | 1,04 | 0,01 | -4,77 | 0,08 |
| **2416** | 0,97 | 0,02 | -4,71 | 0,08 |
| **2420** | 1,01 | 0,02 | -4,91 | 0,03 |
| **2424** | 1,33 | 0,02 | -5,63 | 0,06 |
| **2428** | 1,41 | 0,03 | -4,80 | 0,11 |
| **2436** | 1,24 | 0,04 | -4,97 | 0,05 |
| **2440** | 1,65 | 0,02 | -4,67 | 0,02 |
| **2444** | 1,62 | 0,03 | -5,75 | 0,46 |
| **2448** | 1,59 | 0,02 | -8,02 | 0,02 |
| **2452** | 1,83 | 0,17 | -8,00 | 0,68 |
| **2456** | 1,73 | 0,01 | -8,03 | 0,04 |
| **2460** | 1,73 | 0,01 | -8,30 | 0,04 |
| **2464** | 1,54 | 0,50 | -9,31 | 1,70 |
| **2468** | 1,34 | 0,01 | -9,70 | 0,03 |
| **2472** | 1,56 | 0,01 | -7,66 | 0,02 |

**Table 8.** Carbon isotope and oxygen isotope values of core and cutting samples of K-11 well

| | Carbon Isotope | | Oxygen Isotope | | | Carbon Isotope | | Oxygen Isotope | |
|---|---|---|---|---|---|---|---|---|---|
| | | std | | std | | | std | | std |
| **1642,00** | 1,48 | 0,02 | -5,30 | 0,06 | **1726,85** | 1,73 | 0,02 | -3,10 | 0,03 |
| **1644,00** | 1,84 | 0,02 | -3,54 | 0,04 | **1728,00** | 1,71 | 0,03 | -3,33 | 0,06 |
| **1646 (a)** | 2,35 | 0,02 | -5,19 | 0,05 | **1730,10** | 1,84 | 0,01 | -4,38 | 0,08 |
| **1646 (b)** | 1,42 | 0,04 | -4,22 | 0,04 | **1734,00** | 1,40 | 0,03 | -2,99 | 0,03 |
| **1648,00** | 1,45 | 0,02 | -4,69 | 0,04 | **1738,00** | 1,21 | 0,02 | -3,49 | 0,04 |
| **1649,12** | 2,97 | 0,02 | -4,11 | 0,04 | **1739,00** | 1,39 | 0,03 | -3,24 | 0,05 |
| **1650,90** | 0,61 | 0,01 | -4,55 | 0,04 | **1742,00** | 1,19 | 0,02 | -4,42 | 0,11 |
| **1653,10** | 1,28 | 0,02 | -6,10 | 0,04 | **1746,00** | 1,55 | 0,03 | -3,56 | 0,08 |
| **1655,10** | 1,28 | 0,02 | -6,50 | 0,08 | **1750,00** | 1,57 | 0,03 | -4,74 | 0,03 |
| **1657,10** | 1,12 | 0,02 | -6,74 | 0,10 | **1754,00** | 1,61 | 0,01 | -5,01 | 0,05 |
| **1658,50** | 1,33 | 0,02 | -5,99 | 0,08 | **1758,00** | 1,43 | 0,02 | -4,09 | 0,06 |
| **1660,00** | 1,41 | 0,02 | -6,10 | 0,03 | **1762,00** | 1,34 | 0,02 | -5,95 | 0,06 |
| **1664,00** | 1,89 | 0,02 | -4,38 | 0,12 | **1764,16** | 2,00 | 0,03 | -3,69 | 0,04 |
| **1668,00** | 2,38 | 0,03 | -4,46 | 0,05 | **1766,00** | 1,53 | 0,02 | -4,20 | 0,05 |
| **1672,00** | 2,28 | 0,01 | -5,60 | 0,02 | **1768,13** | 1,56 | 0,02 | -4,51 | 0,13 |
| **1676,00** | 2,25 | 0,04 | -6,50 | 0,07 | **1770,16** | 1,40 | 0,02 | -5,61 | 0,04 |
| **1678,13** | 1,62 | 0,02 | -5,38 | 0,04 | **1772,07** | 1,30 | 0,01 | -6,80 | 0,03 |
| **1680,00** | 2,32 | 0,02 | -4,17 | 0,07 | **1774,00** | 1,78 | 0,01 | -3,59 | 0,09 |
| **1684,00** | 1,93 | 0,01 | -4,96 | 0,05 | **1774,10** | 1,21 | 0,01 | -5,19 | 0,05 |
| **1688,00** | 3,29 | 0,02 | -4,80 | 0,04 | **1774,12** | 1,68 | 0,02 | -4,92 | 0,04 |
| **1692,00** | 3,42 | 0,02 | -4,27 | 0,12 | **1776,12** | 1,21 | 0,02 | -6,83 | 0,02 |
| **1694,02** | 2,13 | 0,01 | -4,02 | 0,05 | **1778,00** | 1,55 | 0,02 | -4,14 | 0,05 |
| **1695,79** | 1,64 | 0,03 | -3,84 | 0,05 | **1778,04** | 1,58 | 0,02 | -8,05 | 0,03 |
| **1696,00** | 2,50 | 0,03 | -4,53 | 0,05 | **1780,01** | 0,97 | 0,04 | -5,90 | 0,05 |
| **1696,75** | 1,62 | 0,05 | -3,47 | 0,04 | **1782,00** | 1,23 | 0,03 | -8,60 | 0,13 |
| **1698,40** | 2,45 | 0,03 | -3,37 | 0,08 | **1782,11** | 1,50 | 0,02 | -6,34 | 0,03 |
| **1700,56** | 2,00 | 0,01 | -3,59 | 0,07 | **1784,00** | 1,49 | 0,02 | -7,22 | 0,05 |
| **1702,55** | 2,91 | 0,02 | -3,77 | 0,06 | **1786,00** | 1,36 | 0,02 | -7,83 | 0,08 |
| **1704,00** | 1,99 | 0,03 | -3,90 | 0,07 | **1788,00** | 1,59 | 0,02 | -4,97 | 0,05 |
| **1708,00** | 2,43 | 0,02 | -4,95 | 0,06 | | | | | |
| **1712,00** | 2,22 | 0,02 | -4,53 | 0,05 | | | | | |
| **1716,00** | 1,33 | 0,01 | -5,42 | 0,07 | | | | | |
| **1719,06** | 1,95 | 0,04 | -3,12 | 0,05 | | | | | |
| **1721,05** | 2,05 | 0,02 | -4,02 | 0,02 | | | | | |
| **1723,05** | 1,82 | 0,03 | -2,93 | 0,03 | | | | | |
| **1725,25** | 1,65 | 0,02 | -2,99 | 0,05 | | | | | |

In this study carbon isotope data which is supposed to be positive excursion is used to reinforce the C-T boundary and OAE-2 defined by biostratigraphic data, microfacies and INPEFA logs (**Figure 97** and **Figure 98**). Where C-T boundary is located in the K-11 well, positive excursion in carbon isotope values is observed (**Figure 98**). However, in the carbon isotope values of K-2 well, there is significant negative excursion nearby C-T boundary which is also associated with OAE-2 (**Figure 97**). In the study of Beil et. al. (2018), it is stated that this initial negative excursion on carbon isotope excursion is related with OAEs which cause rapid release of large volume of $^{13}C$ depleted carbon either as methane or $CO_2$ (Dickens et al., 1995; Jenkyns, 2003; Turgeon and Creasar, 2008; Du Vivier et al., 2014; Beil et. al., 2018). The positive carbon isotope excursion followed by this negative shift in carbon isotope values is associated with greater burial rates of $^{12}C$ enriched organic carbon in organic rich shales (Jenkyns, 1980; Schlanger et al., 1987; Arthur et al., 1988; Scholz et. al., 2019). The increase in the burial rates has substantial impact on the carbon balance and biological productivity which enhances globally defined ocean anoxia (Scholz et. al., 2019).

When the carbon isotope curves of K-11 and K-2 wells are compared, it is realized that there are similarities in the curves of the wells. Sample frequency is higher in K-11 well compared to K-2 well; since both cutting and core samples are considered together in K-11. In K-2 well, $\delta^{13}C$ values are lower during Cenomanian time interval compared to Turonian, which is between 1 to 2 values (**Figure 97**). During the Turonian time, $\delta^{13}C$ values are higher, which is between 1.5 to 3.5 values. There is only one outlier value which can be considered as negative shift in $\delta^{13}C$ values, which is associated with greater burial rates of $^{12}C$ just after positive carbon excursion (**Figure 97**). Similar to K-2 well, $\delta^{13}C$ values are lower during Cenomanian compared to Turonian in K-11 well, which varies from 1 to 2. During Turonian, $\delta^{13}C$ values become higher and changes from 1 to 3.5. There is only one value which is less than 1 (**Figure 98**) and (**Table 7** and **Table 8**).

As a general speaking, eustatic sea-level fall and regression is resulted in the increased weathering rates, which causes the increased flux of siliciclastic sediments to shelf, increased carbon burial, and a positive $\delta^{13}C$ excursion (Gröcke et. al., 1999). Eustatic sea-level rise could have decreased the $\delta^{13}C$ of dissolved inorganic carbon in the ocean and the

effect of organic-carbon burial on isotopic values by leading to eustatic sea-level rise and relatively negative $\delta^{13}C$ excursions (Gröcke et. al., 1999). Negative shift observed on the carbon isotope curves just after the C-T boundary in Turonian time is not obvious in K-11 well as much as in K-2 well. This difference can be related with the depth of the Derdere Formation. Depth of the Derdere Formation in K-2 well is much more compared to K-11 well which can affect carbon isotope values and anoxia; since carbon isotope values have direct relationship with anoxia. Due to the fact that basin is getting deeper through K-2 well with the increasing relative sea level, basin can be more anoxic which can create greater negative shift on carbon isotope curve.

Oxygen isotope curves of the K-2 and the K-11 wells are compared and general trends and oxygen isotope values are similar (**Table 7** and **Table 8**). In K-2 well, oxygen isotope values varies from -10 to -8 in the early Cenomanian whereas they are fluctuating between -6 to -4 in the late Cenomanian (**Figure 99**). These lower oxygen isotope values correspond to first two sequences at the bottom of the succession. In K-11 well, oxygen isotope values changes from -9 to -4 in early Cenomanian while they vary from -6 to -3 in the late Cenomanian (**Figure 100**). Lower oxygen isotope values correspond to first two sequences in the Derdere succession similar to K-2 well. More negative oxygen isotope values can be the indicator of the meteoric diagenesis. Meteoric diagenesis does not affect carbon isotopic values since they are not prone to diagenesis as much as oxygen isotopes (Valladares et. al., 1996). Oxygen isotope results of K-2 well vary from -6 to -3 in the Turonian time whereas they are fluctuating from -7 to -3 in K-11 well. In Turonian, there are some negative shifts on oxygen isotopes which can be associated with the meteoric diagenesis. When oxygen isotope curves and sequences are correlated, negative excursions correspond to the highstand systems tracts with some exceptions. As a summary, general trends of oxygen isotope curves of K-2 and K-11 wells are same. At the bottom of the succession, lowest oxygen isotope results are recorded and the values increase towards the upper part of the succession (**Figure 99** and **Figure 100**). Oxygen and carbon isotope ratios become more negative with increasing carbonate content higher than about %60 (Thierstein and Roth, 1991). Therefore, these negative isotope ratios at the bottom of the succession can be explained with increasing carbonate content with the decreasing rate of the relative sea level during the early Cenomanian time interval (Haq, 2014).

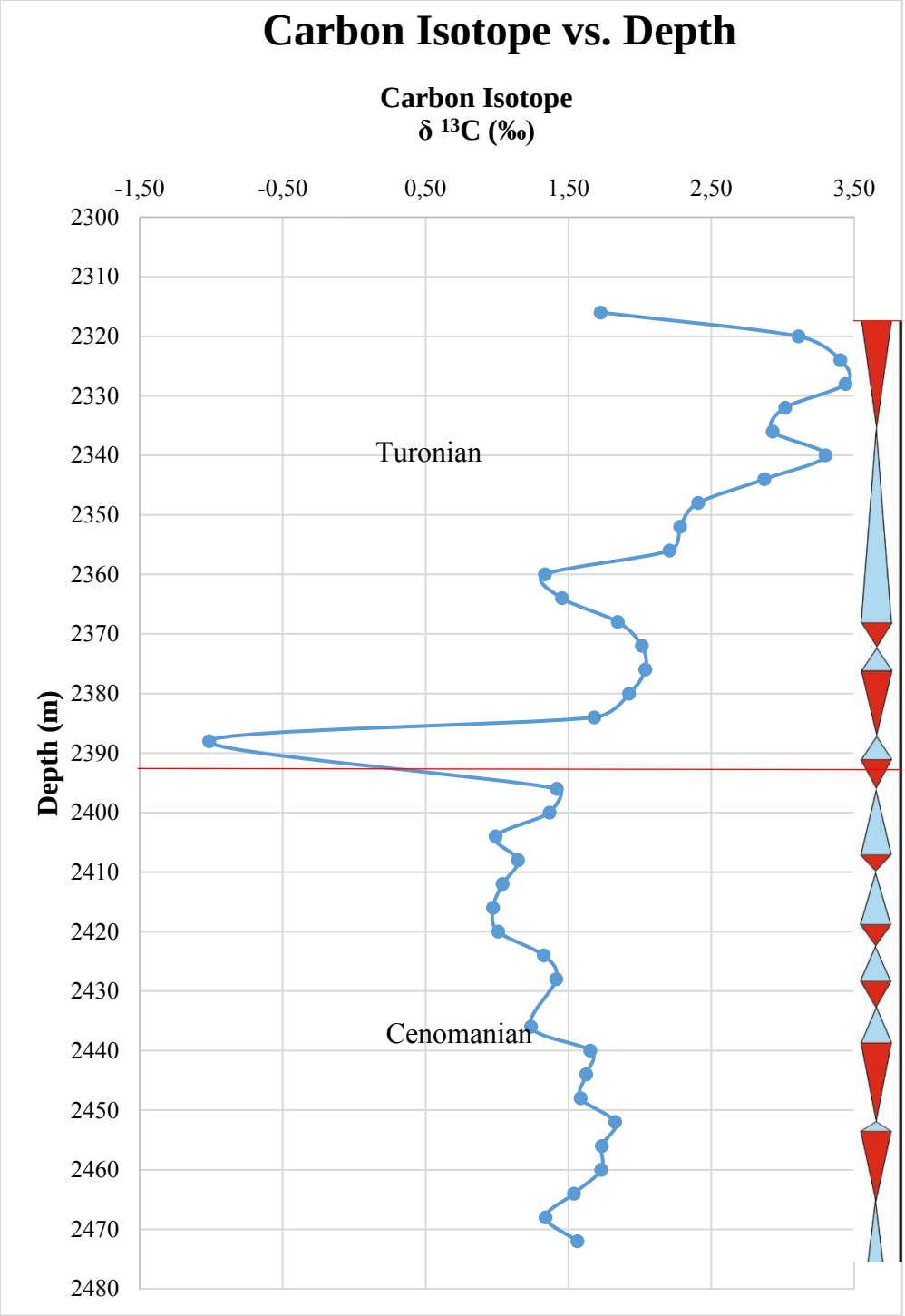


**Figure 97.** Carbon isotope data vs. depth (m) graph of K-2 well based on the data of **Table 7**(Red line shows the C-T boundary)

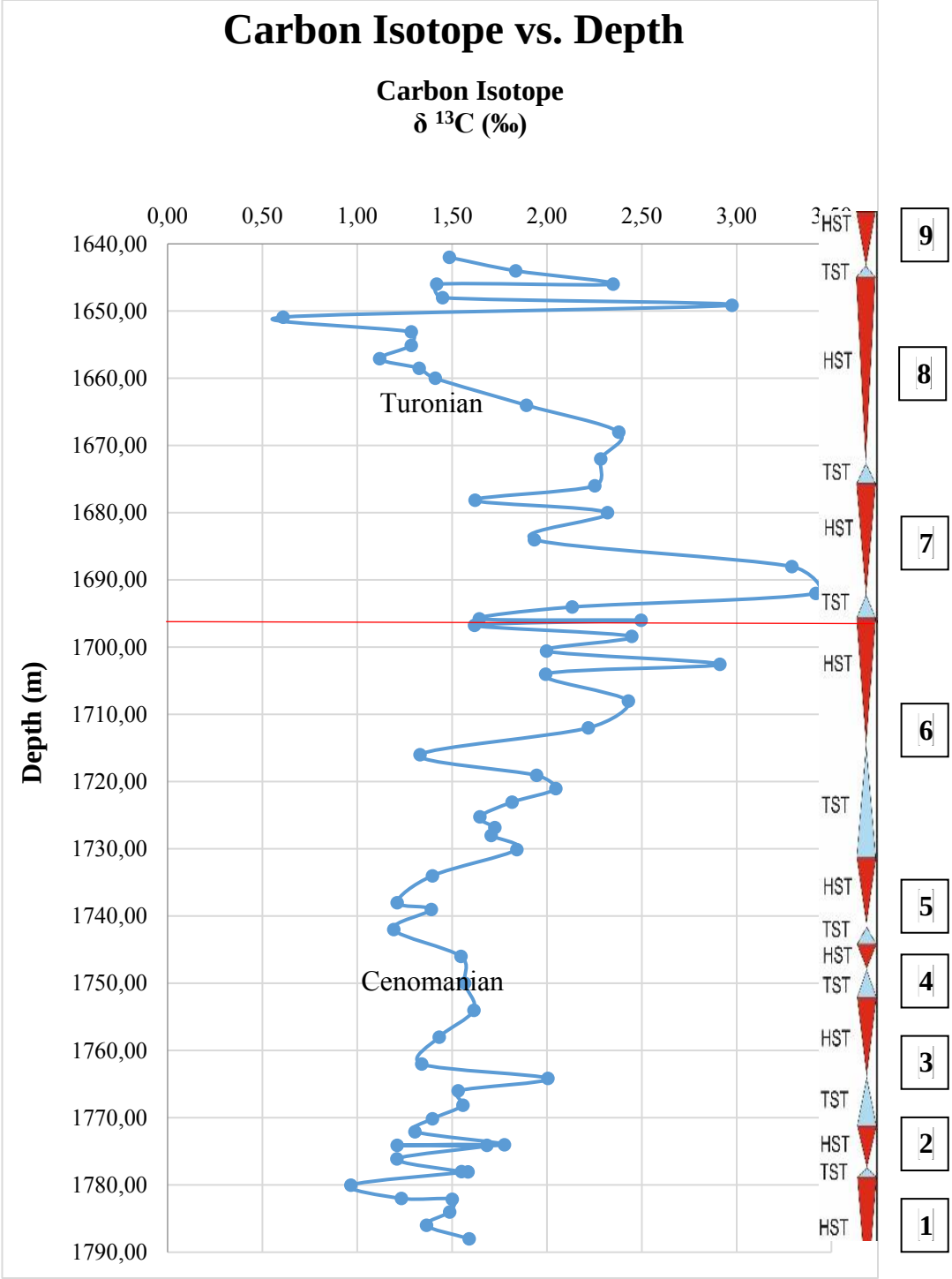


**Figure 98.** Carbon isotope data vs. depth (m) graph of K-11 well based on the data of **Table 8** (Red line shows the C-T boundary)

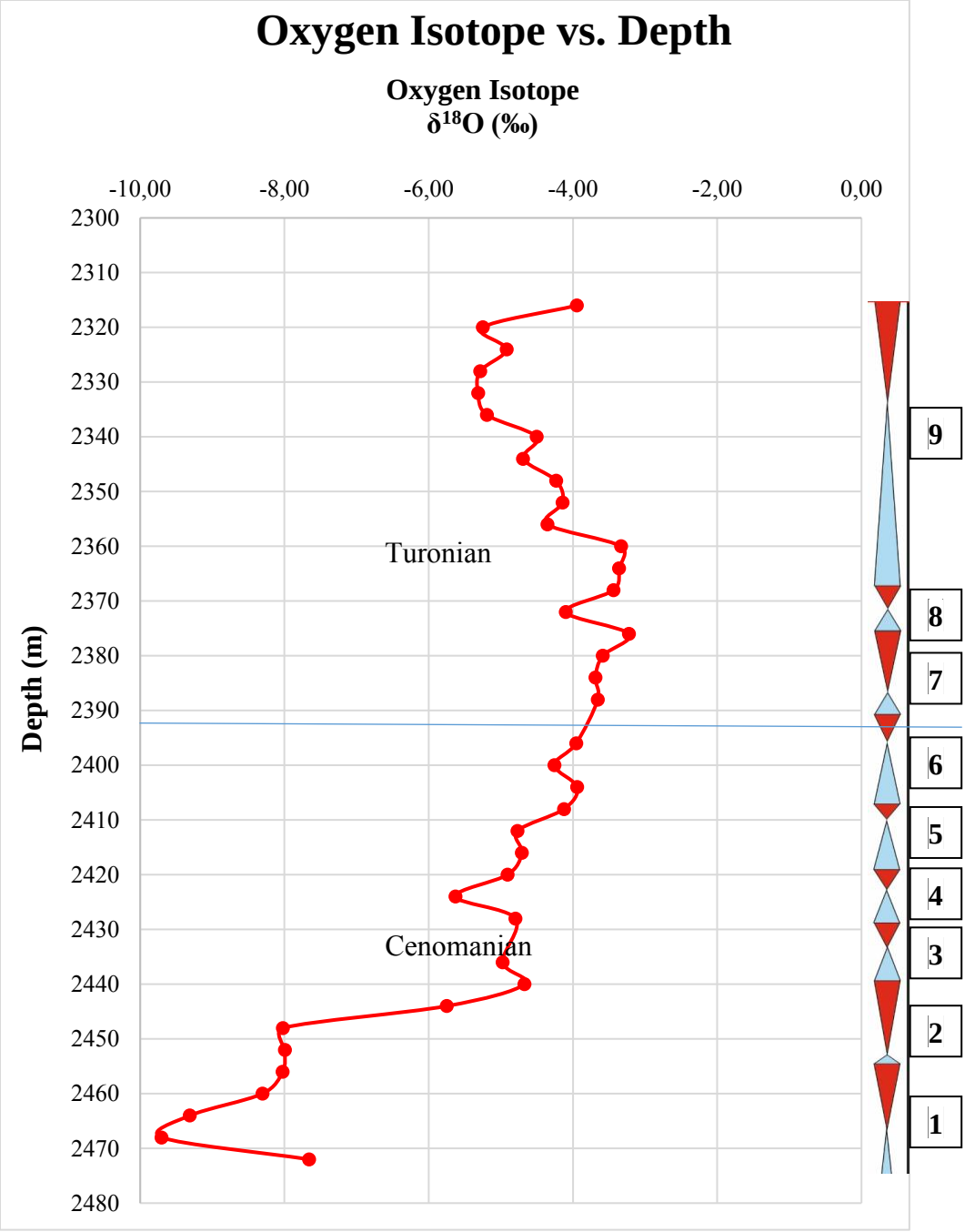


**Figure 99.** Oxygen isotope data vs. depth (m) graph of K-2 well based on the data of **Table 7** (Blue line shows the C-T boundary)

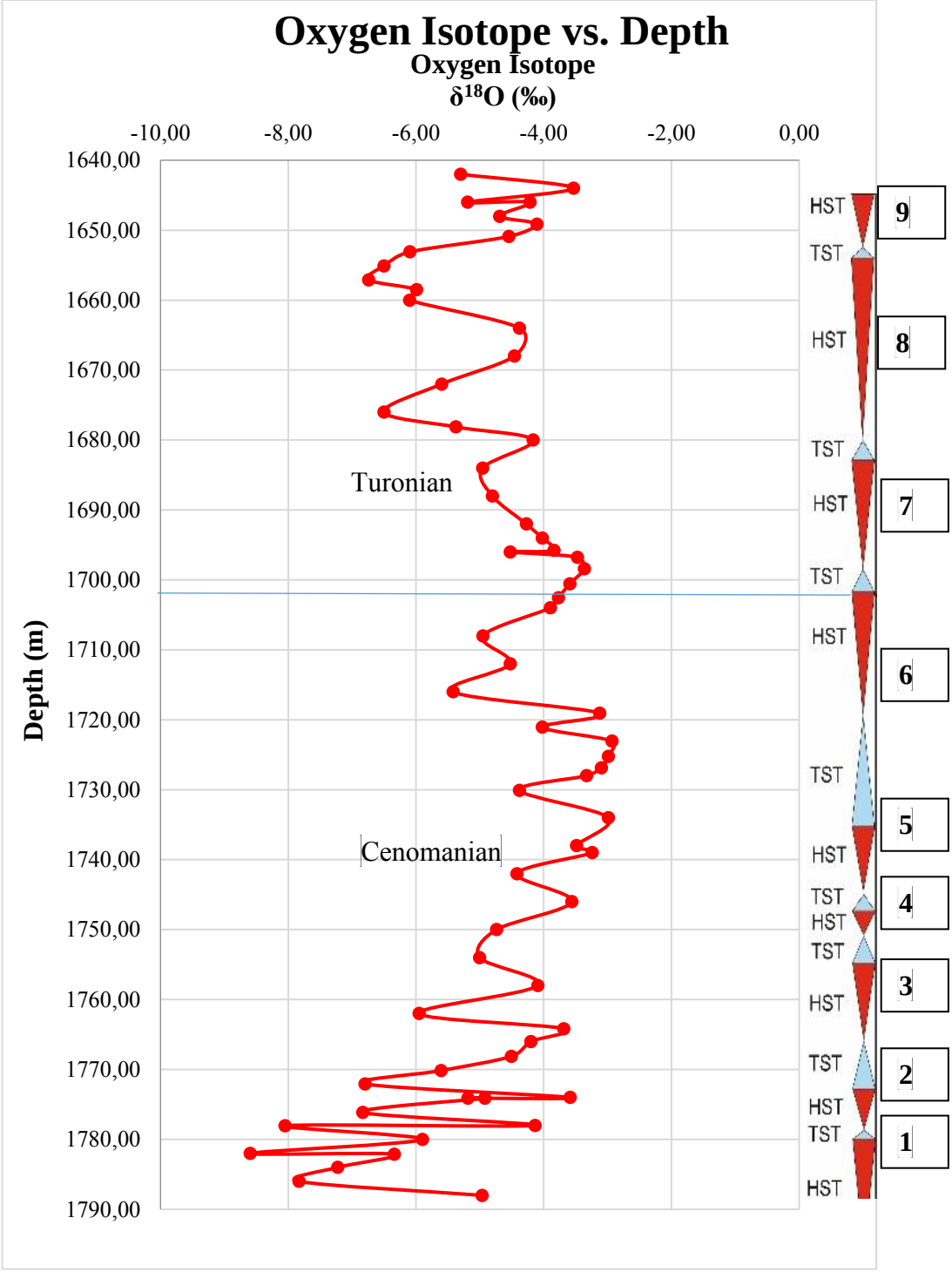


**Figure 100.** Oxygen isotope data vs. depth (m) graph of K-11 well based on the data of **Table 8** (Blue line shows the C-T boundary)

Reference sections of carbon isotope curves of Brac succession, Eastbourne, Sussex, UK, Pueblo, Colorado (Jarvis et. al., 2006) and the Türkoğlu section are compared with the carbon isotope curves of K-2 and K-11 wells (**Figure 101**). General trend of K-11 well seems similar to the reference curves and Turkoglu section in terms of peaks (Pearce et. al., 2009) defined on the curves. There are some differences in the K-2 well and the other reference sections and Türkoğlu section. There is a sharp negative shift in carbon isotope values, which can be explained by the greater burial rates of $^{12}C$ just after positive carbon excursion in K-2 well.

Oxygen isotope curves of K-2 and K-11 wells are compared with the Türkoğlu section, Eastbourne, Sussex and Pueblo, Colorado. General trends of the curves are similar in K-2, K-11 wells and Türkoğlu sections (**Figure 102**). Oxygen isotope values become more negative below the Cenomanian-Turonian boundary in the K-2 and K-11 wells, the Türkoğlu section and Pueblo, Colorado; however isotope values tend to be more positive in Eastbourne, Sussex section. Positive shifts are observed just above the Cenomanian-Turonian boundary in K-2 and K-11 wells, in the Türkoğlu section and in Eastbourne and Pueblo reference sections. It is suggested that positive shifts on the oxygen isotope curve is the indicator of marine incursion and negative shifts show the fresh water influx in the study of Keller and Pardo (2004). Marine incursion can be interpreted as transgression and fresh water influx can be considered as regression and they are also suggested in this study.

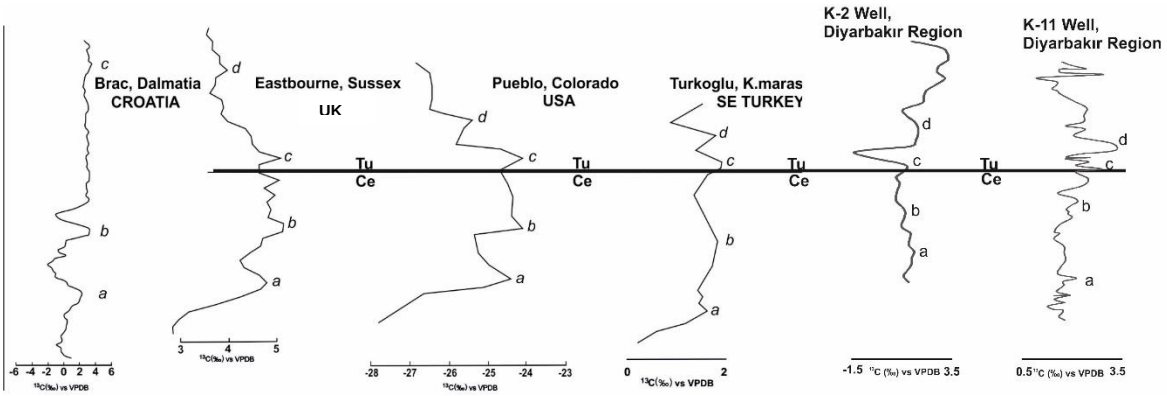


**Figure 101.** Correlation of C-isotope curve of K-2 and K-11 wells with the curves of Türkoğlu section, the Cenomanian-Turonian time of Eastbourne and Pueblo reference sections and Brac succession (modified from Mülayim et. al., 2019)

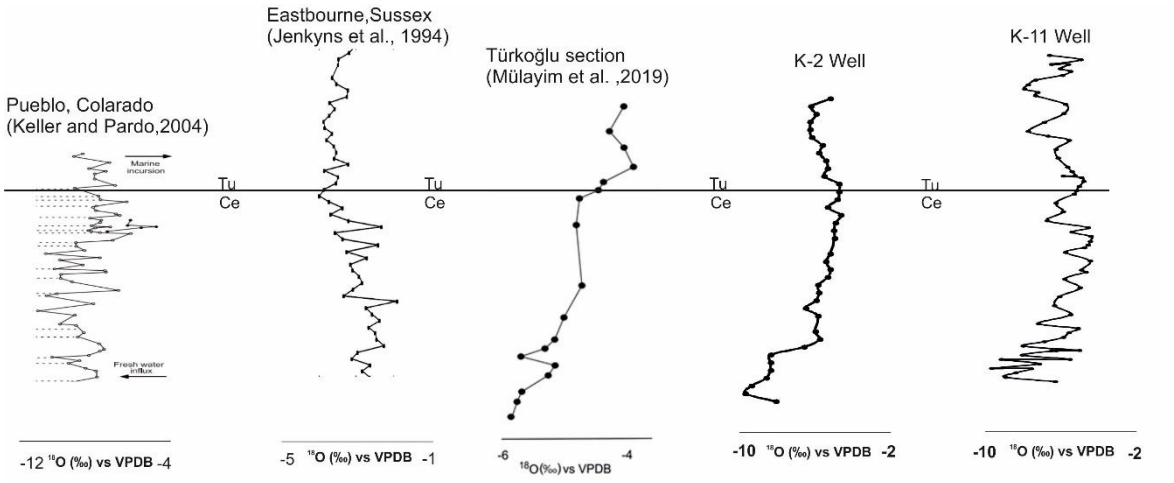


**Figure 102.** Correlation of O-isotope curve of K-2 and K-11 wells with the curves of Türkoğlu section, the Cenomanian-Turonian time of Eastbourne and Pueblo reference sections

# CHAPTER 5

# DIAGENESIS

## 5.1 DIAGENETIC MECHANISMS AND RESERVOIR PROPERTIES OF THE DERDERE FORMATION

Diagenesis contains both mechanical and chemical processes in the subsurface that occur after the deposition and continue until metamorphism or weathering begins (Muller, 1967; Bjorlykke, 1983; Milliken, 2003; Scholle and Ulmer-Scholle, 2003). Diagenesis begin at the sea floor (syngenetic or eogenetic alteration), continue through deep burial (mesogenetic alteration) and also include subsequent uplift (telogenetic alteration) (Scholle and Ulmer-Scholle, 2003). In other words, diagenesis is the process that encompasses the transformation of unconsolidated sediment to hard sedimentary rocks and it contains dolomitization, dissolution, cementation, replacement, stylolization, compaction, fracturing, authigenic mineral formation, type diaganetic mechanisms. It is one of the most important processes in the evolution of mechanical rock parameters and reservoir parameters of the rocks. Cementation can be considered as significant affect on the sediment strength, brittleness, deformation, and porosity due to the binding effect on grain contacts (White et. al., 2011; Milliken, 2013; Ergene, 2014). Diagenesis can mask the primary depositional features and it can also keep information about the post depositional settings, pore water compositions and temperatures. It can cause porosity and permeability loss or gain. Having general information about diagenetic processes provides perception of the factors behind the porosity loss, and relative timing of porosity evolution and oil migration which is considered as significant in terms of hydrocarbon exploration (Scholle and Ulmer-Scholle, 2003).

### 5.1.1 Diaganetic Mechanisms

Diagenesis generally includes numerous mechanical and chemical processes. The most common ones are dolomitization, dissolution, cementation, replacement, and stylolization. Dolomitization is the formation of dolomite mineral by the replacement of magnesium ions with calcite ions in mostly calcite minerals (Scholle and Ulmer-Scholle, 2003). Dissolution is leaching of unstable minerals and forming secondary pores. Cementation means that filling the open primary or secondary pore spaces with newly precipitated material. Replacement is the inversion of one polymorph of a mineral by another. Chemical compaction is the formation of stylolites and means dissolution along surfaces.

#### 5.1.1.1 Dolomitization

The main diagenetic process observed in the thin sections is dolomitization. In the upper levels of the Derdere Formation, most of the samples are intensely dolomitized and mostly dolomicrosparite to dolosparite type microfacies are identified. Among the dolomite-rock textures, dolomites defined in the Derdere Formation are classified as very fine to fine crystalline, subhedral characteristics of dolomites (**Figure 103-106**). This type of dolomites is composed of dense, dark mosaics of interlocking sub-to anhedral crystals. Due to dense mosaics of crystals, allochems and sedimentary structures are unlikely to be preserved and between the crystals streaks of pyrite are commonly observed. In the study of Amthor and Friedman (1991), this type of fine crystalline dolomites are interpreted as restricted to subtidal to supratidal setting and the fine crystal size may be the result of an early replacement of precursor peritidal lime mudstone or neomorphism of penecontemporaneous or early diaganetic dolomite.

Sibley (1980) suggested cloudy core-clear rimmed dolomites which are formed as a result of the precipitation of the different type of fluids which are calcite saturated and dolomite saturated. Cloudy core part of the dolomite crystal is resulted from the fluids saturated with respect to calcite and clear rimmed dolomite is formed by fluids saturated with respect to dolomite; hence this type of dolomite indicates the calcite replacement of dolomite and they are formed in the mixed marine-meteoric water zone (**Figure 107**). This dolomite type

is frequently observed at the top of the Derdere Formation where Derdere and Sayındere formations are in contact in the studied wells. In the sequence stratigraphic framework, these dolomites are in the 9$^{th}$ sequence of the Derdere Formation (**Figure 103-106**).

Euhedral dolomite crystals can replace bioclasts and the micrite dominated matrix (**Figure 108**). In addition to this type of dolomites, euhedral interlocking dolosparites are described and some primary constituents belong to original fabric are preserved. These preserved consitituents provides an opportunity to make an interpretation about the microfacies and shoaling to deepening sequences (1$^{st}$ sequence of the K-8 well) (**Figure 108** and **Figure 109**).

Intense dolomitization can cause some problems to study sequence stratigraphy due to the masking of the original fabric and primary constitunets. On the other hand, some preserved depositional features and the type of dolomite texture whether it is dolosparite, dolomicrosparite, or dolomicrite provide the data for the depositional microfacies (**Figure 109**). In order to reveal the sequences in the studied wells, these approaches related with the crystals size of the dolomites and original fabrics are used. Crystal size of dolomite is associated with the rate of nucleation and the rate of growth. Due to the larger surface area of fine particles, nucleation rate is higher than growth rate which makes crystal size small. In other words, in general mud dominated facies tend to form more finely crystalline dolomites (**Figure 103** and **Figure 104**) and grain dominated facies tend to form more coarsely crystalline dolomites. Early diagenetic product dolomites tend to be more finely crystalline than burial dolomites according to crytal growth rates (Scholle and Ulmer-Scholle, 2003). That is why as a result of the early dolomitization of subtidal to supratidal lime muds, very fine to fine grained dolomite crystals are formed.

Dolomites of the Derdere Formation are commonly the product of the mixing zone and early diagenesis and they are formed in the lower temperatures due to planar fabrics of dolomites (**Figure 106-108)**. Mixing zone dolomites range from microcrystalline to clear zoned replacements of dolomites and cements (Scholle and Ulmer-Scholle, 2003).Uniform or unimodal size distribution of dolomites means single phase of formation. Planar fabrics of dolomites represent lower temperutures for precipitation while non-planar fabrics offer

higher tempertures which are above 50-100 ºC (Gregg and Sibley, 1984; Sibley and Gregg, 1987; Scholle and Ulmer-Scholle, 2003).

Since High-Mg calcite and aragonite are less stable compared to low-Mg calcite, they are more susceptible to dolomitization which is resulted in partial dolomitization (**Figure 103-105)**. Among high-Mg calcite and aragonite, high-Mg calcite is more stable which is resulted in more preserved tests/shells as a result of dolomitization compared to aragonitic tests/shells. For instance peloids are mostly preserved and peloidal facies are partially dolomitized (**Figure 105**).

Light microscope based cathodoluminescence studies are conducted on the dolomite samples in order to reveal the zoning of dolomites and formation stages of dolomites (**Figure 110-115**). Some euhedral dolomites are mostly observed as zoned (**Figure 108** and **Figure 109**) even under the plane polar light. Different timing of the formation of the dolomites with zoning is observed under the CL light. Two stages of the crystallization are realized with the dark color at the middle of the rhombs and bright red color at the edges of the dolomite crystals (**Figure 113-115**).

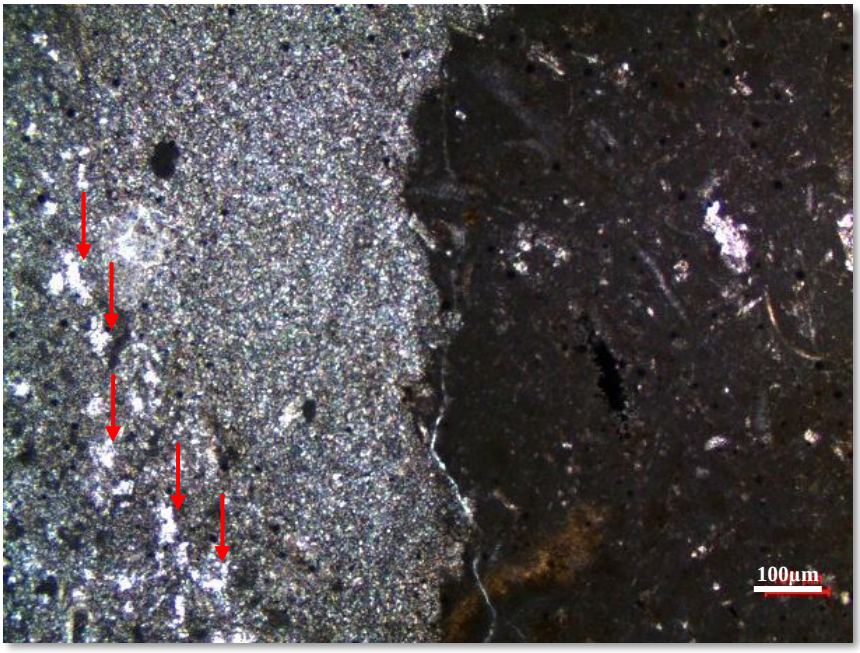


**Figure 103.** Partially dolomitized skeletal, peloidal packstone to grainstone microfacies from the thin section at 1649.35 m of the K-11 well (Note that the original fabric of peloidal facies is partially preserved. Red arrows show pore spaces.)

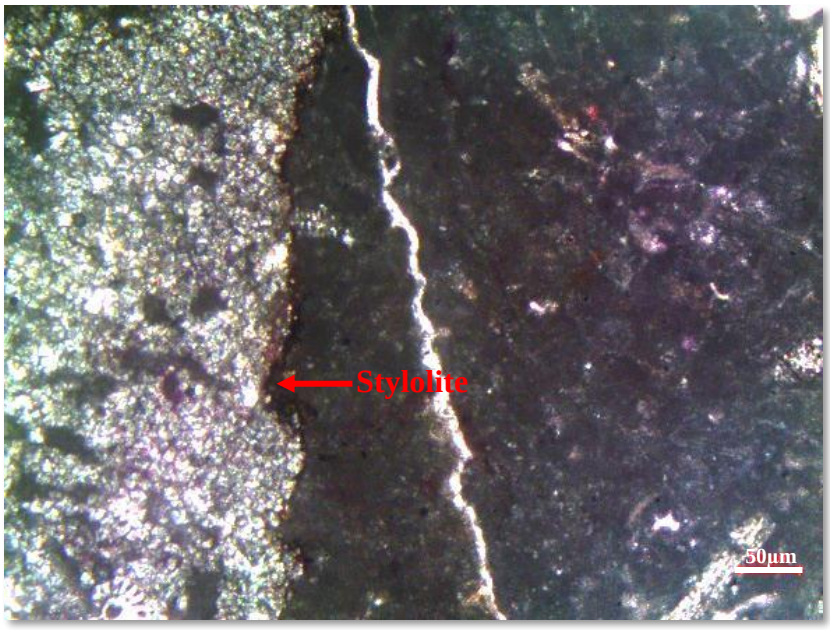


**Figure 104.** Partially dolomitized skeletal, peloidal packstone to grainstone microfacies from the thin section at 1650.11 m of the K-11 well (Note that original fabric of the peloidal facies is partly preserved and Stylolite enhances dolomitization.)

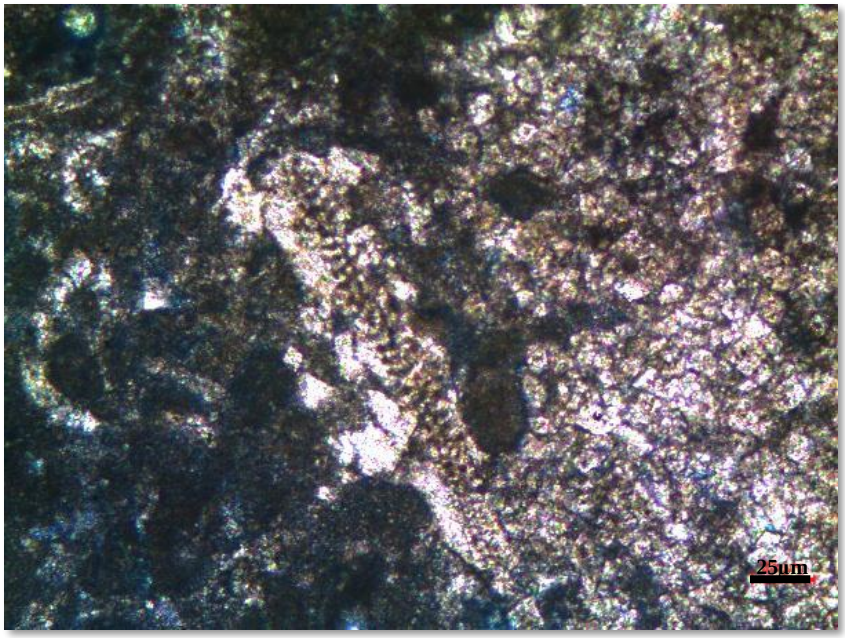


**Figure 105.** Partially dolomitized benthic foraminiferal, skeletal, peloidal packstone to grainstone microfacies from the thin section at 1650.23 m of the K-11 well (Note that original fabric of the peloidal facies is partly preserved.)

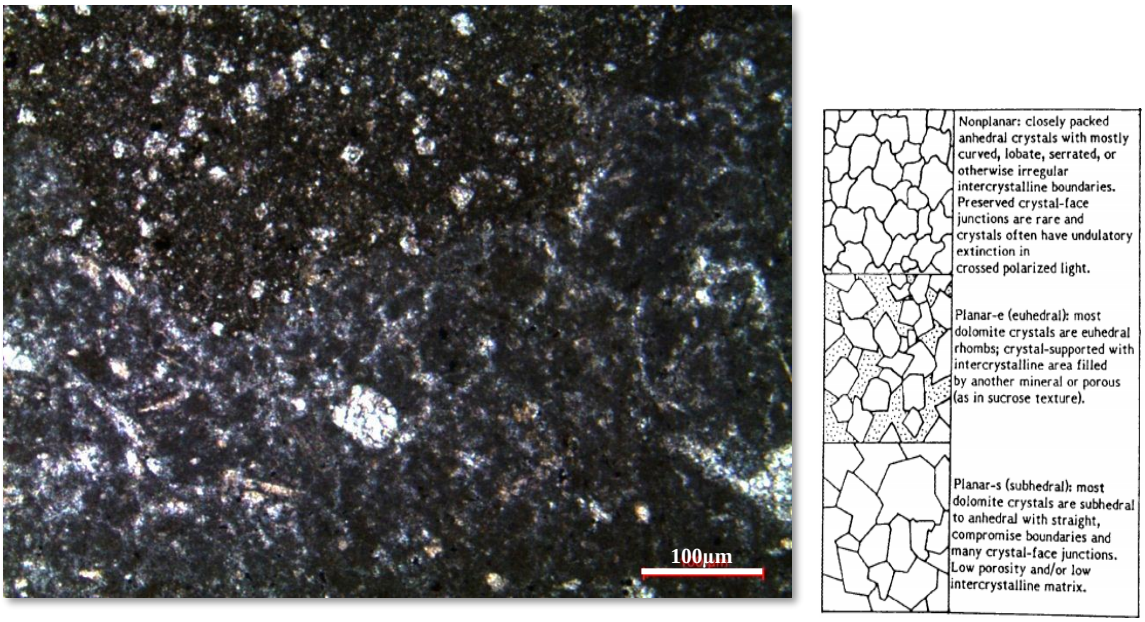


**Figure 106.** Planar-e dolomite with unreplaced peloids, recrystallized skeletal fragments and matrix microfacies from the thin section at 1764.67 m of the K-11 well [(Note that original fabric of the peloidal facies is preserved.) (Dolomite rock texture classification of Gregg and Sibley (1984) is on the right).]

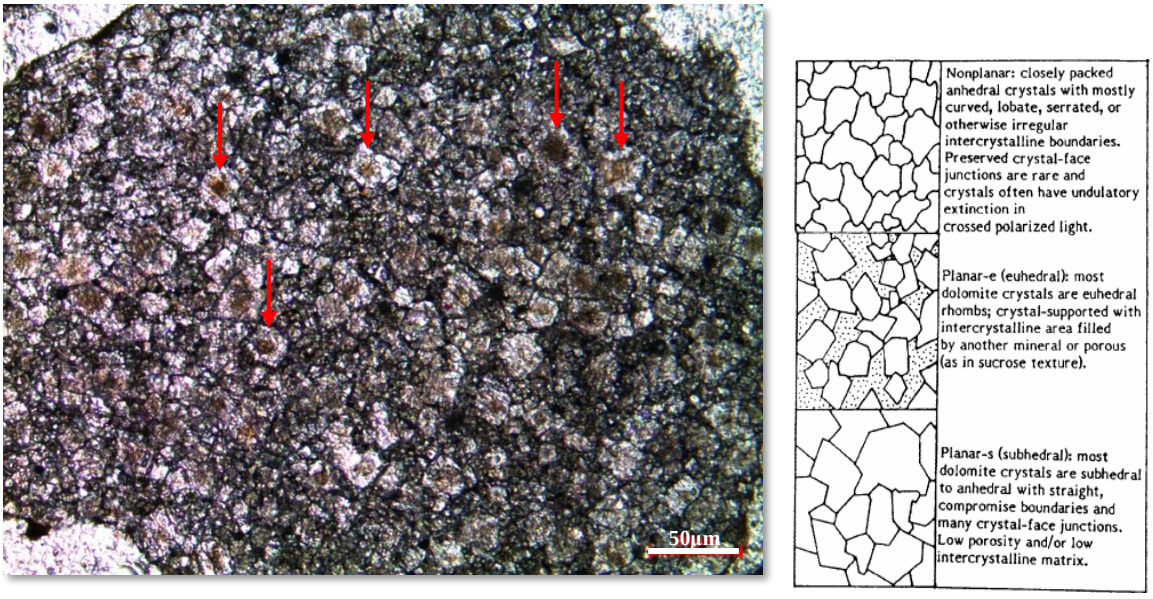


**Figure 107.** Planar-s cloudy core-clear rimmed dolomite with low porosity and low intercrystalline matrix showing zoning from the thin section at 1872 m of the K-8 well [Dolomite rock texture classification of Gregg and Sibley (1984) is on the right.]

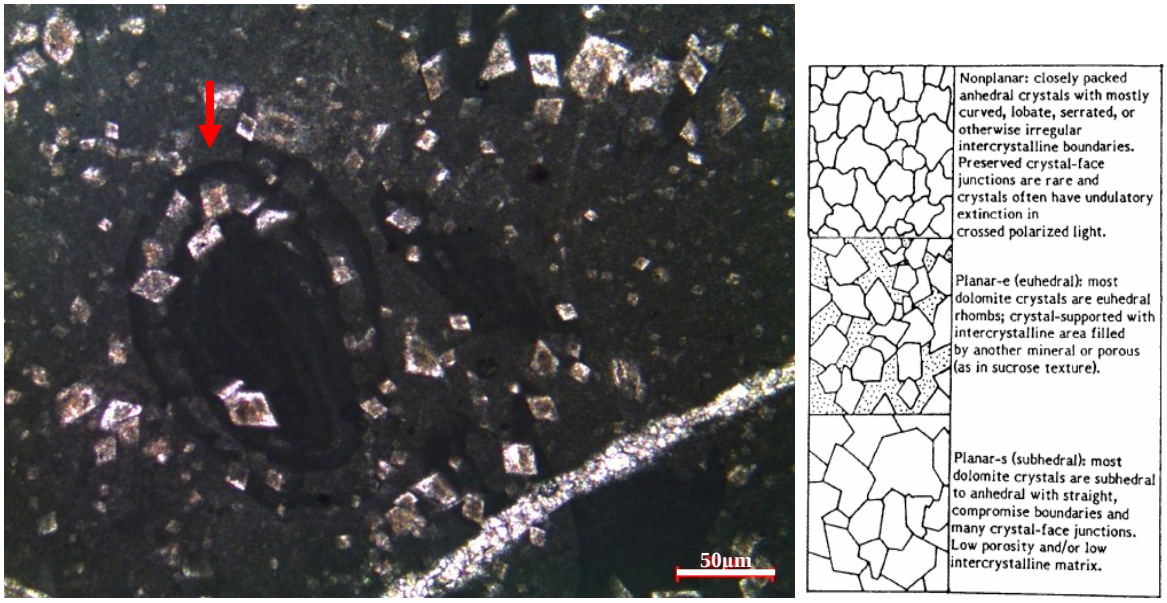


**Figure 108.** Planar-e dolomite with partly replaced benthic foraminifera and the micrite dominated matrix from thin section at 1800 m of the K-8 well (Dolomite rock texture classification of Gregg and Sibley (1984) is on the right.)

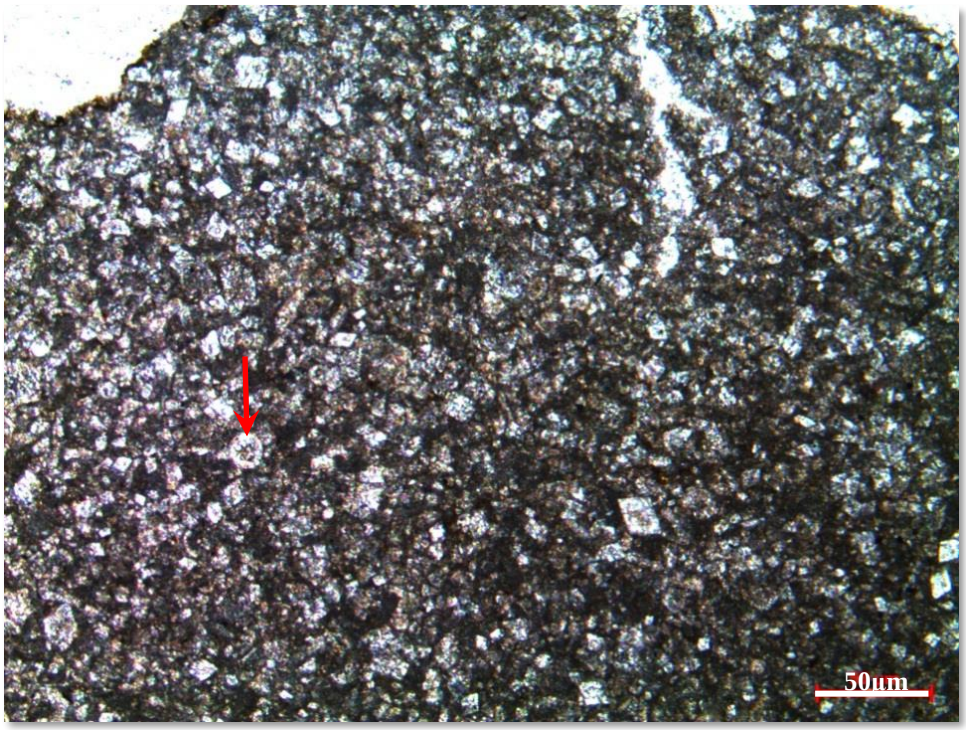


**Figure 109.** Calcareous dolosparite from the thin section at 1866 m of the K-8 well (Note that original fabric including calcisphaerulids is partially preserved.)

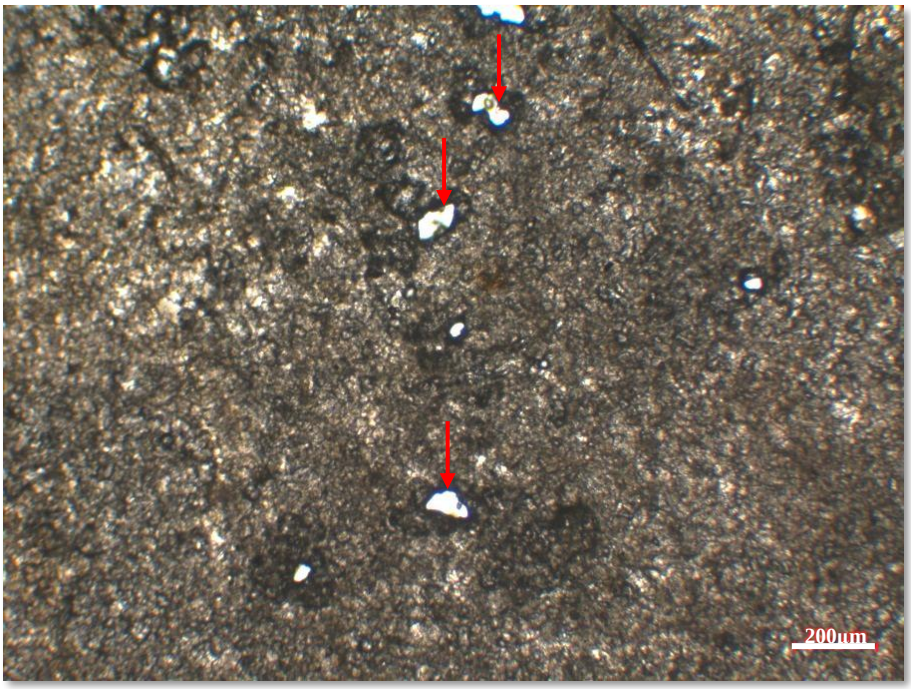


**Figure 110.** Dolomicrosparite and pore spaces of the K-11 well, plane polar light

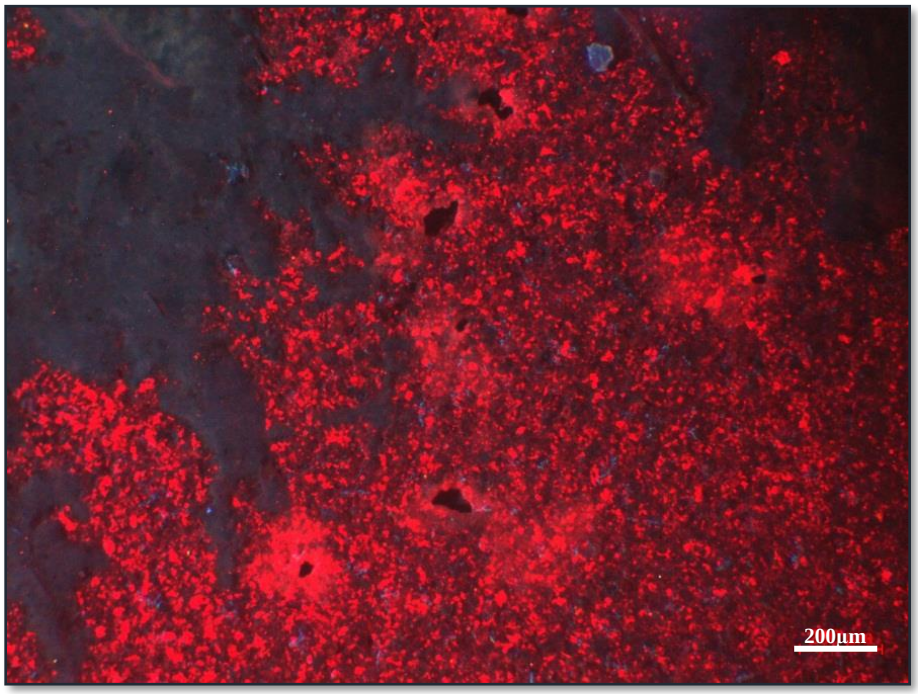


**Figure 111.** Dolomicrosparite and pore spaces of K-11 well, light microscope based cathodoluminescence image of **Figure 110**

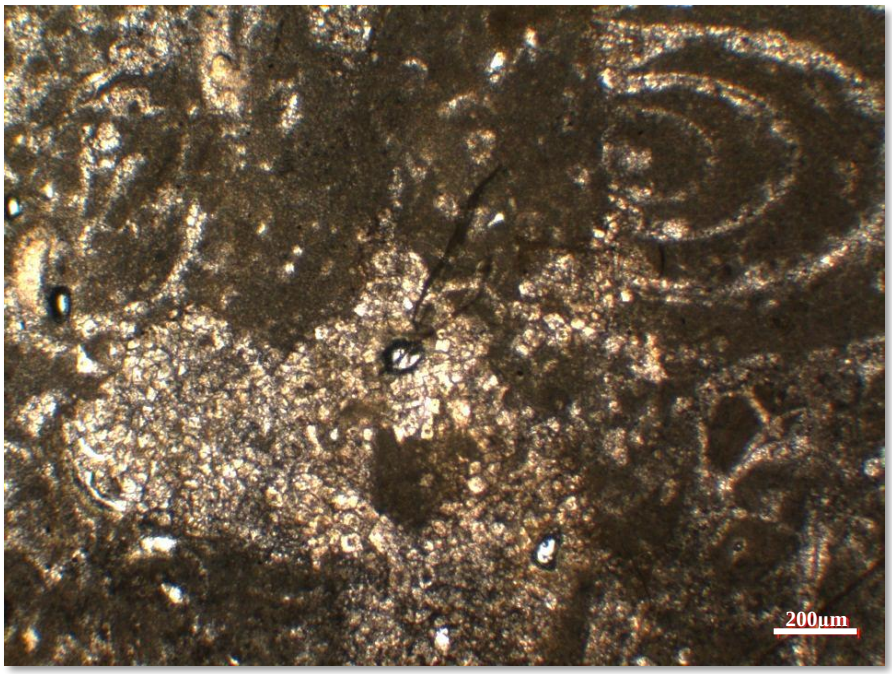


**Figure 112.** Partially dolomitized recrystallized skeletal fragments and pore spaces, at 1650.69 m of the K-11 well, plane polar light

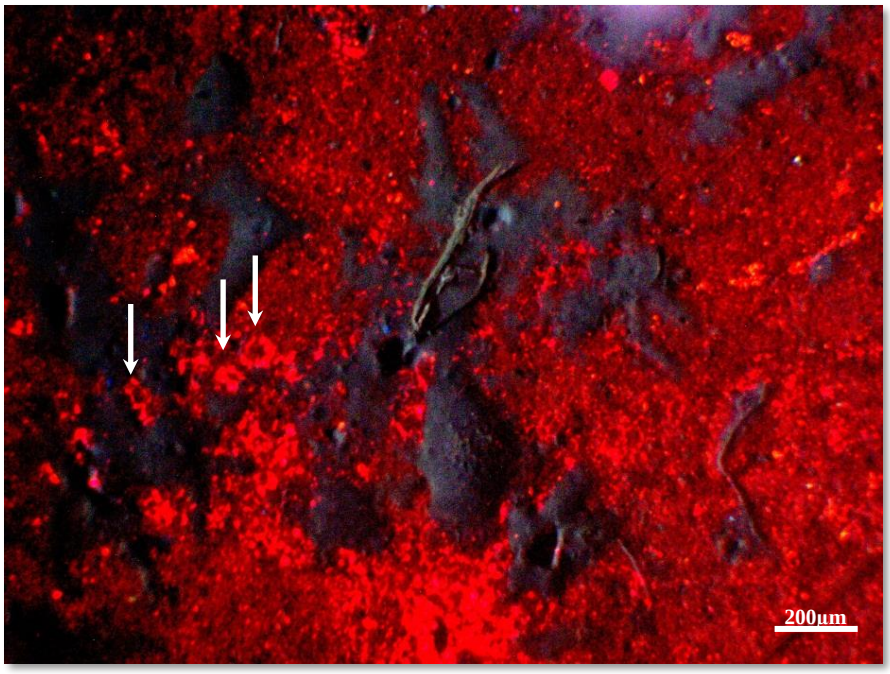


**Figure 113.** Partially dolomitized recrystallized skeletal fragments and pore spaces, at 1650.69 m of the K-11 well, light microscope based cathoduluminescence image of **Figure 112** (White arrows show zoning on the dolomites with dull red to brown colored center and bright red colored rims.)

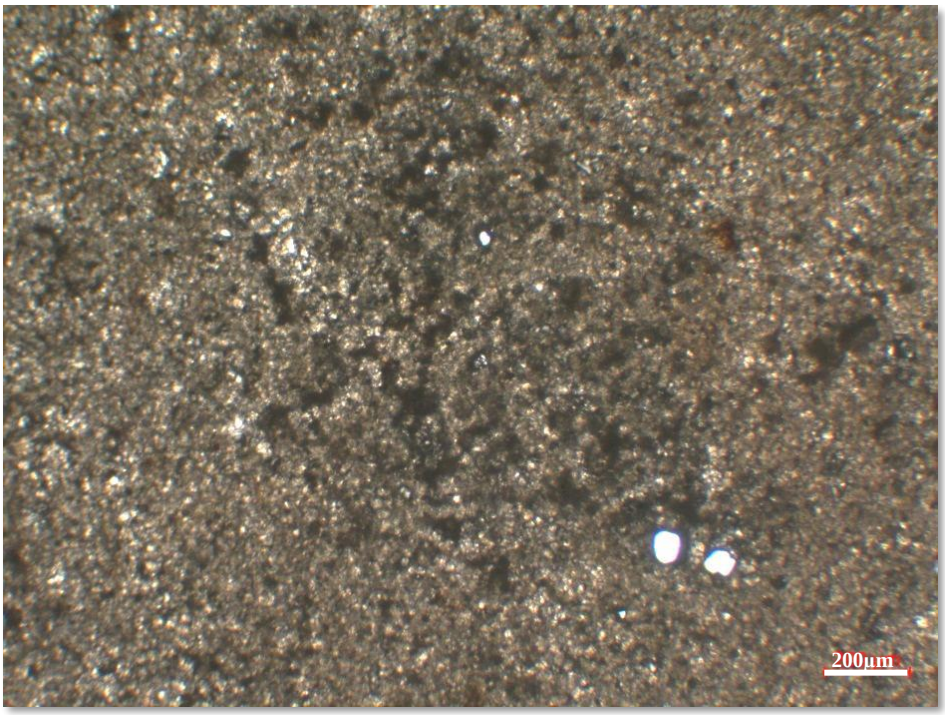


**Figure 114.** Dolomicrosparite and pore spaces of K-11 well, plane polar light

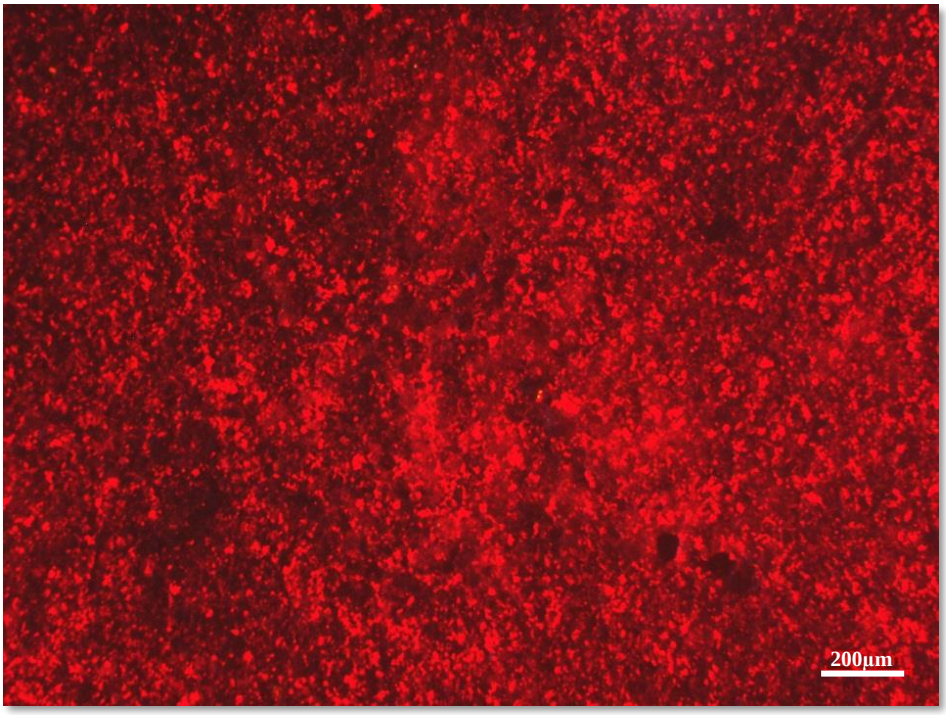


**Figure 115.** Dolomicrosparite and pore spaces of K-11 well, light microscope based cathoduluminescence image of **Figure 114**

Dolomitization in the Derdere Formation is commonly observed in the upper levels of the formation at the top of highstand systems tracts mostly in the inner ramp depositional settings with the presence of dissolution vugs (**Figure 116**) which is also stated in the study of Morad et. al. (2012). Additionally, in the highstand systems tract of 7$^{th}$ sequence of the K-11 well where distal middle ramp environmental conditions are prevailing, thin dolomite beds and dissolution vugs are detected. The observations related with the dolomitization and highstand systems tracts defined in the sequence stratigraphic framework are also stated in the study of Özkan and Altiner (2019). Dolomitization can be associated with the fall in the relative sea-level and occur as a consequence of the evaporation of marine pore water, mostly in near-shore environments (Zenger, 1972; M'Rabet, 1981; Machel and Mountjoy, 1986) and in the mixed meteoric/marine (brackish) pore water zone which is between phreatic marine and phreatic meteoric pore water zone (Badiozamani, 1973; Humphrey, 1988; Morad et. al., 2012). This type of dolomitization is related with the development of moldic vuggy pores by selective or non-selective dissolution of aragonite or Mg-calcite-bearing components. In the evaporate model, due to the increase in Mg/Ca ratio, dolomitization occurs with the precipitation of gypsum and anhydrite (Adams and Rhodes, 1960; Hardie, 1987; Machel and Mountjoy, 1986; Morrow, 1990; Morad et. al., 2012).

As a petrographical observation, if the dolomite packages are thicker at the top of the Derdere, degree of the dolomitization decreases from top to bottom. In order words, at the topmost part of the formation totally dolomitized microfacies (dolomicrosparite to dolosparite) are defined. Calcareous dolomite and dolomitic limestone lithologies become dominant at the lower levels of these thick dolomite packages described at the top of the Derdere Formation. These types of observations are also stated in the study of Morad et. al. (2012). During the relative fall of sea level, the mixed marine/meteoric pore water zone is shifted landwards which causes upward increase in dolomitization in carbonate successions (Taghavi et al., 2006; Morad et. al., 2012) (**Figure 116**). In order words, in the case of dolomitization caused by relative sea level fall, intensity of dolomitization decreases from top to bottom.

Mixing zone diagenesis results in the dissolution of less stable aragonite and high-Mg calcite and precipitation of bladed and overgrowth of more stable low-Mg calcite (Csoma et al., 2004; Morad et. al., 2012). After the pronounced fall in relative sea level and following subaerial exposure of peritidal deposits, dolomitization of the deposits of HST and TST below the sequence boundaries occur, which is also suggested in supratidal-evaporative seepage reflux model during warm arid climatic conditions (Tucker, 1993; Morad et. al., 2012).

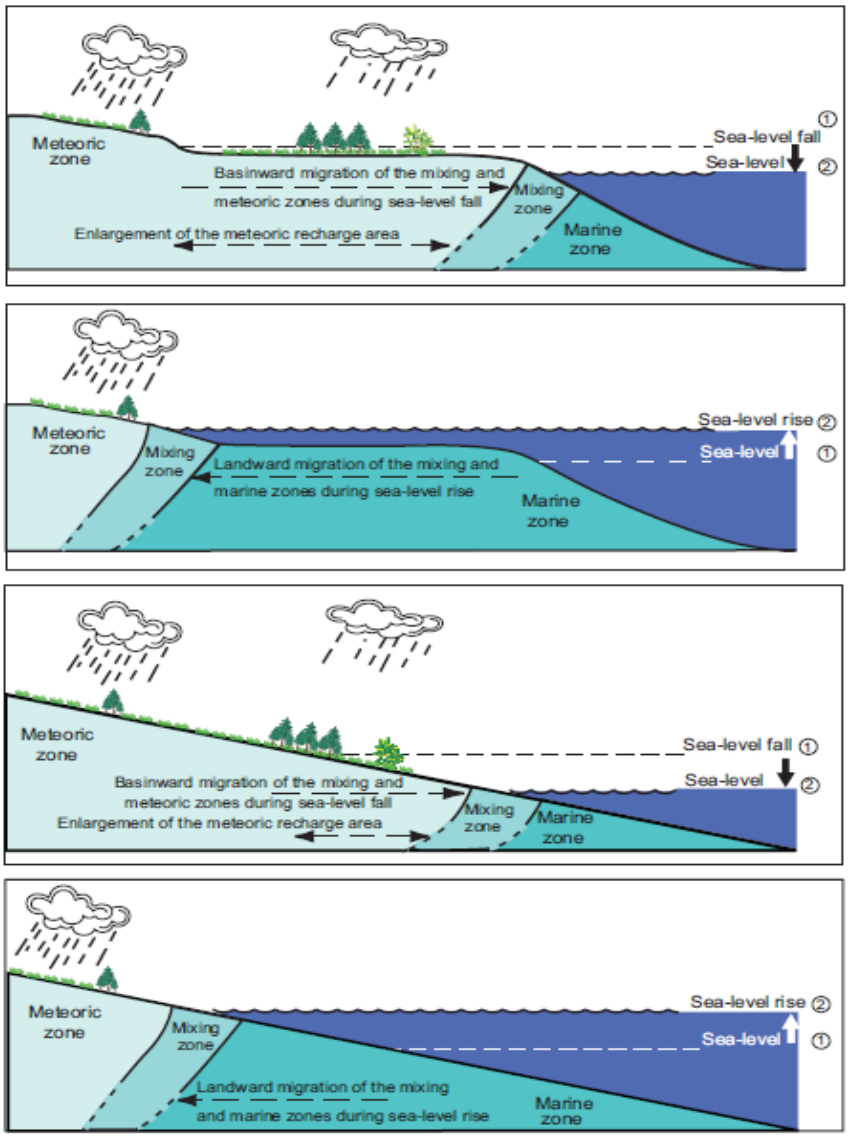


**Figure 116.** Change in the meteoric, mixing and marine phreatic zones in platforms and ramps during relative sea level rise and fall. Large area is affected in platforms rather than homoclinal ramps (Morad et. al., 2012)

#### 5.1.1.2 Dissolution

Dissolution is the major diagenetic mechanism which enhances reservoir quality including porosity and permeability (**Figure 117-120**). Solubility of the minerals is variable, which affects the dissolution rates. Dolomites are more stable than calcite minerals (Bosence, 2002) and among the calcite minerals; low magnesium calcite minerals are more stable than high magnesium calcite minerals and aragonite.

The most common porosity type observed in this study is vuggy porosity and formation of vuggy porosity is mostly observed as non-fabric selective including matrix, cement and grains (Choquette and Pray, 1970) and it is most likely to be observed in dolomitic intervals in this study. Dissolution occurs in the vadose zone of solution due to meteroric diagenesis and it is observed in the mixed marine-fresh water zone. The main mechanisms generate dissolution are fresh water entrance due to sea level fluctuations, compaction of shales and the release of water and pressure solution (Moore, 1989).

In this study, dissolution is associated with subaerial exposure and entrance of meteoric water to the system due to sea level fluctuations and it is frequently observed at the top of the highstand systems tracts of the sequences. Since calcite minerals are more unstable than dolomite, remnants of calcite can dissolve during dolomitization and it generates vuggy porosity between dolomite crystals.

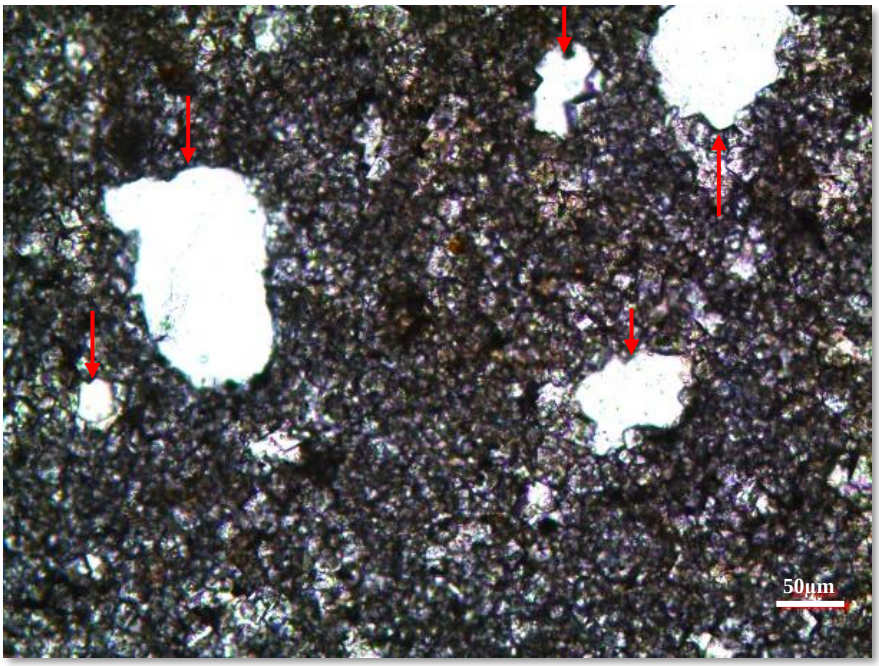


**Figure 117.** Vuggy porosity in dolomicrosparite formed as a result of dissolution from the thin section at 1649.76 m of the K-11 well (Red arrows show pore spaces.)

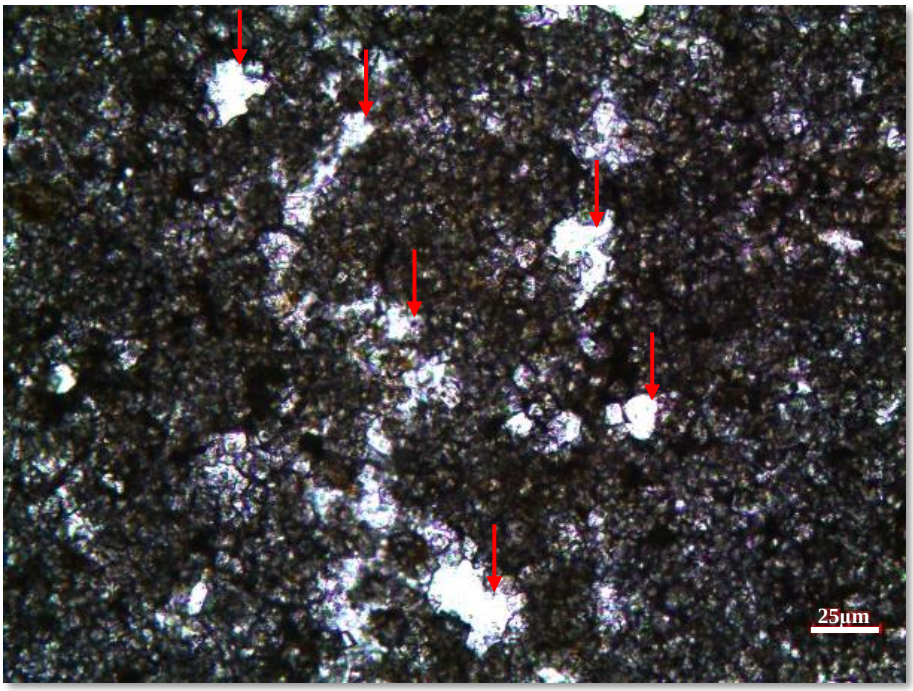


**Figure 118.** Porous dolomicrosparite microfacies from the thin section at 1649.83 m of the K-11 well (Red arrows show vuggy porosity.)

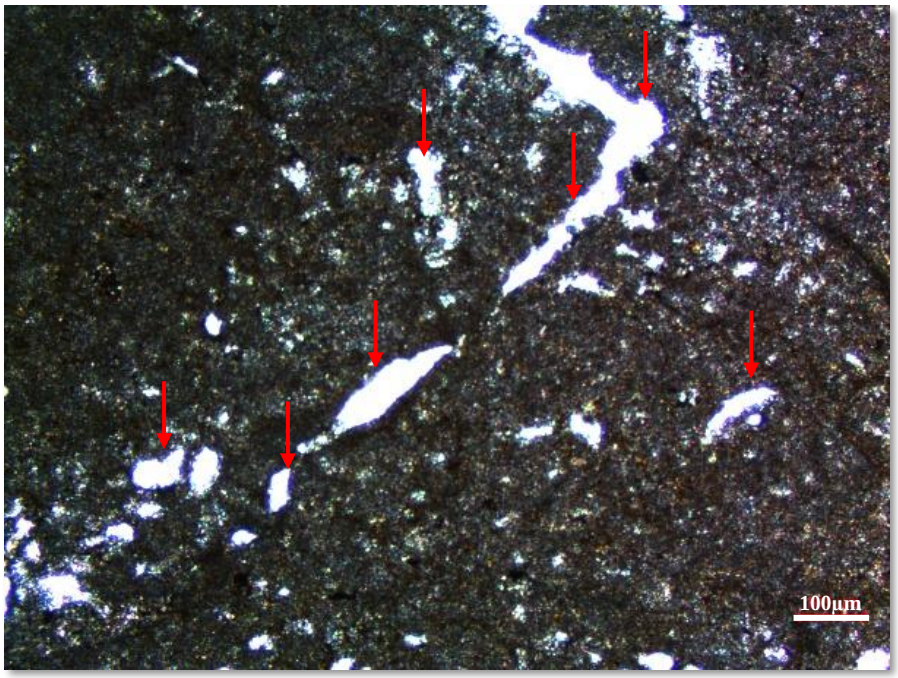


**Figure 119.** Porous dolomicrosparite microfacies from the thin section samples of 1649.62 m of K-11 well (Red arrows show vuggy porosity.)

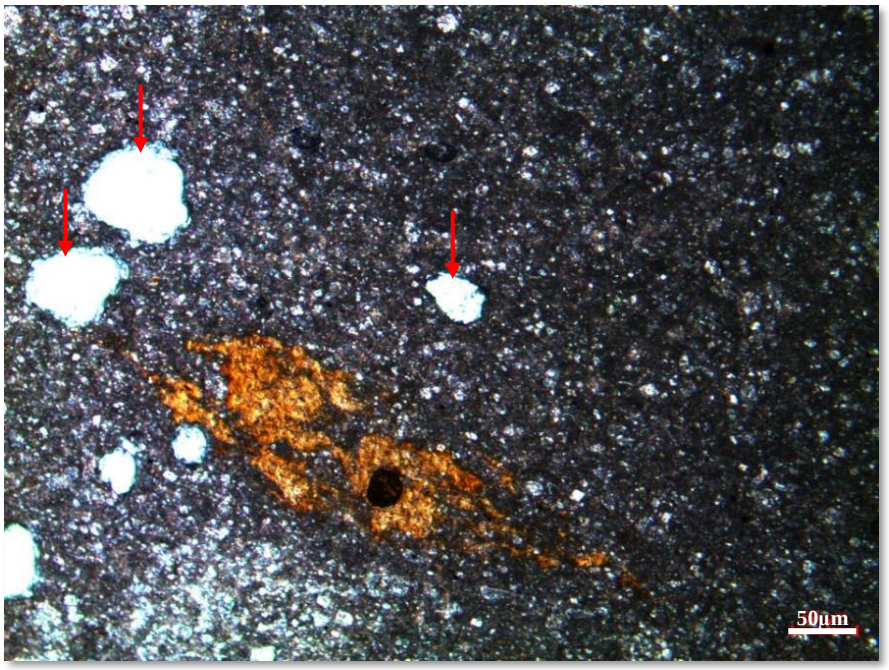


**Figure 120.** Partially dolomitized skeletal calcisphaerulid-bearing wackestone microfacies from the thin section at 1697.20 m of the K-11 well (Note that original fabric of the peloidal facies is partly preserved. Red arrows show vuggy porosity.)

#### 5.1.1.3 Cementation

The other main diagenetic process is cementation intensely observed in the samples of the Derdere Formation. The most common and distinctive calcite cement types observed in the samples of the studied wells are (1) micritic envelope type cement around the skeletal fragments as micritic isopachous Mg calcite (**Figure 121** and **Figure 122**) and (2) abundant equant calcite cement inside the leached grains and both interparticle and intraparticle porosity is filled with sparry calcite (**Figure 122-124**), and (3) isopachous bladed calcite cement (**Figure 125**). Also, syntaxial overgrowth of echinoderm (**Figure 126**) particles is pervasively observed in the samples, where packstone to grainstone microfacies deposited in the inner ramp depositional settings are defined. Isopachous equant calcite and bladed calcite cements are the most commonly observed in the freshwater active phreatic zone. Due to preservation of stable micritic envelopes, outlines of the grains are still can be observed (Scholle and Ulmer-Schoelle, 2003).

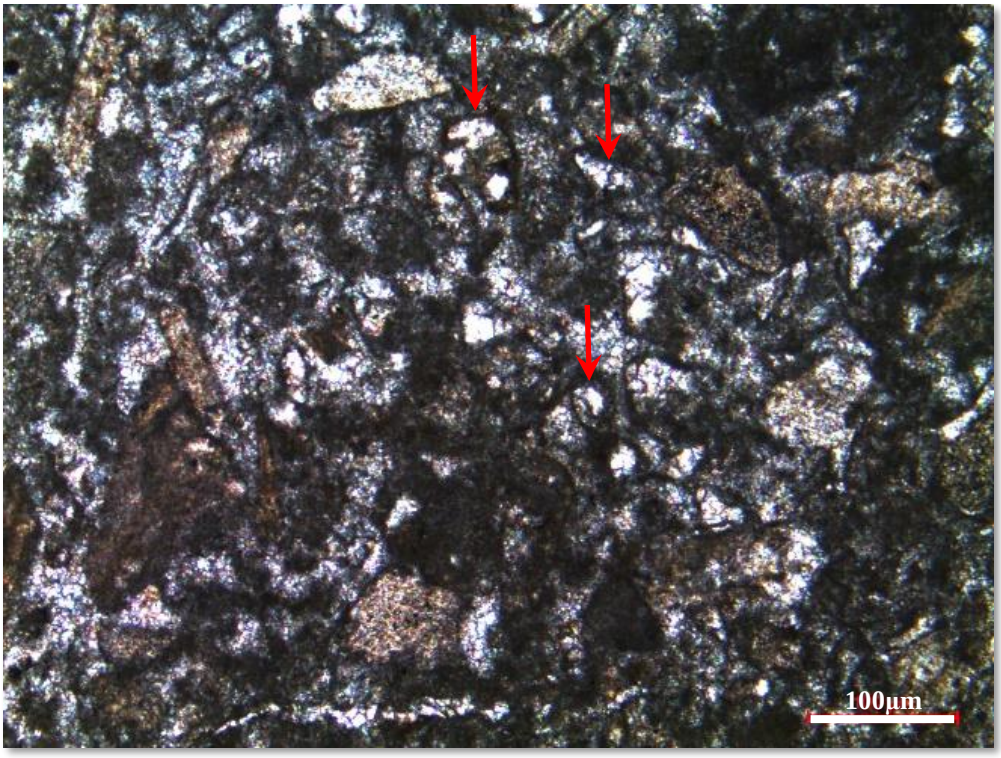


**Figure 121**. Micritic isopachous Mg calcite and sparry calcite cement as interparticle pore filling from the thin section at 1770.8 m of the K-11 well (Red arrows show the micritic isopachous cement at around the skeletal grains.)

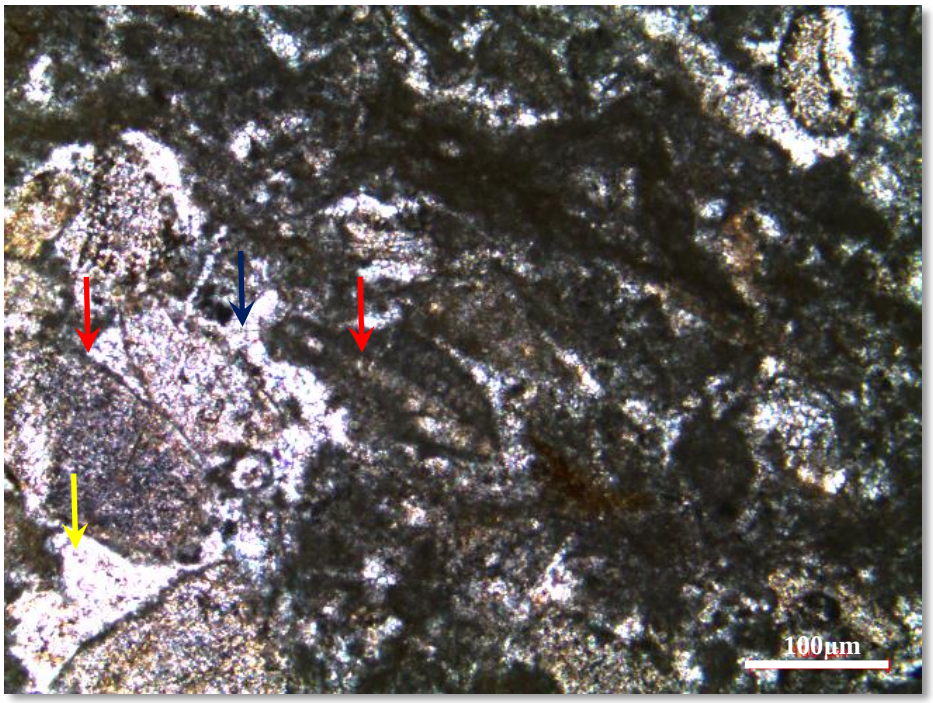


**Figure 122.** Micritic isopachous Mg calcite and sparry calcite cement as interparticle pore filling from the thin section at 1771.4 m of the K-11 well (Red arrows show the micritic isopachous cement. Yellow arrows show sparry calcite cement.)

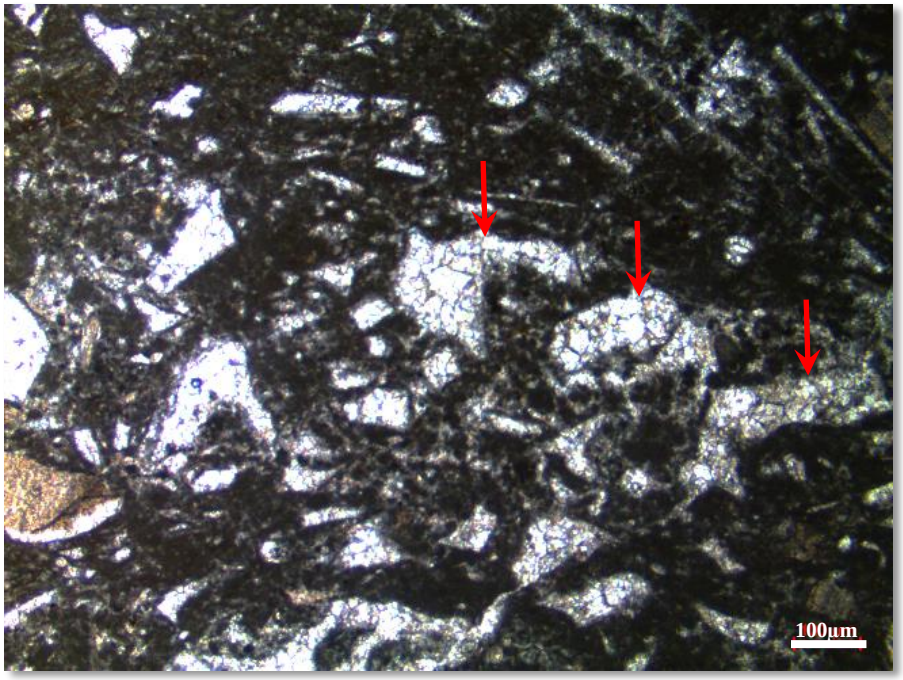


**Figure 123.** Sparry calcite cement formed as a result of neomorphism inside the skeletal fragments from the thin section at 1765.16m of the K-11 well

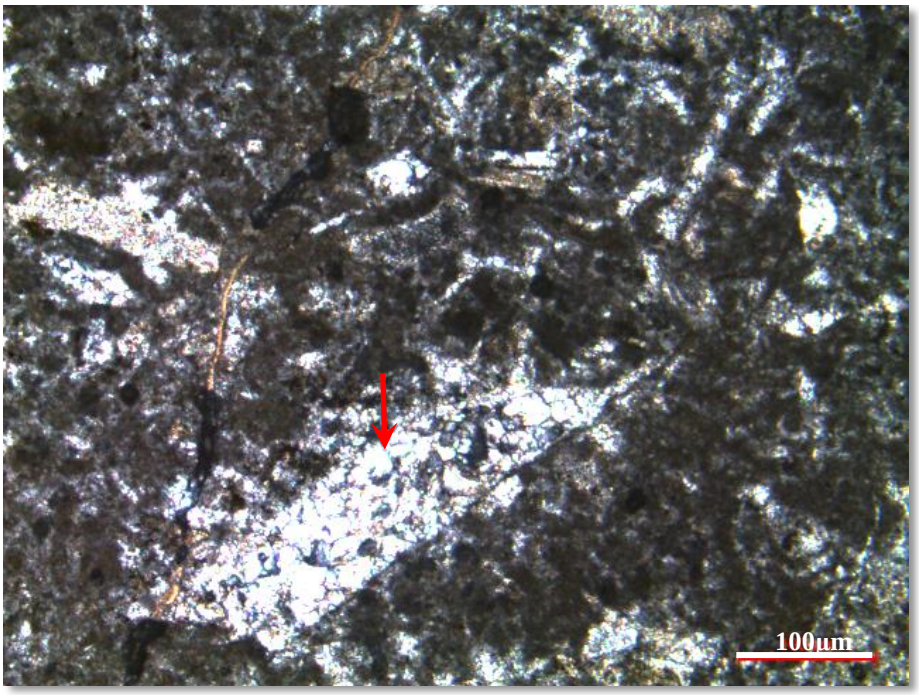


**Figure 124.** Sparry calcite cement formed as a result of neomorphism inside the skeletal fragments from the thin section at 1765.78 m of the K-11 well

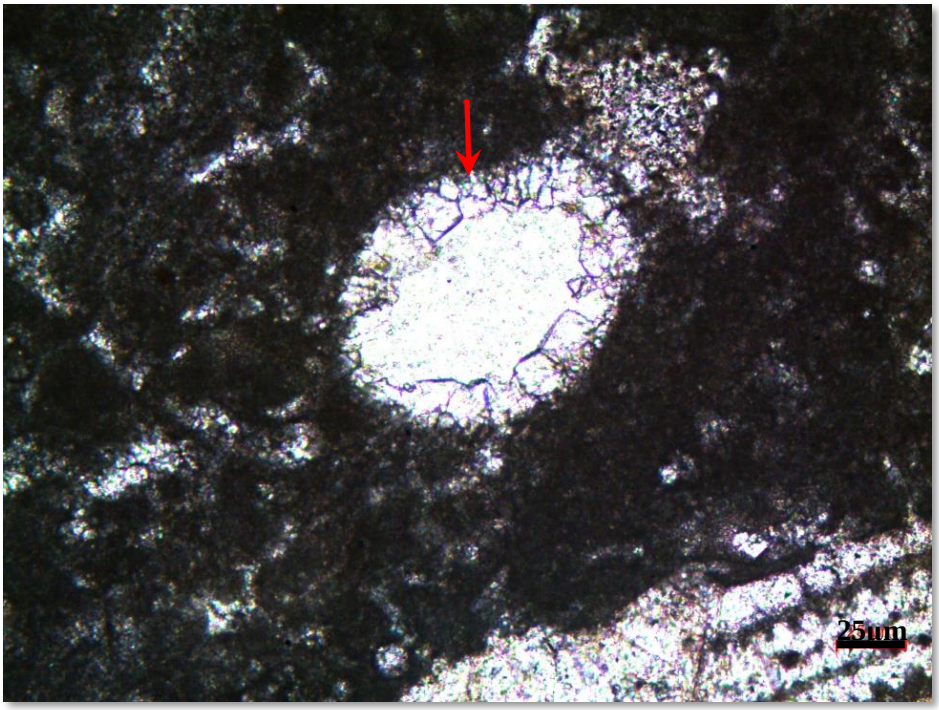


**Figure 125.** Isopachous equant rim cement formed in the pore space of the skeletal fragment from the thin section at 1650 m of the K-11 well

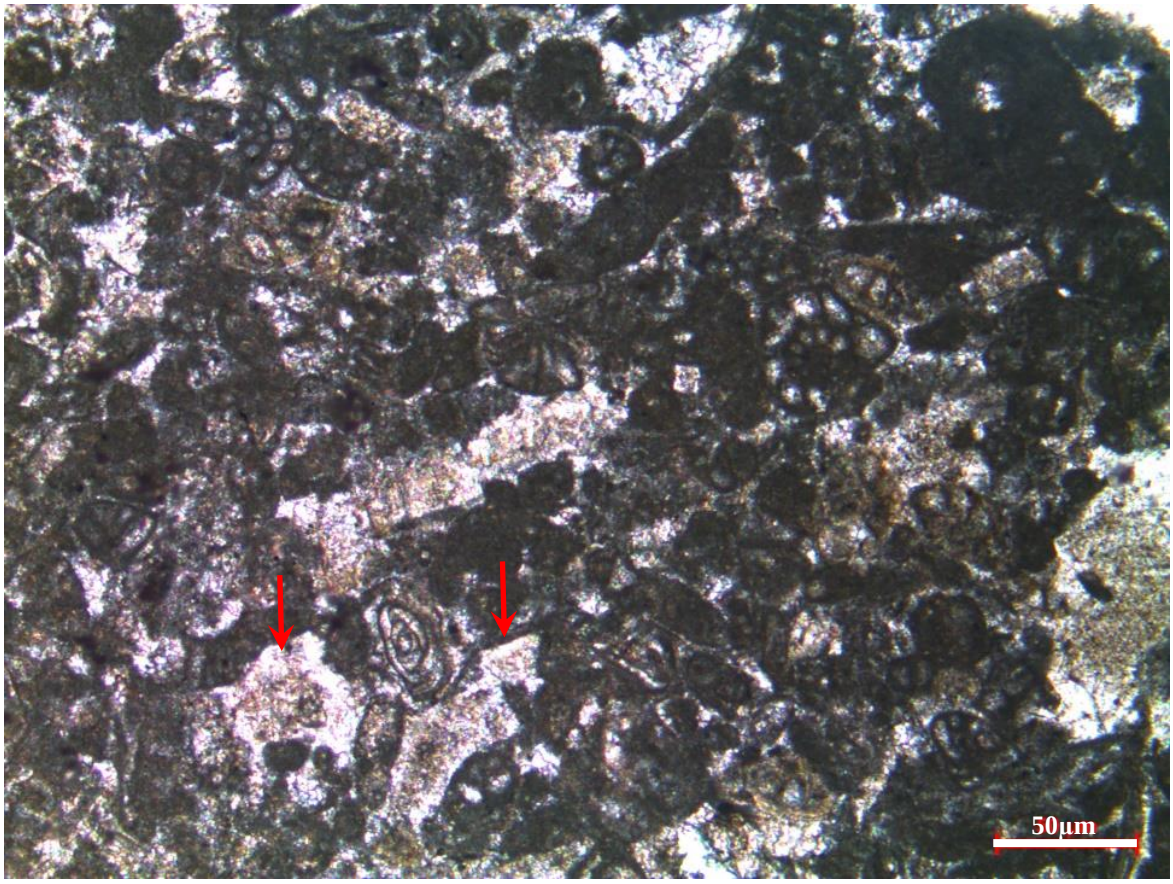


**Figure 126.** Syntaxial overgrowth of echinoderm particles in the thin section sample at 1808 m of the K-8 well

In the thin section samples of the Derdere Formation where extensive solution of some skeletal fragments are observed, isopachous bladed calcite cement is formed, bright red rimmed luminescence cement is detected on the light microscope based CL studies (**Figure 127** and **Figure 128**).

In the study of Hajikazemi et. al. (2010), it is stated that luminescence properties of the cements are the indicator of diagenetic environments due to oxidizing and reducing conditions depend on the presence or absence of Fe. As a general speaking, the non-luminescent characteristic of isopachous rim cement, equant calcite cements and syntaxial cement can be formed either in marine or meteoric vadose diaganetic environments due to being exposed to oxidizing conditions and the bright rims of the surrounding crystals can be the indicator of reducing conditions of a meteoric phreatic type diagenetic enevironment (Moldovany and Lohmann 1984; Hajikazemi et. al. 2010).

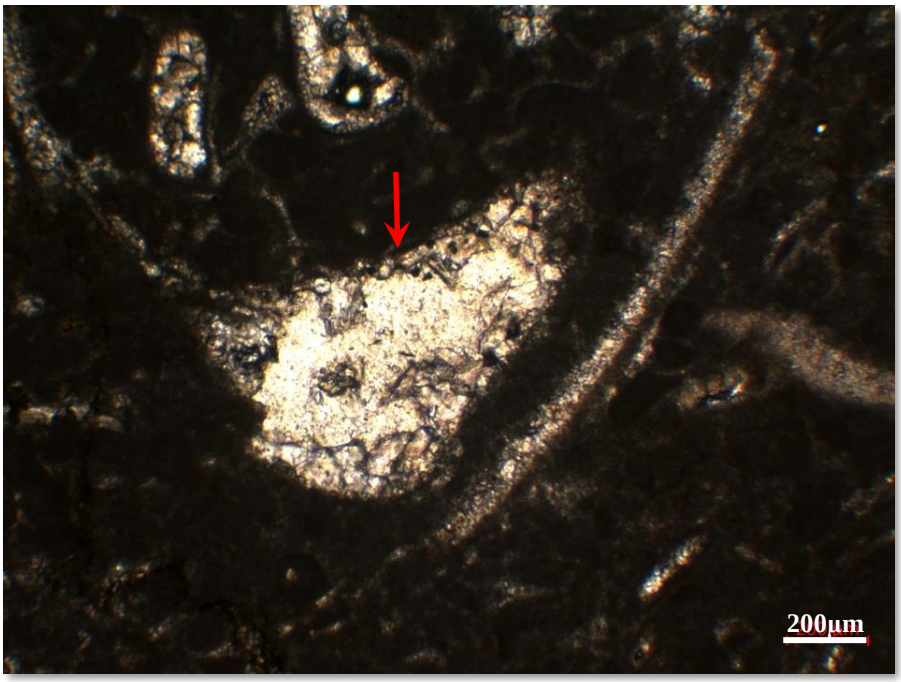


**Figure 127.** Isopachous bladed calcite cement inside the pore space of the skeletal fragments from the thin section at 1650.69 m of the K-11 well

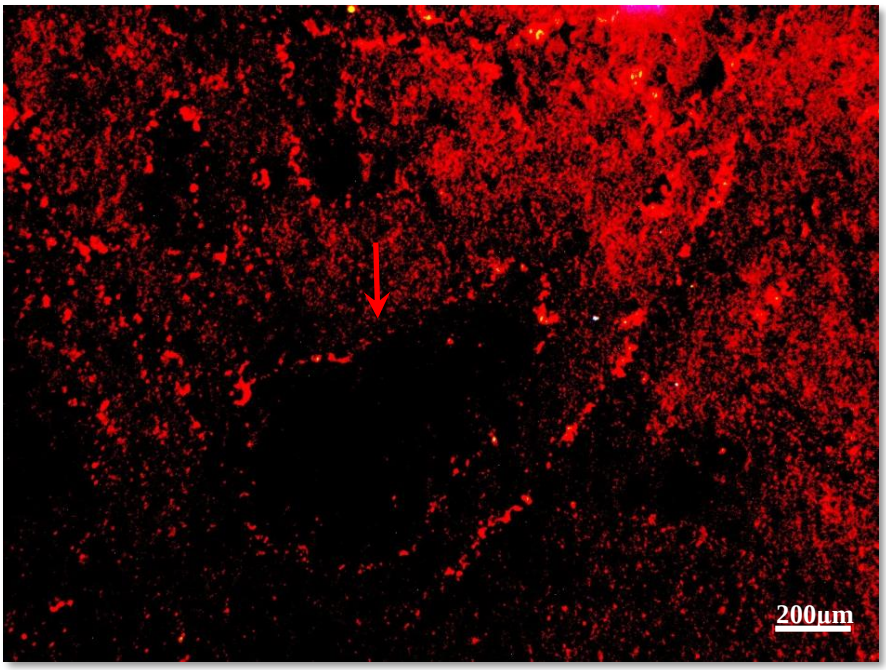


**Figure 128.** Isopachous bladed calcite cement inside the pore spaced of the skeletal fragments from the thin section at 1650.69 m of the K-11 well, light microscope based cathodoluminescence image of **Figure 127**

#### 5.1.1.4 Replacement

Petrographic studies show the existence of totally calcitized radiolaria in the thin section of sample 1697.42m, taken from core#2 (mentioned above) (**Figure 129** and **Figure 130**). During the deposition of the Derdere Formation, OAE2 defined in the study of Schlanger and Jenkyns (1976) occurs in the pelagic sedimentary sequences of C-T age. These events, which are related with transgressive episodes, occur globally in oceans, nutrient enrichment and organic matter production, have an impact on climate and bottom-water currents (Schlanger and Jenkyns, 2007; Arthur and Sageman, 2005; Ergene, 2014).

This organic enrichment, which is expected during OAE2 event, is observed in the petrographic studies of thin sections below the radiolaria-bearing level which is also observed in the study of Milliken et. al. (2016) and this is supported by log data as well. Silica originated radiolaria is totally replaced by calcite. In order to reveal the replacement of silica, some SEM studies were conducted (**Figure 131**) and X-ray maps were obtained and presence of authigenic silica was detected on X-ray maps (**Figure 132**). On the other hand, the more certain results are revealed with the study of light microscope based cathodoluminescence (CL) by its working principle of making fabrics visible that are not visible by light microscopy. Therefore, totally calcitized, broken and fragmented parts (spicules) of radiolaria is differentiated from background calcite. Silica replacement of dolomites is also another common replacement type observed in the Derdere Formation. It is petrographically observed that silicification postdates the dolomite formation (**Figure 133** and **Figure 134**) in the diagenetic history of the Derdere Formation.

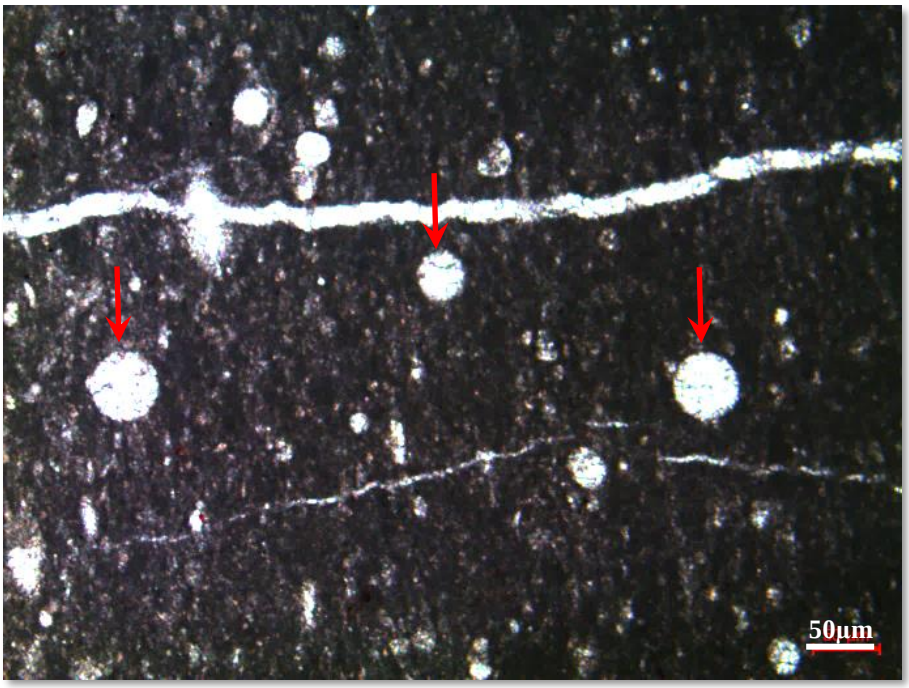


**Figure 129.** Calcite replaces silica in radiolaria-bearing mudstone microfacies from the thin section at 1697.42 m of the K-11 well

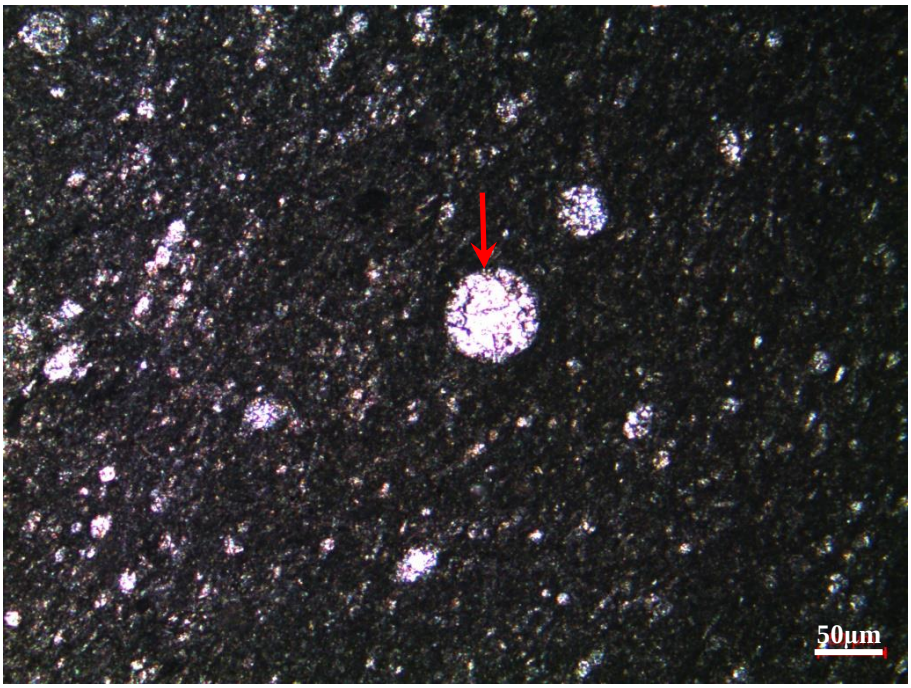


**Figure 130.** Calcite replaces silica in radiolarian-bearing mudstone microfacies from the thin section at 1697.42 m of the K-11 well

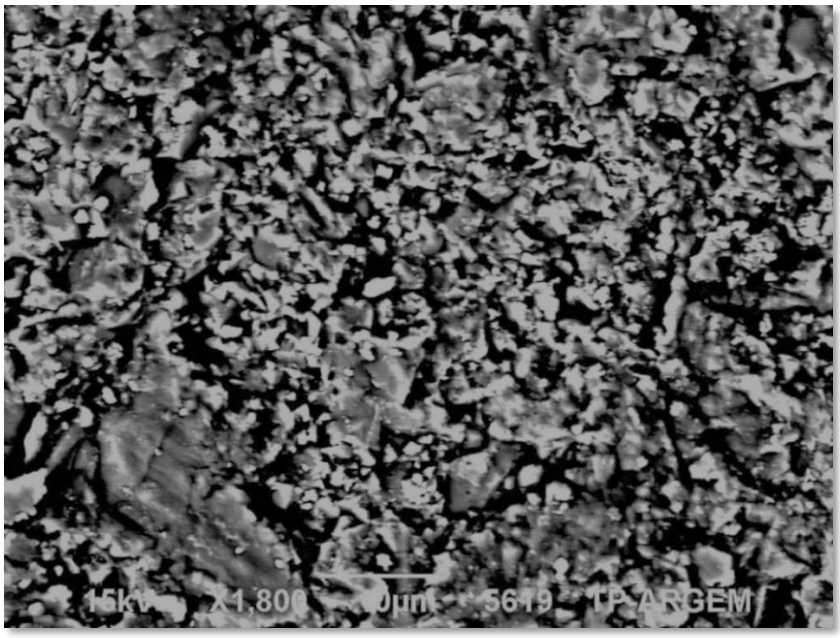


**Figure 131.** Scanning electron microscope photomicrograph of radiolaria-bearing mudstone microfacies from the thin section of 1697.42 m of K-11 well

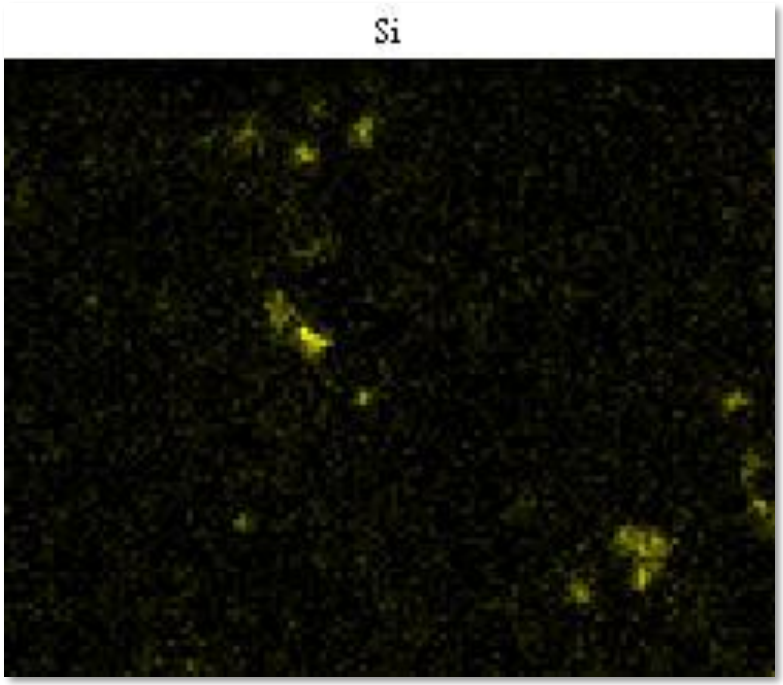


**Figure 132.** X-ray mapping of silica element shown in **Figure 131** (bright yellow areas show the presence of authigenic silica due to its size and anhedral shape)

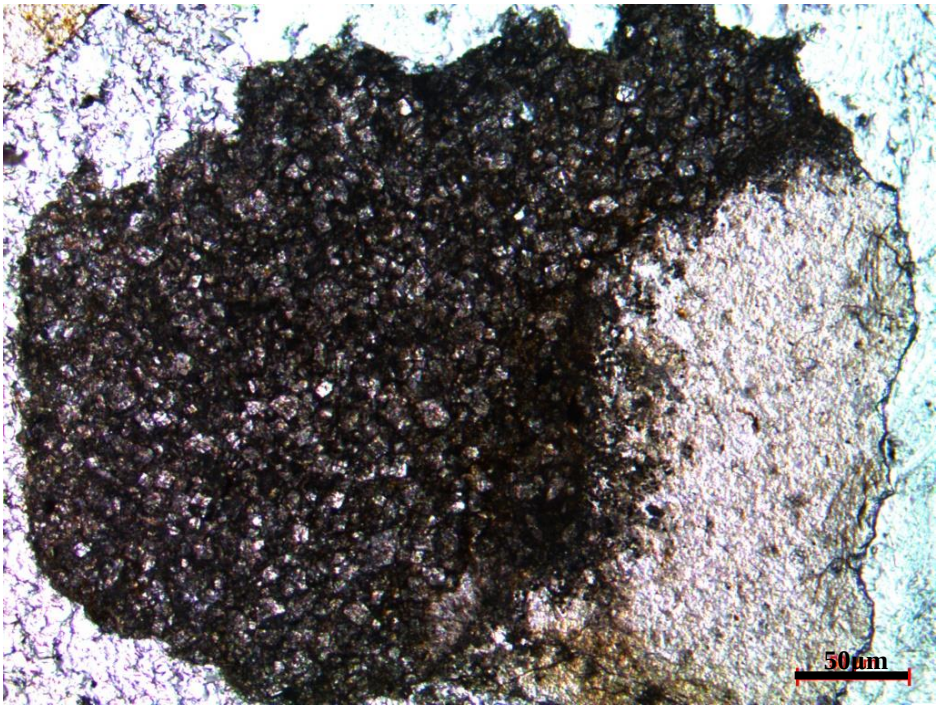


**Figure 133.** Silica replacement of dolosparite from the thin section at 1866 m of the K-8 well, plane polar light

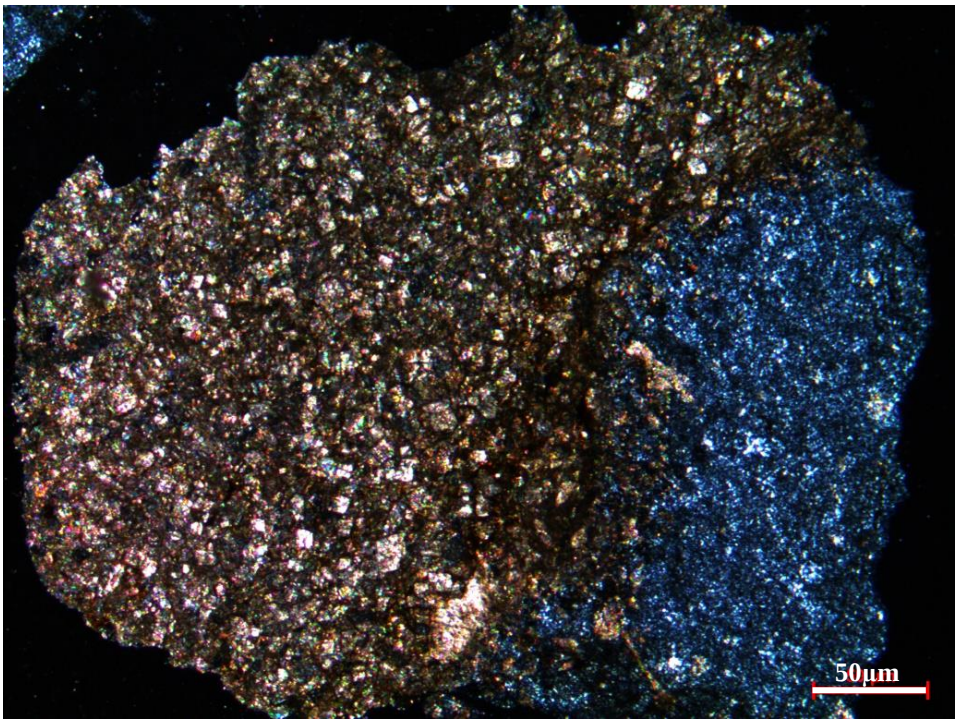


**Figure 134.** Silica replacement of dolosparite from the thin section at 1866 m of the K-8 well, cross polar light

### 5.1.1.5 Chemical Compaction (Stylolitization)

Stylolites are commonly observed in the samples of the Derdere Formation in thin sections, core and sometimes on the cutting samples. They are mostly filled with clay minerals and/or organic matter (**Figure 135** and **Figure 136**). Since their formation is related with the pressure solution of the grains, they are mostly observed at around the grains especially skeletal fragments (**Figure 137**, **Figure 138**, and **Figure 140**). Another parameter related with the formation of stylolites is their association with fluid flow and dolomitization. Dolomites are formed where stylolites are observed or the size of the dolomite crystals enlarges due to the fluid flow at around stylolites (**Figure 138-140**) in the Derdere Formation.

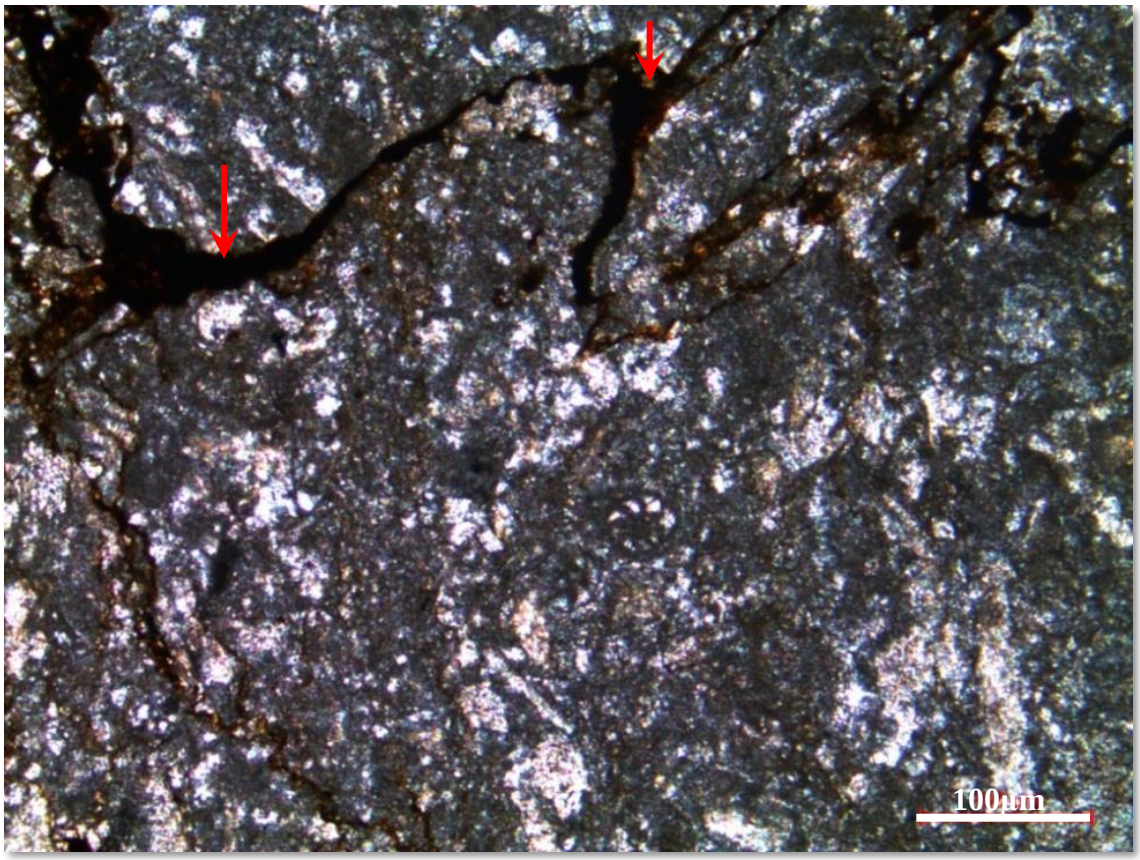


**Figure 135.** Stylolites filled with organic matter and clay from the thin section at 1769.03 m of the K-11 well

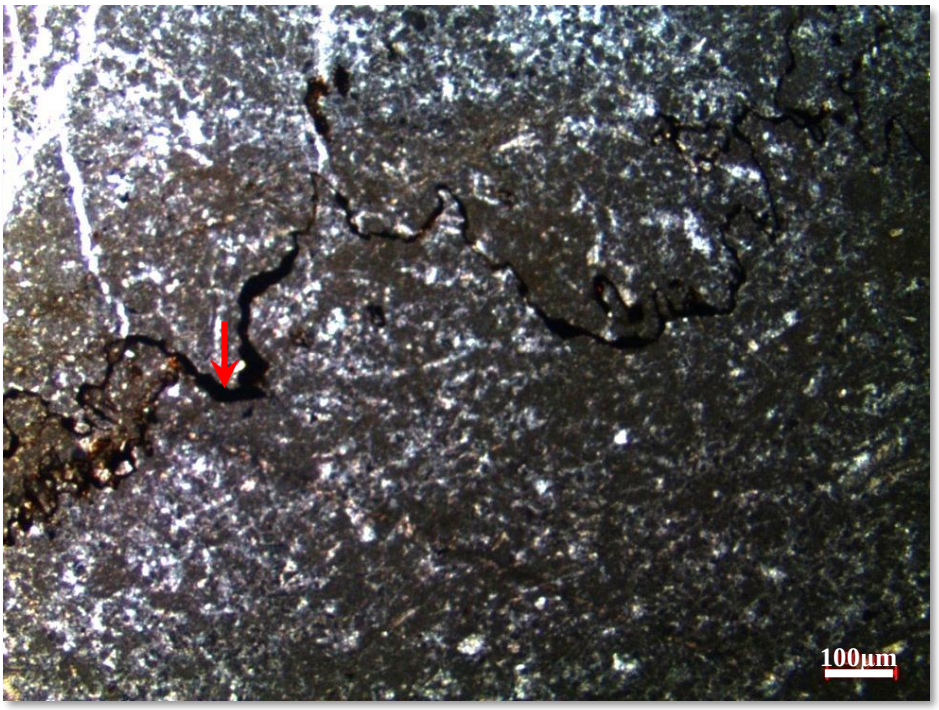


**Figure 136**. Stylolites filled with organic matter and clay from the thin section at 1765.40 m of the K-11 well

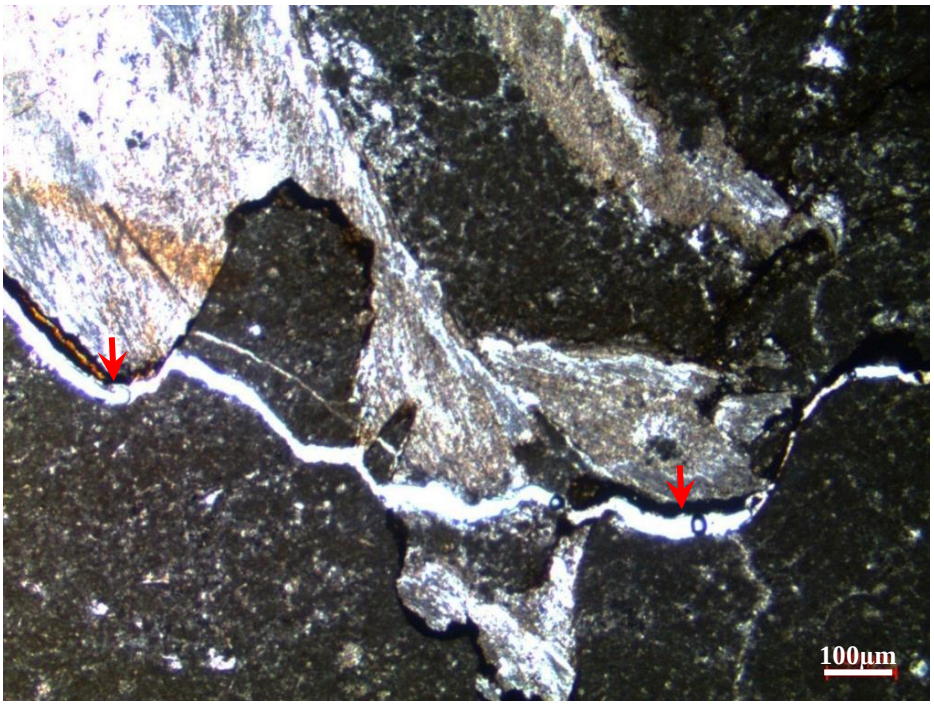


**Figure 137**. Stylolites formed at around the skeletal fragment from the thin section at 1764.89 m of the K-11 well

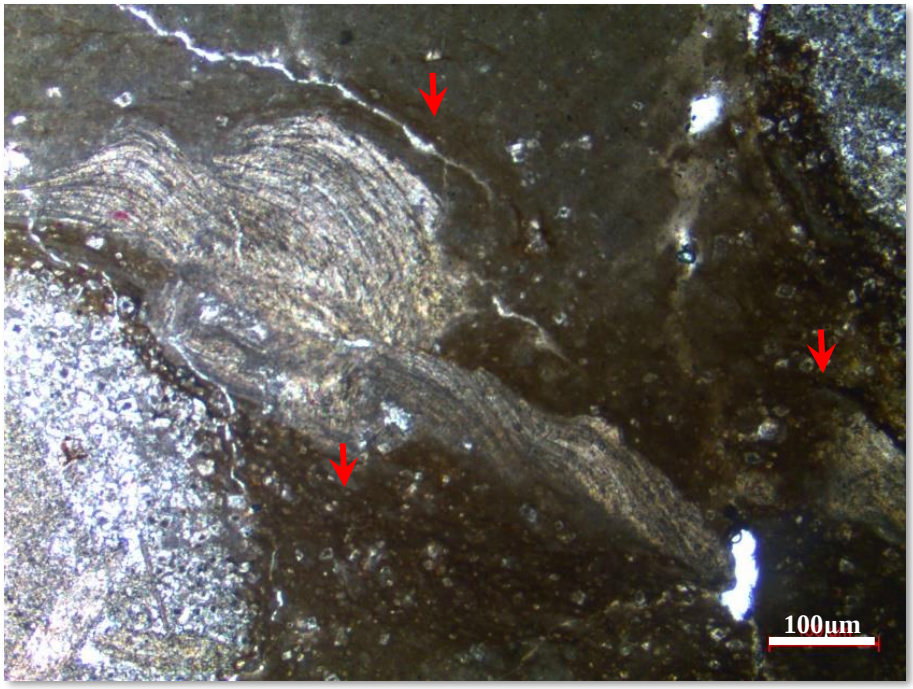


**Figure 138.** Stylolites associated with dolomitization from the thin section at 1776.86 m of the K-11 well

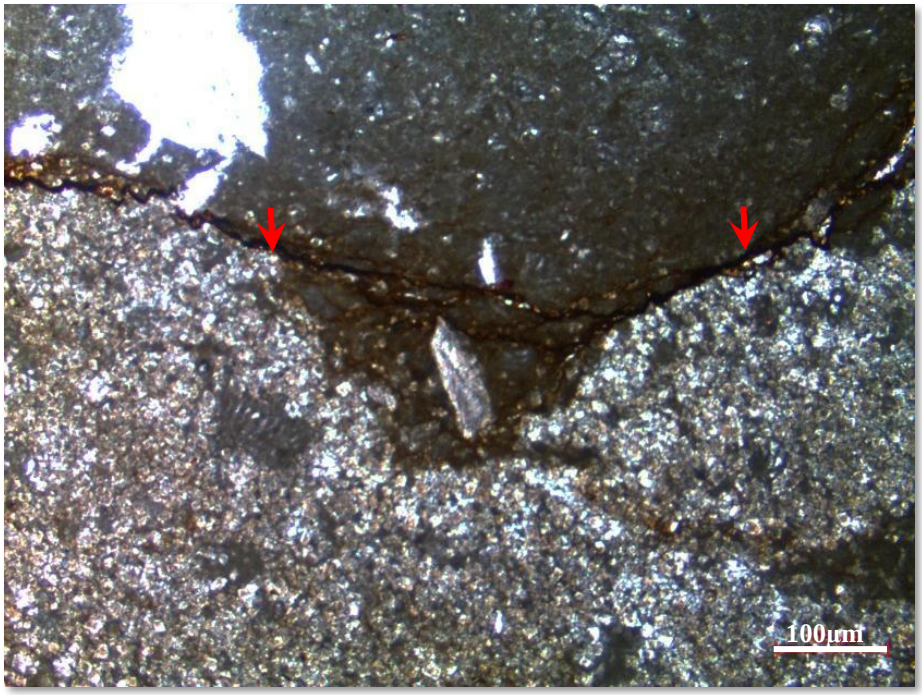


**Figure 139.** Stylolites associated with dolomitization from the thin section at 1779.53 m of the K-11 well

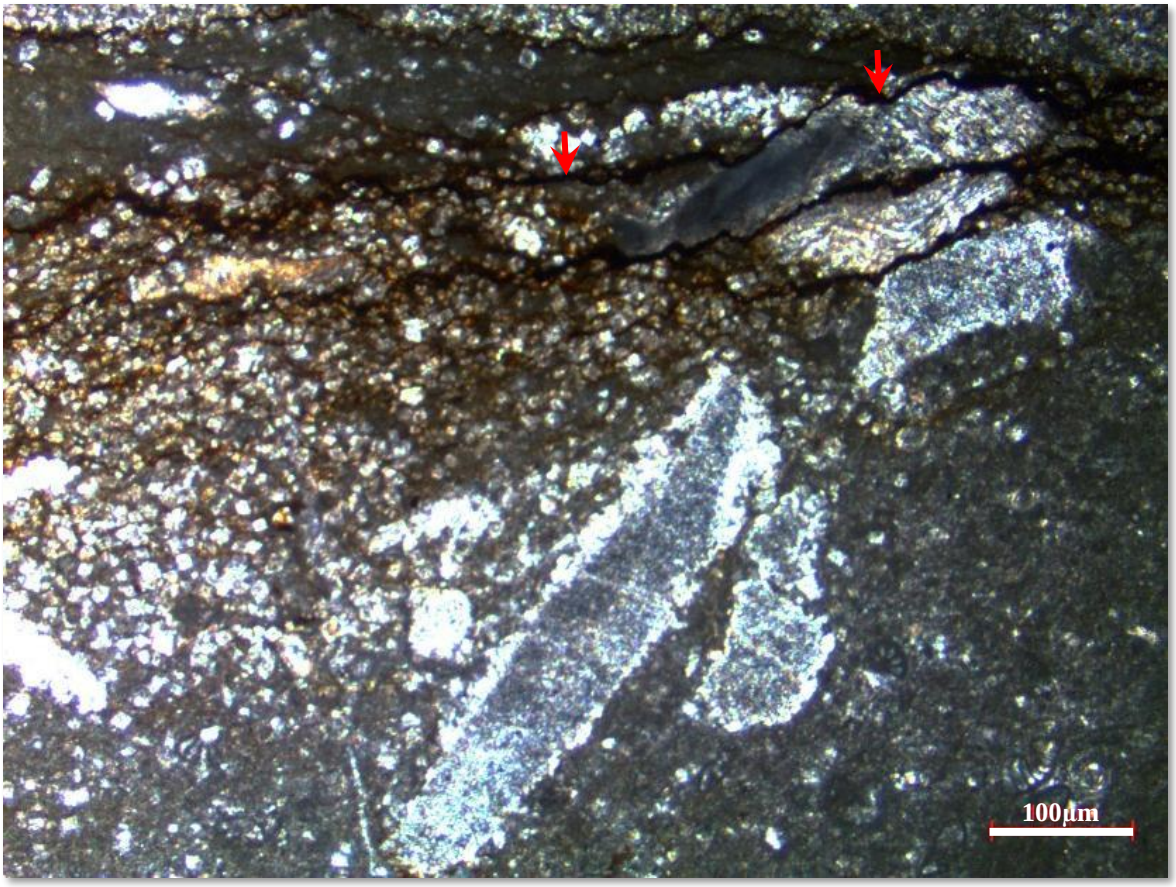


**Figure 140.** Stylolites associated with dolomitization and formed around the skeletal grains from the thin section at 1780.93 m of the K-11 well

Stylolitization is considered as common phenomenon observed in oil and carbonate reservoirs in the world (Paganoni et. al., 2016) including reservoir levels of southeastern Turkey which is the main concern of this study, the Derdere Formation. Authigenic mineral formations along stylolites and related fractures are generally associated with the fluid flow (Evans and Elmore, 2006; Baron and Parnell, 2007; Neilson and Oxtoby, 2008; Heap et al., 2014; Paganoni et. al., 2016).

Microstylolites are surface produced by tectonic or burial related pressure dissolution of soluble carbonate typically marked by the presence of clays, organic matter or other insoluble material. Stylolites generate secondary porosity zones. Generally dolomite formation postdates stylolite formation which is also observed in the Derdere Formation. At the time of burial diagenesis, euhedral dolomites can develop on early formed anhedral or subhedral dolomite crystals (Schoelle and Ulmer-Schoelle, 2003).

### 5.1.2 Diagenetic Environments

For hydrocarbon exploration in carbonate rocks, it is crucial to understand the products and mechanisms of carbonate diagenesis and diaganetic environments. Four major diaganetic environments which are vadose zone, meteoric phreatic zone, mixing zone and marine phreatic zone are described in the study of Longman (1980). These diagenetic environments can be divided into numerous zones regarding the rate of water movement and saturation of water with respect to calcium carbonate.

In the Derdere Formation, the main diaganetic mechanisms observed are dolomitization, dissolution of some skeletal fragments, formation of dissolution vugs, cementation including micritic and isopachous Mg calcite, abundant equant calcite cement, isopachous bladed calcite cement and syntaxial overgrowths on echinoderm fragments. The presence of abundant equant calcite cement, isopachous bladed calcite cement and syntaxial overgrowths and relatively low porosity observed in the Derdere Formation shows the freshwater phreatic active zone conditions in terms of diagenetic environments.

In the freshwater phreatic environment there are active saturated zone and stagnant saturated zone (Longman, 1980) (**Figure 141**). The characteristics of the active saturated zone are leaching in the zone of solution, neomorphism of grains and extensive intergranular calcite cementation and the characteristics of stagnant saturated zone are neomorphsim of grains without cementation (Longman, 1980). Syntaxial overgrowths on echinoderm fragments and equant calcite cementation that coarsen toward pore centers are other characteristics of active freshwater phreatic zone in the Derdere Formation (**Figure 141**).

In addition to these cement types, presence of isopachous and micritic Mg calcite is the indicator of marine phreatic active zone in the Derdere Formation. Marine phreatic environment is one of the most common diagenetic environments for carbonates and it is divided into a zone of relatively little water circulation and a zone of good water circulation. Fibrous aragonite and micritic Mg-calcite are common cement types of this diaganetic environment (Longman, 1980) (**Figure 141**).

It is interpreted that during the diagenesis of the Derdere Formation, both freshwater phreatic zone and marine phreatic zone conditions are prevailing. Hence diagenetic environment of the Derdere Formation can be concluded as mixed zone. Also, in this study extensive solution and formation of dissolution vugs as a result of subaerial exposure are another remarkable observation in the studied wells of the Derdere Formation which is observed in the vadose zone of solution type of diagenetic environment.

In the isotope studies, during subaerial exposure, due to entrance of freshwater to the system, it replaces sea water in the pores of shallow-water carbonates and mixing zone of fresh and marine water occurs. In the mixing zone, active water circulation causes dolomitization or cementation. In the long term mixing zones, dolomite formation is observed if the salinity of water is low whereas bladed-Mg calcite formation can occur if marine water is dominant (Longman, 1980). At the topmost part of the Derdere Formation, dolomitization is common where freshwater is dominant and below this level, cementation becomes more pervasive where marine water is prominent.

The freshwater vadose environment is where both air and meteoric water are found together in the pores and it is divided into zone of solution and zone of precipitation. Climate has crucial role on early diagenesis if there is subaerial exposure. In other words, in arid climates, cementation is not intensely observed which prevents cementation of primary pores while in humid climates, primary pores are more susceptible to cementation and secondary pores are more likely to be formed in pronounced amounts (Longman, 1980) (**Figure 141**). Since the primary pores of the Derdere Formation is highly cemented and some secondary pores are formed at the topmost part of the Derdere Formation, it is interpreted as the humid climatic conditions are prevailing during the deposition of the Derdere Formation.

When the microfacies deposited during highstand systems tract of the carbonate ramp model seaward progradation of the margin and thinning of topsets are observed and during this time interval, subaerial exposure of the microfacies are supposed to be observed (Emery and Myers, 1996) (**Figure 142**).

Light microscope based cathodoluminescence studies are conducted in the well samples of the Derdere Formation. The sample with the isopachous bladed calcite cement precipitated

inside the skeletal fragments are analyzed under the light microscope based cathodoluminescence light and non-luminescence to bright red rimmed luminescence of the carbonate cement is detected which is the indicator of the impact of meteoric water (**Figure 128**). In the study conducted for Upper Sarvak Formation which can be considered as equivalent of the Derdere Formation by Hajikazemi et. al. (2010) based on CL, meteoric water effect is also interpreted. The zonation of dark and bright colors observed in CL photomicrographs may be evaluated as associated with sea-level fluctuations and periodic change in the diagenetic environment of Upper Sarvak Formation as phreatic and vadose zones and available oxygen level. Non-luminescent to bright yellow rimmed luminescence cement is considered as originated from meteoric or shallow burial environement (Meyers 1974; Moldovany and Lohmann 1984; Carpenter and Lohmann 1989).

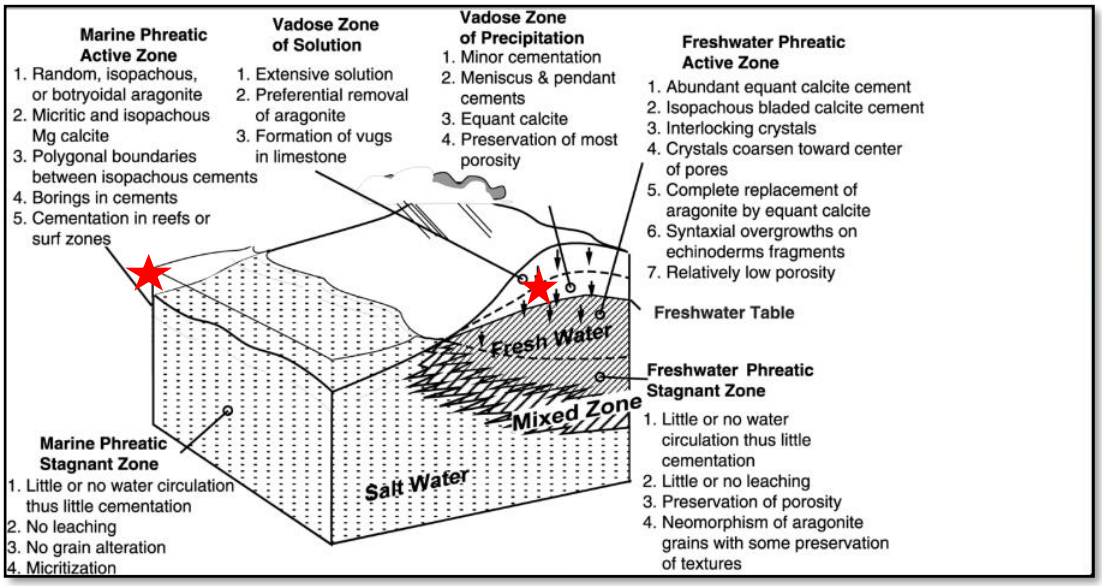


**Figure 141.** Common carbonate cements and diagenetic features formed in different diagenetic environments (Longman, 1980) (Red stars show the diagenetic environenments of the Derdere Formation)

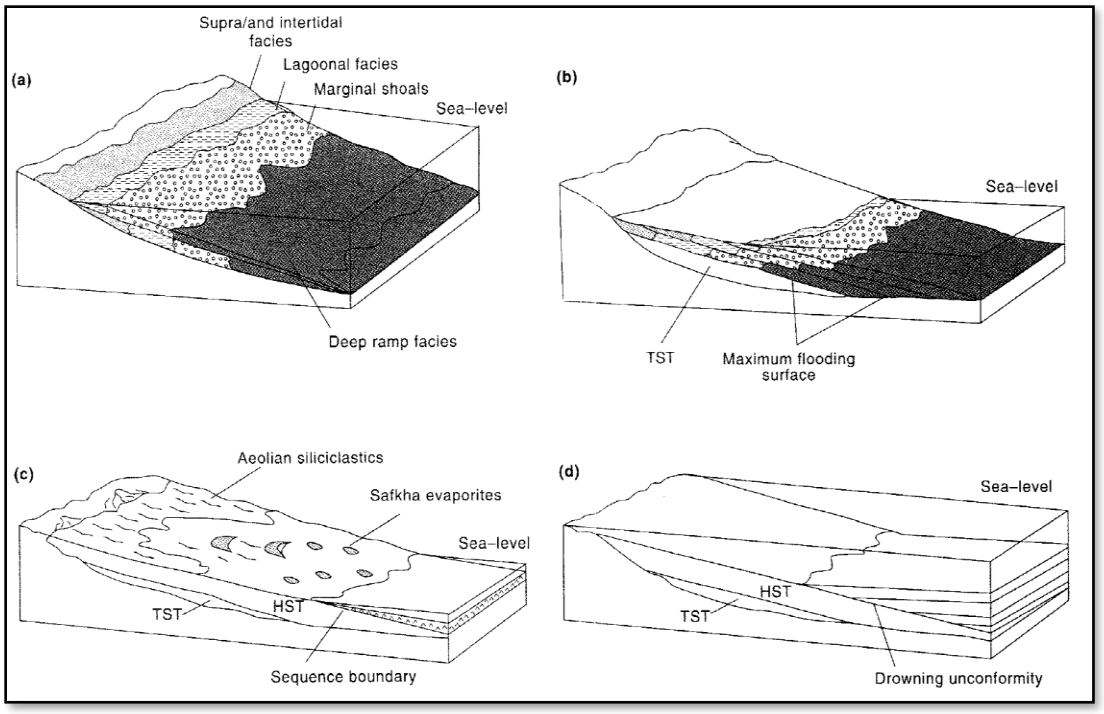


**Figure 142.** Sequence stratigraphic models for ramp (a) transgressive systems tract shows landward stepping of ramp facies (b) highstand systems tract shows seaward progradation of the margin (c) lowstand systems tract in arid, restricted basins (d) drowning of carbonate ramp systems (Emery and Myers, 1996)

### 5.1.3 Reservoir Quality of Derdere Formation

Reservoir quality is defined as the hydrocarbon storage capacity and reservoir quality evaluation depends mainly on the effective porosity and deliverability which is the function of the permeability of the formation. Generally, good reservoirs have higher porosity and permeability values. Porosity and permeability generation in carbonate rocks are related with both primary factors including depositional factors and secondary factors including diagenetic features. For instance, among diagenetic features cementation and compaction can be considered as most important factors to decrease porosity and permability of the rocks.

The Derdere Formation is one of the important oil and gas reservoir units in southeastern of Turkey. Although both depositional and diagenetic factors have a role on the reservoir quality of the formation, diagenesis is the major controlling factor impacting in a both positive and negative way.

Destructive role of diagenesis is to decrease permeability by cementation (destroys primary porosity and disconnects pore throats) and to decrease porosity by compaction (causes loss of water between the grains and closer intergrain contacts). Constructive role of diagenesis is the dolomitization and dissolution which enhances porosity and permeability. Dolomitization which is major diagenetic mechanism improves reservoir quality if it is associated with dissolution and meteoric diaganesis. Hence, diagenesis is under the control of sea-level which should be revealed with the sequence stratigraphic framework.

In the Derdere Formation, dissolution and dolomitization are associated with the time of falling of relative sea level and observed in the uppermost part of highstand systems tracts. Dolomitization can occur in both transgressive and highstand systems tracts; however it enhances reservoir quality of the formation in case it is associated with highstand systems tracts. Early cementation is also observed at the time of shoaling during falling of relative sea-level. Other diagenetic mechanisms including stylolitization and fracturing are not associated with relative sea-level; on the contrary they are formed as a result of compaction. Similarly in the Upper Sarvak Formation which is the time equivalent of the Derdere Formation, if dolomitization is related with the relative sea-level fall and exposure, it improves reservoir quality of the formation (Taghavi et. al., 2006) (**Figure 143**).

Petrographic and lithologic analysis showed that, microfacies defined in core#1 were deposited in the inner ramp/proximal middle ramp setting, microfacies defined in core#2 belongs to the distal middle ramp setting, microfacies of core#3 is characteristic to the outer ramp depositional setting, and microfacies of core#4 and core #5 represents the inner ramp/shoal type depositional environment. When porosity vs. permeability plots of all cores of K-11 well are considered, facies defined in core #1 can be considered as the best reservoir level among the facies defined in other cores of K-11 well. In addition to core#1, facies defined in core#4 and core#5 are other most promising reservoir levels (**Figure 144**).

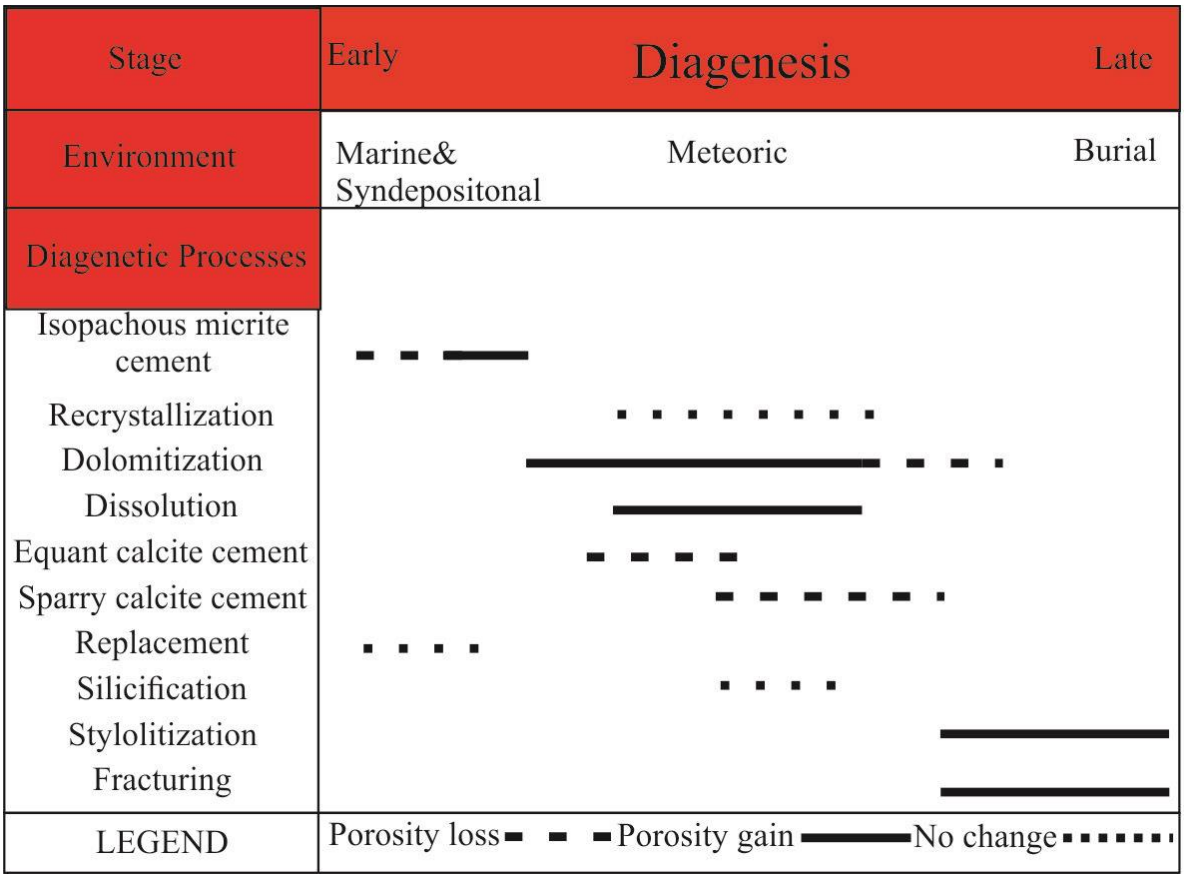


**Figure 143.** Type and timing of diagenetic processes of the Derdere Formation in Diyarbakır Region

Generally, facies defined in core #1, core#4 and core#5 are similar and they were laid down in an inner ramp type environment. Hence, facies of the inner ramp type environment in the Derdere Formation have good reservoir properties with the porosity values measured (**Table 9** and **Figure 144**). Facies defined in the other cores of K-11 well belong to distal middle ramp to outer ramp type depositional environments and their reservoir parameters are not as good as the samples of the inner ramp depositional setting. These samples are located in the low porosity and low permeability side of porosity and permability plots. The difference between the porosity values of the samples deposited in the inner ramp and distal middle ramp/outer ramp settings are also observed petrographically in thin sections. As mentioned above not only depositional features but also diagenetic features are vital for the reservoir quality assessment. From this point of view, in addition to facies, dolomitization is another aspect to predict reservoir quality (**Table 9** and **Figure 144**) which is also detected petrographically.

Core samples are more reliable for porosity and permeability calculations. Porosity vs. permeability plots is used to compare reservoir qualities (**Figure 144-146**). When porosity vs. permeability plot is taken into account, two samples of core#1 have better reservoir quality from the rest of the samples of core#1. These samples have the highest porosity and permeability values where grain densities are also highest among the samples of core#1 (**Table 9**). The reason of higher grain density is the dolomitization since dolomites have higher grain densities compared to limestones, calcareous dolomites or dolomitic limestones.

The porosity and permability values of the two cores obtained from K-8 well are plotted (**Figure 145**). First core is taken from distal middle ramp depositional environment and second core is taken from proximal middle ramp type depositional environment. Except for two samples, porosity and permeability values of the core samples are not that much high. The samples, which have highest porosity and permeability, have grain densities, which are similar to dolomite (2.87 g/cm$^3$) and different from the limestone (2.71 g/cm$^3$) (**Table 10**). This shows that reservoir quality of the Derdere Formation in the K-8 well is mainly affected by dolomitization similar to the plots of K-11 well (**Figure 145**). Similarly, porosity and permeability values of the core of the K-9 well are plotted and except for three values of the core#1 of K-9 well, porosity and permeability values are low which are considered to be deposited in distal to outer ramp depositional setting (**Table 11** and **Figure 146**). The reason of higher porosity values of three samples are similar to the scenario given for the samples of the K-11 and the K-8 wells which is the constructive affect of dolomitization to the reservoir quality.

There are some grain density values less than 2.71 g/cm$^3$, which is pure limestone. When the depths of these samples whose grain densities are at around 2.64 g/cm$^3$ are considered, they correspond to the samples deposited in the outer ramp and distal middle ramp depostional setting. They are observed with greater abundance of clay lithologically and at around the depths of these samples gamma ray values are high. One of the samples is the sample classified as radiolaria-bearing mudstone and it can be interpreted that the samples with lowest grain density among all the samples correspond to the OAE-2 zone.

To conclude although primary depositional microfacies play important role for the reservoir characterization, the most significant mechanism to develop good reservoir properties are diagenesis and especially dolomitization in the studied wells of the Derdere Formation in the Diyarbakır Region.

**Table 9.** Reservoir properties of the cores of K-11 well

| Well Name | Core Number | Box Number | Sample Number (m) | Pore Volume (cc) | Porosity (%) | Air Permeability (md) | Permeability (md) | Grain Density (g/cc) |
|---|---|---|---|---|---|---|---|---|
| K-11 | 1 | 1 | 1649,20 | 23,10 | 27,58 | 79,68 | 70,45 | 2,85 |
| K-11 | 1 | 1 | 1649,60 | 17,10 | 23,67 | 41,46 | 35,25 | 2,85 |
| K-11 | 1 | 2 | 1649,95 | 13,51 | 19,29 | 3,91 | 2,89 | 2,77 |
| K-11 | 1 | 2 | 1650,40 | 11,51 | 16,47 | 1,26 | 0,87 | 2,73 |
| K-11 | 1 | 3 | 1651,00 | 15,41 | 18,98 | 1,85 | 1,30 | 2,72 |
| K-11 | 1 | 3 | 1651,45 | 12,07 | 15,81 | 0,86 | 0,58 | 2,72 |
| K-11 | 1 | 4 | 1652,10 | 19,18 | 23,11 | 1,93 | 1,36 | 2,73 |
| K-11 | 1 | 5 | 1652,80 | 12,02 | 23,04 | 2,25 | 1,61 | 2,74 |
| K-11 | 1 | 5 | 1653,15 | 12,63 | 15,44 | 0,50 | 0,33 | 2,74 |
| K-11 | 1 | 5 | 1653,30 | 14,51 | 17,39 | 0,81 | 0,54 | 2,75 |
| K-11 | 1 | 6 | 1653,65 | 12,72 | 15,62 | 0,54 | 0,35 | 2,75 |
| K-11 | 1 | 6 | 1654,15 | 13,18 | 16,07 | 0,77 | 0,52 | 2,74 |
| K-11 | 1 | 7 | 1654,75 | 12,79 | 15,29 | 0,55 | 0,36 | 2,74 |
| K-11 | 1 | 8 | 1655,40 | 9,81 | 14,78 | 1,65 | 1,16 | 2,74 |
| K-11 | 1 | 8 | 1656,05 | 13,34 | 15,99 | 1,78 | 1,25 | 2,76 |
| K-11 | 1 | 9 | 1656,95 | 10,93 | 12,94 | 0,29 | 0,19 | 2,77 |
| K-11 | 1 | 10 | 1657,40 | 5,23 | 19,65 | 2,36 | 1,69 | 2,79 |
| K-11 | 1 | 10 | 1657,85 | 12,40 | 15,05 | 0,45 | 0,29 | 2,74 |
| K-11 | 1 | 11 | 1658,45 | 8,27 | 9,90 | 0,70 | 0,46 | 2,72 |
| K-11 | 2 | 1 | 1694,20 | 1,76 | 2,08 | 0,04 | 0,02 | 2,70 |
| K-11 | 2 | 1 | 1694,75 | 0,92 | 1,10 | 0,03 | 0,02 | 2,67 |
| K-11 | 2 | 4 | 1697,00 | 2,50 | 4,79 | 0,04 | 0,02 | 2,72 |
| K-11 | 2 | 5 | 1698,00 | 1,80 | 2,38 | 0,03 | 0,02 | 2,64 |
| K-11 | 2 | 8 | 1700,30 | 0,67 | 1,77 | 0,16 | 0,10 | 2,64 |
| K-11 | 3 | 2 | 1720,50 | 0,37 | 0,45 | 0,02 | 0,01 | 2,67 |
| K-11 | 3 | 4 | 1722,20 | 0,58 | 0,73 | 0,02 | 0,01 | 2,64 |
| K-11 | 3 | 7 | 1725,40 | 0,83 | 1,01 | 0,04 | 0,02 | 2,67 |
| K-11 | 4 | 1 | 1764,30 | 4,38 | 5,28 | 0,03 | 0,02 | 2,73 |
| K-11 | 4 | 1 | 1764,55 | 2,01 | 2,60 | 0,16 | 0,10 | 2,73 |

**Table 9** (continued). Reservoir properties of the cores of K-11 well

| Well Name | Core Number | Box Number | Sample Number (m) | Pore Volume (cc) | Porosity (%) | Air Permeability (md) | Permeability (md) | Grain Density (g/cc) |
|---|---|---|---|---|---|---|---|---|
| K-11 | 4 | 2 | 1764,85 | 5,53 | 6,66 | 0,13 | 0,08 | 2,72 |
| K-11 | 4 | 2 | 1765,30 | 7,03 | 8,47 | 0,11 | 0,06 | 2,71 |
| K-11 | 4 | 3 | 1765,95 | 10,91 | 12,81 | 0,57 | 0,38 | 2,71 |
| K-11 | 4 | 3 | 1766,50 | 9,67 | 11,72 | 0,25 | 0,16 | 2,72 |
| K-11 | 4 | 4 | 1767,30 | 8,02 | 9,89 | 0,11 | 0,07 | 2,71 |
| K-11 | 4 | 4 | 1767,80 | 7,95 | 9,64 | 0,13 | 0,08 | 2,71 |
| K-11 | 4 | 5 | 1768,40 | 8,78 | 10,78 | 0,18 | 0,11 | 2,71 |
| K-11 | 4 | 6 | 1769,00 | 9,66 | 11,97 | 0,18 | 0,11 | 2,72 |
| K-11 | 4 | 6 | 1769,50 | 11,54 | 13,77 | 0,32 | 0,20 | 2,72 |
| K-11 | 4 | 7 | 1770,00 | 11,78 | 14,54 | 0,39 | 0,25 | 2,72 |
| K-11 | 4 | 8 | 1770,75 | 12,83 | 15,73 | 0,61 | 0,40 | 2,72 |
| K-11 | 4 | 8 | 1771,40 | 13,61 | 16,47 | 0,80 | 0,54 | 2,72 |
| K-11 | 4 | 9 | 1771,90 | 13,06 | 16,23 | 0,89 | 0,60 | 2,72 |
| K-11 | 4 | 9 | 1772,30 | 9,88 | 17,27 | 1,11 | 0,76 | 2,72 |
| K-11 | 5 | 1 | 1773,25 | 13,87 | 16,97 | 0,99 | 0,67 | 2,72 |
| K-11 | 5 | 1 | 1773,70 | 14,07 | 17,14 | 1,14 | 0,78 | 2,72 |
| K-11 | 5 | 2 | 1774,30 | 14,73 | 18,01 | 1,41 | 0,98 | 2,71 |
| K-11 | 5 | 2 | 1774,90 | 13,68 | 16,95 | 0,97 | 0,66 | 2,72 |
| K-11 | 5 | 3 | 1775,40 | 13,02 | 15,83 | 0,79 | 0,53 | 2,72 |
| K-11 | 5 | 3 | 1775,90 | 12,26 | 15,05 | 0,63 | 0,41 | 2,73 |
| K-11 | 5 | 4 | 1776,40 | 12,04 | 14,68 | 0,60 | 0,39 | 2,73 |
| K-11 | 5 | 4 | 1776,80 | 9,36 | 11,40 | 0,30 | 0,19 | 2,72 |
| K-11 | 5 | 5 | 1776,95 | 10,43 | 15,81 | 0,78 | 0,52 | 2,74 |
| K-11 | 5 | 5 | 1777,35 | 12,77 | 15,45 | 0,46 | 0,30 | 2,76 |
| K-11 | 5 | 6 | 1777,80 | 8,01 | 9,96 | 0,14 | 0,09 | 2,73 |
| K-11 | 5 | 6 | 1778,10 | 10,55 | 12,76 | 0,26 | 0,16 | 2,73 |
| K-11 | 5 | 7 | 1778,50 | 4,83 | 6,43 | 0,21 | 0,13 | 2,72 |
| K-11 | 5 | 8 | 1779,20 | 6,97 | 8,60 | 0,42 | 0,27 | 2,75 |
| K-11 | 5 | 9 | 1779,80 | 3,90 | 4,77 | 0,05 | 0,03 | 2,73 |
| K-11 | 5 | 9 | 1780,35 | 6,65 | 8,24 | 0,07 | 0,04 | 2,72 |
| K-11 | 5 | 10 | 1780,80 | 12,82 | 15,82 | 0,60 | 0,39 | 2,74 |
| K-11 | 5 | 10 | 1781,20 | 7,87 | 9,51 | 0,17 | 0,10 | 2,76 |
| K-11 | 5 | 11 | 1781,65 | 4,10 | 5,12 | 0,09 | 0,05 | 2,72 |
| K-11 | 5 | 11 | 1781,95 | 7,20 | 12,54 | 0,41 | 0,27 | 2,76 |

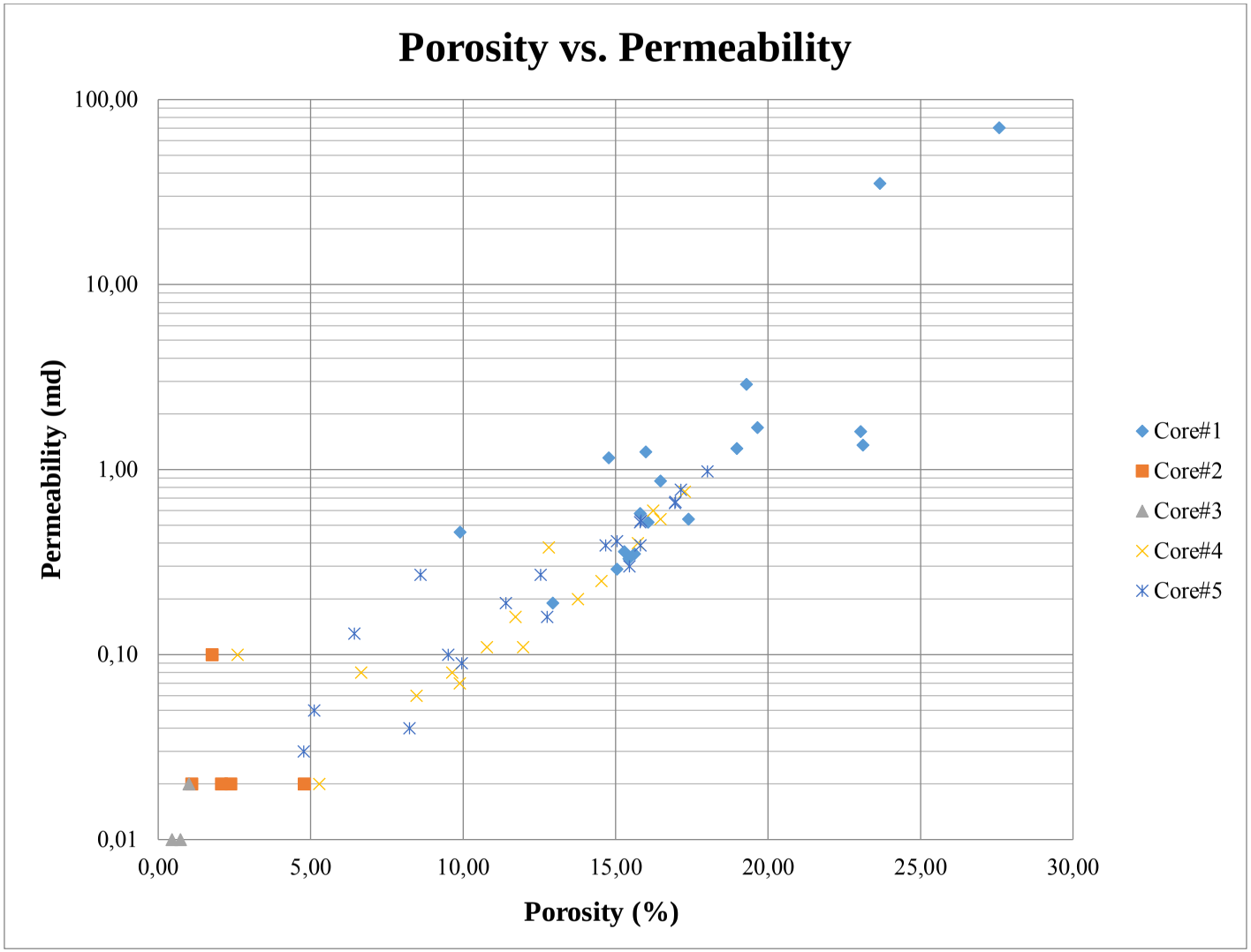


**Figure 144.** Porosity vs. Permeability Graph of the cores of K-11 well

**Table 10.** Reservoir Properties of the cores of K-8 well

| Well Name | Core Number | Box Number | Sample Depth (m) | Pore Volume (cc) | Porosity (%) | Air Permeability (md) | Permeability (md) | Grain Density (g/cc) | Pmean (absatm) |
|---|---|---|---|---|---|---|---|---|---|
| K-8 | 1 | 1 | 1712,15 | 9,36 | 11,58 | 0,41 | 0,27 | 2,74 | 2,52 |
| K-8 | 1 | 2 | 1713,15 | 7,76 | 9,72 | 0,14 | 0,08 | 2,75 | 2,52 |
| K-8 | 1 | 2 | 1713,60 | 6,62 | 10,50 | 0,11 | 0,06 | 2,74 | 3,81 |
| K-8 | 1 | 3 | 1714,75 | 19,04 | 30,00 | 56,85 | 49,26 | 2,83 | 1,65 |
| K-8 | 1 | 4 | 1715,20 | 18,44 | 29,69 | 32,30 | 27,05 | 2,83 | 2,50 |
| K-8 | 1 | 4 | 1715,80 | 4,82 | 8,00 | 0,19 | 0,12 | 2,71 | 3,80 |
| K-8 | 1 | 4 | 1715,85 | 7,32 | 9,25 | 0,44 | 0,29 | 2,71 | 2,52 |
| K-8 | 2 | 1 | 1822,00 | 5,35 | 6,57 | 2,51 | 1,81 | 2,72 | 2,52 |
| K-8 | 2 | 1 | 1822,30 | 4,09 | 6,06 | 0,06 | 0,03 | 2,72 | 2,53 |

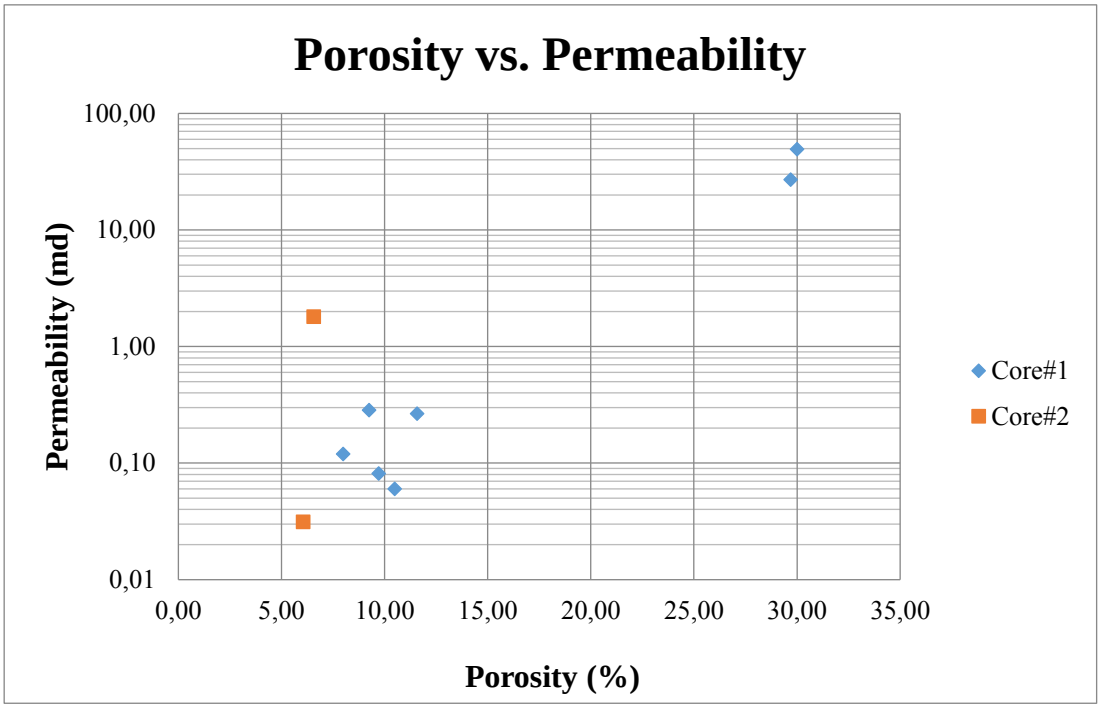


**Figure 145.** Porosity vs. Permeability Graph of the cores of K-8 well

**Table 11.** Reservoir Properties of Cores of K-9 Well

| Well Name | Core Number | Box Number | Sample Depth (m) | Pore Volume (cc) | Porosity (%) | Air Permeability (md) | Permeability (md) | Grain Density (g/cc) | Pmean (absatm) |
|---|---|---|---|---|---|---|---|---|---|
| K-9 | 1 | 5 | 2433,70 | 0,11 | 0,17 | 0,04 | 0,02 | 2,70 | 2,34 |
| K-9 | 1 | 4 | 2432,90 | 0,39 | 0,61 | 0,02 | 0,01 | 2,69 | 2,34 |
| K-9 | 1 | 4 | 2432,60 | 0,29 | 0,45 | 0,05 | 0,03 | 2,69 | 2,34 |
| K-9 | 1 | 3 | 2432,25 | 0,43 | 0,67 | 0,01 | 0,01 | 2,69 | 2,34 |
| K-9 | 1 | 3 | 2431,70 | 0,21 | 0,33 | 0,02 | 0,01 | 2,71 | 2,18 |
| K-9 | 1 | 3 | 2431,35 | 10,88 | 17,07 | 0,23 | 0,14 | 2,79 | 1,96 |
| K-9 | 1 | 2 | 2431,10 | 11,13 | 18,04 | 1,17 | 0,80 | 2,81 | 1,95 |
| K-9 | 1 | 2 | 2430,90 | 5,45 | 16,53 | 0,52 | 0,34 | 2,81 | 1,95 |

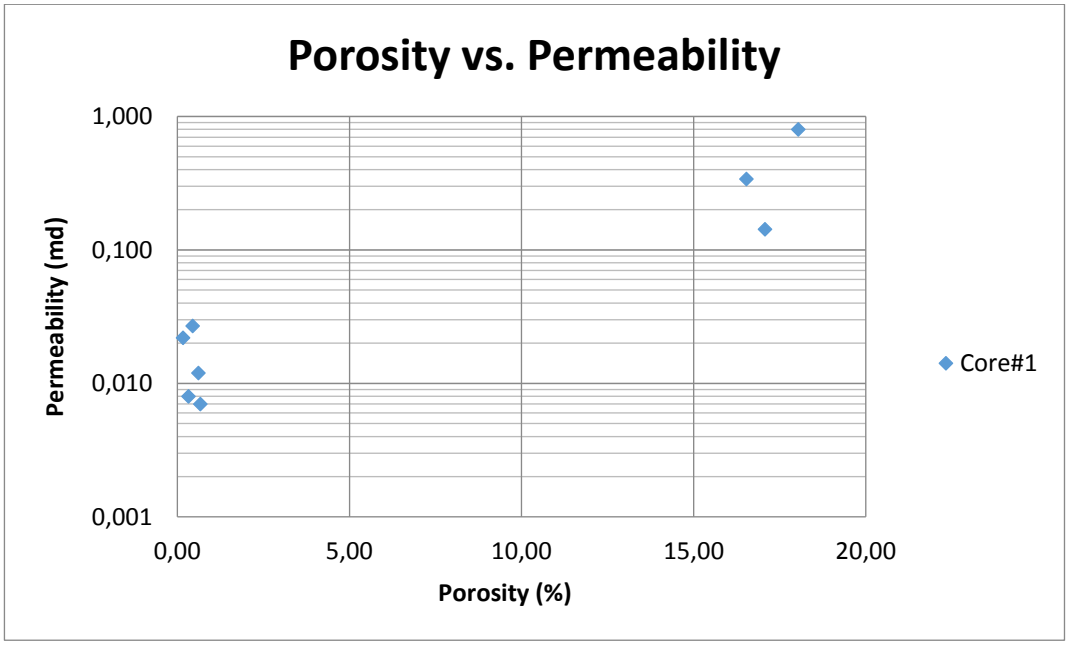


**Figure 146.** Porosity vs. Permeability Graph of Cores of the K-9 well

# CHAPTER 6

# DISCUSSION AND CONCLUSION

## 6.1 DISCUSSION

### 6.1.1 Depositional Model

In order to organize stratigraphical and sequential framework of the Derdere Formation with the detailed microfacies analysis, the K-11 well was selected to start with due to the presence of numerous complete cores. Petrographic analysis and description of the microfacies are completed for the Derdere Formation including five cores and cuttings. In addition to the K-11 well, K-8, K-3, K-2, K-4, K-9 and the K-7 wells are studied petrographically to reveal the variety of microfacies in the Derdere Formation and the depositional model.

Depositional environments of each microfacies are defined and it is revealed that the different types of microfacies were under the control of sea level fluctuations in all seven wells. From this point of view, the depositional model depends on the type and relative abundances of constituents and the change in microfacies defined in the succession. In the carbonate ramp type depositional model of the Derdere Formation (modified from Wilson model (1975)) mainly three types of depositional environment were recognized including the inner ramp (tidal flat, lagoon and shoal), the middle ramp (proximal middle and distal middle ramp), and the outer ramp. The carbonate model of the Derdere Formation differs from Wilson carbonate model (1975) by the barrier frame and reef bodies with boundstone type microfacies defined in the Wilson model and reef-building organisms (except for some broken rudists and algae fragments) in this study area.

By seperating the Derdere Formation lithologically and biostratigraphically from the Sabunsuyu Formation, the deposition of the Derdere Formation is considered in the interval of Cenomanian to Turonian in this study. Therefore, the depositional model of

the Derdere Formation is compared with the other models of the Cenomanian-Turonian succesions from different parts of the world including the Campos Basin in Brazil, northern Germany, the Sarvak Formation in Bi Hakimeh oil field, and the Guerrero–Morelos Basin, Southern Mexico. Common depositional features and constituents are recognized with some minor differences.

The depositional model developed for the Derdere Formation has numerous common features with the model of Macae Formation in Campos Basin, Brazil defined in the study of Spadini et. al. (1988). These similarities (1) grainstone microfacies rich in peloids characteristic for a shoal environment, (2) wackestone microfacies identified in fine-grained limestones with few and low diversity benthic foraminifera, planktonic foraminifera, skeletal fragments and rare calcisphaerulids in the middle ramp setting, and (3) packstone microfacies described in fine-grained limestones with greater amount of calcisphaerulids as a bloom in the outer ramp. Fenestral fabric type is observed in the thin section of lime mudstone with some benthic foraminifers is interpreted as peritidal environment of the inner ramp setting.

One of the important bases of the depositional model of the Derdere Formation is that the abundance of calcisphaerulids is under the control of the fluctuations in the relative sea level. This is supported by the study of Wilmsen (2003). It is stated that calcisphaerulid blooms are controlled by the fairweather wavebase and the storm wavebases in the Cenomanian stage of the northern Germany.

In the model developed for the Sarvak Formation, the depositional model is divided as inner shelf, middle shelf and outer shelf with the similar constituents of the model of the Derdere Formation. Although there are numerous common features with our depositional model, the scarcity of benthic foraminifera in our model is different from Sarvak Formation. This difference can be related to the more restricted depositional area of the Derdere Formation, when compared to the Sarvak Formation. Also studies conducted for Sarvak Formation show that not only depositional features but also diagenetic mechanisms and their timing are similar to the Derdere Formation (Taghavi et. al., 2006).

### 6.1.2 INPEFA Logs and Sequence Stratigraphy

Sedimentological logs, which are another aspect of the study, are considered with the depositional environments described in the model and microfacies. Total gamma ray and uranium gamma ray log responses are interpreted together where they are available in order to see the influence of lithology rather than the organic matter. INPEFA log, which shows general trends with turning points recording significant events depend on lithology change, is created using both total gamma ray and uranium free gamma ray for seven wells. By correlating INPEFA logs and lithofacies, 3rd order sequences are defined. In total, nine 3rd order sequences are described in the wells which have penetrated entirely to the Derdere Formation. These sequences defined in the K-11 well were correlated with the sequences of other wells using INPEFA logs. These 3rd order sequences identified in the other wells were also tested on whether they are associated with the change in microfacies with shoaling and deepening upward trends. It is concluded that microfacies change is controlled by eustasy and microfacies are the same with some minor differences in terms of the primary constituents in the studied wells. From this aspect, wells of the Diyarbakır Region are able to be correlated from west to east.

### 6.1.3 Microfacies and Sequence Stratigraphy

Due to the dominance of the outer ramp facies during the Albian time in the Mardin area, it is interpreted as being deeper compared to Albian time in the Diyarbakır Region. The deposition of the Derdere Formation is considered as in the time interval of Cenomanian to Turonian and it is different from the Mardin, Derik section where the deposition of the Derdere Formation started in mid-Albian. Hence, the Derdere deposition should be considered as time-transgressive and the time interval of the deposition differs from Mardin at the south to the Diyarbakır Region at the north.

When the deposition of the Derdere Formation during the Turonian time is compared in the wells and in the field, it was observed that planktonic foraminiferal assemblage dominated the fauna. Nonetheless, *Marginotruncana* type planktonic foraminifera are

mostly found in the upper parts of the Derdere Formation drilled in the wells of the Diyarbakır Region and in the Karababa Formation of the Derik field section, which is the upper contact of the Derdere Formation. On the other hand, in the well section of K-11 pilot well, *Marginotruncana* are mostly detected in the lower levels of the Turonian in the Derdere Formation. In the well sections of Diyarbakır, Derdere and Sayındere formations are in contact and Karababa Formation is missing.

In the Turonian time, three sequence boundaries and three and a half sequences are described. Whereas there are five sequence boundaries defined in the study of Haq (2014). Although the number of the sequences are the same both in the field section of the Derik and in the studied wells, one sequence is absent at the uppermost part of the Derdere Formation in the studied wells. In the field section, the Derdere and Karababa Formations are in contact and the deposition of Karababa Formation continues during the Turonian time; however, in the studied wells, the Derdere Formation is overlain by the Sayındere Formation deposited during Campanian. In other words, the number of the sequences defined in the Turonian time of the Derik section is the same with the number of sequences described in the study of Haq (2014), however the last sequence of the Turonian is eroded or not deposited in the studied wells of the Diyarbakır Region.

The sequences defined in the wells are correlated with the other carbonate platforms of the Cenomanian-Turonian. The number and the thickness of the sequences defined in the present study are similar to the sequences defined in the succession of Jordan (Schulze et. al., 2003). There are four sequence boundaries identified in the Cenomanian time and three sequence boundaries in the Turonian time in Jordan according to Schulze et. al. (2003).

### 6.1.4 Isotope Studies

An isotope study is carried out in order to define some important events in the deposition of the Derdere Formation including the C-T boundary event and the related Oceanic Anoxic Event 2. Carbon isotopes are used to detect C-T boundary and OAE-2 together with biostratigraphy, microfacies and INPEFA logs. On the isotope curves the

positive carbon isotope excursion followed by negative shift and it is related with greater burial rates of $^{12}C$ enriched organic carbon in organic rich shales. Globally defined ocean anoxia is developed by the increase in the burial rates and biological productivity. This negative shift observed on the carbon isotope curves is more obviously observed in the samples of K-2 well compared to K-11 well. It is explained by the greater anoxia in K-2 well due to deeper basin conditions where K-2 well is drilled. Since basin is getting deeper through K-2 well, basin is supposed to be more anoxic with the increasing rates of relative sea level, which is resulted in the greater negative shift on carbon isotope curve.

Shifts on the carbon isotope curves of K-2 and K-11 wells are similar in terms of lower $\delta^{13}C$ values during Cenomanian time and higher $\delta^{13}C$ values during Turonian time interval.

Negative and positive excursions observed on the oxygen isotope curves are used to make correlation with relative sea level changes, sequence boundaries and maximum flooding surfaces, although oxygen isotope values are intensively affected by diagenesis. Hence, oxygen isotope studies are considered as a secondary tool to define sequences and major stratigraphic surfaces and should be used together with other primary tools including microfacies change, INPEFA logs and biostratigraphy.

General trends observed on the oxygen isotope curves are similar in the two wells. At the bottom of the succession, lowest $\delta^{18}O$ values are recorded and $\delta^{18}O$ values increase through the upper part of the succession. During the early Cenomanian time interval, carbonate content increases with the decreasing rate of relative sea level. Carbon and oxygen isotope ratios become more negative with the increasing carbonate content which can be the explanation to the negative isotope ratios at the bottom of the succession. More negative oxygen isotope values are the indicator of the meteoric diagenesis. There are some negative shifts on the oxygen isotope curves in Turonian time interval, which is explained by the meteoric diagenesis.

### 6.1.5 Diagenesis

In addition to depositional descriptions, dolomitization, dissolution, cementation, replacement and chemical compaction type diagenetic features are identified. Micritic isopachous Mg calcite cement, sparry calcite cement as neomorphism of skeletal fragments and interparticle pore filling and syntaxial overgrowths are the main cement types identified in the samples. The diagenetic environment is interpreted as marine phreatic zone to freshwater phreatic zone according to these cement types. Calcite replacement of originally siliceous radiolaria is the other diagenetic mechanism observed in thin sections which is also supported with the existence of authigenic silica observed in X-ray mapping technique.

Another aspect of this reserach is to study reservoir properties of the Derdere Formation which depend on the measurements of the core samples. Cores of K-11, K-8 and K-9 wells are evaluated with this point of view and it is concluded that depositional and diagenetic features both affect the reservoir quality of the formation. Microfacies deposited in inner ramp/shoal type depositional environment have higher primary porosity compared to the microfacies deposited in distal middle ramp to outer ramp in the K-11 well.

In general, compaction and cementation are two major pore reducing diagenetic mechanisms. Cementation during the early diagenesis causes low intergranular porosity and destroys pore connections; therefore the effect of cementation on the porosity loss is more than the effect of compaction in the Derdere Formation. Due to the early cementation, physical compaction does not have a significant impact on the reservoir quality reduction.

The main mechanism responsible for the formation of secondary porosity and having influence on the reservoir quality is dolomitization process. Reservoir quality of the samples whose grain densities are close to dolomites are better than other samples of calcareous dolomites, dolomitic limestones or limestones in the K-11, K-8 and K-9 wells. From top to bottom decreasing intensity of dolomitization from dolomite to calcareous dolomite and dolomitic limestones make us think that the dolomitization is associated with the fall in relative sea levels at the top highstand systems tracts.

Another indication of this dolomitization is the presence of vuggy pores formed by non-selective dissolution as an indicator of meteoric water and subaerial exposure.

Dolomitization enhancing reservoir quality of the formation occurs at the top of highstand systems tract during subaerial exposure (**Figure 147**). Cloudy core-clear rimmed dolomites are observed in shoal depositional environment and from the aspect of being associated with highstand systems tracts and meteoric diagenesis, they enhance reservoir quality of the formation. On the other hand, dolomitization observed in the transgressive systems tract does not have any constructive effect on the reservoir quality.

Chemical compaction (stylolitization) is a common phenomenon and is associated with dolomites. Dolomite formation both predates and postdates the stylolite generation. Dolomites are formed not only during the meteoric diagenesis and before the burial compaction but also after the formation of stylolites during burial compaction. Stylolite related dolomitization also causes the increase in the crystal size of dolomites along stylolites.

### 6.1.6 Sequence Stratigraphic Model and Diagenesis

Various petrographic studies and isotope studies provide data to show the relationship between dolomitization and sequence stratigraphy. Petrographic studies (including light microscope, light microscope based cathodoluminescence studies, and isotope studies) show that there is mixing with meteoric water. Additionally, studies of Özkan and Altiner (2019) in the field revealed the subaerial exposure surfaces in the Derdere Formation which is interpreted as mixing with meteoric water.

A model for highstand deposition on the Derdere ramp platform and diaganetic mechanisms generated during sea level fluctuations is proposed in this study. The model shows the highstand deposition on the last 3$^{rd}$ order sequence of the Derdere Formation. During highstand systems tract and relative fall of sea-level, the outer ramp, the distal middle ramp and the proximal middle ramp facies are supposed to be shifted toward the basin (progradation of the middle and the outer ramp facies), and thickness

of the strata toward the maximum flooding surface decreases (**Figure 147**). In this study parasequences could not be defined due to the restrictions of the sample resolution. In the model proposed for highstand deposition of the Derdere Formation, stratal geometries are drawn by considering sea-level fluctuations during the progradational deposition of the parasequences and parasequence sets in 3$^{rd}$ order sequences (**Figure 147**).

Micritization and isopachous Mg calcite cement formation are characteristics for marine diagenesis and it is observed as micritic envelopes around the bioclasts in the Derdere Formation (**Figure 147**). It is an early diagenetic process and it has both destructive and constructive effects on the reservoir quality in terms of decreasing permeability by filling pore throats and reducing porosity loss due to compaction, respectively in the Derdere Formation. During the meteoric water infiltration, in the meteoric vadose zone there are solution and precipitation zones and in the precipitation zone, equant calcite cement is observed in minor amount. In the meteoric phreatic zone equant calcite cement becomes abundant and calcite crystals are getting coarser towards the center of pores in the Derdere Formation (**Figure 147**). Also, recrystallization of bioclasts and matrix of the sediments are considered as the product of meteoric diagenesis below the sequence boundary in the inner ramp deposits of the Derdere Formation.

At the time of the deposition of highstand systems tract, facies deposited on the inner ramp depositional setting were subaerially exposed and experienced meteoric water infiltration process; therefore dissolution and dolomitization type diagenetic mechanisms are observed. Mixing marine-fresh water zone was shifted toward the basinward, and mixing zone dolomites experienced dissolution process. Dissolution took place at the time of dolomitization due to the solubility of the remnants of the calcite minerals and vuggy pores were formed between the dolomite crystals (**Figure 147**). Below the dolomicrosparites with vugs at the topmost part of the formation, partially dolomitized facies are observed at the lower parts of the highstand systems tract of the last sequence and more stable low Mg calcite peloids and other stable constituents are preserved (**Figure 147**).

# HIGHSTAND DEPOSITION ON THE DERDERE RAMP PLATFORM

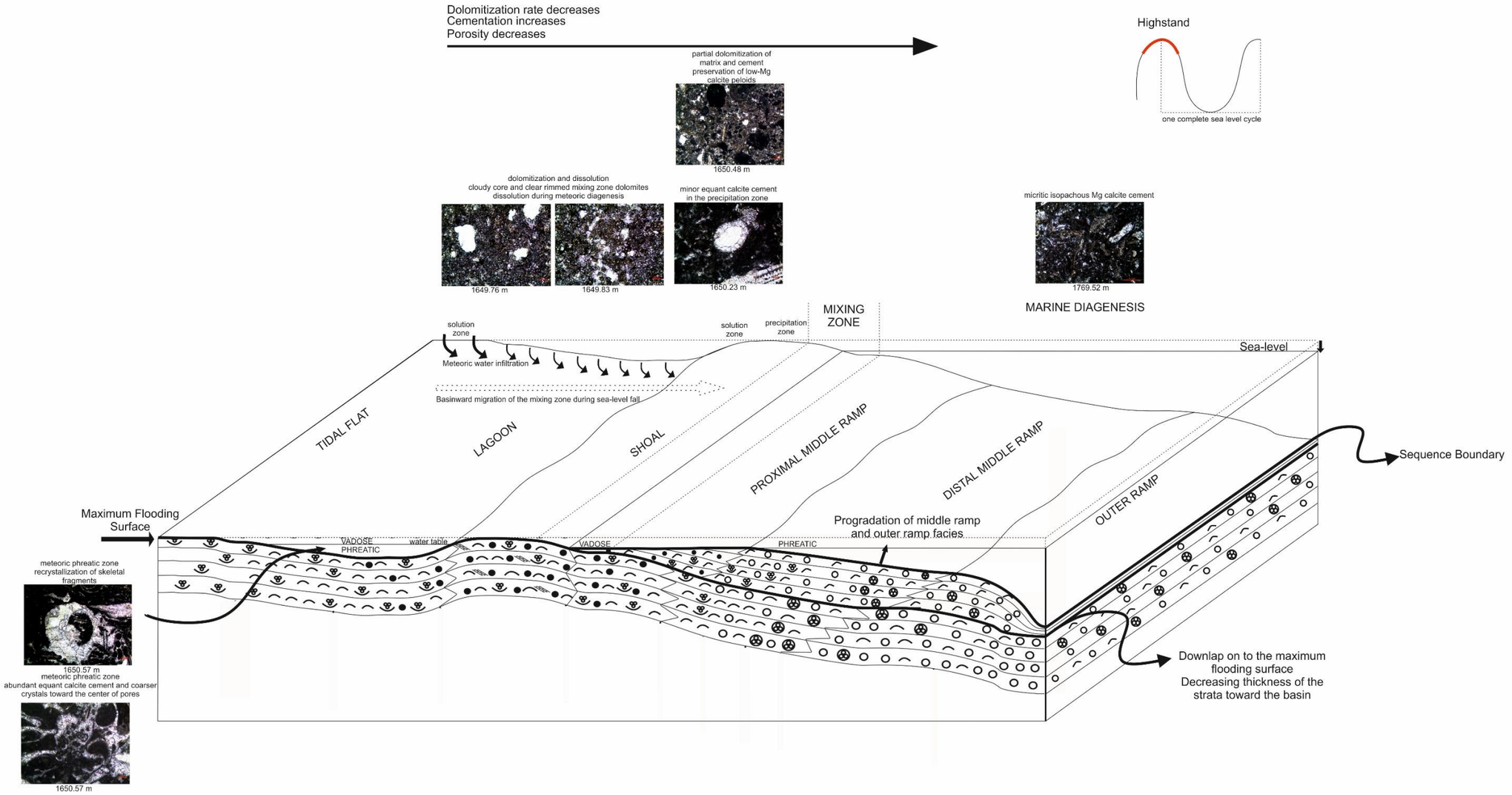


**Figure 147**. Depositional environments and diagenetic environments on the ramp model of the Derdere Formation during highstand systems tract and relative sea-level fall

## 6.2 CONCLUSION

Detailed microfacies analysis show that deposition is under the control of sea level fluctuations in the studied wells of Diyarbakır Region and carbonate ramp type depositional model of the Derdere Formation (modified from Wilson carbonate model (1975)) depends on the variations in microfacies is proposed in this study.

The deposition of the Derdere Formation is defined as in the time interval of Cenomanian-Turonian by drawing upper and lower contacts of the Derdere Formation in the study area. When it is compared with Derik, Mardin fieldsection, it is concluded that Derdere deposition is time-transgressive and it started later in the studied wells of Diyarbakır at the north than in the fieldsection at the south.

The depositional model of the Derdere Formation is compared with the other carbonate models deposited in the time interval of Cenomanian-Turonian worldwide and it is concluded that both depositional and diagenetic features defined in the Derdere Formation are quite similar to the other Cenomanian-Turonian successions.

3$^{rd}$ order sequences are defined by using INPEFA logs, microfacies change and biostratigraphy. In total, nine 3$^{rd}$ order sequences are described in the wells and it differs from twelve 3$^{rd}$ order sequences of the Derik, Mardin fieldsection due to the absence of three 3$^{rd}$ order sequences of the wells defined in the Albian time.

When the upper contact of the Derdere Formation is considered, the number of the sequences of the Turonian time defined in the study of Haq (2014) is different from the number of the sequences of the Turonian described in the wells of Diyarbakır. To conclude, the last 3$^{rd}$ order sequence of the Derdere Formation defined in the wells is eroded or not deposited. From the aspect of eustasy controlled microfacies, sequences defined in the wells of the Diyarbakır Region are able to be correlated from west to east. Also, the 3$^{rd}$ order sequences defined in the wells are compared with the other sequence stratigraphic studies conducted on Cenomanian-Turonian carbonate platforms worldwide. The number and the thickness of the sequences defined in the present study are quite similar to the sequences defined in the succession of Jordan.

Negative excursions on the carbon isotope studies conducted to detect C-T boundary and OAE-2 are more clearly observed in the K-2 well, where anoxia is interpreted as greater due to the depth of the basin where K-2 well is drilled. Lower $\delta^{13}C$ values during Cenomanian time and higher $\delta^{13}C$ values during Turonian time interval are quite similar in two isotopically studied wells.

Lowest $\delta^{18}O$ values are recorded at the bottom of the Derdere Formation and $\delta^{18}O$ values increase through the upper parts of the succession. During the early Cenomanian time interval, carbonate content increases with the decreasing rate of relative sea level and oxygen isotope ratios become more negative with the increasing carbonate content. Negative excursions are detected on the oxygen isotope curves in Turonian time interval at the top of the Derdere Formation, which is considered as the indicator of meteoric diagenesis.

Not only diagenetic mechanisms but also depositional features have a pronounced effect on the reservoir quality of the formation. Microfacies of the inner ramp/shoal type depositional environment have higher primary porosity than the microfacies of the distal middle ramp to outer ramp depositional setting. On the other hand, the main mechanism behind the formation of secondary porosity and having constructive effect on the reservoir quality is the dolomitization.

The diagenetic environment is interpreted as marine phreatic zone to freshwater phreatic zone according to the cement types observed. Calcite replacement of originally siliceous radiolaria is the other significant conclusion of this study. Among the major diagenetic mechanisms reducing porosity, the effect of cementation overweighs the effect of compaction in the Derdere Formation due to the early cementation.

The relationship between the dolomitization and the sequence boundaries capping the facies deposited in inner ramp settings is another important conclusion of this study. Decreasing intensity of dolomitization from top to bottom of the packages and the presence of vuggy pores are the indicator of being associated with the meteoric diagenesis and subaerial exposure during the fall in relative sea levels at the top of highstand systems tracts. Cloudy core-clear rimmed dolomites formed during meteoric diagenesis enhance reservoir quality of the formation whereas dolomitization of the

deposits of transgressive systems tract does not have any constructive effect on the reservoir quality.

A model for highstand deposition on the Derdere ramp platform and diaganetic mechanisms generated during sea level fluctuations is the most important conclusion of this study. Progradation of middle ramp and outer ramp facies was observed while facies deposited on the inner ramp depositional setting were subaerially exposed and experienced meteoric water infiltration during the relative sea level fall at the highstand systems tract. Hence, mixing marine-fresh water zone was shifted toward the basinward, and mixing zone dolomites experienced dissolution process.

## REFERENCES


-Abreu, V. (Ed.). (2010). *Sequence Stratigraphy of Siliciclastic Systems: The ExxonMobil Methodology; Atlas of Exercises* (Vol. 9). SEPM Soc for Sed Geology.

-Adams, J. E., & Rhodes, M. L. (1960). Dolomitization by seepage refluxion. *AAPG Bulletin*, *44*(12), 1912-1920.

-Aguilera-Franco, N. & Romano, U. H. (2004). Cenomanian–Turonian facies succession in the Guerrero–Morelos Basin, Southern Mexico. *Sedimentary Geology*, 170(3-4), 135-162.

-Aksu, R. (1980). Hakkari-Çukurca, Harbol, Derik-Bedinan, Hazro bölgelerinin jeolojisi: TPAO Arama Grubu, Rapor no. 1460. 1460, 58 s.

-Al-aasm, I. S. & Veizer, J. (1986). Diagenetic stabilization of aragonite and low-Mg calcite, II. Stable isotopes in rudists. *Journal of Sedimentary Petrology*, 56, 763–770.

-Ala, M. A. & Moss, B. J. (1979). Comparative petroleum geology of southeast Turkey and northeast Syria. *Journal of Petroleum Geology*, 1(4), 3-27.

-Allan, J. R. & Matthews, R. K. (1982). Isotope signatures associated with early meteoric diagenesis. *Sedimentology*, 29(6), 797-817.

-Altiner, D. (1989). An example for the tectonic evolution of the Arabian Platform margin (SE Anatolia) during Mesozoic and some criticisms of the previously suggested models. In *Tectonic Evolution of the Tethyan Region* (pp. 117-129). Springer, Dordrecht.

-Amthor, J. E. & Friedman, G. M. (1991). Dolomite-rock textures and secondary porosity development in Ellenburger Group carbonates (Lower Ordovician), west Texas and southeastern New Mexico. *Sedimentology*, 38, 343-362.

-Araç, M. & Yılmaz, E. (1991). XI ve XII. Bölge güneyindeki kuyularda kesilen Cudi ve Mardin Gruplarının sedimantolojisi ile fasiyes, diyajenez ve rezervuar özellikleri: TPAO Araştırma Merkezi, Rapor no. 1715, 154 s.

-Arthur, M. A., Dean, W. E., & Pratt, L. M. (1988). Geochemical and climatic effects of increased marine organic carbon burial at the Cenomanian/Turonian boundary. *Nature*, *335*(6192), 714-717.

-Arthur, M. A. & Sageman B. B. (2005). Sea level control on source rock development: Perspectives from the Holocene Black Sea, the mid-Cretaceous Western Interior Basin of North America, and the Late Devonian Appalachian Basin, in *The Deposition of Organic Carbon-Rich Sediments: Models, Mechanisms and Consequences*, edited by N. B. Harris, pp. 35 – 59, SEPM Soc. for Sed. Geology.

-Aydemir, A. (2011). Comparison of Mississippian Barnett Shale, Northern-Central Texas, USA and Silurian Dadas Formation in Southeast Turkey. *Journal of Petroleum Science and Engineering*, *80*(1), 81-93.

-Badiozamani, K. (1973). The dorag dolomitization model, application to the middle Ordovician of Wisconsin. *Journal of Sedimentary Research*, 43(4), 965-984.

-Baron, M., & Parnell, J. (2007). Relationships between stylolites and cementation in sandstone reservoirs: Examples from the North Sea, UK and East Greenland. *Sedimentary Geology*, 194(1-2), 17-35.

-Beil, S., Kuhnt, W., Holbourn, A. E., Aquit, M., Flögel, S., Chellai, E. H., & Jabour, H. (2018). New insights into Cenomanian paleoceanography and climate evolution from the Tarfaya Basin, southern Morocco. *Cretaceous Research*, *84*, 451-473.

-Bosence, D. (2002). Carbonate Reservoirs Porosity Evolution and Diagenesis in a Sequence Stratigraphic Framework-Developments in Sedimentology, Vol. 55; Clyde H. Moore; Elsevier, Amsterdam, *Marine and Petroleum Geology*, *10*(19), 1295-1296.

-Bragina, L., & Bragin, N. (2010, May). Radiolaria and Global Oceanic Anoxic Event-2 in the Upper Cretaceous sections of Western Caucasus. In *EGU General Assembly Conference Abstracts* (p. 1995).

-Brand, U., & Veizer, J. (1981). Chemical diagenesis of a multicomponent carbonate system; 2, Stable isotopes. *Journal of Sedimentary Research*, *51*(3), 987-997.

-Bryant, G.F., 1960, Stratigraphic report of the Korudag area, Petroleum District VI, Southeast Turkey (American Overseas Petroleum (AMOSEAS) Report): Petrol İşleri Genel Müdürlüğü Teknik Arşivi. Kutu no. 323, Rapor no. 12, 23 s.

-Bordenave, M. L., & Hegre, J. A. (2010). Current distribution of oil and gas fields in the Zagros Fold Belt of Iran and contiguous offshore as the result of the petroleum systems. *Geological Society, London, Special Publications*, *330*(1), 291-353.

-Bjørlykke, K. (1983). Diagenetic reactions in sandstones. In *Sediment diagenesis* (pp. 169-213). Springer, Dordrecht.

-Castro, J. M., Company, M., De Gea, G. A., & Aguado, R. (2001). Biostratigraphy of the Aptian–Middle Cenomanian platform to basin domain in the Prebetic Zone of Alicante, SE Spain: calibration between shallow water benthonic and pelagic scales. *Cretaceous Research*, *22*(2), 145-156.

-Catuneanu, O. (2002). Sequence stratigraphy of clastic systems: concepts, merits, and pitfalls. *Journal of African Earth Sciences*, 35(1), 1-43.

-Catuneanu, O. (2006). *Principles of Sequence Stratigraphy*. Amsterdam, (pp. 375). Elsevier.

-Catuneanu, O. (2019). Scale in sequence stratigraphy. *Marine and Petroleum Geology*, *106*, 128-159.

-Carpenter, S. J., & Lohmann, K. C. (1989). 18O and 13C variations in late Devonian marine cements from the Golden Spike and Nevis reefs, Alberta, Canada. *Journal of Sedimentary Research*, 59(5).

-Carter, R. M., Abbott, S. T., Fulthorpe, C. S., Haywick, D. W., & Henderson, R. A. (1991). Application of global sea-level and sequence-stratigraphic models in Southern Hemisphere Neogene strata from New Zealand. *Sedimentation, Tectonics, and Eustasy: Sea Level Changes at Active Margins*, *12*, 41-65.

-Cater, J. M. L., & Gillcrist, J. R. (1994). Karstic reservoirs of the mid-Cretaceous Mardin Group, SE Turkey: tectonic and eustatic controls on their genesis, distribution and preservation. *Journal of Petroleum Geology*, *17*(3), 253-278.

-Choquette, P. W., & Pray, L. C. (1970). Geologic nomenclature and classification of porosity in sedimentary carbonates. *AAPG bulletin*, *54*(2), 207-250.

-Craig, H. (1957). Isotopic standards for carbon and oxygen and correction factors for mass-spectrometric analysis of carbon dioxide. *Geochim. Cosmochim. Acta*, 12, 133–149.

-Csoma, A.E., Goldstein, R.H., Mindszenty, A. & Simone, L. (2001). Diagenesis of platform strata as a tool to predict downslope depositional sequences, Monte Camposauro, Italy. In *AAPG Annual Meeting Expanded Abstracts* (p. 45).

-Celikdemir, M. E., Dülger, S., Görür, N., Wagner, C., & Uygur, K. (1991). Stratigraphy, sedimentology and hydrocarbon potential of the Mardin Group, SE Turkey. *Generation, Accumulation and Production of Europe's Hydrocarbons. European Association of Petroleum Geoscientists. Special Publication*, *1*, 439-454.

-Cordey, W. G., & Campbell, A. S. (1971). Stratigraphy and sedimentation of the Cretaceous Mardin Formation in southeastern Turkey. In *Geology and history of Turkey: 13th Annual Field Conference of the Petroleum Exploration Society of Libya* (pp. 317-348).

-Cros, P., Dercourt, J., Günay, Y., Fourcade, E., Bellier, J.P., Lauer, J.P., Manivit, H., & Kozlu, H. (1999). The Arabian Platform in southeastern Turkey: an Albian–Cenomanian carbonate ramp collapsed during the Senonian. *TAPG Bulletin 11*,1, 55–77.

-Çelikdemir, E. & Dülger, S. (1990). Güneydoğu Anadolu'da Mardin Grubu Karbonatlarının Stratigrafisi, Sedimantolojisi ve Rezervuar Özellikleri. TPAO Arama Grubu Raporu No: 2665, s.93.

-Çelikdemir, E. M., Dülger, S., Görür, N., Wagner, C., & Uygur, K. (1991). Stratigraphy, sedimentology, and hydrocarbon potential of the Mardin Group, SE Turkey. *Special Publications of the European Association of Petroleum Geoscientists 1*, 439–454.

-Çoruh, T. (1981). Mardin Grubu karbonatlarının X. Bölge Bölükkonak-2/A, Alıçl-2, Dodan-6M, Tavan-1, Kavikadağ-1 kuyularıyla; IX. Bölge Körkandil, Ballıkaya ve Mehmet Yusuf ölçülmüş stratigrafik kesitlerindekimikropaleontolojik incelenmesi: *TPAO Araştırma Merkezi*, Rapor no. 403/A, s.12.

-Çoruh, T., Yakar, H., & Ediger, V. (1997). Güneydoğu Anadolu Bölgesi Otokton İstifinin Biyostratigrafi Atlası. Ankara: Türkiye Petrolleri A.O. Araştırma Merkezi Grubu Başkanlığı.

-Darwish, M. H., Zakhera, M. S., Abdel-Maksoud, N. A., & Obaidalla, N. A. (2015, November). Macro-biostratigraphy integration of the Cenomanian-Turonian transition at North Eastern Desert and Southwestern Sinai, Egypt. In *The 8th International Conference on The Geology of Africa Assiut-Egypt* (pp. 99-131).

-Demirel, I. H., & Guneri, S. (2000). Cretaceous carbonates in the Adiyaman region, SE Turkey: an assessment of burial history and source-rock potential. *Journal of Petroleum Geology*, *23*(1), 91-106.

-De Righi, M. R., & Cortesini, A. (1964). Gravity tectonics in foothills structure belt of southeast Turkey. *AAPG Bulletin*, *48*(12), 1911-1937.

-Dias-Brito, D. (1985). Calcisphaerulidae do Albiano da Bacia de Campos, Rio de Janeiro, Brasil. Investigações taxonômicas: biocronoestratigráficas e paleoambientais. *Coletânea de Trabalhos Paleontológicos, Geologia*, *27*, 295-306.

-Dias-Brito, D. (2000). Global stratigraphy, palaeobiogeography and palaeoecology of Albian–Maastrichtian pithonellid calcispheres: impact on Tethys configuration. *Cretaceous Research*, *21*(2-3), 315-349.

-Dickens, G. R., O'Neil, J. R., Rea, D. K., & Owen, R. M. (1995). Dissociation of oceanic methane hydrate as a cause of the carbon isotope excursion at the end of the Paleocene. *Paleoceanography*, *10*(6), 965-971.

-Duran, O., Şengündüz, N., Sayılı, A., Soylu, C., & Aras, M. (1996). XI ve XII. Bölgelerde (GDA) Üst Kretase karbonatlarının stratigrafisi, sedimantolojisi, rezervuar özellikleri, jeokimyasal değerlendirmesi ve hidrokarbon potansiyeli: *TPAO Araştırma Merkezi*, Rapor no. 2165, s.76.

-Duval, B, Cramez, C., and Vail, P. R. (1998). Stratigraphic cycles and major marine source rocks. *In Mesozoic and Cenozoic Sequence Stratigraphy of European Basins* (P. C. De Graciansky, J. Hardenbol, T. Jacquin and P. R. Vail, Eds.), pp. 43–51. *SEPM Special Publication* 60.

-Du Vivier, A. D., Selby, D., Sageman, B. B., Jarvis, I., Gröcke, D. R., & Voigt, S. (2014). Marine $^{187}Os/^{188}Os$ isotope stratigraphy reveals the interaction of volcanism and ocean circulation during Oceanic Anoxic Event 2. *Earth and Planetary Science Letters*, *389*, 23-33.

-Ehrenberg, S. N., & Svana, T. A. (2001). Use of spectral gamma-ray signature to interpret stratigraphic surfaces in carbonate strata: An example from the Finnmark carbonate platform (Carboniferous-Permian), Barents Sea. *AAPG bulletin*, *85*(2), 295-308.

-Einsele, G., Ricken, W. & Seilacher, A. (Eds.) (1991). *Cycles and Events in Stratigraphy*. Springer-Verlag, pp. 955.

-Emery, D., & Myers, K. (Eds.). (2009). *Sequence stratigraphy*. John Wiley & Sons.

-Erbacher, J., Thurow, J., & Littke, R. (1996). Evolution patterns of radiolaria and organic matter variations: A new approach to identify sea-level changes in mid-Cretaceous pelagic environments. *Geology*, *24*(6), 499-502.

-Erenler, M. (1989). XI.-XII. Bolge guney alanlarindaki kuyularda Mesozoyik coke1 istifi mikropaleontolojik incelenmesi. TPAO Report 1364, pp.44.

-Ergene, S. M. (2014). *Lithologic heterogeneity of the Eagle Ford Formation, south Texas* (Master's Thesis, University of Texas at Austin).

-Evans, M. A., & Elmore, R. D. (2006). Fluid control of localized mineral domains in limestone pressure solution structures. *Journal of Structural Geology*, *28*(2), 284-301.

-Farinacci, A., & Köylüoğlu, M. (1982). Evolution of the Jurassic-Cretaceous Taurus Shelf (southern Turkey). *Boletino della Società Paleontologica Italiana*, *21*, 267-276.

-Flügel, E. (2004). Microfacies data: fabrics. In *Microfacies of Carbonate Rocks* (pp. 177-242). Springer, Berlin, Heidelberg.

-Fontaine, J. M., Monod, O., & Perincek, D. (1989). The Hezan Units: a fragment of the south neo-Tethyan passive continental margin in SE Turkey. *Journal of Petroleum Geology*, *12*(1), 29-50.

-Fourcade, E., Dercourt, J., Gunay, Y., Azéma, J., Kozlu, H., Bellier, J. P., ... & Vrielynck, B. (1991). Stratigraphie et paléogéographie de la marge septentrionale de la plate-forme arabe au Mésozoïque (Turquie du Sud-Est). *Bulletin de la Societé géologique de France*, *162*(1), 27-41.

-Galloway, W. E. (1989). Genetic stratigraphic sequences in basin analysis I: architecture and genesis of flooding-surface bounded depositional units. *AAPG bulletin*, 73(2), 125-142.

-Ghanem, H., & Kuss, J. (2013). Stratigraphic control of the Aptian–Early Turonian sequences of the Levant Platform, Coastal Range, northwest Syria. *GeoArabia*, *18*(4), 85-132.

-Gossage, D. W. (1956). Compiled progress report on the geology of part Petroleum District VI, Southeast Turkey: N. V. Turkse Shell, Report no. GRT. p.2,22.

-Gregg, J. M., & Sibley, D. F. (1984). Epigenetic dolomitization and the origin of xenotopic dolomite texture. *Journal of Sedimentary Research*, *54*(3), 908-931.

-Gröcke, D. R., Hesselbo, S. P., & Jenkyns, H. C. (1999). Carbon-isotope composition of Lower Cretaceous fossil wood: Ocean-atmosphere chemistry and relation to sea-level change. *Geology*, 27(2), 155-158.

-Güven, A., Dincer, A., Tuna, M. E., Tezcan Ü.Ş. & Çoruh, T. (1988). Güneydoğu Anadolu'da Mardin ve Midyat Grupları arasında yer alan birimlerin stratigrafisi (ön rapor): *TPAO Ayılrama Grubu*, Rapor no. 2414, s.154.

-Güven, A., Dinçer, A., Tuna, M. E., & Çoruh, T. (1991). Güneydoğu Anadolu Kampaniyen-Paleosen Otokton istifinin Stratigrafisi. *TPAO Arama Grubu*, Rapor no. 2414.

-Hajikazemi, E., Al-Aasm, I. S., & Coniglio, M. (2010). Subaerial exposure and meteoric diagenesis of the Cenomanian-Turonian Upper Sarvak Formation, southwestern Iran. *Geological Society, London, Special Publications*, *330*(1), 253-272.

-Handfield, R. W., Bryant, G.F., & Keskin, C. (1959). Measured section, Korudag (American Overseas Petroleum): *TPAO Arama Grubu*, Rapor no. 523.

-Handford, C. R., & Loucks, R. G. (1993). Carbonate depositional sequences and systems tracts--responses of carbonate platforms to relative sea-level changes: Chapter 1.

-Haq, B. U., & Al-Qahtani, A. M. (2005). Phanerozoic cycles of sea-level change on the Arabian Platform. *GeoArabia*, *10*(2), 127-160.

-Haq, B. U. (2014). Cretaceous eustasy revisited. *Global and Planetary change*, *113*, 44-58.

-Hardenbol, J., Thierry, J., Farley, M. B., Jacquin, T., Graciansky, P.-C. D.&Vail, P. R. (1998). Mesozoic and Cenozoic sequence chronostratigraphic framework in European basins. In Mesozoic and Cenozoic Sequence Stratigraphy of European Basins (eds P.-C. d. Graciansky, J. Hardenbol, T. Jacquin and P. R. Vail), pp. 3–13. *SEPM Special Publication 60*.

-Hardie, L. A. (1987). Dolomitization; a critical view of some current views. *Journal of Sedimentary Research*, *57*(1), 166-183.

-Hattin, D. E. (1981). Petrology of Smoky Hill Member, Niobrara Chalk (Upper Cretaceous), in type area, western Kansas. *AAPG Bulletin*, *65*(5), 831-849.

-Heap, M. J., Baud, P., Reuschlé, T., & Meredith, P. G. (2014). Stylolites in limestones: Barriers to fluid flow?. *Geology*, *42*(1), 51-54.

-Heckel, P. H. (1986). Sea-level curve for Pennsylvanian eustatic marine transgressive-regressive depositional cycles along midcontinent outcrop belt, North America. *Geology*, *14*(4), 330-334.

-Hortstink, F. (1971). The Late Cretaceous and Tertiary geological evolution of eastern Turkey, *Proceedings of the 1st Petroleum Congress*, p.25-41.

-Husinec, A., & Sokač, B. (2006). Early Cretaceous benthic associations (foraminifera and calcareous algae) of a shallow tropical-water platform environment (Mljet Island, southern Croatia). *Cretaceous Research*, *27*(3), 418-441.

-Humphrey, J. (1988) Late Pleistocene mixing zone dolomitization, southeastern Barbados, West Indies. *Sedimentology*, 35, 327–348.

-Hüsing, S. K., Zachariasse, W. J., Van Hinsbergen, D. J., Krijgsman, W., Inceöz, M., Harzhauser, M., ... & Kroh, A. (2009). Oligocene–Miocene basin evolution in SE Anatolia, Turkey: constraints on the closure of the eastern Tethys gateway. *Geological Society, London, Special Publications*, *311*(1), 107-132.

-James, N. P., Choquette, P. W., McIlreath, I., & Morrow, D. (1990). Limestone diagenesis, the meteoric environment. *Sediment Diagenesis: Geological Association Canada Reprint Series, St-John's, Newfoundland*, 36-74.

-Jarvis, I., Carson, G. A., Cooper, M. K. E., Hart, M. B., Leary, P. N., Tocher, B. A., & Rosenfeld, A. (1988). Microfossil assemblages and the Cenomanian-Turonian (Late Cretaceous) oceanic anoxic event. *Cretaceous Research*, 9(1), 3-103.

-Jarvis, I. A. N., Murphy, A. M., & Gale, A. S. (2001). Geochemistry of pelagic and hemipelagic carbonates: criteria for identifying systems tracts and sea-level change. *Journal of the Geological Society*, 158(4), 685-696.

-Jarvis, I. A. N., Gale, A. S., Jenkyns, H. C., & Pearce, M. A. (2006). Secular variation in Late Cretaceous carbon isotopes: a new δ13C carbonate reference curve for the Cenomanian–Campanian (99.6–70.6 Ma). *Geological Magazine*, *143*(5), 561-608.

-Jenkyns, H. C. (1980). Cretaceous anoxic events: from continents to oceans. *Journal of the Geological Society*, 137(2), 171-188.

-Jenkyns, H. C. (1985). The Early Toarcian and Cenomanian-Turonian anoxic events in Europe: comparisons and contrasts. *Geologische Rundschau*, *74*(3), 505-518.

-Jenkyns, H. C., Gale, A. S., & Corfield, R. M. (1994). Carbon-and oxygen-isotope stratigraphy of the English Chalk and Italian Scaglia and its palaeoclimatic significance. *Geological Magazine*, 131(1).

-Jenkyns, H. C. (2003). Evidence for rapid climate change in the Mesozoic–Palaeogene greenhouse world. *Philosophical Transactions of the Royal Society of London. Series A: Mathematical, Physical and Engineering Sciences*, *361*(1810), 1885-1916.

-Keller, G., & Pardo, A. (2004). Age and paleoenvironment of the Cenomanian–Turonian global stratotype section and point at Pueblo, Colorado. *Marine Micropaleontology*, 51(1-2), 95-128.

-Kellogg, H. E. (1960). Stratigraphic Report, Derik-Mardin Area, Petroleum District V, Southeast Turkey (American Overseas Petroleum (AMOSEAS) Report) Report no: 1367 (unpublished).

-Kellogg H. E. (1961) Regional stratigraphy and petroleum possibilities of Southeast Turkey. Petroleum District V, SE Turkey. (American Overseas Petroleum (AMOSEAS) Report): Petrol İşleri Genel Müdürlüğü Teknik Arşivi, Kutu no: 201, Rapor no.1, 29s. (*TPAO Arama Grubu*, Rapor no.767). (unpublished).

-Kennedy, W. J., & Cobban, W. A. (1991). Stratigraphy and interregional correlation of the Cenomanian-Turonian transition in the Western Interior of the United States near Pueblo, Colorado, a potential boundary stratotype for the base of the Turonian stage. *Newsletters on Stratigraphy*, 1-33.

-Keskin, G., & Can, C. (1986). Upper Cretaceous carbonate reservoirs of the Raman field, southeast Turkey. *Carbonates and Evaporites*, 1(1), 25.

-Ketin, İ. (1966). Tectonic units of Anatolia (Asia minor). *Maden Tetkik ve Arama Dergisi*, *66*(66), 23-34.

-Köylüoğlu, M. (1986). Güneydoğu Anadolu otokton birimlerin kronostratigrafisi, mikrofasiyes ve mikrofosilleri, *TPAO Araştırma Merkezi*, Eğitim Yayınları No:9, s. 53.

-Krapez, B. (1996). Sequence stratigraphic concepts applied to the identification of basin-filling rhythms in Precambrian successions. *Australian Journal of Earth Sciences*, *43*(4), 355-380.

-Lehrmann, D.J. & Goldhammer, R.K. (1999). Secular variation in parasequence and facies stacking patterns of platform carbonates: a guide to application of stacking

pattern analysis in strata of diverse ages and settings. In: Harris, P.M., Saller, A.H., Simo, J.A. (Eds.), Advances in Carbonate Sequence Stratigraphy: Application to Reservoirs, Outcrops and Models. *SEPM Special Publication 63*, 187-226.

-Longman, M. W. (1980). Carbonate diagenetic textures from nearsurface diagenetic environments. *AAPG bulletin*, *64*(4), 461-487.

-Lucia, F. J., & Major, R. P. (1994). Porosity evolution through hypersaline reflux dolomitization. *Dolomites: A Volume in Honour of Dolomieu*, 325-341.

-Machel, H. G. (1985). Cathodoluminescence in calcite and dolomite and its chemical interpretation. *Geoscience Canada*, *12*(4).

-Machel, H. G., & Mountjoy, E. W. (1986). Chemistry and environments of dolomitization—a reappraisal. *Earth-Science Reviews*, *23*(3), 175-222.

-Martin, A. Z. (2001). Late Permian to Holocene paleofacies evolution of the Arabian Plate and its hydrocarbon occurrences. *GeoArabia*, *6*(3), 445-504.

-Mathey, B., Alzouma, K., Lang, J., Meister, C., Néraudeau, D., & Pascal, A. (1995). Unusual faunal associations during Upper Cenomanian-Lower Turonian floodings on the Niger ramp (central West Africa). *Palaeogeography, Palaeoclimatology, Palaeoecology*, *119*(1-2), 63-75.

-Matyszkiewicz, J. (1996). The significance ofSaccocoma-calciturbidites for the analysis of the Polish epicontinental late Jurassic Basin: An example from the Southern Cracow-Wielun Upland (Poland). *Facies*, *34*(1), 23-40.

-Meyers, W. J. (1974). Carbonate cement stratigraphy of the Lake Valley Formation (Mississippian) Sacramento Mountains, New Mexico. *Journal of Sedimentary Research*, 44(3), 837-861.

-Miall, A.D. (2010). "Historical and Methodological Background", dalam The Geology of Stratigraphic Sequences, eds. Miall, A. D., Springer, Berlin, Heidelberg, hal. 3-45.

-Milliken, K. L. (2003). *Late diagenesis and mass transfer in sandstone shale sequences* (Vol. 7, p. 407).

-Milliken, K. L., & R. Day-Stirrat (2013). Cementation in mudrocks: Brief review with examples from cratonic basin mudrocks, in J.-Y. Chatellier and D. M. Jarvie, eds., Critical assessment of shale resource plays: *AAPG Memoir* 103, p. 133–160.

-Milliken, K. L., Ergene, S. M., & Ozkan, A. (2016). Quartz types, authigenic and detrital, in the upper cretaceous eagle ford formation, South Texas, USA. *Sedimentary Geology*, 339, 273-288.

-Mohseni, H., & Al-Aasm, I. S. (2004). Tempestite deposits on a storm-influenced carbonate ramp: An example from the Pabdeh Formation (Paleogene), Zagros Basin, SW Iran. *Journal of petroleum geology*, 27(2), 163-178.

-Moix, P., Beccaletto, L., Kozur, H. W., Hochard, C., Rosselet, F., & Stampfli, G. M. (2008). A new classification of the Turkish terranes and sutures and its implication for the paleotectonic history of the region. *Tectonophysics*, 451(1-4), 7-39.

-Moldovanyi, E. P., & Lohmann, K. C. (1984). Isotopic and petrographic record of phreatic diagenesis; Lower Cretaceous Sligo and Cupido formations. *Journal of Sedimentary Research*, *54*(3), 972-985.

-Moore, C. H. (1989). *Carbonate diagenesis and porosity*. Amsterdam, (pp. 338). Elsevier.

-Morad, S., Ketzer, J. M., & De Ros, L. F. (2012). Linking diagenesis to sequence stratigraphy: an integrated tool for understanding and predicting reservoir quality distribution. *Linking Diagenesis to Sequence Stratigraphy. Special Publication of the International Association of Sedimentologists*, *45*, 1-36.

-Morrow, D. W. (1990). Dolomite — Part 1: the chemistry of dolomite and dolomite precipitation. In: *Diagenesis* , I. A. McIlreath and D. W. Morrow (Eds.). *Geoscience Canada Reprint Series* No. 4, pp. 113 – 123

-Morrow, D. W. (1990). Dolomite–Part 2: Dolomitization models and ancient dolostones. *Geoscience Canada Reprint Series*, *4*, 125-139.

-Mouthereau, F., Lacombe, O., & Vergés, J. (2012). Building the Zagros collisional orogen: timing, strain distribution and the dynamics of Arabia/Eurasia plate convergence. *Tectonophysics*, *532*, 27-60.

-M'rabet, A. (1981). Differentiation of environments of dolomite formation, Lower Cretaceous of Central Tunisia. *Sedimentology*, *28*(3), 331-352.

-Müller, G. (1967). Diagenesis in argillaceous sediments. In *Developments in sedimentology* (Vol. 8, pp. 127-177). Elsevier.

-Mülayim, O. (2013). *Microfacies analysis, depositional environments and sequence stratigraphy of the late Cretaceous Karababa and Derdere formations in the Cemberlitas oil field, Adiyaman, Southeastern Turkey* (Master's Thesis, University of Alabama Libraries).

-Mülayim, O., Mancini, E., Cemen, I., & Yılmaz, İ. Ö. (2016). Upper Cenomanian-Lower Campanian Derdere and Karababa formations in the Çemberlitaş oil field, southeastern Turkey: their microfacies analyses, depositional environments, and sequence stratigraphy. *Turkish Journal of Earth Sciences*, *25*(1), 46-63.

-Mülayim, O., Yilmaz, İ.Ö., Sarı, B. & Taslı, K. (2019). Carbon–isotope stratigraphy of the Cenomanian–Turonian carbonate succession of the Türkoğlu section (SE Turkey): implications for the timing of Late Cretaceous sea–level rise and anoxic event. IESCA 2019, Conference Abstracts.

-Mülayim, O., Yılmaz, İ. Ö., Özer, S., Sarı, B., & Taslı, K. (2020). A Cenomanian–Santonian rudist–bearing carbonate platform on the northern Arabian Plate, Turkey: facies and sequence stratigraphy. *Cretaceous Research*, *110*, 104-414.

-Mülayim, O. (2020). *Cenomanian–turonian platform evolution and records of OAE 2 on the drowned northern arabian carbonate platform (se Turkey): Integration of biostratigraphy, sequence stratigraphy, sedimentology, and stable isotopes* (Doctoral Dissertation, Middle East Teachnical University).

-Neilson, J. E., & Oxtoby, N. H. (2008). The relationship between petroleum, exotic cements and reservoir quality in carbonates–A review. *Marine and Petroleum Geology*, *25*(8), 778-790.

-Nio, S. D., Brouwer, J. H., Smith, D., de Jong, M., & Böhm, A. R. (2005). Spectral trend attribute analysis: applications in the stratigraphic analysis of wireline logs. *first break*, *23*(4).

-O'Dogherty, L. (1994). *Biochronology and paleontology of mid-Cretaceous radiolarians from northern Apennines (Italy) and Betic Cordillera (Spain)* (Vol. 21, pp. 1-415). Section des sciences de la terre, Université de Lausanne.

-Ogg, J. G., Hinnov, L. A., & Huang, C. (2012). Chapter 26. Jurassic. Chapter 27. Cretaceous. *The Geologic Time Scale*, 731-853.

-Okay, A. I., & Tüysüz, O. (1999). Tethyan sutures of northern Turkey. *Geological Society, London, Special Publications*, *156*(1), 475-515.

-Okay, A. I. (2008). Geology of Turkey: a synopsis. *Anschnitt*, *21*, 19-42.

-Özkan, R., & Altiner, D. (2019). The Cretaceous Mardin Group carbonates in southeast Turkey: Lithostratigraphy, foraminiferal biostratigraphy, microfacies and sequence stratigraphic evolution. *Cretaceous Research*, 98, 153-178.

-Paganoni, M., Al Harthi, A., Morad, D., Morad, S., Ceriani, A., Mansurbeg, H.,& Sirat, M. (2016). Impact of stylolitization on diagenesis of a Lower Cretaceous carbonate reservoir from a giant oilfield, Abu Dhabi, United Arab Emirates. *Sedimentary geology*, 335, 70-92.

-Pasin C., Akgül, A. & Dülger, S. (1982). Güneydoğu Anadolu'da Mardin Grubu: *TPAO Arama Grubu*, Rapor no. 1635, s.81.

-Pearce, M. A., Jarvis, I., & Tocher, B. A. (2009). The Cenomanian–Turonian boundary event, OAE2 and palaeoenvironmental change in epicontinental seas: new insights from the dinocyst and geochemical records. *Palaeogeography, Palaeoclimatology, Palaeoecology*, *280*(1-2), 207-234.

-Perinçek, D. (1979). The geology of Hazro-Korudağ-Çüngüş-Maden-Ergani-Hazar-Elazığ Malatya region. *Guide Book, TJK, Ankara*.

-Perincek, D. (1980). Sedimentation on the Arabian shelf under the control of tectonic activity in Taurid belt. In *Proceedings of the 1st Petroleum Congress* (pp. 77-93).

-Perinçek, D., & Özkaya, I. (1981). Tectonic evolution of the northern margin of Arabian plate. *Yerbilimleri*, *8*, 91-101.

-Perinçek, D., Duran, O., Bozdoğan, N., & Çoruh, T. (1991). Stratigraphy and paleogeographical evolution of the autochthonous sedimentary rocks in SE Turkey, in Turgut, S., ed., Tectonics and Hydrocarbon Potential of Anatolia and Surrounding Regions: Ozan Sungurlu Symposium Proceedings: Ankara, Turkey, *Turkish Association of Petroleum Geologists*, p. 274–304.

-Posamentier, H. W., Allen, G. P., James, D. P., & Tesson, M. (1992). Forced regressions in a sequence stratigraphic framework: concepts, examples, and exploration significance. *AAPG bulletin*, *76*(11), 1687-1709.

-Posamentier, H. W., & Weimer, P. (1993). Siliciclastic sequence stratigraphy and petroleum geology—where to from here?. *AAPG bulletin*, *77*(5), 731-742.

-Pollastro, R. M., Jarvie, D. M., Hill, R. J., & Adams, C. W. (2007). Geologic framework of the Mississippian Barnett shale, Barnett-paleozoic total petroleum system, Bend arch–Fort Worth basin, Texas. *AAPG bulletin*, 91(4), 405-436.

-Ramsbottom, W. H. C. (1979). Rates of transgression and regression in the Carboniferous of NW Europe. *Journal of the Geological Society*, *136*(2), 147-153.

-Razin, P., Taati, F., & Van Buchem, F. S. P. (2010). Sequence stratigraphy of Cenomanian–Turonian carbonate platform margins (Sarvak Formation) in the High Zagros, SW Iran: an outcrop reference model for the Arabian Plate. *Geological Society, London, Special Publications*, *329*(1), 187-218.

-Reid, S. K. & Dorobek, S. L. (1993). Sequence stratigraphy and evolution of a progradational, foreland carbonate ramp, lower Mississippian Mission Canyon Formation and stratigraphic equivalents, Montana and Idaho. In: Loucks, R. G., Sarg, J. F. (eds.), Carbonate sequence stratigraphy – Recent developments and applications. *AAPG Memoir* 57, 327–352.

-Rider, M. (1996). *Geological Interpretation of Well Logs*, 2nd ed. Whittles Publishing , Latheronhouse, UK , 280 pp.

-Rikhtegarzadeh, M., Vaziri, S. H., Aleali, M., Bakhtiar, H. A., & Jahani, D. (2016). Microbiostratigraphy, Microfacies and Depositional Environment of the Sarvak

Formation in Bi Bi Hakimeh Oil Field (Well No. 29), Southwest Iran. *International Journal of Geography and Geology*, *5*(10), 194-208.

-Robertson, A., Boulton, S. J., Taslı, K., Yıldırım, N., İnan, N., Yıldız, A., & Parlak, O. (2016). Late Cretaceous–Miocene sedimentary development of the Arabian continental margin in SE Turkey (Adıyaman region): Implications for regional palaeogeography and the closure history of Southern Neotethys. *Journal of Asian Earth Sciences*, *115*, 571-616.

-Saber, S. G., Salama, Y. F., Scott, R. W., Abdel-Gawad, G. I., & Aly, M. F. (2009). Cenomanian-Turonian rudist assemblages and sequence stratigraphy on the North Sinai carbonate shelf, Egypt. *GeoArabia*, *14*(4), 113-134.

-Saltık, O. & Saka, K. (1971a). İnişdere tip stratigrafi kesiti: *TPAO Arama Grubu*, Arşiv no. 4308.

-Saltık, O. & Saka, K. (1971b). Karababa tip stratigrafi kesiti: *TPAO Arama Grubu*, Arşiv no. 4307.

-Sarg, J. F. (1988). Carbonate sequence stratigraphy. *In Sea Level Changes–An Integrated Approach* (C. K. Wilgus, B. S. Hastings, C. G. St. C. Kendall, H. W. Posamentier, C. A. Ross and J. C. Van Wagoner, Eds.), pp. 155–182. *SEPM Special Publication, 42*.

-Sharland, P. R., Casey, D. M., Davies, R. B., Simmons, M. D., & Sutcliffe, O. E. (2001). *Arabian plate sequence stratigraphy* (Vol. 2, p. 371). Bahrain: Gulf PetroLink.

-Schlager, W. (2004) Fractal nature of stratigraphic sequences. *Geology* 32, 185–188.

-Schlager, W. (2010). Ordered hierarchy versus scale invariance in sequence stratigraphy. *Int. J. Earth Sci*. 99, 139–151.

-Schlanger, S. O., Arthur, M. A., Jenkyns, H. C., & Scholle, P. A. (1987). The Cenomanian-Turonian Oceanic Anoxic Event, I. Stratigraphy and distribution of organic carbon-rich beds and the marine δ13C excursion. *Geological Society, London, Special Publications*, 26(1), 371-399.

-Schlanger, S. O., & Jenkyns, H. C. (2007). Cretaceous oceanic anoxic events: causes and consequences. *Netherlands Journal of Geosciences/Geologie en Mijnbouw*, (Classic Papers).

-Schmidt, G. C. (1964). A review of Permian and Mesozoic formations exposed near the Turkey/Iraq border at Harbol. *Maden Tetkik ve Arama Dergisi*, *62*(62).

Scholle, P. A., & Arthur, M. A. (1980). Carbon isotope fluctuations in Cretaceous pelagic limestones: potential stratigraphic and petroleum exploration tool. *AAPG Bulletin*, *64*(1), 67-87.

-Scholle, P. A., & Ulmer-Scholle, D. S. (2003). *A color guide to the petrography of carbonate rocks: grains, textures, porosity, diagenesis, AAPG Memoir 77* (Vol. 77).

-Scholz, F., Beil, S., Flögel, S., Lehmann, M. F., Holbourn, A., Wallmann, K., & Kuhnt, W. (2019). Oxygen minimum zone-type biogeochemical cycling in the Cenomanian-Turonian Proto-North Atlantic across Oceanic Anoxic Event 2. *Earth and Planetary Science Letters*, 517, 50-60.

-Schulze, F., Lewy, Z., Kuss, J., & Gharaibeh, A. (2003). Cenomanian–Turonian carbonate platform deposits in west central Jordan. *International Journal of Earth Sciences*, *92*(4), 641-660.

-Schulze, F., Kuss, J., & Marzouk, A. (2005). Platform configuration, microfacies and cyclicities of the upper Albian to Turonian of west-central Jordan. *Facies*, 50(3-4), 505-527.

-Serra, O. (1984). *Fundamentals of well-log interpretation*. *The acquisition of logging data:* Amsterdam (Vol. 1 pp. 423). Elsevier.

-Sibley, D.F. (1980). Climatic control of dolomitization, Seroe Domi Formation Pliocene , Bonaire, N.A. In: Zenfger, D.H., Ž . Dunham, J.B., Ethington, R.L. Eds., Concepts and Models of Dolomitization. *SEPM Special Publication, 28*, 247–258.

-Sibley, D. F. & Gregg, J. M. (1987). Classification of dolomite rock textures. *Journal of sedimentary Research*, *57*(6), 967-975.

-Sinanoglu E. & Erkmen, U. (1980). Güneydoğu Anadolu Apsiyen-Albiyen palinostratigrafisi ve bölgenin Alt Kretase palinoprovenansları içindeki yeri: *Türkiye Beşinci Petrol Kongresi, Jeoloji-Jeofizik Bildirileri*, 51-59.

-Soleimani, B., Bahadori, A., & Meng, F. (2013). Microbiostratigraphy, microfacies and sequence stratigraphy of upper cretaceous and paleogene sediments, Hendijan oilfield, Northwest of Persian Gulf, Iran. *Natural Science*, *5*(11), 1165.

-Soua, M. (2012). Application of facies associations, integrated prediction error filter analysis, and chemostratigraphy to the organic-rich and siliceous Cenomanian-Turonian sequence, Bargou Area, Tunisia: Integrated sequence stratigraphic analysis. *Journal of Geological Research*, *2012*.

-Spadini, A. R., Esteves, F. R., Dias-Brito, D., Azevedo, R. M., & Rodrigues, R. (1988). The Macaé Formation, Campos basin, Brazil: Its evolution in the context of the initial history of the South Atlantica. *Rev. Bras. Geocienc*, *18*(3), 261-272.

-Stoll, H. M., & Schrag, D. P. (2000). High-resolution stable isotope records from the Upper Cretaceous rocks of Italy and Spain: Glacial episodes in a greenhouse planet?. *Geological Society of America Bulletin*, *112*(2), 308-319.

-Sungurlu, O. (1973). VI. Bölge Gölbaşı-Gerger arasındaki sahanın jeolojisi: *TPAO Arama Grubu*, Rapor no. 802, s.30.

-Sungurlu, O. (1974). VI. Bölge kuzeyinin jeolojisi ve petrol imkanları. *Türkiye İkinci Petrol Kongresi, Tebliğler*, 85-107.

-Swart, P. K., Reijmer, J. J., & Otto, R. (2009). A reevaluation of facies on Great Bahama Bank II: Variations in the δ13C, δ18O and mineralogy of surface sediments. *Int. Assoc. Sedimentol. Spec. Publ*, 41, 47-59.

-Şenel, M. (2002). Geological map of Turkey, Denizli 1: 500.000 scale sheet. *General Directorate of Mineral Research and Exploration, Ankara, Turkey*.

-Şengör, A. C., & Yilmaz, Y. (1981). Tethyan evolution of Turkey: a plate tectonic approach. *Tectonophysics*, *75*(3-4), 181-241.

-Şengör, A. M. C., Yılmaz, Y., & Sungurlu, O. (1984). Tectonics of the Mediterranean Cimmerides: nature and evolution of the western termination of Palaeo-Tethys. *Geological Society, London, Special Publications*, *17*(1), 77-112.

-Şengündüz, N. & Aras, M. (1986). XI. ve XII. Bölgelerde Mardin Grubu karbonatlarının ve Karaboğaz Formasyonu'nun fasiyes dağılımı, diyajenetik özellikleri ve çökelme modeli: *TPAO Araştırma Merkezi*, Rapor no. 1005, s.75.

-Taghavi, A. A., Mørk, A., & Emadi, M. A. (2006). Sequence stratigraphically controlled diagenesis governs reservoir quality in the carbonate Dehluran Field, southwest Iran. *Petroleum Geoscience*, *12*(2), 115-126.

-Tardu, T. (1991). A sequence stratigraphic approach to the Mardin Group. Tectonics and hydrocarbon potential of Anatolia and surrounding regions. In *Ozan Sungurlu Symposium Proceedings, Ankara, Turkey*.

-Temple, P. G., & Perry, L. J. (1962). Geology and oil occurrence, southeast Turkey. *AAPG Bulletin*, *46*(9), 1596-1612.

-Terry, R. D., Chilingar, G. V., & Hancock, A. (1955). Comparison charts for visual estimation of percentage composition. *Journal of Sediment Petrology*, *25*, 229-234.

-Thierstein, H. R., & Roth, P. H. (1991). Stable isotopic and carbonate cyclicity in Lower Cretaceous deep-sea sediments: dominance of diagenetic effects. *Marine Geology*, 97(1-2), 1-34.

-Tovey, N. K., & Krinsley, D. H. (1991). Mineralogical mapping of scanning electron micrographs. *Sedimentary Geology*, *75*(1-2), 109-123.

-Tucker, M. E. (1993). Carbonate diagenesis and sequence stratigraphy. *Sedimentology Review/1*, 51-72.

-Tuna, D. (1973). VI. Bölge Litostratigrafi Birimleri Adlamasının Açıklayıcı Raporu: *TPAO Arama Grubu*, Rapor no. 813, s.131.

-Tuncer, M. (2013). *Balanced cross section of the northeast of Adiyaman, Turkey.* (Master's Thesis, Missouri University of Science and Technology).

-Turgeon, S. C., & Creaser, R. A. (2008). Cretaceous oceanic anoxic event 2 triggered by a massive magmatic episode. *Nature*, *454*(7202), 323-326.

-Vail, P. R., Mitchum, R. M. Jr., & Thompson, S., III. (1977). Seismic stratigraphy and global changes of sea level, part four: global cycles of relative changes of sea level. *American Association of Petroleum Geologists Memoir 26*, 83–98.

-Vail, P. R. (1991). The stratigraphic signatures of tectonics, eustacy and sedimentology-an overview. *Cycles and events in stratigraphy*, 617-659.

-Valladares, I., Recio, C., & Lendinez, A. (1996). Sequence stratigraphy and stable isotopes (δ13C, δ180) of the Late Cretaceous carbonate ramp of the western margin of the Iberian Chain (Soria, Spain). *Sedimentary Geology*, *105*(1-2), 11-28.

-van Buchem, F. S., Razin, P., Homewood, P. W., Philip, J. M., Eberli, G. P., Platel, J. P., ... & Cantaloube, S. (1996). High resolution sequence stratigraphy of the Natih Formation (Cenomanian/Turonian) in northern Oman: distribution of source rocks and reservoir facies. *GeoArabia*, *1*(1), 65-91.

-Vanneau, A. & Silva, I. (1995). Biostratigraphy and systematic description of benthic foraminifers from mid-Cretaceous shallow-water carbonate platform sediments at Sites 878 and 879 (MIT and Takuyo-Daisan Guyots). In *Proceedings of the Ocean Drilling Program. Scientific results* (Vol. 144, pp. 199-219).

-Arnaud-Vanneau, A., & Sliter, W. V. (1995). Early Cretaceous shallow-water benthic foraminifers and fecal pellets from Leg 143 compared with coeval faunas from the Pacific Basin, Central America, and the Tethys: Northwest Pacific atolls and guyots. In *Proceedings of the Ocean Drilling Program. Scientific Results* (Vol. 142, pp. 537-564).

-Van Wagoner, J. C., Posamentier, H. W., Mitchum, R. M. Jr., Vail, P. R., Sarg, J. F., Loutit, T. S., and Hardenbol, J. (1988). An overview of sequence stratigraphy and key definitions. *In Sea Level Changes–An Integrated Approach* C. K. Wilgus, B. S. Hastings, C. G. St. C. Kendall, H. W. Posamentier, C. A. Ross and J. C. Van Wagoner, Eds.), pp. 39–45. *SEPM Special Publication 42*.

-Van Wagoner, J. C., Mitchum, R. M. Jr., Campion, K. M., and Rahmanian, V. D. (1990). Siliciclastic sequence stratigraphy in well logs, core, and outcrops: concepts for

high-resolution correlation of time and facies. *American Association of Petroleum Geologists Methods in Exploration Series 7*, p. 55.

-Velić, I. (2007). Stratigraphy and Palaeobiogeography of Mesozoic Benthic Foraminifera of the Karst Dinarides (SE Europe)-PART 1. *Geologia Croatica*, *60*(1), 1-60.

-Wanless, H. R., & Weller, J. M. (1932). Correlation and extent of Pennsylvanian cyclothems. *Bulletin of the Geological Society of America*, *43*(4), 1003-1016.

-Weyl, P. K. (1960). Porosity through dolomitization--Conservation-of-mass requirements. *Journal of Sedimentary Research*, 30(1), 85-90.

-White, R. J., Spinelli, G. A., Mozley, P. S., & Dunbar, N. W. (2011). Importance of volcanic glass alteration to sediment stabilization: offshore Japan. *Sedimentology*, *58*(5), 1138-1154.

-Williams, D. F. (1988). Evidence for and against sea-level changes from the stable isotopic record of the Cenozoic, in C. K. Wilgus, B. S. Hastings, C. G. St. C. Kendall, H. W. Posamentier, C. A. Ross, and J. C. Van Wagoner, eds., Sea-level changes: an integrated approach: Tulsa, *SEPM Special Publication 42*, 31–36.

-Williams, T. A., Graham, S. A., & Constenius, K. N. (1998). Recognition of a Santonian submarine canyon, Great Valley Group, Sacramento basin, California: Implications for petroleum exploration and sequence stratigraphy of deep-marine strata. *AAPG bulletin*, *82*(8), 1575-1595.

-Wilmsen, M. (2003). Sequence stratigraphy and palaeoceanography of the Cenomanian Stage in northern Germany. *Cretaceous Research*, *24*(5), 525-568.

-Wilmsen, M., & Voigt, T. (2006). The middle–upper Cenomanian of Zilly (Sachsen-Anhalt, northern Germany) with remarks on the Pycnodonte Event. *Acta Geologica Polonica*, *56*(1), 17-31.

-Wilson, H. H. & Krummenacher, R. (1959). Geology and oil prospects of the Gaziantep Region, Southeast Turkey (N. V. Turkse Shell Report): Petrol İşleri Genel

Müdürlüğü Teknik Arşivi, Kut no. 351, Rapor no. 1, 53 s. (*TPAO Arama Grubu*, Rapor no. 839).

-Wilson, J. L. (1975). The lower carboniferous Waulsortian facies. In *Carbonate Facies in Geologic History* (pp. 148-168). Springer, New York, NY.

-Yalçın, N. (1976). Geology of the Narince-Gerger area (Adıyaman province) and its petroleum possibilities. *Revue de la Faculté des Sciences de l'Université d'Istanbul B*, *41*, 57-82.

-Yildiz, G. (2019). *Reservoir Heterogeneity, Sedimentology, and Diagenesis of Ordovician Bedinan Formation, Southern Diyarbakir Basin, SE Turkey: Paleogeographic Implications* (Master's Thesis, Middle East Technical University).

-Yilmaz, Y. (1990). Allochthonous terranes in the Tethyan Middle East: Anatolia and the surrounding regions. *Philosophical Transactions of the Royal Society of London. Series A, Mathematical and Physical Sciences*, *331*(1620), 611-624.

-Yılmaz, E. (1982). Hazro (Diyarbakır) güneybatı yöresinin jeolojisi (Diploma çalışması): İstanbul Teknik Üniversitesi. *Jeoloji Kürsüsü*.

-Yılmaz, Y., Yigitbas, E., & Yildirim, M. (1987). Güneydogu Anadolu'da Triyas sonu tektonizmasi ve bunun jeolojik anlami. In *Proceedings of the Turkish 7th Petroleum Congress* (pp. 65-77).

-Yılmaz, Y. (1993). New evidence and model on the evolution of the southeast Anatolian orogen. *Geological Society of America Bulletin*, *105*(2), 251-271.

-Yılmaz, E., & Duran, O. (1997). Güneydoğu Anadolu Bölgesi Otokton ve Allokton Birimler Stratigrafi Adlama Sözlüğü " Lexicon". Ankara: TPAO.

-Zenger, D. H. (1972). Significance of supratidal dolomitization in the geologic record. *Geological Society of America Bulletin*, *83*(1), 1-12.

-Zhao, Z., Wang, J., & Wang, P. (2017). Carbon and oxygen isotope variation and its implication for marine sequence: A case study of Ordovician in Tarim Basin. *Petroleum Research*, *2*(3), 281-290.

## CURRICULUM VITAE

### PERSONAL INFORMATION

Surname, Name: Yetim, Suzan Müge
Nationality: Turkish (TC)
Date and Place of Birth: 22 July 1988, Ankara
Marital Status: Married
Phone: +90 543 337 73 94
email: smergene@tpao.gov.tr

### EDUCATION

| Degree | Institution | Year of Graduation |
|---|---|---|
| MS | Univeristy of Texas at Austin, Jackson School of Geosciences | 2014 |
| BS | METU Geological Engineering | 2011 |
| High School | Etimesgut Anadolu High School, Ankara | 2006 |

### WORK EXPERIENCE

| Year | Place | Enrollment |
|---|---|---|
| 2014-Present | Turkish Petroleum Cooperation | Sedimentologist |
| 2011-2012 | METU Dept. of Geological Eng. | Teaching Assistant |
| 2010 July | Esri Turkey | Intern Eng. Student |
| 2009 August | Turkish Petroleum Cooperation | Intern Eng. Student |

### FOREIGN LANGUAGES

Advanced English

### PUBLICATIONS

Ergene, S. M. (2014). Lithologic Heterogeneity of the Eagle Ford Formation. South Texas [MS thesis]: University of Texas at Austin.

Milliken, K. L., Ergene, S. M., & Ozkan, A. (2016). Quartz types, authigenic and detrital, in the Upper Cretaceous Eagle Ford Formation, south Texas, USA. Sedimentary Geology, 339, 273-288.

Ergene, S. M., & Milliken, K. (2016) Petrography of Silica Diagenesis in the Eagle Ford Formation, South Texas. In AAPG Annual Convention and Exhibition.

Müge Yetim, S., & Altıner, D. (2019). Evaluation of Reservoir Quality of Mardin Group Carbonates within the Sequence Stratigraphy Framework in Adiyaman and Diyarbakir Regions, SE Turkey. EGUGA, 982.